

CENTRAL LIBRARY  
TEZPUR UNIVERSITY  
Accession No. T316  
Date \_\_\_\_\_

**MICROSTRIP PATCH ANTENNAS - SOME  
TECHNIQUES ON SIZE REDUCTION AND TUNING**

**A thesis submitted in partial fulfillment of the requirements  
for the degree of  
Doctor of Philosophy**

**By  
Anup Kumar Bordoloi  
Registration No: 010 of 2010**



**Department of Electronics and Communication Engineering  
Tezpur University  
Tezpur-784028  
Assam, India**

**December, 2013**

*This thesis is dedicated to my beloved parents*

*Late Chandra Nath Bordoloi and Mrs Usha Devi*

## ABSTRACT

Mobile and handheld wireless technology, in the contemporary world scenario has become increasingly ubiquitous. In particular the field of RF wireless communication is experiencing unprecedented technological advancements and market growth, evident by rapid increase in use of cellular telephony, mobile data and wireless local area network (WLAN) technologies as well as satellite communication. In the wireless systems, the antenna, which acts as the frontends at the transmitting and receiving ends, is a critical component.

Applications in present day mobile communications essentially require smaller antenna size for mobile handheld devices. For this reason, there has been great emphasis on achieving broad band operations with compact microstrip antenna introduction of new mobile wireless systems such as Wi Max 2400 (2595-2690 MHz), Wi Fi (2400-2483 MHz), WCDMA in 3G (2.1 GHz), 4G mobile telecommunication network and the development of systems that integrate these with mobile phones, newer design approaches for built in, multiband antennas for combined mobile system has been emerging. S-, C- and X- band which are studied in this work can find applications as is discussed below.

The current work originates from the need to develop microstrip antenna structures to operate in S-, C- and X- band for dual-frequency operation on a single plane with less design complexity and low profile. Also tuning of one or both the frequencies by varying just one design parameter can simplify design process to a great extent. Bandwidth enhancement is another design aspect that needs to be addressed while designing the antenna. The work emphasizes on size reduction, bandwidth enhancement and tuning of resonant frequencies.

S- Band communication (2.0 GHz to 4.0 GHz) is broadly used for weather radar, ship radar and some communication satellites. Other uses include digital cordless telephone, microwave ovens(2.495GHz or 2.450 GHz), Wi Max standards (2.595 GHz to 2.695GHz), consumer electronics including Bluetooth (2.402 GHz to 2.480 GHz) etc.

C- Band communication (4.0 GHz to 8.0 GHz) has wide applications ranges which cover satellite communication, cordless devices, commercial communication via satellite (uplink: 5.925 GHz - 6.425 GHz; downlink: 3.7 GHz -4.2 GHz), Wi-Fi devices including personal computers, video game console, smart phones, digital camera, tablet and weather RADAR systems to mention a few.



X- Band communication (8.0 GHz to 12.0 GHz) also covers wide range of applications which includes RADAR, terrestrial communications, space communications, and amateur radio (10 GHz -10.5 GHz). Other sub bands are used for civil and military applications, government institutions for weather monitoring, air traffic controls, defense technologies etc.

Microstrip patch antennas, which are popular antennas in wireless communication systems, have limiting narrow band response which limits its use in many applications. It is a challenge for antenna designers to modify the geometry of microstrip antenna to enhance its bandwidth without significant increase in mounting space requirements.

Compared to broadband antennas, reconfigurable antennas can offer advantages such as compact size with comparable radiation patterns and gain for designed frequency bands and frequency selectivity with requisite performance characteristics. In recent years, reconfigurable antennas have received significant attention for their applications in S-, C- and X- band communications band by adapting their properties to achieve selectivity in frequency, bandwidth, polarization and gain. Studies have been carried out by different researchers to demonstrate electronic tunability for different antenna structures which include use of varactor diodes, applications of electrically and magnetically tunable substrates with the use of barium strontium titanate and ferrite materials, slot loading, MEMS etc.

One of the design approaches involves drawing a slit parallel to the radiating edges. The structure is then modified by varying the slit lengths to less than the width of the patch width. The second structure is a profiled patch. Both the structures yield dual and multi band characteristics. Size reduction as much as 49% is achieved.

Bandwidth enhancement of up to 30% has been achieved with introduction of a pair of 100  $\mu\text{m}$  slits parallel to the radiating edges and equidistant from the two edges when the electrically isolated sections (due to the slits) were elevated with a slant angle from the plane of the patch. A large frequency envelope with at least -10 dB return loss in the range of 6.84 GHz to 9.24 GHz for elevation angle  $65^\circ$  extending from the C- on to the X- band. At the elevation angle  $85^\circ$ , the -10 dB bandwidth covers the frequency range from 8.45 GHz to 10.54 GHz with a bandwidth of 22%.

A patch geometry obtained by a notionally superposing a finite strip line section is designed for dual band operations. Tuning range from 2.04 GHz to 2.17 GHz and

and 4.83 GHz to 5.19 GHz is obtained for lower and upper frequencies with this oblique arm being rotated from 0° to 45° with respect to the radiating edge.

A spike edged rectangular patch antenna (SEMPA), where spike shaped triangular conductor sections are added to the rectangular patch at the radiating edges has been investigated for bandwidth enhancement. The number, position and dimensions of the spikes are varied to study the effect on resonant frequency. Dual band characteristics with almost the same return loss values are obtained for the modified structure. Two adjacent spikes has been bridged using a line section of 2 mm width resulting in a second resonance frequency of almost half of the first resonant frequency obtained without the bridge section. Shifting of this line section inwards (towards the main patch) results in increase of the upper resonant frequency and hence the bridge section can be adjusted to tune the frequency from 4.7 GHz to 5.27 GHz.

Design and testing of a reconfigurable patch antenna with a rectangular air pocket in the substrate layer between the patch and the ground is carried out for post fabrication tuning. A sliding section of the same material with the dimension of the air pocket is moved into the air pocket for tuning the resonant frequency. The approach for tuning the resonant frequency is simple and does not involve complicated and costly devices. The measured results indicate a frequency tuning from 3.25 GHz to 3.40 GHz. The structure can also possibly be improved by careful tailoring of the air pocket dimensions.

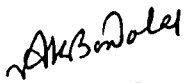
A PC controlled antenna measurement set up has been developed for measuring the antenna characteristics which include measurement for  $S_{11}$  parameter and radiation pattern measurements. All radiation pattern measurements are carried out using this developed setup.

## DECLARATION BY THE CANDIDATE

I hereby declare that the thesis “**Microstrip Patch Antennas- Some techniques on size reduction and tuning**”, submitted to **Department of Electronics and Communication Engineering, Tezpur University, Tezpur, Assam** in partial fulfillment for the award of the degree of Doctor of Philosophy in Electronics and Communication Engineering has not been previously considered for the award of any degree, diploma, associate ship, fellowship or any other similar title or recognition from any University, Institute or other organizations.

Date: 24.12.2013

Place: Tezpur

  
(Anup Kumar Bordoloi)

Enrollment No: ELP08101

Department of Electronics & Communication

School of Engineering

Tezpur University



**TEZPUR UNIVERSITY**  
(A Central University established by an Act of Parliament)  
**Napaam, Tezpur- 784028**  
**DISTRICT: SONITPUR:: ASSAM::INDIA**

Dr. S. Bhattacharyya, Ph.D. (University of Delhi)  
Professor

Phone: +91-3712-275255 (O)  
+91-9435381270 (M)  
Fax: +91-3712-267005/6 (O)  
Email: sb@tezu.emet.in

---

**CERTIFICATE OF THE PRINCIPAL SUPERVISOR**

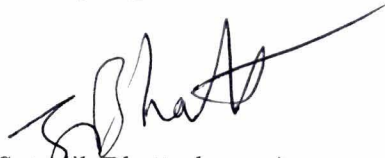
This is to certify that the work presented in the thesis entitled “**Microstrip Patch Antennas-Some techniques on size reduction and tuning**”, has been carried out by **Mr. Anup Kumar Bordoloi** under my supervision and guidance. The thesis embodies accounts of his own findings and these have not been submitted previously anywhere for the award of any degree either by him or by anyone else.

All help received from various sources have been duly acknowledged.

No part of this thesis has been submitted elsewhere for award of any degree.

Date: 24/12/2013

Place: Tezpur, Assam

  
(Satyajib Bhattacharyya)



**TEZPUR UNIVERSITY**  
(A Central University established by an Act of Parliament)  
**Napaam, Tezpur- 784028**  
**DISTRICT: SONITPUR::ASSAM:: INDIA**

Phone: +91-3712-275255(O)  
+91-9435381270 (M)

Fax: +91-3712-267005(O);  
Email: adm@tezu.ernet.in

---

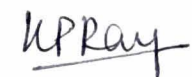
**Certificate of the External Examiner and ODEC**

This is to certify that the thesis entitled “**Microstrip patch antennas- some techniques on size reduction and tuning**” submitted by **Mr. Anup Kumar Bordoloi, Department of Electronics & Communication, School of Engineering** to Tezpur University in partial fulfillment for the award of the degree of **Doctor of Philosophy in Electronics & Communication** has been examined by us on December 12, 2014 and found to be satisfactory.

The committee recommends for the award of the degree of Doctor of Philosophy.

  
**Supervisor**

(Satyajib Bhattacharyya)

  
**External Examiner**

( Dr. K. P. Ray )

Date: 12/12/2014

Date: 12/12/2014

## ***Acknowledgements***

I would like to express my heartfelt gratitude to Prof. Satyajib Bhattacharyya, my research supervisor, for his guidance, valuable suggestions, untiring moral support and useful critiques of this research work.

I am grateful to Prof. J. C. Dutta, Head of the Department, Electronics & Communication Engineering, for his academic support and the facilities provided to carry out the research work.

I would like to thank Hon'ble Vice Chancellor of Tezpur University, Prof. Mihir Kanti Chaudhuri for giving encouragement and beneficial advice throughout my research work.

I sincerely thank Prof. Nidhi S. Bhattacharyya, Department of Physics, for her useful and constructive recommendations on my research work..

I specially thank Mr. Riku Chutia and Dr. Santanu Sharma, for guiding me in developing the measurement setup.

My thanks are due to Mr. Mantu Mali (Machine operator), Mitharam Handique (Central workshop), Khargeswar Rangpi (Central workshop) and B. Tech students, Nitesh, Anupam for their help in the accomplishment of the measurement setup.


I would like to extend my heartfelt thanks to my fellow co-worker in the microwave research group, Pranjali for his constant support and helping me throughout.

I thank all the research scholars of ECE Dept., Soma, Nilima, Shashi, Lachit, Champak, Nimisha, Bidyut and Aradhana for sharing a wonderful time during my research work.

Also I am thankful to my friends Subasit, Kunal, Debashis, Jyoti, Sikha, Pragyan, Arunav, Lutu, Anil, Azhar, Mayur, Rahul and Dushyanta for their well wishes.

My dear Maa, dada, baideu and bou, without your love, blessings and untiring help and support it would not have been possible to reach here. Words are not enough to express my gratitude towards you.

Above all, I feel grateful for the immense blessings of Almighty God in carrying out this research work and enabling me to its completion.

  
Anup Kumar Bordoloi

<b>Contents</b>	<b>Page no.</b>
<b>LIST OF FIGURES</b>	iv -xi
<b>LIST OF TABLES</b>	xii-xiii
<b>LIST OF SYMBOLS AND ABBREVIATION</b>	xiv-xvi
 <b>Chapter I</b>	
<b>Introduction to the Research Problem</b>	1
1.1 Introduction	2
1.2 Reported work on tuning and size reduction	5
1.2.1 <i>Tuning techniques</i>	5
1.2.2 <i>Size reduction techniques</i>	9
1.3 Motivation for the present work	11
1.4 Thesis outline	12
References	14-18
 <b>Chapter II</b>	
<b>Measurement Setup Integration</b>	19
2.1 Introduction	20
2.2 Measurement setup	20
2.2.1 <i>Return loss measurement setup</i>	20
2.2.2 <i>PC controlled radiation pattern measurement set- up</i>	21
2.2.3 <i>Antenna mounting system design</i>	25
2.3 Interfacing	26
2.4 Algorithm and interfacing	27
2.5 Results	29
2.6 Chapter summary	30-31
 <b>Chapter III</b>	
<b>Planar and Elevated Microstrip Patch Antenna with Slits</b>	32
3.1 Introduction	33
3.2 Planar patch prior to introduction of slits	34
3.3 Simulation for feed point and slit widths	39
3.4 Fabrication of patch with slits	43
3.5 Measured results	46
3.6 Patch with single partial slit	48
3.6.1 <i>Measured return loss for patch with varying slit length</i>	49
3.6.2 <i>Radiation pattern measurement for patch different slit length</i>	52

<b>Contents</b>	<b>Page no.</b>
<b>3.7 Patch with slit isolated elevated sections</b>	<b>58</b>
<b>3.7.1 Design and fabrication of elevated patch antenna with slits</b>	<b>59</b>
<b>3.7.2 Return loss measurement of simple patch antenna</b>	<b>63</b>
<b>3.7.3 Return loss measurement of elevated patch antenna</b>	<b>64</b>
<b>3.7.4 Radiation pattern measurements of profiled patch antenna</b>	<b>66</b>
<b>3.8 Chapter Summary</b>	<b>71-72</b>
References	<b>73</b>
 <b>Chapter IV</b>	
<b>Microstrip Patch Antenna with Notionally Superposed Microstrip Line</b>	<b>74</b>
<b>4.1 Introduction</b>	<b>75</b>
<b>4.2 Design of patch with asymmetrically superposed strip line section</b>	<b>75</b>
<b>4.2.1 Feed point location</b>	<b>75</b>
<b>4.3 Antenna performance studies with varying strip line width and tilt angle</b>	<b>78</b>
<b>4.3.1 Variation of strip line width and its effect on RL performance</b>	<b>78</b>
<b>4.3.2 Variation of tilting angle and its effect on RL performance</b>	<b>82</b>
<b>4.3.3 Variation of tilt angle and its effect on antenna size</b>	<b>86</b>
<b>4.4 Measured results</b>	<b>88</b>
<b>4.4.1 Return loss measurements of simple and modified patch with the strip line</b>	<b>89</b>
<b>4.5 Comparison of measured and simulated results</b>	<b>93</b>
<b>4.5.1 Return loss performance</b>	<b>93</b>
<b>4.5.2 Antenna size reduction</b>	<b>102</b>
<b>4.6 Radiation pattern measurements of modified patch with tilted superposed strip line section</b>	<b>103</b>
<b>4.7 Chapter summary</b>	<b>109-110</b>
References	<b>111</b>
 <b>Chapter V</b>	
<b>Spike edged Rectangular patch antenna</b>	<b>112</b>
<b>5.1 Introduction</b>	<b>113</b>
<b>5.2 Design of patch with number spike section on radiating edges</b>	<b>113</b>
<b>5.2.1 Feed point Location</b>	<b>113</b>
<b>5.3 Simulated antenna performance studies with spikes at radiating edges</b>	<b>116</b>
<b>5.3.1 Return loss performance of patch with six spikes on each edge</b>	<b>117</b>
<b>5.4 Measured results</b>	<b>120</b>
<b>5.4.1 Return loss measurement of simple patch</b>	<b>121</b>
<b>5.4.2 Return loss measurements of modified patch with spikes</b>	<b>121</b>



<b>Contents</b>	<b>Page no.</b>
5.5 Radiation pattern measurement of SEMPA and SEMPA with strip line	126
5.6 Chapter summary	129-130
References	131
 <b>Chapter VI</b>	
<b>Microstrip patch antenna with substrate pocket</b>	132
6.1 Introduction	133
6.2 Design and fabrication of patch with air pocket underneath the patch (Prototype 1)	133
6.2.1 <i>Return loss measurements of patch with substrate pocket and plunger (Prototype 1)</i>	136
6.3 Design and fabrication of patch with air pocket underneath the patch (Prototype 2)	138
6.3.1 <i>Return loss measurement of patch with substrate pocket and plunger (Prototype 2)</i>	141
6.4 Chapter summary	143-144
References	145
 <b>Chapter VII</b>	
<b>Conclusion and future work</b>	146
7.1 Conclusion	147
7.2 Future work	149
<b>Publications</b>	158
<b>Appendices A</b>	

## **List of figures**

<b>Figure no.</b>	<b>Figure Caption</b>	<b>Page no.</b>
<b>Chapter -II</b>		
2.1	Coaxial Dual-Directional Coupler (11692D)	22
2.2	Block diagram of test set up for measurement of $S_{11}$ parameter	22
2.3	Schematic diagram of set up for antenna radiation pattern	23
2.4	Stepper motor drive circuit	25
2.5	Antenna Mount designed for antenna pattern measurement	26
2.6	Photograph of the measurement system	27
2.7	Flowchart for data acquisition of power (dB) vs. angle of rotation ( $\theta$ )	28
2.8	Measurement of received power vs. angle for antenna under test	29
<b>Chapter -III</b>		
3.1	Coaxially fed rectangular patch antenna (a) Top view (b) Side view (c) Coordinate system	34
3.2	Rectangular microstrip patch antenna in the $TM_{10}$ mode (a) E-field distribution (b) Voltage and current variation (c) Radiating slots of RMSA (d) Equivalent transmission line model	35
3.3	Simulated plot of return loss vs. feed point location (at 4.2 GHz)	39
3.4	Simulated plot of VSWR vs. feed point location	40
3.5	Simulated plot of impedance (real part) vs. feed point location	40
3.6	Simulated plot of smith chart at 4.2 GHz for frequency sweep 2-6 GHz	41
3.7	Simulated plot of slit width variation vs. shift in resonant frequency (a) 1 -100 $\mu\text{m}$ (b) 10-100 $\mu\text{m}$	42
3.8	(a) Planar RMSA (b) Planar RMSA with double slit (c) Planar RMSA with single slit ( $\ell_s = 2.5 \text{ mm}$ ) near to the feed point (d) Planar RMSA with single slit ( $\ell_s = 2.5 \text{ mm}$ ) further from the feed point	44

### List of figures (contd.)

Figure no.	Figure Caption	Page no.
3.9	Return loss vs. resonant frequency for RMSA (feed point at 2.5 mm from patch centre)	46
3.10	Return loss vs. frequency for simple patch and patch with slits	47
3.11	Measured return loss vs. resonant frequency for simple patch and patch with single slit	48
3.12	(a) Patch antenna with partial slit [table 3.4 (a)] (b) Fabricated patch antenna with partial slit	49
3.13	Measured return loss vs. frequency for different slit lengths(s)	49
3.14	Slit length vs. resonant frequency (measured)	50
3.15	Measured return loss plot for different slit length (lower resonant frequencies)	51
3.16	Measured return loss plot for different slit length (upper resonant frequencies)	51
3.17	Measured radiation pattern of simple patch at 4.25 GHz (a) E- plane (b) H- plane	53
3.18	Measured radiation pattern of patch with slit ( $s = W$ ) at 2.17 GHz (a) E- plane (b) H- plane	53
3.19	Measured radiation pattern of patch with slit ( $s = W$ ) at 4.86 GHz (a) E- plane (b) H- plane	54
3.20	Measured radiation pattern of patch with slit ( $s = 16$ ) at 2.33GHz (a) E- plane (b) H- plane	54
3.21	Measured radiation pattern of patch with slit ( $s = 16$ ) at 5.11GHz (a) E- plane (b) H- plane	54
3.22	Measured radiation pattern of patch with slit ( $s = 13$ ) at 2.78 GHz (a) E- plane (b) H- plane	55
3.23	Measured radiation pattern of patch with slit ( $s = 13$ ) at 5.04 GHz (a) E- plane (b) H- plane	55
3.24	Measured radiation pattern of patch with slit ( $s = 14$ ) at 2.49 GHz (a) E- plane (b) H- plane	55
3.25	Measured radiation pattern of patch with slit ( $s = 14$ ) at 4.98 GHz (a) E- plane (b) H- plane	56
3.26	Measured radiation pattern of patch with slit ( $s = 15$ ) at 2.56 GHz (a) E- plane (b) H- plane	56
3.27	Measured radiation pattern of patch with slit ( $s = 15$ ) at 4.90 GHz (a) E -plane (b) H -plane	56

### List of figures (contd.)

Figure no.	Figure Caption	Page no.
3.28	Measured directivity vs. slit length (s) for E- and H- plane	58
3.29	Measured directivity vs. slit length (s) for E- and H- plane	58
3.30	Microstrip patch antenna with slits (a) Planar conventional structure with slits (top and side view) (b) Structure with slits and elevated sections (oblique side view) (c) Fabricated profiled antenna with slits (top and oblique view)	60
3.31	(a) Planar conventional structure without slits (top and side view) (b) Fabricated central conductor (top view)	62
3.32	(a) Miter saw with single sided copper laminated substrate sample (b) Fabricated elevated substrate section ( $\theta_e = 45^\circ$ )	62
3.33	(a) Isolated substrate section before adding to elevated patch section (b) Fabricated elevated section before addition ( $\theta_e = 45^\circ$ ) (c) Isolated substrate section added to elevated patch section	62 63 63
3.34	Return loss vs. frequency of simple patch antenna (resonant frequency = 4.42 GHz)	63
3.35	Measured return loss plot for patch with different $\theta_e$ (a) $\theta_e = 0^\circ, 45^\circ, 50^\circ, 55^\circ, 65^\circ, 70^\circ, 75^\circ, 85^\circ$ (b) $\theta_e = 0^\circ, 65^\circ, 85^\circ$	64
3.36	Measured plot for two best return loss values (at $f_L$ and $f_U$ ) vs. angle of elevation ( $\theta_e$ )	66
3.37	Measured radiation pattern for simple patch at 4.42 GHz (a) E - plane (b) H - plane	66
3.38	Measured radiation pattern for patch with slits ( $\theta_e = 0^\circ$ ) at 7.53 GHz (a) E - plane (b) H - plane	67
3.39	Measured radiation pattern for patch with slits ( $\theta_e = 0^\circ$ ) at 8.43 GHz (a) E - plane (b) H - plane	67
3.40	Measured radiation pattern of patch with slits ( $\theta_e = 65^\circ$ ) at 4.04 GHz (a) E - plane (b) H - plane 4	68
3.41	Measured radiation pattern of patch with slits ( $\theta_e = 65^\circ$ ) at 8.83 GHz (a) E - plane (b) H - plane	68
3.42	Measured radiation pattern of patch with slits ( $\theta_e = 85^\circ$ ) at 4.23 GHz (a) E - plane (b) H - plane	68
3.43	Measured radiation pattern of patch with slits ( $\theta_e = 85^\circ$ ) at 10.26 GHz (a) E - plane (b) H - plane	69

### List of figures (contd.)

Figure no.	Figure Caption	Page no.
3.44	Measured directivity vs. angle of elevation ( $\theta_e$ ) for E- plane	70
3.45	Measured directivity vs. angle of elevation ( $\theta_e$ ) for E- and H- plane	71
<b>Chapter -IV</b>		
4.1	(a) Dimension for simple patch resonating at 4.55 GHz (CST Microwave Studio) (b) Simple patch shown with notionally superposed strip line section (Dimensions are given in table 4.2) (c) Actual modified patch geometry	76
4.2	Simulated return loss vs. feed point location (from patch centre)	77
4.3	Simulated plot of impedance ( $\Omega$ ) vs. feed point location	77
4.4	Simulated plot of VSWR vs. feed point location	78
4.5	Variation of RL value with strip line for $\theta_t = 10^\circ$	79
4.6	Variation of RL value with strip line for $\theta_t = 20^\circ$	79
4.7	Variation of RL value with strip line for $\theta_t = 30^\circ$	80
4.8	Variation of RL value with strip line for $\theta_t = 40^\circ$	81
4.9	Variation of RL value with strip line for $\theta_t = 45^\circ$ (resonant frequency shown in brackets)	82
4.10	Variation of RL value with tilt angle ( $\theta_t$ ) for strip line $w = 1$ mm	82
4.11	Variation of RL value with tilt angle ( $\theta_t$ ) for strip line $w = 2$ mm	83
4.12	Variation of RL value with tilt angle ( $\theta_t$ ) for strip line $w = 3$ mm	83
4.13	Variation of RL value with tilt angle ( $\theta_t$ ) for strip line $w = 4$ mm	84
4.14	Variation of RL value with tilt angle ( $\theta_t$ ) for strip line $w = 5$ mm	84
4.15	(a) 3-D plot of return loss as a function of $\theta_t$ and $w$ (simulated) for lower and upper resonant frequency (b) 3-D plot of resonant frequency as a function of $\theta_t$ and $w$ (simulated) for lower and upper resonant frequency	86
4.16	Size reduction (%) for different strip line width ( $w$ ) for varied tilt angle ( $\theta_t$ )	87
4.17	(a) Fabricated simple patch designed at 4.75 GHz (b) One of the fabricated patch antenna with superposed strip line ( $\theta_t = 40^\circ$ )	88
4.18	Measured and simulated return loss plot for the simple patch	89

### List of figures (contd.)

Figure no.	Figure Caption	Page no.
4.19	Measured return loss plot for different values of tilt angle, $\theta_t$ (both LRF and URF)	90
4.20	Measured return loss plot for different values of tilt angle, $\theta_t$ for lower resonant frequency	90
4.21	Measured return loss plot for different values of tilt angle, $\theta_t$ for upper resonant frequency	91
4.22	Variation of resonant frequency with different tilt angle ( $\theta_t$ )	93
4.23	Return loss vs. frequency for $\theta_t = 10^\circ$ (lower resonant frequency)	94
4.24	Return loss vs. frequency for $\theta_t = 10^\circ$ (upper resonant frequency)	94
4.25	Return loss vs. frequency for $\theta_t = 20^\circ$ (lower resonant frequency)	95
4.26	Return loss vs. frequency for $\theta_t = 20^\circ$ (upper resonant frequency)	95
4.27	Return loss vs. frequency for $\theta_t = 30^\circ$ (lower resonant frequency)	96
4.28	Return loss vs. frequency for $\theta_t = 30^\circ$ (upper resonant frequency)	96
4.29	Return loss vs. frequency for $\theta_t = 40^\circ$ (lower resonant frequency)	97
4.30	Return loss vs. frequency for $\theta_t = 40^\circ$ (upper resonant frequency)	97
4.31	Return loss vs. frequency for $\theta_t = 45^\circ$ (lower resonant frequency)	98
4.32	Return loss vs. frequency for $\theta_t = 45^\circ$ (upper resonant frequency)	98
4.33	Comparison plot of return loss values with tilt angle $\theta_t$ for lower resonant frequency	99
4.34	Comparison plot of return loss values with tilt angle $\theta_t$ for upper resonant frequency	100
4.35	Measured and simulated values of the lower resonant frequency as a function of tilt angle ( $\theta_t$ )	101
4.36	Measured and simulated values of the upper resonant frequency as a function of tilt angle ( $\theta_t$ )	101
4.37	Comparison plot showing the reduction in size with different tilt angle ( $\theta_t$ )	102
4.38	Measured radiation patterns of simple rectangular patch at 4.75 GHz (a) E- plane      (b) H- plane	103
4.39	Measured radiation patterns of patch with $\theta_t = 10^\circ$ at 2.17 GHz (a) E- plane      (b) H- plane	104
4.40	Measured radiation patterns of patch with $\theta_t = 10^\circ$ at 5.19 GHz (a) E- plane      (b) H- plane	104

### List of figures (contd.)

Figure no.	Figure Caption	Page no.
4.41	Measured radiation patterns of patch with $\theta_t = 20^\circ$ at 2.13 GHz (a) E- plane (b) H- plane	104
4.42	Measured radiation patterns of patch with $\theta_t = 20^\circ$ at 5.09 GHz (a) E- plane (b) H- plane	105
4.43	Measured radiation patterns of patch with $\theta_t = 30^\circ$ at 2.08 GHz (a) E- plane (b) H- plane	105
4.44	Measured radiation patterns of patch with $\theta_t = 30^\circ$ at 4.83 GHz (a) E- plane (b) H- plane	105
4.45	Measured radiation patterns of patch with $\theta_t = 40^\circ$ at 2.17 GHz (a) E- plane (b) H- plane	106
4.46	Measured radiation patterns of patch with $\theta_t = 40^\circ$ at 5.05 GHz (a) E- plane (b) H- plane	106
4.47	Measured radiation patterns of patch with $\theta_t = 45^\circ$ at 2.04 GHz (a) E- plane (b) H- plane	107
4.48	Measured radiation patterns of patch with $\theta_t = 45^\circ$ at 5.01 GHz (a) E- plane (b) H- plane	107
4.49	Measured directivity vs. tilt angle ( $\theta_t$ ) for E- plane	108
4.50	Measured directivity vs. tilt angle ( $\theta_t$ ) for H- plane	109

### Chapter -V

5.1	Simple square patch resonating at 4.40 GHz (CST Microwave Studio)	114
5.2	Simulated return loss vs. feed point distance from patch centre	114
5.3	Simulated plot of impedance ( $\Omega$ ) vs. feed point location	115
5.4	Simulated plot of VSWR vs. feed point location	115
5.5	Patch structure with spikes at radiating edges	116
5.6	Simulated return loss plots for feed points at 7 mm and 9.5 mm from patch centre	117
5.7	Patch structure with alternate spikes at symmetric positions	118
5.8	(a) Simulated return loss plots for patch with 12 and 6 symmetrically placed spikes (p=9.5 mm)	118
	(b) Simulated return loss plots for patch with 12 and 6 asymmetrically placed spikes (p=9.5 mm)	119

## List of figures (contd.)

Figure no.	Figure Caption	Page no.
5.10	Simulated return loss for simple patch and modified geometries	120
5.11	(a) Fabricated simple patch (b) Fabricated patch antenna with spikes	121
5.12	Simulated RL plot ( $p=9.5$ mm)	121
5.13	Return loss plot for simple patch and SEMPA	122
5.14	(a) SEMPA with strip line connecting 2 spike vertices (b) SEMPA with strip line connecting 3 spike vertices	123
5.15	(a) Return loss plots for SEMPA with line connecting two outer spike vertices [figure 5.14 (a)] (b) Return loss plots for SEMPA with line connecting three outer spike vertices [figure 5.14 (b)]	123 124
	(c) Return loss plots for figures 5.14 (a) and 5.14 (b)	124
5.16	(a) SEMPA geometry with strip line showing shifting of the strip line (b) Fabricated SEMPA with single strip ( $d=1$ mm)	125
5.17	Return loss plots for SEMPA with strip line at 3 different positions	126
5.18	Measured radiation pattern of SEMPA at 4.67 GHz (a) E - plane (b) H- plane	126
5.19	Measured radiation pattern of SEMPA at 5.09 GHz (a) E - plane (b) H-plane	127
5.20	Measured radiation pattern at 4.79 GHz of SEMPA with strip line connecting 2 vertices (a) E - plane (b) H - plane	127
5.21	Measured radiation pattern at 4.89 GHz of SEMPA with strip line connecting 3 spike vertices (a) E - plane (b) H - plane	127
5.22	Measured radiation pattern at 5.40 GHz of SEMPA with strip line connecting 3 spike vertices (a) E - plane (b) H - plane	128
5.23	Measured radiation pattern at 5.40 GHz of SEMPA with strip line connecting 3 spike vertices (a) E - plane (b) H - plane	128

## Chapter -VI

6.1	Antenna geometry demarcating assembled segments (a) End view looking into air pocket (b) Top view (c) Plunger dimension	135
-----	--	-----



### List of figures (contd.)

<b>Figure no.</b>	<b>Figure Caption</b>	<b>Page no.</b>
<b>6.2</b>	(a) Fabricated patch with air pocket beneath the patch (b) Fabricated patch with plunger section inserted into the air Pocket	136
<b>6.3</b>	Measured return loss plot for patch with different dielectric section (%) below the patch	137
<b>6.4</b>	Shift in resonant frequency with different air pocket beneath the patch	138
<b>6.5</b>	(a) Single side copper clad substrate showing region to be machined out (end view) (b) Copper clad substrate after machining of region R (end view) (c) Patch on substrate after etching (end view) (d) Patch on substrate with ground plane introduced (end view) (e) Top view of the antenna structure (f) Plunger dimensions	139
<b>6.6</b>	Picture showing the process of preparing patch with milled away section	140
<b>6.7</b>	(a) Fabricated patch structure with air pocket (oblique end view) (b) Fabricated patch and plunger section	141
<b>6.8</b>	Measured return loss plot for patch with different dielectric section (%) below the patch	142
<b>6.9</b>	Measured return loss for patch with different air pocket dimension at the respective resonant frequencies	142
<b>6.10</b>	Measured resonant frequency vs. different air pocket dimension	143

## **List of tables**

<b>Table no.</b>	<b>Table Caption</b>	<b>Page no.</b>
<b>Chapter –II</b>		
2.1	Specifications of Dual Directional Coupler (DDC)	21
2.2	Specification of the stepper motor	23
2.3	LPT1 pin configuration	24
2.4	Performance evaluation of automated set-up	30
<b>Chapter –III</b>		
3.1	(a) Slit width variation (1-10 $\mu\text{m}$ ) (b) Slit width variation (0-100 $\mu\text{m}$ )	43
3.2	Design parameter of RMSA	45
3.3	Fabricated slit width measurement using travelling microscope	46
3.4	(a) Variation of resonant frequencies and RL with different slit lengths(s) (b) Antenna size reduction corresponding to LRF for different slit lengths(s)	52
3.5	Measured directivity with different slit lengths (s)	57
3.6	Design specification of profiled RMSA	61
3.7	Resonant frequency and return loss for different elevation angles ( $\theta_e$ )	65
3.8	Best bandwidth enhancement for two specific elevation angles	65
3.9	Measured directivity for two frequencies ( $f_L$ and $f_U$ ) with best return loss values	70
<b>Chapter –IV</b>		
4.1	Size reduction for strip line width w of 4 mm	87
4.2	Specifications of RMSA and strip line [in reference to figure 4.1 (b)]	88
4.3	Variation of resonant frequencies and return loss with different tilt angle ( $\theta_t$ )	92
4.4	Size reduction with different angle of rotation ( $\theta_r$ )	92
4.5	Resonant frequencies for different tilt angles ( $\theta_t$ )	100

<b>List of tables (contd.)</b>		<b>Page no.</b>
<b>Table no.</b>	<b>Table Caption</b>	
		102
4.6	Resonant frequency difference between measured and simulated values	108
4.7	Measured directivity for different tilt angles ( $\theta_t$ ) of the strip line section	
 <b>Chapter -V</b>		
5.1	Design parameters of the spike edged patch	116
5.2	Design parameter of MPA with spikes	120
5.3	Variation of resonant frequency and return loss of the modified SEMPA	125
5.4	Resonant frequencies and RL values of SEMPA with strip line positions	126
5.5	Measured directivity with SEMPA and SEMPA with strip line	129
 <b>Chapter -VI</b>		
6.1	Specifications for the patch and assembled segments	134
6.2	Resonant frequency with position of plunger	136
6.3	Specifications for the patch with air pocket	138
6.4	Resonant frequency with plunger end position	141

## List of symbols and abbreviations

WLAN	Wireless Local Area Network
LAN	Local Area Network
FDTD	Finite Difference Time Domain
GHz	Giga Hertz
KHz	Kilo-Hertz
UWB	Ultra Wide Band
MEMS	Micro Electro Mechanical Switch
AMC	Artificial Magnetic Conductor
FSS	Frequency Selective Surface
$\mu$ s	Micro Second
RF	Radio Frequency
dB	Decibel
PIFA	Printed Inverted F Antenna
dBi	Decibels relative to an isotropic antenna gain
UMTS	Universal Mobile Telecommunication System
PIL	Planar Inverted-L
CSRR	Complementary Split Ring Resonator
TM	Transverse Magnetic
VSWR	Voltage Standing Wave Ratio
MWS	Mobile Wireless Systems
DBS	Direct Broad Cast Satellites
BW	Band Width
CST	Computer Simulated Technology
SEMPA	Spike Edged Microstrip Patch Antenna
MHz	Mega Hertz

SCPI	Standard Commands for Programmable Instruments
dBm	Decibel-mill watt
GPIO	General Purpose Interface Bus
DALN	Displayed Average Noise Levels
VBW	Video Bandwidth
ACLR	Residual Adjacent Channel Leakage Ratio
EVM	Residual Error Voltage Magnitude
DDC	Dual Directional Coupler
VISA	Virtual Instrument Software Architecture
MOSFETS	Metal Oxide Semiconductor Field Effect Transistor
MPA	Microstrip Patch Antennas
RL	Return Loss
LRF	Lower Resonance Frequency
URF	Upper Resonance Frequency
RMSA	Rectangular Microstrip Antenna
$\epsilon_{reff}$	Effective Dielectric Constant
$\lambda_0$	Free Space Wavelength
TLM	Transmission Line Model
h	Height
$L_e$	Effective Length
$W_e$	Effective Width
E	Electric Field Vector
$f_0$	Resonance Frequency
$G_m$	Mutual Conductance
H	Magnetic Field Vector
$\theta_e$	Elevated Angle

$\epsilon_r$	Relative Permittivity
$\lambda$	Wavelength
$f_r$	Resonance Frequency
kg	Kilogram

# CHAPTER I

## INTRODUCTION TO THE RESEARCH PROBLEM

---

### 1.1 Introduction

### 1.2 Literature on tuning and size reduction

#### *1.2.1 Tuning techniques*

#### *1.2.2 Size reduction techniques*

### 1.3 Motivation and Importance of the work

### 1.4 Thesis Outline

### References

## 1.1 Introduction

Mobile and handheld wireless technology, in the contemporary global scenario, has become ubiquitous to say the least. In particular the field of RF wireless communication is experiencing unprecedented technological advancements and market growth, spurred by the rapid increase in the use of cellular telephony, mobile data and wireless local area network (WLAN) as well as satellite communication [1 - 5]. This growth is only but likely to proliferate in the near future as widespread deployment of wireless networks are revolutionizing the concept of communication and information processing of business, professional and private applications. Furthermore, military agencies deploy high end wireless devices for use in tactical environment including portable devices providing extensive computational powers for soldiers. In this backdrop, it is only but obvious that the world of communication is bound to experience an ever increasing momentum in development of wireless networks and related fields replacing its erstwhile counterpart of wired technology which was the backbone of communication technology until very recently. In this wireless era, the antenna, which acts as the frontends at the transmitting and receiving sides is a critical component.

The device at the transmitting end which launches the signal into free space and at the receiving end which receives the transmitted signals, i.e. the antennas, must have characteristics that conform to the specific requirements of the system. Characteristics of antennas are, therefore, of prime importance in deciding the overall performance of any communication system.

In the microwave region, because of the wavelengths involved, antennas can be designed within a practical size while catering to the performance requirements of a system. In addition, a channel in this frequency range occupying a fixed percentage bandwidth can carry far more data than in the lower frequency range. As a consequence, most long and short range RF wireless communication links operate in this frequency range although higher frequencies are also used nowadays having larger channel capacity.

There are two major aspects that need to be addressed while designing an antenna. First, the bandwidth over which its desired characteristics remain within an acceptable range. This requirement becomes all the more significant in view of the present day broadband and multichannel systems. Multi frequency antenna, on the other hand, can operate at a number of desired frequencies rather than over the whole frequency range, for which it is more difficult to design the antenna with the given characteristics. These



can also eliminate the need for additional space for mounting a number of antennas for different frequencies. Secondly, the shape of the radiation pattern that will determine what part of the total power will be radiated and received in the desired direction. For instance, highly directional radiation patterns with sharp pencil beam can be useful in establishing point to point links and therefore the same frequency can be used at adjacent locations to establish another link, obviating the requirement for additional frequency bands. This also reduces the total power required to be transmitted to establish the link. Another example of shaped beam antennas are the satellite DTH antennas with beam shape designed for particular intended area of coverage, known as the footprint.

Microstrip antennas are well suited for mobile or radio communications, military applications and applications involving aircraft and space craft, where small size, light weight and low profile is a necessity [6 - 15]. Microstrip antennas are also preferred for wireless LAN systems due to their versatility, conformability, mechanical ruggedness, low cost and low sensitivity to manufacturing tolerances. Many of the antenna applications for satellite links, mobile communications, wireless local area networks etc. require broadband, dual/multi frequency operation, frequency agility and polarization control. These can be achieved by suitably loading the simple microstrip antenna and altering the basic antenna structure by introducing slots, structural modifications etc. [16 - 17].

Microstrip antennas began gaining prominence from the year 1970, although the idea of microstrip antenna is reported in the literature way back in 1953 by G.A. Deschamps [18] and was first patented by H. Gutton and G. Bassinot in 1955 [19]. In the years that followed, microstrip antennas received significant attention of the research community and work on different patch configurations, array designs as well as patches with different loading are reported in the literature [20 - 23]. Modelling of antennas for design and analysis has also seen continued development alongside [24 - 27].

The inherent limitation of narrow bandwidth in patch antenna requires to be enhanced for many practical applications, posing a challenge for designers. As a consequence, increasing the bandwidth of microstrip patch antennas has been a major thrust area of research. Some of the approaches for broadband techniques are: (i) lowering the value of  $Q$  which involves selection of different radiator shapes, increasing the substrate thickness and using substrates with lower dielectric constant, (ii) using impedance matching techniques which include inserting matching networks, adding tuning elements, slotting and notching of patches, use of aperture and proximity

coupling (iii) introducing multiple resonators which include use of parasitic (stacked or coplanar) elements in combination with (i) and (ii) [28 - 33].

Another limitation is its inherently low power handling capability which is a constraint for use in the transmitting mode. Various techniques, including use of arrays, are employed to overcome this. Surface wave propagation is another limiting factor affecting efficiency, which increases with increase in frequency and cross-coupling among others. Techniques such as use of photonic band gap structures, which are obtained by periodic loading of the substrate, are generally used to suppress this unwanted propagation within the antenna structure [34 - 36].

Size reduction and bandwidth enhancement are also becoming major design considerations for practical applications. Application in present day mobile communication requires smaller antenna size for mobile handheld devices. For this reason, there has been great emphasis on achieving compact and broad band operations of microstrip antennas. With the introduction of new mobile wireless systems such as WiMax 2400 (2595 - 2690 MHz), Wi-Fi (2400 - 2483.5 MHz), WCDMA in 3G mobile telecommunication network etc., a notable change in antenna design approaches has come about. Significant progress in the design of compact microstrip antenna with broad band, dual band-frequency, dual-polarized, circularly polarized and gain enhanced operations has been reported [37 - 42].

The feeding mechanism is another important design consideration for antenna performance characteristics. The microstrip antennas can be excited directly either by a coaxial probe or by a microstrip line. It can be also excited indirectly using electromagnetic coupling, aperture coupling and a coplanar wave guide feed with no direct electrical contact between the feed line and patch. Aperture coupling is often chosen by designers as this type of feed arrangement allows physical separation of the two functions, antenna excitation and radiation, and the freedom to use optimal substrates for radiator and transmission line [43 - 45].

The development of complex antenna structures using inhomogeneous dielectric material, multilayered dielectric structures, periodic loading of the substrate to suppress surface waves, aperture coupling of the feed to the antenna, use of staked configuration to achieve larger bandwidth, loading of the antenna to improve characteristics and integration of the circuit functions to antenna functions has ushered in the development of various modelling and numerical techniques for these complex structures. These include full wave techniques such as the integral equation approach and FDTD technique. Many

commercial softwares such as CST Microwave Studio, HFSS, IE3D which are based on numerical methods such as MoM, FEM are nowadays available for computation of antenna performance. These are widely used by researchers and designers for validation of experimental results as well as for pre fabrication evaluation of proposed antenna performance.

## 1.2 Literature on tuning and size reduction

A detailed survey of contemporary literature on microstrip antenna research and the aspects that require attention vis-a-vis their current applications in communication has been carried out. It is with this basis and background that the two aspects as mentioned earlier have been taken up for study in the present work.

### 1.2.1 Tuning techniques

Iskandar Fitri et al. proposed a compact microstrip slot antenna fed by a microstrip line with multi tuning stubs for UWB applications [46]. They reported an acceptable impedance match in the frequency ranges of 1.3 GHz to 5.1 GHz for single antenna element and 1.1 GHz to 6.4 GHz for stub array composed of two antenna elements. Matching condition can be controlled by tuning the stubs under the slot and shorting the tuning stub connected in shunt for bandwidth enhancement. This technique can be used in antenna array for further enhancement of bandwidth. The technique is complex requiring adjustment of many parameters of the tuning arms.

H.K. Ng et al. proposed frequency tuning of a the dielectric resonator antenna using loading cap [47]. Tuning of resonant frequency can be achieved by changing the radius of the loading cap. Exciting the dielectric resonator antenna with its fundamental  $TE_{111}$  mode by a coupling aperture need very careful adjustment as a small parametric variation can generate higher order modes.

J.A Tirado- Mendez et al. reported an alternative to the commonly used tuning techniques such as use of stubs, posts, variable air gap etc. by applying defected microstrip structure in tuning a square patch antenna [48]. Poor matching and lower gain issues are to be tackled in this technique.

P. Blondy et al. developed a wide tuning range MEMS switched patch antenna [49]. The antenna operates at 23.8 GHz without bias and 12.4 GHz with an applied bias of 150 V.

J. Ollikainen et al. proposed a thin dual resonant stacked shorted patch antenna for mobile communications [50]. The antenna was designed with a bandwidth of 10%

necessary for GSM 1800 or GSM 1900 applications. The structure needs a controlled coupling between the driven patch and parasitic patch for impedance bandwidth.

P.J. Rainville et al. fabricated a microstrip patch antenna on a ferrite film which can be tuned by applying a magnetic field bias [51]. The radiation polarization can be varied by application of small in-plane magnetic bias field.

A tunable bow tie radiating element mounted above an artificial magnetic conductor (AMC) with a geometry consisting of a frequency selective surface (FSS) was presented by Fabio Michele Valeri [41]. The FSS was designed on a thin grounded dielectric slab where chip-set varactor diodes were placed between metallic elements and the backing plane through vias. The antenna was tuned over the S-band by varying capacitances through an appropriate voltage. The technique needs larger volume and external voltage source.

A wideband bow-tie slot antenna with tuning stubs was reported by Abdelnasser et al. [52]. Many of the antenna parameters such as width and height of bow tie slot, width of the stub, inner and outer heights of the metal stub, inner slot height were adjusted to improve the bandwidth up to 88% for a centre frequency of 10.0 GHz with a gain of approximately 6.7 dB. The technique involves many tuning parameters in achieving the requisite gain over the operating frequency range.

Peroulis et al. reported a reconfigurable slot antenna which was compact, efficient and electronically tunable [53]. Tuning is realized by changing its effective length, controlled by the bias voltages of solid state shunt switches. An effective bandwidth of 1.7:1 was obtained by using this tuning method without the need for any other additional matching network.

A compact multi-band antenna with broad individual bands consisting of semi-disk radiating elements was presented by Pouhe et al. [54]. Using angular displacement of probe position, operation in the frequency range from 1.71 GHz to 2.55 GHz for 3G mobile communications and in the C-band from 3.78 GHz to 4.38 GHz for satellite TV communication were obtained. The structure is sensitive to off-set positioning of the probe feed leading of excitation of higher order modes.

Sylvain Loizeau et al. presented a reconfigurable antenna with a low tuning range and with an additionally switchable UWB [55]. Two types of reconfigurability components were used; PIN diode for enabling discrete configuration change and a varicap diode which allows continuous tuning of the resonant frequency. Loading extra components poses matching issues in addition to a large volume for integration.

P. Rocc et al. reported synthesis of a quad-band patch antenna [56]. The shape modification was evolved based on fractal-shaped erosion strategy. The antenna was designed to meet the requirements for Galileo frequency bands  $E_5$  and  $L_1$  ( $f_{E5} = 1191.795$  MHz,  $f_{L1} = 1575.42$  MHz) and Wi-Max frequency bands ( $f_{WM1} = 2.5$  GHz and  $f_{WM2} = 2.5$  GHz).

A dual band antenna, using two stacked shorted patches for applications in the GSM 1800 and GSM 1900 cellular system handsets for increased bandwidth has been presented by Gwo -Yun Lee et al. [57]. Two resonant frequencies close to each other were obtained by adjustment of lengths of the stacked shorted patches although the length adjustments affect radiation pattern and the stacked configuration need reasonable precision in packaging for specific application requirements.

A technique for obtaining dual-band operation using a reconfigurable slot antenna has been reported by Nader Behdad et al. [58]. Frequency ratio achieved for the design ranges from  $1.3 \leq f_R \leq 2.67$  by changing dc bias voltages of its two varactors in the range of 0.5 V to 30.0 V. This type of antenna needs simultaneous matching at both bands for entire range of bias voltages.

M. Nishigaki et al. proposed an UWB tunable antenna with built-in piezoelectric MEMS variable capacitors [59]. A tuning ratio of 11 and a quality factor of the order of 37 at 650 MHz for bias voltage from 0V to 8.0 V were obtained. Issues such as nonlinearity of using varactor diodes where RF signal also varies the capacitance of the varactors diodes need to be tackled.

N.X. Sun et al. reported an electronically tunable magnetic patch antenna with metal magnetic film between the alumina substrate and the copper patch designed to operate at 2.10 GHz [60]. With appropriate external magnetic biasing perpendicular and parallel to the feed line, an enhanced bandwidth of 50% over the conventional patch antenna with its directivity increasing from 5.58 dB to 6.73 dB was achieved. In this technique, external field applied has a wide range of variations from 20 to 1000 Oe to control the frequency shift and the direction of external field has to be precisely controlled at the same time.

Antennas with metallic magnetic films and self biased magnetic films for electronic tuning have been reported by Guo-Min Yang et al. [61]. One layer just above a ring and another under the ground plane lowers the resonant frequency to 1.7 GHz from 1.72 GHz for the non magnetic antenna. The ferrite film loading effectively changes the geometrical dimensions thereby shifting down the resonant frequency. Fabrication

complexity is of concern as two layers below and above the patch was loaded with magnetic films.

Zammit et al. presented a tuneable microstrip antenna using switchable patches [62]. The design was obtained with 13 different copper strip bridges in place of switch combinations which tunes the frequency from 1.36 GHz to 1.92 GHz. The co-planar parasitic patches acting as capacitive load need large volume posing compactness problem. Combination of switches needs to be precisely controlled for getting uniform current distribution on the patch.

Davor Bonafacic et al. reported a PIFA with slotted PIFA loading for mobile communication devices [63]. Maximum gain of 3.2 dBi was obtained with capacitive loading to the slotted PIFA. The reduction in antenna dimension was made at the expense of bandwidth, gain and efficiency.

Abdelaziz et al. presented a compact microstrip patch antenna designed for application in civilian GPS (1.575GHz) [64]. Reduction in size of up to 24.6% was obtained. Gain was reduced by low radiation efficiency though good circular polarization was obtained for applications in mobile system.

Jing Liang et al. reported a microstrip patch antenna on tunable electromagnetic band-gap substrates [65]. Tuning was achieved by the diode loaded EBG substrate rather than on the antenna itself. A 4-by-4 EBG unit is embedded underneath the radiating patch and proximity coupled by a microstrip line with edged loaded SMA connector.

Carson R. White et al. developed single and dual polarized tunable slot ring antennas [66] for both single and dual polarized frequency tuning. The design achieved tuning range from 0.95 GHz to 1.85 GHz and 0.93 GHz to 1.6 GHz using two varactor diodes for single polarization antenna and four varactor diodes for dual polarization.

Se-Keun Oh et al. designed a varactor tunable slim antenna [67] which covers frequencies for Digital Cellular Systems (DCS: 1710-1880 MHz), Personal Communication Systems (PCS: 1850-1990MHz), Universal Mobile Telecommunication System (UMTS:1900-2200MHz), WiBro (2300-2390 MHz), Industrial, Scientific and Medical band (ISM) and WLAN (5150-5250 MHz and 5725-5850 MHz). The designed antenna combines the use of slots, Planar Inverted -L (PIL) and varactor diode for obtaining frequency tuning. In this technique, the total volume of components is an important issue for applications in portable handheld devices.

A tunable via-patch loaded PIFA with size reduction was presented by Chi Chiu et al. [68] for application in the 2.4 ISM band. In the designed patch, the adjustment of the

height of the via patch was done by turning a screw. Tuning was obtained in the range from 2.5 GHz to 3.3 GHz. An L-Shaped opening was cut on the ground plane under the patch for enhancing the impedance bandwidth. This type of mechanical tuning needs large parametric variations posing a challenge to the designer in catering to specific application requirements.

J.-C Langer et al. proposed a micro machined reconfigurable out of plane microstrip patch antenna using plastic deformation magnetic actuation [69]. Measurement was done for four angular positions of the antenna:  $0^\circ$ ,  $15^\circ$ ,  $45^\circ$  and  $90^\circ$ . Practical issues that arise for these designs are stress failure at the joints over the life time of the antenna. Moreover, the strength of the external magnetic field necessary to bend the antenna limits the size reduction. Also the presence of magnetic material on the patch causes significant losses.

### ***1.2.2 Size reduction techniques***

X.L. Bao et al. presented a miniature wide band patch for portable and cellular applications [70]. A cross-slot was placed in the ground plane which can achieve reduction of patch size and introduction of cross slot-ring provides broadband characteristics. Appropriate adjustment of antenna parameters is essential as the concentric annular ring-patch and the slot ring in the ground plane may generate multiple resonant modes.

W.-L Chen et al. presented a Sierpinski carpet microstrip antenna based on capacitive loading technique and obtained size reduction of 33.9 % [71].

Investigations on an H- shaped microstrip patch antenna with inductive loading had been reported by Pradyot Kala [72]. Theoretical calculations were done for adjustment of the H- shaped patch antenna loaded with multiple shorting posts based on the transmission line theory. Optimizing the parameters connecting the two arms of the 'H' and other patch dimensions is claimed to have the potential for size reduction.

Shaoqiu et al. presented a method for combining bandwidth enhancement with size reduction for design of ultra low profile antenna [73]. Commercially available Ansoft HFSS software was used for simulation. Results were obtained by using inset fed loaded and slots, for exciting two orthogonal modes,  $TM_{10}$  and  $TM_{01}$  simultaneously.

B.R. Holland et al. presented a tunable co- planar patch antenna using varactor [74] operating in the frequency range of 4.92 GHz to 5.40 GHz. Possible applications include next generation multi-standard wireless communication systems. The capacitive loading effect introduced by the varactor at the top radiating edge caused phase alteration between top and bottom radiating edges which tilted the pattern.

Ricky Chair et al. proposed a miniature half slot wide-band, half U-slot and half E-shaped patch antennas [75]. U-slot was introduced to improve size reduction compared to that obtained using shorting post. Bandwidth in the range of 20-30% was obtained using relatively thick substrate ( $\approx 0.08\lambda$ ). The radiation patterns were asymmetrical in the XZ-plane with a strong  $E_\phi$  field in the YZ-plane caused by structural asymmetry of the half U-slot.

Davor Bonefacic et al. proposed small H-shaped antennas [76]. Modifications to the H-shaped antennas were performed for three different cases: shorting the patch, introducing shorting posts and shorting with folded radiating edges of the patch. All the antennas were designed for 2 GHz. Maximum measured gain obtained was in the range from 3.6 dBi to 5.3 dBi. Reduction in size was observed at the expense of bandwidth. Again, shorting influenced cross polarization level when the lengths become larger than the width of the patch.

Yonghoon Kim et al. presented a size reduction technique by elevating the centre of the patch [77]. A size reduction of 53% was obtained at a single frequency of 3 GHz. Further size reduction was obtained by additional notch on the patch. In this approach, impedance and gain were degraded due to radiation from the edges of the notch.

Hang Wong et al. proposed size reduction of a patch antenna using parasitic shorting elements [78]. A symmetrical arrangement was employed to avoid unwanted radiation from vertical shorting pins. The design exhibited 3.25% impedance bandwidth with a gain of 2 dBi. Narrow bandwidth was a limitation in the design.

Korkontzila et al. designed a square patch antenna on top of EBG substrate comprising of two layers, each carrying a biperiodic array of circular patches, which resonate at 2.4 GHz [79]. A size reduction of 24% was obtained. The structure involves several steps which make the design complex and time consuming. Use of adhesives between layers of laminations, proper machining and spacing between periodic structures were required in this design.

Y.J. Wang et al. reported a compact and broadband microstrip patch antenna [80]. An impedance bandwidth of 17.8% was obtained in the frequency range from 1.862 GHz to 2.225 GHz.

E.E.M Khaled et al. proposed a compact patch antenna based on slot matching [81]. Four frequency bands in the range from 2 GHz to 5 GHz were obtained with return loss of about -9.54 dB and a VSWR of less than 2.



A small size broadband microstrip patch with small ground plane was reported by Ji-Hyuk Kim et al. [82]. Broadband characteristics were obtained from 5 GHz to 6 GHz with multiple layers of substrates. The antenna was divided into three segments and each segment was connected to a microstrip line. The fabrication process involved many steps such as thermal evaporation, molding, electroplating, wafer preparation etc. due to which the cost of fabrication becomes a limiting factor .

Michal Pokorny et al. reported a planar tri-band inverted F-antenna using slots and parasitic patches to cover the GSM 900, GSM 1800 and ISM 2400 bands [83]. Multi-objective optimization was chosen for genetic algorithm (GA) for improvement in the impedance matching and the direction of maximum gain. The practical design revealed some shift in resonant frequency ostensibly caused due to manual assembly and soldering of the antenna and metal pins.

J.Vekataraman et al. proposed a small microstrip patch antenna [84]. Three patches were designed for size reduction of up to 70%. In one method, genetic algorithm was used to optimize size and location of the slots on the patch. In another method, the patch was loaded with multiple slots along its edges where particle swarm algorithm interfaced with HFSS has been utilized for optimizing the dimension of the slots. In yet another approach, Complementary Split Ring Resonator (CSRR) has been placed in the ground plane of the patch to create left handed effect that results in negative permittivity.

### 1.3 Motivation for the present Work

As mentioned earlier, compact and broadband antenna characteristics are two of the prime considerations for present day wireless systems such as Wireless Access Systems (WAS) and Mobile Wireless Systems (MWS) including WLAN, WiMax, RFID, UWB etc. for short, middle and long range communication systems. Antenna designed for these applications should therefore be easily customizable and configurable to cater to different application requirements with minor alterations in the structure; be it at the fabrication stage or after.

One method for size reduction of microstrip antenna is to use high permittivity substrates. However, the difficulty in achieving this is compounded by the fact that one needs to maintain performance characteristics within the acceptable limit for a particular application. Antennas for mobile systems need specific minimum band width, high efficiency, impedance matching and acceptable radiation pattern bandwidth for practical applications. In particular, the excitation of surface waves within the substrate may deteriorate the antenna gain and the shape of the radiation pattern. Again, size

miniaturization of normal patch has been accomplished by loading, which may take various forms such as use of high dielectric constant substrates, modifications of basic patch shapes, use of shorting elements and combinations of the above techniques.

Bandwidth enhancement techniques employed for conventional patch antenna include use of a thick substrate with low dielectric constant, using planar and gap coupled multi resonators, stacked electromagnetically coupled or aperture coupled patches, impedance matching techniques, log periodic configurations and use of ferrite substrates. However, these techniques have to satisfy the ever increasing demand for low cost, simple fabrication, ease of integration, reliability as well as multi band antennas that can operate at different frequency bands or cover a wide frequency spectrum. All these existing and widely used designs have some limitations; for instance, use of high dielectric constant material for size reduction exhibits narrow bandwidth, high loss and poor efficiency due to surface wave generation. Major modification of the basic patch structure may also cause inefficient use of the available space.

A tunable antenna on the other hand provides an alternative to a broadband antenna in which an antenna with a small BW is tuned over a large frequency range. Tunable multi-frequency antennas rather than broadband antennas can be a preferred alternative when the system needs to operate only at one frequency in each band at any given time. Thus size reduction as well as tuning the resonant frequency at more than one frequency or one frequency within the band or multiband is two major areas that need attention. An antenna that can operate in more than one band with continuous or discrete tuning is a requirement for present day wireless applications. The challenge here is to evolve an acceptable trade off between these requirements and other antenna performance characteristics.

The motivation for the proposed work is essentially driven by the need for lower cost antennas providing the performance characteristics required without significant increase in weight or compromise on profile.

The thesis presents some new structures which are designed in this work for:

- Size reduction
- Dual/Multi-frequency operation with tuning of the lower and/or higher frequencies or both.

#### **1.4 Thesis Outline**

The present work carried out has been organized into 7 chapters covering the different design techniques with measured and simulation results. High frequency

simulation software CST Microwave Studio, based on FDTD numerical technique is used for pre-fabrication assessment of design as well as comparison with measured results. Various new designs such as modifying the conventional planar patch structures, adding new elements to the patch for tuning, bandwidth enhancement and size reduction are highlighted.

Chapter 1 gives an overview of microstrip antenna technology, tuning and size reduction techniques.

Integration of the constituent units and PC automation of a test and measurement setup is described in Chapter 2. The automated system can carry out antenna performance measurements which include S parameters and antenna radiation pattern. System performance evaluation has been carried out using standard antennas.

Chapter 3 details studies on a planar patch antenna with slits near the radiating edge and the effect of electromagnetic coupling through it on antenna characteristics and tuning. The effect of elevation of the cut out patch sections at different angles of elevation was studied in detail. Radiation patterns are also presented and comparison of measured pattern shapes with that of the conventional planar structure is included.

Chapter 4 describes a patch antenna with notionally superposed finite microstrip line section for size reduction. Performance is studied with respect to angular position of the line section near one of the radiating edges.

Chapter 5 presents spike edged microstrip patch antenna (SEMPA) designed for bandwidth enhancement. A detailed study on variation of spike number, position as well as strip line loading of spike vertices is carried out with respect to return loss, bandwidth and radiation pattern characteristics.

Chapter 6 includes the design of a reconfigurable patch antenna with a rectangular air pocket in the substrate layer between the patch and the ground plane. A plunger of the same substrate material with the dimensions of the air pocket is inserted into the air pocket for tuning the resonant frequency.

Chapter 7 summarizes the results on the designed antenna structures; highlighting the major achievements, shortcoming and scope for future work.

---

**References**

- [1] J. R. James, P. S. Hall, (Eds.), "Handbook of Microstrip Antennas," *Peter Peregrinus, London, UK*, 1989.
- [2] J. Hung, "Microstrip antennas for commercial applications," in *Microstrip Antennas: The Analysis and Design of Microstrip Antennas and Arrays*, D. M. Pozar and D. H. Schaubert (Eds.), *IEEE Press, New York*, pp. 371-379, 1995.
- [3] A. Curiel da Silva, "The First Generation INMARSAT System," *IEEE 3<sup>rd</sup> Int. conf. on satellite systems for mobile commun. and navigation*, pp. 1-7, 1983.
- [4] W. Refferty, K. Dessouky, and M. Sue, "NASA's mobile satellite development program," *Proc. of the mobile satellite conf*, pp. 11-22, 1988.
- [5] J. J. Schuss, et al., "Design of Iridium phased array antennas," *IEEE AP-S Int. Symp. Digest*, pp. 218-221, 1993.
- [6] I. J. Bahl, and P. Bhartia, "Microstrip antennas," *Artech House, Dedham, MA*, 1980.
- [7] J. R., James, and P. S., Hall, and C., Wood, "Microstrip antennas, theory and design," *Peter Peregrinus, London, UK*, 1981.
- [8] J. R. James, P. S. Hall, (Eds.), "Handbook of Microstrip Antennas," *Peter Peregrinus, London, UK*, 1989.
- [9] P. Bhartia, K. V. S. Rao, and R. S. Tomar, "Millimeter- wave microstrip and printed circuit antennas," *Artech House, Norwood, MA*, 1991.
- [10] D. M. Pozzar, and D. H. Schaubert (Eds.), "The analysis and design of microstrip antenna and arrays," *IEEE press, New York*, 1996.
- [11] J. F. Zucher, and F. E. Gardiol, "Broad band patch antennas," *Artech House, Norwood, MA*, 1995.
- [12] R. A. Sainati, "CAD microstrip antennas for wireless applications," *Artech House, Norwood, MA*, 1996.
- [13] D. M. Pozar, "Microstrip antennas," *Proc. IEEE*, Vol. 80, pp. 79-92, 1992.
- [14] Issue of "*IEEE Trans. on antennas and propagation*," Vol. AP- 29.
- [15] J. P. Daniel et al., "Research on planar antennas and arrays: Structures Rayonnantes," *IEEE Antenna propag. magazine*.
- [16] K. C. Gupta et al., "Microstrip lines and slot lines", 2nd ed., *John Willey, New York*, Chap 14, 1981.
- [17] D. M. Pozar, "A Microstrip antenna aperture coupled to a microstrip line," *Electronics Letters*, Vol. 21, pp. 49-50.
- [18] G. A. Deschamps, "Microstrip microwave antennas," *presented in the 3<sup>rd</sup> USAF symp. on antennas*, 1953.
- [19] H. Gutton and G. Baissinot, "Flat aerial for ultra high frequencies," *French patent no. 703113*, 1955.
- [20] V. Palaniswamy, and R. Garg, "Rectangular ring and H shape microstrip antennas- alternative approach to rectangular microstrip antenna," *Electronics letters*, Vol. 21, No. 19, pp. 874-876, 1985.

- [21] G. Kumar, and K. C. Gupta, "Broadband microstrip antennas using additional resonator gap- coupled to radiating edges," *IEEE transaction on antenna propagation*, Vol. AP-32, pp. 1375-1379, 1984.
- [22] G. Zhou, "Shorting -pin loaded annular ring microstrip antennas," *IEEE AP-S Int. Symp. Digest*, pp. 900-903, 1998.
- [23] M. T. Ma, "Theory and applications antenna arrays," *Willey-Interscience, New York*, 1974.
- [24] D. C. Chang, D. I. Wu, J. C. Moore, "Modelling and computer-aided design of microstrip antenna arrays," European space agency workshop on active antennas, 1992.
- [25] K. C. Gupta, R. Garg, and R. Chanda, "Computer aided-design of microwave circuits," *Artech House, Dedham, MA*, 1981.
- [26] R. E. Munson, "Conformal microstrip antennas and microstrip patch arrays," *IEEE transaction on antenna propagations*, Vol. AP-22, no. 1, pp. 74-77, 1974.
- [27] A. G. Demeryd, "Linear microstrip array antennas," *Chalmer univ. tech., Goteborge, Sweden, Tech. Rep. TR n7505*, 1975.
- [28] D. M. Pozar and D.H. Schaubert, "Microstrip antennas: The analysis and design of microstrip antennas and arrays," *New York, IEEE press*, 1995.
- [29] H. G. Puels, and A. R. Van De Capelle, "An matching technique for increasing the bandwidth of microstrip antennas", *IEEE trans. Antenna propagation*, Vol. AP-37, No. 11, pp. 1345-1354, 1989.
- [30] H. G. Puels, and A. R. Van De Capelle, "Wideband impedance matching resonator antennas," *Proc. IEE 2<sup>nd</sup> Int. Conf. Antennas Propagation*, Pt. 1, pp. 402-405, 1981.
- [31] K. S. Fong, H. F. Pues, and M. J. Withers, "Wideband multilayer coaxial-fed microstrip antenna elements," *Electronic Letters, Vol. 21*, pp. 497-498, 1985.
- [32] H. Legay, and L. Shafai, "A new stacked microstrip antenna with large bandwidth and high gain," *IEEE AP-S Int. Sym. Digest*, pp. 948-951, 1993.
- [33] B. Balakrishnan, and G. Kumar, "Wideband and high gain electromagnetically coupled circular patch antenna" *IEEE AP-S Int. Sym. Digest*, pp. 1112-1115, 1998.
- [34] V. Radisic et al., "Novel 2-D photonic band gap structures for microstrip lines," *IEEE Microwave Guided Wave Lett.*, Vol. 8, pp. 69-71.
- [35] Y. Qian et al., "Microstrip patch antenna using novel photonic bandgap structures," *Microwave Journal*, Vol. 42, pp. 66-76, 1999.
- [36] R. Coccioli et al., "Aperature coupled patch antenna on UC-PBG substrate," *IEEE Trans. On Microwave Theory and Technique*, Vol. MTT-47, pp. 2123-2130, 1999.
- [37] M. Du. Plessis, and J. H. Cloete, "Tuning stub for microstrip patch antenna," *IEEE AP-S Int. Symp. Digest*, pp. 964-967, 1993.
- [38] K. P. Ray, and G. Kumar, "Tunable and dual-ban circular microstrip antenna with stubs," *IEEE Trans. Antenna Propagation*, Vol. 48, pp. 1036-1039, 2000.
- [39] P. Bhartia, and I. J. Bahl, "A frequency agile microstrip antenna," *IEEE AP-S Int. Symp. Digest*, pp. 304-307, 1982.

- [40] S. Maci, and G. B. Gentili, "Dual frequency patch antennas," *IEEE AP Magazine*, Vol. 39, pp. 13-19, 1997.
- [41] H. Schaubert et al., "Microstrip antennas with frequency agility and polarization diversity," *IEEE Trans. Antenna Propagation*, Vol. AP-29, pp. 118-123, 1981.
- [42] W. F. Richards, S. E. Davidson, and S. A. Long, "Dual band reactively loaded microstrip antenna," *IEEE Trans. Antenna Propagation*, Vol. AP-33, pp. 556-561, 1985.
- [43] D. M. Pozar, "Microstrip antenna aperture coupled to microstrip line," *Electronics Letters*, Vol. 21, No. 2, pp. 49-50, 1985.
- [44] D. M. Pozar, and S. D. Targonski, "Improved coupling for aperture coupled microstrip antennas," *Electronics Letters*, Vol. 27, No. 13, pp. 1129-1131, 1991.
- [45] V. Rathi, and G. Kumar, and K. P. Ray, "Improved coupling for aperture coupled microstrip antennas," *IEEE Trans. Antenna Propagation*, Vol. AP-44, No. 8, pp. 1196-1198, 1996.
- [46] Iskandar Fitri and Eko Tjipto Rahardjo, "A compact microstrip slot antenna fed by microstrip line with a multi tuning stubs for UWB applications," *Proceeding of Asia-Pasific Microwave Conference*, pp- 1640- 1643, 2006.
- [47] H.K. Ng and W. Leung, "Frequency tuning of the dielectric resonator antenna using a loading cap," *IEEE Transactions on Antennas and Propagation*, Vol.53, pp. 1229- 1232, 2005.
- [48] J. A. Tirado-Mendez and H. Jardon-anguilar, "Application of defected microstrip structure in tuning a square patch antenna," *International Conference on Electrical and Electronics Engineering*, pp.382-384, 2005.
- [49] P. Blondy, D. Bouyge, A. Crunteanu, A. Pothier, "A Wide Tuning Range MEMS Switched Patch Antenna," *IEEE MTT-S International Conference on Microwave Symposium Digest*, pp.152- 154, 2006.
- [50] J. Ollikainen, M. Fischer and P. Vainikainen, "Thin dual-resonant stacked shorted patch antenna for mobile communications," *Electronics Letters*, Vol. 35, No. 6, pp.437 – 438, 1999.
- [51] P. J. Rainville and F. J. Harackiewicz, "Magnetic tuning of a microstrip patch antenna fabricated on a ferrite film," *IEEE Microwave and Guided Wave letters*, Vol. 9, No. 12, 1992.
- [52] Abdelaziz A. Abdelaziz, Dalia M. Nashaat, "Compact GPS Microstrip Patch Antenna," *Journal of Theoretical and Applied Information Technology*, pp.1-4, 2007.
- [53] Dimitrios Peroulis, Kamal Sarabandhi and Linda P.B. Katehi, "Design of reconfigurable slot antennas," *IEEE Transactions on Antennas and propagation*, Vol. 53, No. 2, pp. 645 – 654, 2005.
- [54] David Pouhe, Cyprian Fusi and Gerhard Monich, "An Improved Compact Multi-band Broadband Patch Antenna for Mobile Communication Systems," *2nd International ITG Conference on Antennas (INICA)*, pp. 158 – 161, 2007.
- [55] Sylvain Loizeau, and Alan Sibille, "A novel reconfigurable antenna with low frequency tuning and switchable UWB band," *3rd European Conference on Antennas and Propagation (EuCAP)*, pp. 1627 – 1631, 2009.
- [56] P. Rocca, R. Azaro, M. Benedetti, F. Viani and A. Massa, "Multi-band patch antenna tuning by a fractal shaped erosion process," *IEEE International, Symp. Antennas and Propagation Society*, AP-S, pp.1-4, 2008.
- [57] Gwo-Yin Lee, Tzung-Wern Chiou and Kin-Lu Wong, "Broadband stacked shorted patch antenna for mobile communication handsets," *Asia-Pacific Microwave Conference APMC*, Vol. 1, pp. 232 – 235, 2001.

- [58] Nader Behdad and Kamal Sarbandi, "Dual-band reconfigurable antenna with a very wide tunability range," *IEEE Transactions on Antennas and Propagation*, Vol. 54, No. 2, 2006.
- [59] M. Nishigaki, T. Miyanki, T. Kawakubo, M. Nishio and S. Sekine, "*IEEE/MTT-S International Microwave Symposium*," pp. 2079 – 2082, 2007.
- [60] N. X. Sun, J. W. Wang, A. Daigle, C. Pettiford, H. Mosallaie and C. Vittoria, "Electronically tunable magnetic patch antennas with metal magnetic films," *Electronics Letters*, Vol.43, No. 8, 2007.
- [61] Guo-Min Yang, X. Xing, A. Daigle, M. Liu, O. Obi, J. W. Wang, K. Naishadham and Nian X. Sun, "Electronically Tunable Miniaturized Antennas on Magnetolectric Substrates With Enhanced Performance," *IEEE Transactions on Magnetics*, Vol.44, No.11, 2008.
- [62] Joseph A. Zammit and Adrian Muscat, "A small tunable antenna using multiple shorting posts and varactor diodes," *3rd International Symposium on Communications, Control and Signal Processing ISCCSP*, pp. 83-86, 2008.
- [63] Davor Bonafacic and Bojan Rapinnac, "Small H- shaped shorted patch antennas," *Radioengineering*, Vol. 17, No.2, pp. 77-82, 2008.
- [64] Abdelaziz A. Abdelaziz, Dalia M. Nashaat, "Compact GPS Microstrip Patch Antenna," *Journal of Theoretical and Applied Information Technology*, pp.1 –4, 2007.
- [65] Jing Liang and H. Y. David Yang, "Microstrip Patch Antennas on Tunable Electromagnetic Band-Gap Substrates," *IEEE Transactions on Antennas and Propagation*, Vol.57, No.6, 2009.
- [66] Carson R. White and Gabriel M. Rebeiz, "Single- and Dual-Polarized Tunable Slot-Ring Antennas," *IEEE Transactions on Antennas and Propagation*, Vol.57, No. 1, 2009.
- [67] Se-Keun Oh, Hyung-Sik Yoon and Seong –Ook Park, "A PIFA-Type Varactor-Tunable Slim Antenna With a PIL Patch Feed for Multiband Applications," *IEEE Antennas and Wireless Propagation Letters*, Vol.6, 2007.
- [68] Chi Yuk Chiu, Kam Man Shum and Chi Hou Chan, "A Tunable Via-Patch Loaded PIFA With Size Reduction," *IEEE Transactions on Antennas and Propagation*, Vol. 55, No. 1, pp. 65-71, 2007.
- [69] J.-C. Langer, J. Zou, C. Liu and J. T. Bernhard, "Micromachined reconfigurable out-of-plane microstrip patch antenna using plastic deformation magnetic actuation," *IEEE Microwave and Wireless Components Letters*, Vol.13, No. 3, pp.120- 122, 2003.
- [70] X. L. Bao and M. J. Ammann, "Investigation on Miniature Wideband Patch Antenna for Portable Wireless and Cellular Applications," *65<sup>th</sup> IEEE Vehicular Technology Conference, VTC*, pp. 1-2, 2007.
- [71] W. –L Chen and G. –M. Wang, "Small size edge fed sierpinski carpet microstrip patch antenna," *Progress In Electromagnetic Research*, Vol.3, pp. 195-202, 2008.
- [72] Pradyut Kala, " Investigation of an H- shaped microstrip patch antenna with inductive loading," *International journal of microwave and optical technology*, Vol.4, No. 2, 2009.
- [73] Shaoqiu Xiao, Bing-Zhong Wang, wei Shao and Yan Zhang, "Bandwidth-enhancing ultralow-profile compact patch antenna," *IEEE Transactions on Antennas and Propagation*, Vol.53, No. 11, pp. 3443-3447, 2005.
- [74] B. R. Holland, R. Ramadoss, S. Pandey and p. Agrawal, "Tunable coplanar patch antenna using varactor," *Electronics Letters*, Vol.42, No. 6, pp. 319-321, 2006.

- [75] Ricky Chair, Chi-Lun Mak, Kai-Fong Lee, Kwai-Man Luk and A. Kishk, "Miniature Wide-Band Half U-Slot and Half E-Shaped Patch Antennas," *IEEE Transactions on Antennas and Propagation*, Vol.53, No. 8, pp. 2645- 2652, 2005.
- [76] Davor Bonafacic and Bojan Rapinnac, "Small H- shaped shorted patch antennas," *Radioengineering*, Vol. 17, No.2, pp. 77-82, 2008.
- [77] Yonghoon Kim, N. J. Francich, S- C., Kim, S., Nam, and P.,M., Asbeck " Size reduction of microstrip antenna by elevating centre of the patch", *Electronics letters*, Vol. 38, No.20, pp. 11631165-82, 2002.
- [78] Hang Wong, Kwok Kan So, Kwai Man Luk, Chi Hou Chan and Quan Xue, "New size reduction for patch antenna by parasitic shorting elements", *International Workshop on Antenna Technology (IWAT)*, pp.1- 4, 2010.
- [79] E. G. Korkontzila, D. B. Pappafilippo, D. P. Chrissoulids, "Miniaturization of microstrip patch antenna for wireless applications by use of multilayered electromagnetic band gap substrate," *First European Conference on Antennas and Propagation*, EuCAP, pp. 1-6, 2006.
- [80] Y. J. Wang, C. K. Lee, "Compact and broadband microstrip patch antenna for the 3G IMT- 2000 handsets applying Styrofoam and shorting post," *Progress In Electromagnetic Research, PIERS*, Vol. 47, pp. 75-85, 2004.
- [81] Michal Pokorny, Jiri Horak, and Zbynek Raida, "Planar tri-band antenna design," *Radioengineering*, Vol. 17, No.1, 2008.
- [82] Ji- Hyuk Kim, Hyeon Cheol Kim and Kukjin Chun, "A small size broadband MEMS antenna for 5 GHz WLAN applications," *Journal of semiconductor technology and science*, Vol. 5, No 3, pp. 204-209, 2005.
- [83] Michal Pokorny, Jiri Horak, and Zbynek Raida, "Planar tri-band antenna design," *Radioengineering*, Vol. 17, No.1, 2008.
- [84] J. Venkataram, A .Wyant, Ch. Wenbo, A. Limaye, G. Shieh, "Small microstrip patch antennas," *Applied Electromagnetics Conference (AEMC)*,pp. 1-4, 2009.



## CHAPTER II

# MEASUREMENT SETUP INTEGRATION

---

### 2.1 Introduction

### 2.2 Measurement Set up

#### *2.2.1 Return loss measurement set up*

#### *2.2.2 PC controlled radiation pattern measurement set- up*

#### *2.2.3 Antenna mounting system design*

### 2.3 Interfacing

### 2.4 Automation software

### 2.5 Results

### 2.6 Chapter summary

### References

## 2.1 Introduction

The experimental setup is automated to overcome the limitations of manual measurement which is time consuming. The automated system is capable of carrying out antenna performance measurements viz.  $S_{11}$  and antenna radiation pattern measurements. The system includes a microwave signal generator, which is interfaced through a USB port using the Virtual Instrument Software Architecture platform in Visual C++ while at the receiving end a spectrum analyzer is interfaced to the automated system via the control PC through a LAN port. System performance evaluation is carried out using standard antennas for accuracy and repeatability, results of which are also included in this chapter.

The development of the automated measurement set up and final implementation of both the software and hardware components are discussed in the following subsections.

## 2.2 Measurement setup

### 2.2.1 Return loss measurement setup

The setup consists of a signal generator, a dual directional coupler and a spectrum analyser for measurement of receiver power.

#### *Signal generator*

An Agilent N5183A signal generator is used as the signal source having a frequency range of 10.0 KHz to 20.0GHz with a frequency setting resolution of 0.01 MHz. Frequency switching speed is  $\leq 5.0$  ms for two modes of operations: SCPI (Standard Commands for Programmable Instruments) mode and list / step sweep mode. Numbers of points that can be set for sweep range within the instrument frequency range are 2 to 65535 for step sweep and 1 to 1601 for line sweep with an output power ranging from -20.0 dBm to +14.0 dBm. Dwell time for digital sweep can be set from 100 $\mu$ s to 100s. Linear and logarithmic step change can be accomplished with available triggering options such as free run, trigger key, external, timer as well as via the interfacing bus (GPIB, LAN, and USB). Different entry modes are possible such as USB/LAN direct power meter, LAN to GPIB and USB to GPIB, remote bus and manual USB/GPIB power meter and power sensor control (when an Agilent power sensor is used). Typical SWR for frequency range of 100.0 kHz to 20.0 GHz is 1.6:1. The system has an inbuilt interfacing feature via the GPIB IEEE-488.2 with listen and talk, LAN 100 based T LAN interface, LXI class C compliant and USB version 2.0. The signal generator supports SCPI 1997 version. The 512 MB of flash memory available in the N5181A MXG is

shared by instrument states, sweep list files and other files. A maximum of 1000 instrument states can be saved depending on utilized memory.

### *Spectrum analyzer*

An Anritsu MS2719B spectrum analyzer is used as receiver having a frequency range of 90 kHz to 20.0 GHz. It has standard built in preamplifier with dynamic range of 100 dB. Displayed average noise levels (DALN) with and without preamplifier are -126 dBm and -150 dBm having a resolution bandwidth of 0.01 MHz. It has a sweep speed of 200 ms with RBW (Resolution bandwidth) and VBW (Video bandwidth) of 30 kHz and 10 kHz respectively. Residual adjacent channel leakage ratio (ACLR) for the spectrum analyzer is -60 dB with a residual error voltage magnitude (EVM) of 1.75%. The spectrum analyzer can be operated with an amplitude accuracy of  $\pm 1.0$  dB up to 20 GHz. Attenuation up to 65 dB is possible in step of 5dB . Phase noise of 800 MHz at 10 kHz offset is -114 dBc/Hz. Input power protection for the spectrum analyzer is 20W (+43 dBm).

### *Dual directional coupler*

An Agilent11692D co-axial dual-directional coupler with a frequency ranging from 2.0 GHz to 18.0 GHz is used for reflectometry ( $S_{11}$ ) measurement. Detailed specifications of DDC are given in a table 2.1.

### **2.2.2 PC controlled radiation pattern measurement set- up**

A PC controlled radiation pattern measurement set- up is developed in the Visual C++ language on the VISA (Virtual Instrument Software Architecture) platform. Initial calibration using standard horn antennas has been carried out to verify the accuracy and repeatability of the measurement system.

**Table 2.1:** Specifications of Dual Directional Coupler (DDC)

Frequency range	2 to 18 GHz
Minimum directivity	2 to 18 GHz: 30 dB
	8 to 18 GHz: 26 dB
Maximum primary line SWR	2 to 12.4 GHz: 1.3
	12.4 to 18 GHz: 1.40
12.4 to 18 GHz: 1.40	1.3
Nominal coupling (dB)	20
Maximum coupling variation with frequency (dB)	$\pm 1$ dB
Tracking auxiliary arms	$\pm 0.7$ dB
Maximum primary line residual loss	< 1.5 dB
Primary line power	50W average
Handling capability	250 $\Omega$ peak

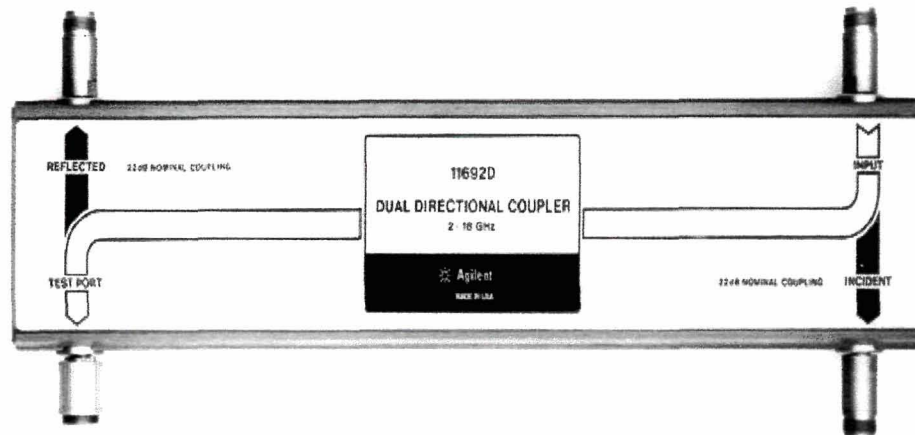


**Figure 2.1:** Coaxial Dual-Directional Coupler (11692D)

The Schematic diagram of the measurement system for  $S_{11}$  is shown in figure 2.2. The main advantage in the automated set up are threefold : first, it drastically reduce the time required for manual measurement which extends up to 10 -12 hour per set of data; secondly, the set-up minimizes involvement required for manual feeding of data and finally, a smoother data curve is obtained without missing out on finer details (variations).

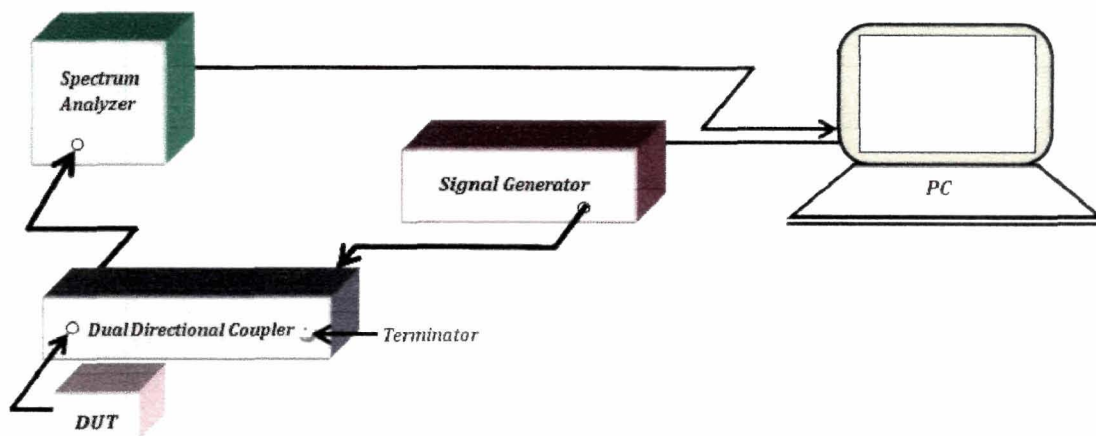


**Figure 2.2:** Block diagram of test set up for measurement of  $S_{11}$  parameter

The setup for antenna radiation pattern measurement consists of a dual tracking DC power source (ST 4076) (30V, 2A) which provides dc power to the stepper motor, signal generator, a PC configured with Windows XP, LAN Hub, stepper motor, and spectrum analyzer connected to the controlling PC to measure the microwave power received by the antenna. The stepper motor is rotated using a driver circuit developed and interfaced to the LPT 1 port of the PC.

The LPT1 port of a PC is used as the I/O port saving the cost on any I/O card.

A PMH stepper motor (12 V, make: Sanyo Denki) which is used for rotating the test antenna mounted on a wooden antenna mount attached to wooden shaft of the antenna turn table.

The schematic radiation pattern measurement system is shown in figure 2.3

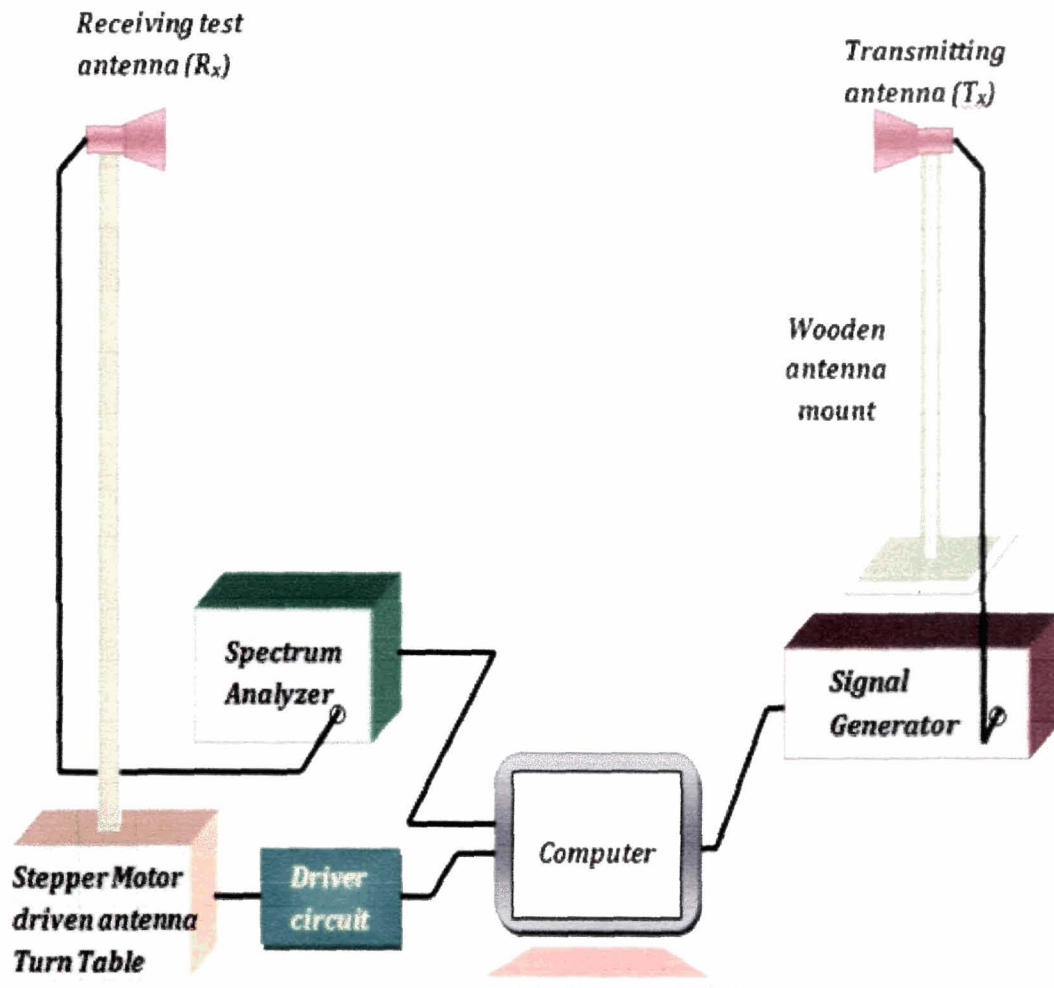


**Figure 2.3:** Schematic diagram of set up for antenna radiation pattern

A PMH stepper motor (12V, make: Sanyo Denki) with a torque 2.0 kg-cm has been used to rotate the antenna under test. Motor specifications are given in table 2.2.

**Table 2.2:** Specification of the stepper motor

Motor type	PMH
Winding resistance (each $\Phi$ )	4.7 $\Omega$
Rated current	1.2 A
Torque	2 Kg-cm
Motor sequence	2,4,6,8

The PMH stepper motor used in the set up is operated in full-step excitation with single phase energized at a time. More precise step reading is evaluated using a wooden shaft attached to the nylon gear having gear ratio of 1:100.

Calculation of number of steps for rotation is evaluated as

Step angle =  $1.8^\circ$  (in an 4 step sequence)

Total no. of steps for complete  $360^\circ$  antenna rotation

$$= \frac{360^\circ}{1.8^\circ} \times \text{gear ratio} = \frac{360^\circ}{1.8^\circ} \times \frac{100}{1} = 20,000$$

Number of steps after 1 power acquisition = 25 steps

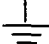
Step angle with gear =  $25 \times 0.018^\circ = 0.45^\circ$

The total number of data for one complete rotation =  $360^\circ / 0.45^\circ = 800$  data points.

### *LPT port interfacing*

The LPT1 port of a PC is used as the I/O port without the need of any external I/O card. Moreover, the data is picked up from Spectrum Analyzer and hence no additional A/D-D/A card is, therefore, necessary. The details of the pin configuration of LPT1 are given in table below.

**Table 2.3:** LPT1 pin configuration

<i>LPT1 Pin number</i>	<i>Signal name</i>	<i>Direction</i>	<i>Address</i>
1	Strobe	→ To printer	37A
2-9	Data bit	→To printer	378H
10-13,15	Acknowledge, Busy, out of paper, select, error	← From printer	379H
14,16,17	Auto line feed, initialize, select-up	→To printer	37A
18-25	Ground		From printer

### Driver circuit

The circuit diagram of the driver circuit designed is given in figure below.

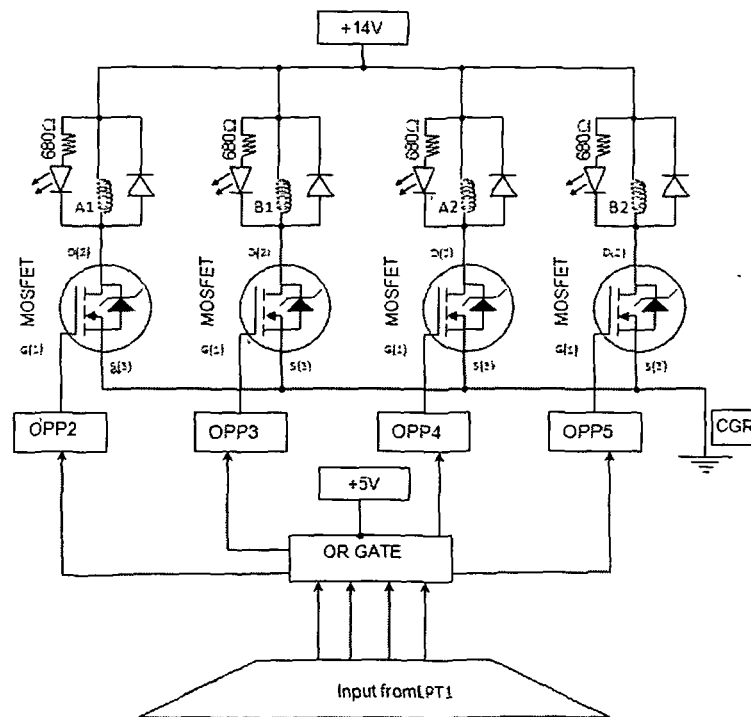


**Figure 2.4:** Stepper motor drive circuit

In this driver circuit, the output from the LPT1 port is fed to the opto couplers (MCT2E) through an OR gate and SN7400N. The four bit stepping sequence generated by the programme appears at 4 of the output pins (bits) of the LPT1 port and is fed to the opto coupler inputs. This is employed as precautionary step to protect the parallel port from unwanted reverse current. MOSFETS (IRF 540N) are used as switches to generate the required motor sequence. Free-wheeling diodes are used in the circuit to maintain the desired current through the coils of the motor.

### 2.2.3 Antenna mounting system design

An azimuthal turn table with mounting system for the test antenna is specially designed and fabricated. On the other hand, a fixed mount is designed so that the test and standard antenna are aligned horizontally along a common axial line. The mounts are made of wood to minimize reflections. A wooden shaft runs through the height of the turn table supported by bearings near both the ends. A nylon gear is specially fabricated and attached to the lower end of the shaft for driving the turn table by a stepper motor (fig. 2.5). To prevent twisting of the co-axial cable connected to the test antenna, a co-axial rotary joint is used on the shaft to isolate the rotating movement of turn table from the static section of the cable connected to the signal detecting system.

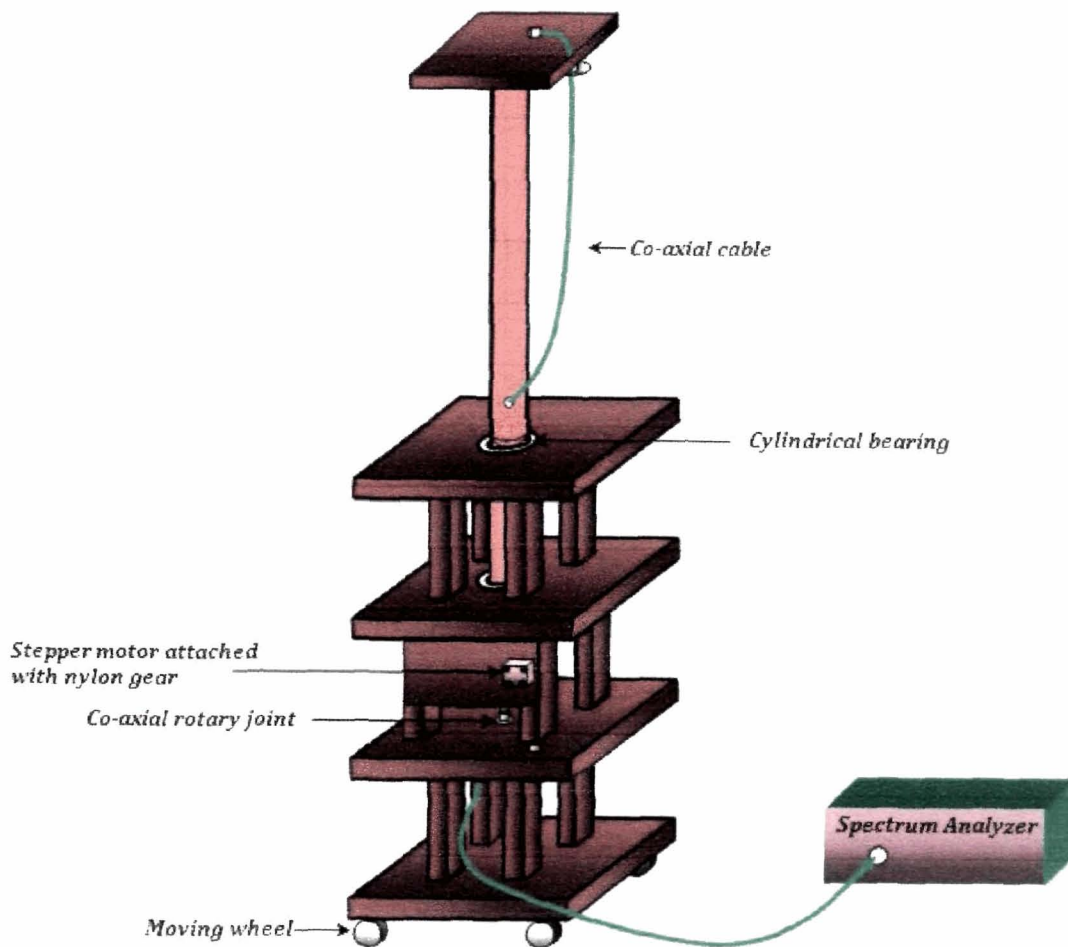


**Figure 2.5:** Antenna Mount designed for radiation measurement

### 2.3 Interfacing

The signal generator which is available in the laboratory is interfaced through the LAN ports using the Virtual Instrument Software Architecture (VISA) platform in the Visual C++ language. Frequency sweep and spot frequency for the automated system on the software developed.





**Figure 2.6:** Photograph of the measurement system

#### **2.4 Automation software**

The flowchart of the data acquisition system for the automated system is shown in figure 2.7. The angular antenna position is stored in a data file (deg.txt) and the corresponding power in dB is acquired from the spectrum analyser and stored in another data file (power.txt). Necessary software developed are given in the program for stabilization of the reading. System initialization routines for the signal generator and spectrum analyzer are included in the developed software. Routines for measurement of  $S_{11}$  parameter with frequency sweeps and patterns with spot frequency are included in the main module. The listing of the programme is included in Appendix A.

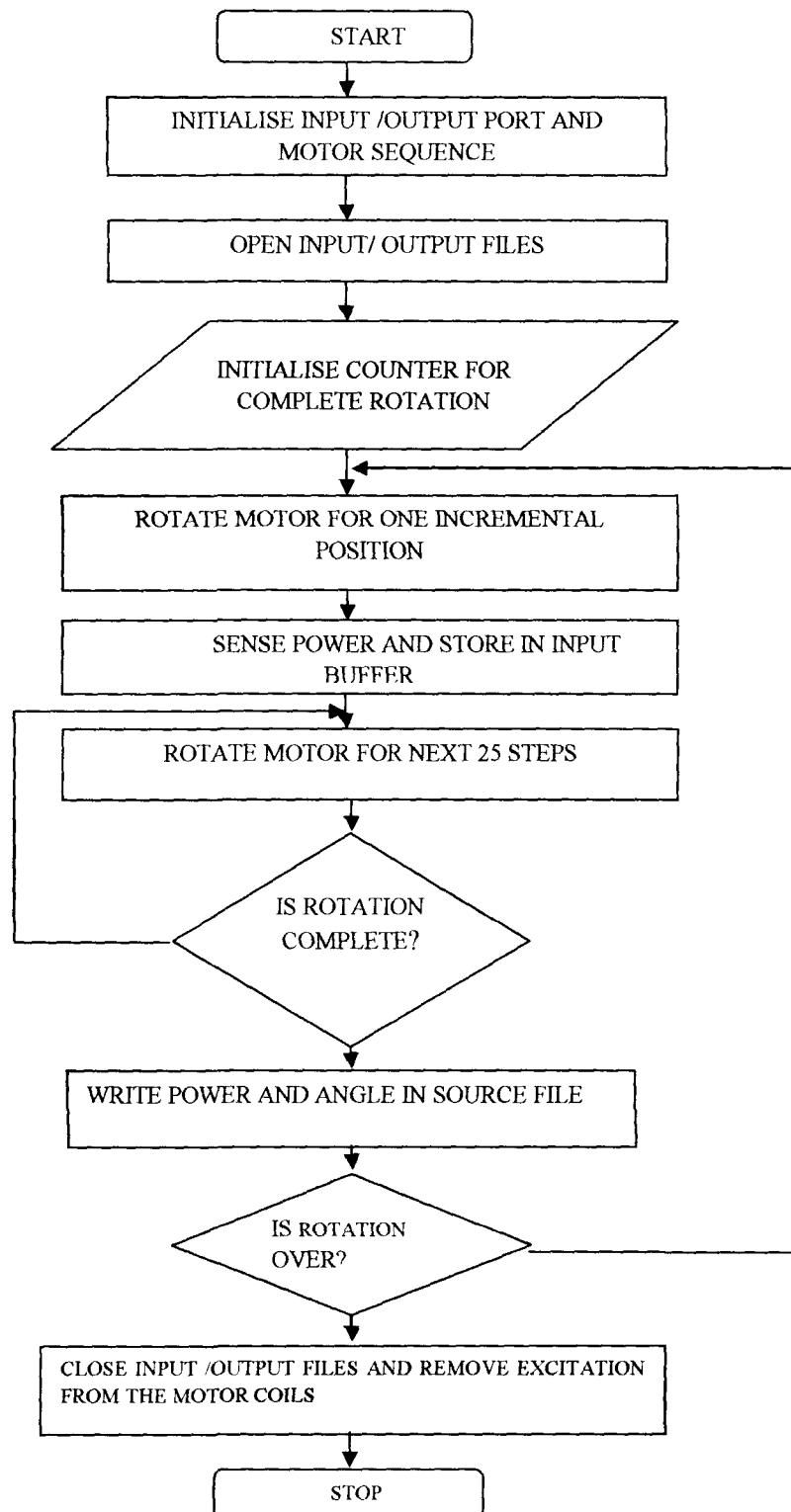


Figure 2.7: Flowchart for data acquisition of power (dB) vs. angle of rotation ( $\theta$ )

## 2.5 Results

Standard horn antenna is antenna is at the receiving end to test the measurement system The radiation pattern acquired using the automated system is shown in figure 2.8 Repetition of the measurements is carried out to verify the accuracy of the results

The time taken for complete set of measurement is about 4 minutes as compared to 10-12 hours for manual measurements

The results show excellent repeatability The performance of automated system is detailed in table 2.4

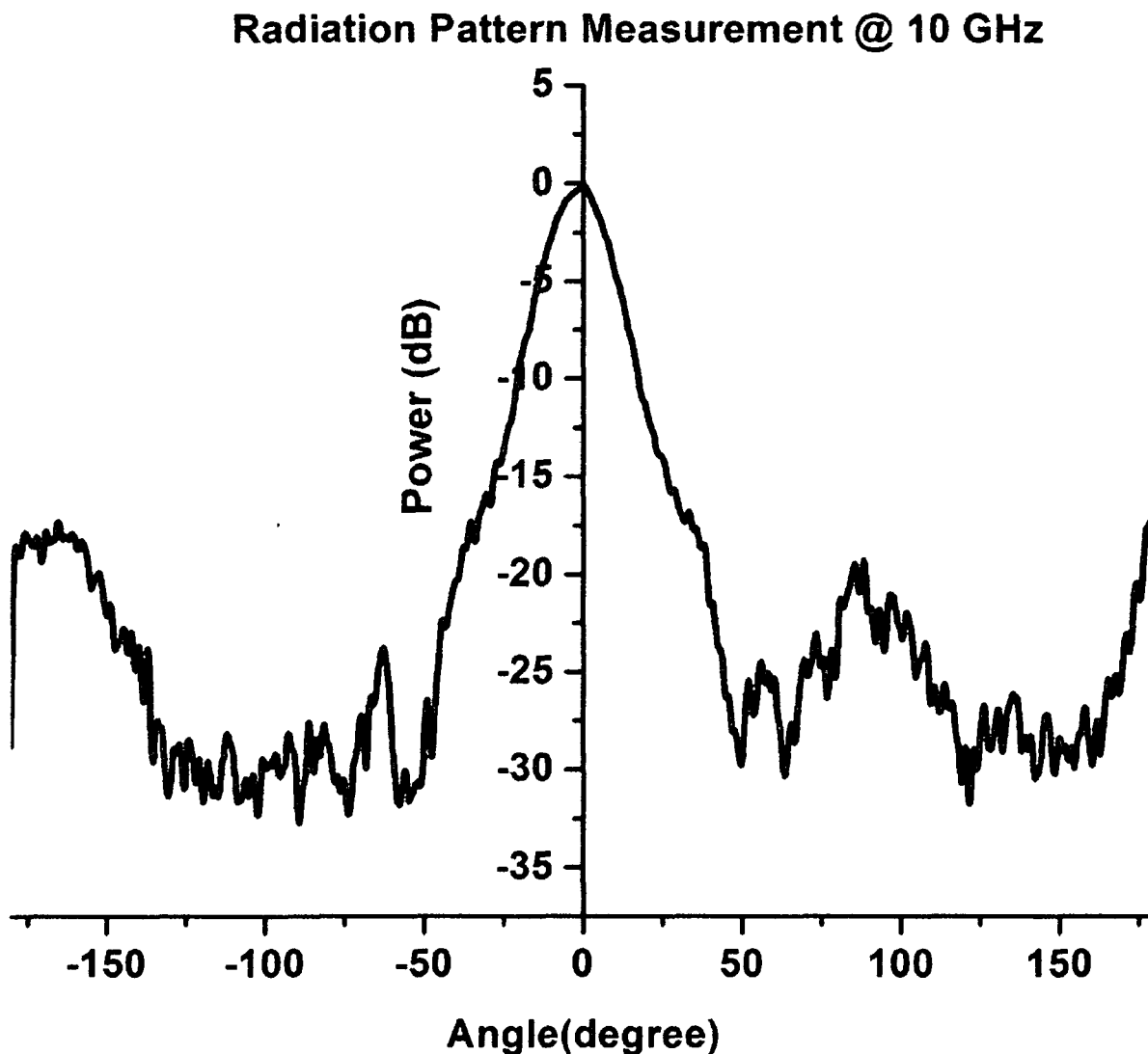


**Figure 2.8:** Measurement of received power vs. angle for antenna under test

Some spikes has been observed in the measured results The spikes generated in the measured results are due to the undesired reflections from different sources such as wall reflections and surrounding objects etc The curve could have been smoother if the measurements were taken in anechoic chamber However the measured radiation pattern

results are almost same with the standard antennas tested for calibration accuracy and repeatability.

A performance comparison measurement results between manually obtained and from the developed automated set-up is carried out which justifies the cost effectiveness (non-anechoic chamber), time and less supervision of users summarized in the following table.

**Table 2.4:** Performance evaluation of automated set-up

<i>Performance</i>	<i>Automated setup</i>	<i>Manual setup</i>
Time(for one complete set of data )	40 minutes 20 seconds	10-12 hours
Number of data points	1600	400
Modified angle increment	0.225 degree	1.8 degree
Minimum measurable angle increment	0.009 degree	1.8 degree

## 2.6 Chapter summary

A PC based automated pattern antenna measurement system has been developed. The system consists of a spectrum analyzer in the frequency range of 10 KHz to 20 GHz for measurement of the received test signal and an Agilent signal generator with a frequency range of 10 KHz to 20 GHz. Alternatively, a USB power sensor Agilent U2008 is also interfaced for power measurement. Antenna rotation in the azimuthal plane is carried out using a specially designed and fabricated wooden antenna turn table driven by a PC controlled stepper motor. Worm and spur gears are designed and fabricated to increase the rotation torque of the turn table. The gears are fabricated out of 1 cm thick nylon sheet. A coaxial rotary joint is mounted on the rotating shaft to couple the signal from the cable mounted on the rotating antenna mount on to the fixed end without twisting of cables.

Driver circuit for the stepper motor is designed and implemented. The LPT1, LAN and USB ports in the controlling PC are used to communicate with the different modules including the stepper motor driver circuit. Computer program for complete automation of the measurement process is developed. System accuracy and repeatability are confirmed using tests on standard pyramidal horn antennas. Test patterns are continuous with smooth curves as compared to the manually obtained patterns as a large number of data points can be acquired with a relatively shorter time. Human involvement is required only for mounting the antenna and setting the frequency of measurement. A program for measurement of return loss is also developed and evaluated for repeatability. The

configuration is essentially a reflectometry measurement set up with a dual directional coupler.

The overall system performs satisfactorily and many of the measured results presented in the subsequent chapters are obtained using the automated measurement system described in the chapter.

## CHAPTER III

# PLANAR AND ELEVATED MICROSTRIP PATCH ANTENNA WITH SLITS

---

### 3.1 Introduction

### 3.2 Planar patch prior to introduction of slits

### 3.3 Simulation for feed point and slit widths

### 3.4 Fabrication of patch with slits

### 3.5 Measured results

### 3.6 Patch with single partial slit

#### *3.6.1 Measured return loss for patch with varying slit length*

#### *3.6.2 Radiation pattern measurements for patch with different slit lengths*

### 3.7 Patch with slit isolated elevated sections

#### *3.7.1 Design and fabrication of elevated patch antenna with slits*

#### *3.7.2 Return loss measurement of simple patch antenna*

#### *3.7.3 Measured results for simple and profiled patch antenna*

#### *3.7.4 Radiation pattern measurements for profiled patch antenna*

### 3.8 Chapter summary

### References

### 3.1 Introduction

The importance of the tuning approach can essentially be attributed to an emphasis on designing a simple patch antenna that can operate simultaneously in different bands as well as tuning of the resonant frequencies within these bands. Development of tunable antennas is of late a prime research interest because of the increasing number of global wireless standards [1-3]. Multiband antennas are required in order to achieve miniaturization in mobile and wireless systems including personal communications, bluetooth, wireless local networks etc. MEMS, PIN diodes and varactor diodes are also used for tuning the resonating frequency of a patch antenna [4-5]. Varying the substrate property using ferrites and ferroelectrics is another approach for tuning [6]. Microstrip patch antennas (MPA) can also be tuned by loading the patch with varying reactive elements (capacitive or inductive). One technique involves changing of the length of a small stub attached to the regular shaped MPA or using varying numbers of shorting posts. Resonant frequency of MPA can also be tuned by varying the air gap between the patch and ground plane [7]. Numerous applications such as satellite links, wireless local area networks, cellular telephones, synthetic aperture radar and radio frequency identifications require dual band antennas [8-10]. Consequently, tunable and dual band antennas are important design considerations for these applications [11-12]. Moreover, two parasitic patch antennas can be gap coupled through cutting a slit near a radiating edge [13].

Tuning of the resonant frequency covering different bands is an important aspect in the context of present day wireless communication and the design approach is focused on achieving reasonable tuning by suitable variation of structural parameters. The main objective of the work is to study the effect of electromagnetic coupling between different sections of the patch obtained by introducing slits near the radiating edges and subsequently profiling the isolated patch sections.

Based on survey of the various techniques available in the literature, an antenna is designed for bandwidth enhancement, size reduction as well as tuning.

In this chapter, at first planar patch antenna with two slits parallel to the radiating edges is studied. The structure is then modified by introducing only one slit near one of the edges, once near the edge closer to the feed point and subsequently near the other edge. The single slit structure is then further modified with the slit length reduced to less than the patch width leaving the outer patch section connected partially to the inner patch section.

The isolated patch sections due to slits running through the patch width are profiled by raising the sections at an angle, the end at the slit side being at the substrate plane while the other end elevated above the substrate plane. Effect of elevation angles on antenna performance is studied. The antennas are fabricated and measured results are presented in this chapter. The results indicate enhancement of bandwidth as well as tunability of both lower and higher frequencies with variation of elevation angles.

### 3.2 Planar patch prior to introduction of slits

The following sections detail the design procedure of the planar patch antenna, which is used as the structural basis for the modified rectangular microstrip patch antenna with slits. The antenna is fabricated and characterized for its return loss ( $RL$ ) and radiation patterns.

The rectangular microstrip antenna (RMSA), because of its structural symmetry, can be analyzed using simple models and hence is one of the simplest and widely used MSA configurations. Figure 3.1 shows the basic structure of a coaxially fed RMSA.

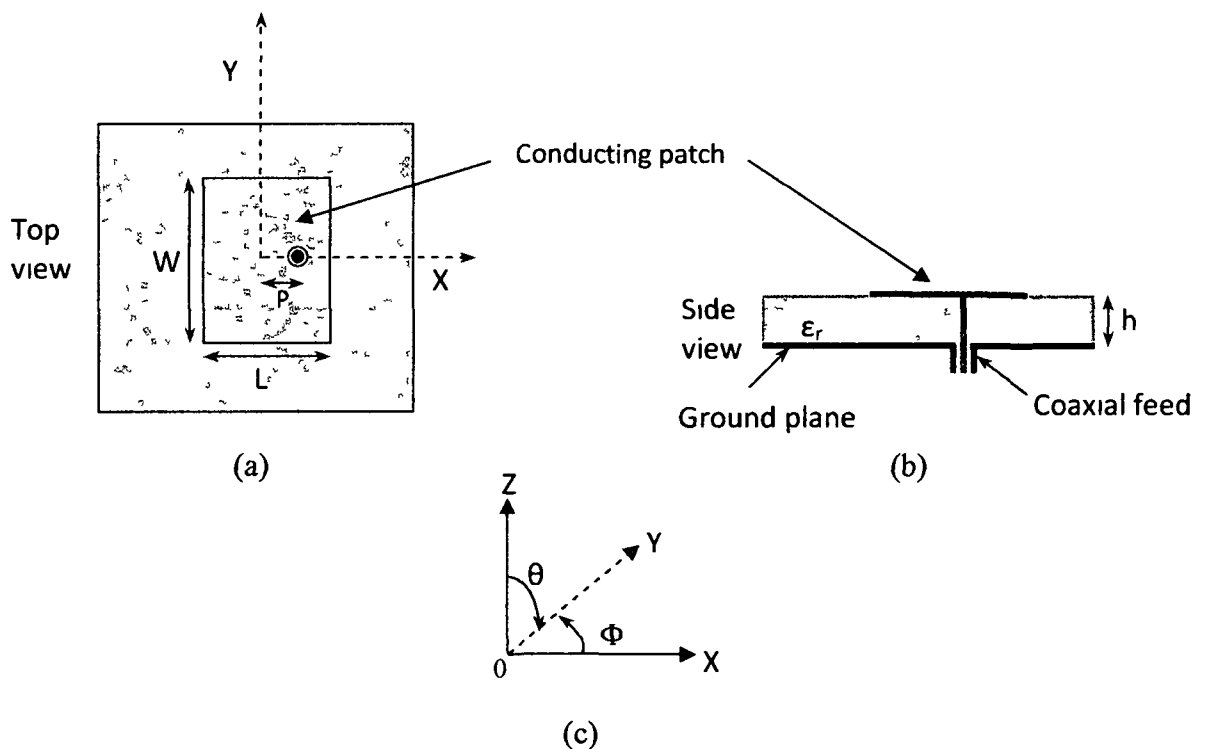


**Figure 3.1:** Coaxially fed rectangular patch antenna

(a) Top view

(b) Side view

(c) Coordinate system.



For the fundamental  $TM_{10}$  mode, the patch length  $L$  (figure 3 1) should be marginally less than  $\lambda/2$ , where  $\lambda$  represents wavelength in substrate medium Here  $\lambda$  is equal to  $\lambda_0 / \sqrt{\epsilon_{reff}}$  where  $\lambda_0$  is the free space wavelength and  $\epsilon_{reff}$  is effective dielectric constant The value of  $\epsilon_{reff}$  is slightly less than  $\epsilon_r$ , as the fringing fields around the periphery of the patch are not confined within the dielectric substrate but also spreads in the air as is evident from figure 3 2 (a) The following expression gives the approximate value of  $\epsilon_{reff}$  [14]

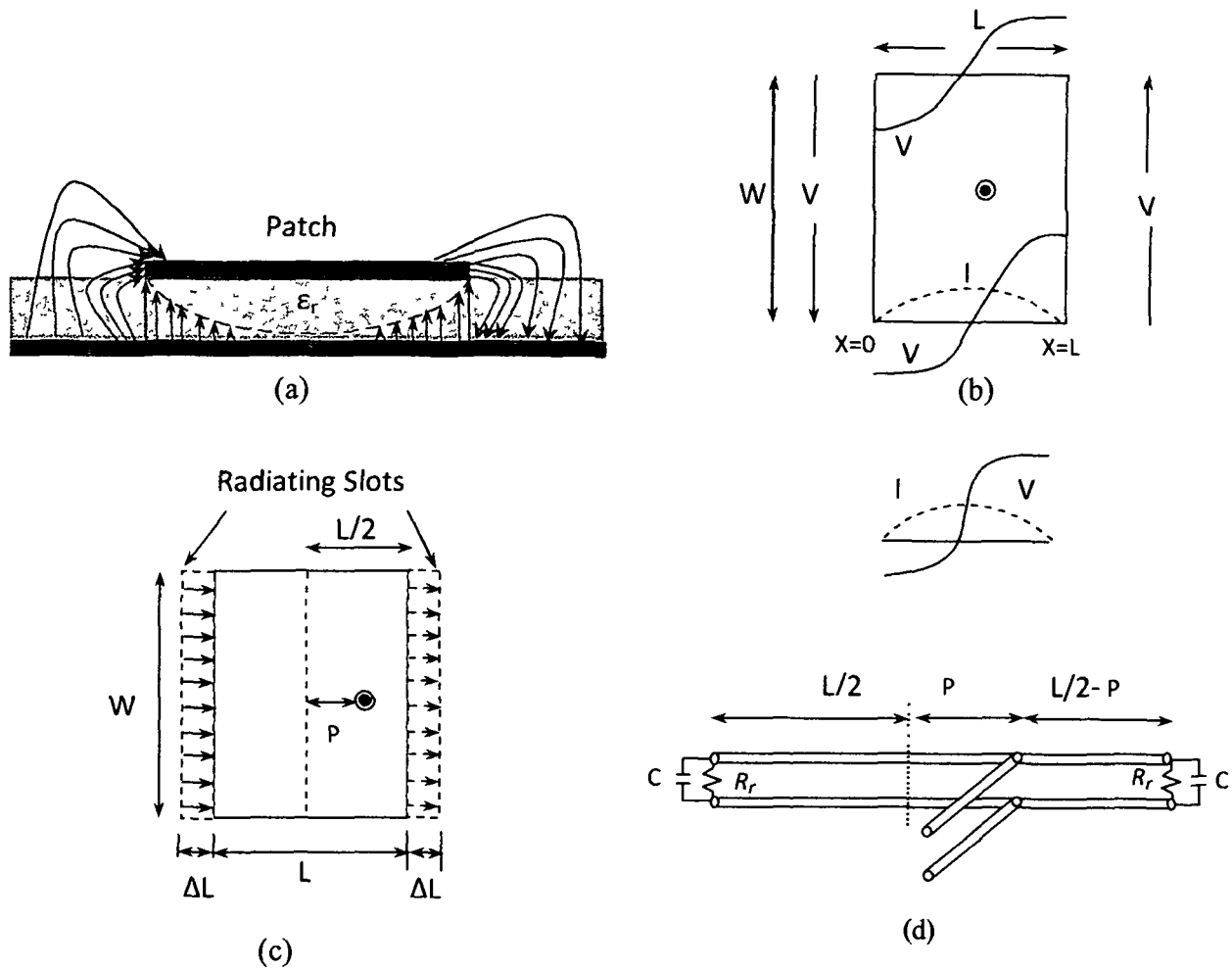


**Figure 3.2:** Rectangular microstrip patch antenna in the  $TM_{10}$  mode

- (a) E-field distribution
- (b) Voltage and current variation
- (c) Radiating slots of RMSA
- (d) Equivalent transmission line model.

$$\epsilon_{re\text{ff}} = \frac{(\epsilon_r + 1)}{2} + \frac{(\epsilon_r - 1)}{2} \left[ 1 + \frac{12h}{W} \right]^{-1/2} \quad \text{-----} \quad (3.1)$$

RMSA operating in the fundamental  $\text{TM}_{10}$  mode can be modeled as a transmission line as the field is uniform along the width and varies along the length. For the transmission line model (TLM), the equivalent capacitance and radiation resistance are as shown in figure 3.2 (d) and the fringing fields along the edges and radiating slots are as shown in figure 3.2 (c).

Ignoring the capacitance due to the fringing fields along the periphery the equivalent capacitance can be estimated by assuming two rectangular conducting plates of dimensions  $L$  and  $W$  separated by dielectric substrate of thickness  $h$  [15] using the following expression:

$$C = \epsilon_0 \epsilon_r \frac{W L}{h} \quad \text{-----} \quad (3.2)$$

The effective capacitance  $C_e$  of the two parallel plates increases due to the fringing capacitance attributable to the fringing fields. The value of  $C_e$  can be estimated from:

$$C_e = \epsilon_0 \epsilon_r \frac{W_e L_e}{h} \quad \text{-----} \quad (3.3)$$

where  $L_e$  and  $W_e$  are the effective length and width of the patch.

Because of the fringing effects, electrically the patch of microstrip antenna looks greater than its physical dimensions. For principal E - plane, the dimension of the patch along its length has been extended on each end by a distance  $\Delta L$ , which is a function of effective dielectric constant  $\epsilon_{re\text{ff}}$  and width to height ratio  $\frac{W}{h}$ . A very popular and practical relation for normalized extension of length is [16]:

$$\frac{\Delta L}{h} = 0.412 \frac{(\epsilon_{re\text{ff}} + 0.3) \left( \frac{W}{h} + 0.264 \right)}{(\epsilon_{re\text{ff}} - 0.258) \left( \frac{W}{h} + 0.8 \right)} \quad \text{-----} \quad (3.4)$$

Since the length of the patch has been extended by  $\Delta L$  on each side, the effective length of the patch is now

$$L_e = L + 2\Delta L \quad \text{-----} \quad (3.5)$$

Since the effective length of the patch is equal to  $\lambda/2$ ,  $L_e$  can be calculated for a given resonant frequency  $f_0$  as:

$$L_e = L + 2\Delta L = \frac{\lambda}{2\sqrt{\epsilon_{reff}}} = \frac{c}{2f_0\sqrt{\epsilon_{reff}}} \quad \text{-----} \quad (3.6)$$

where  $c$  = velocity of light in free space. Hence, equation (3.6) simplifies to:

$$L_e = \frac{15}{f_0\sqrt{\epsilon_{reff}}} \quad \text{-----} \quad (3.7)$$

where  $L_e$  is in cms and  $f_0$  in gigahertz. For a given  $L$ ,  $f_0$  is calculated from

$$f_0 = \frac{c}{2L_e\sqrt{\epsilon_r}} = \frac{15}{L_e\sqrt{\epsilon_r}} \quad \text{-----} \quad (3.8)$$

The resonant frequency for RMSA for any  $T_{mn}$  mode is generally obtained by the following equation [16]

$$f_0 = \frac{c}{2\sqrt{\epsilon_{reff}}} \left[ \left( \frac{m}{L} \right)^2 + \left( \frac{n}{W} \right)^2 \right]^{\frac{1}{2}} \quad \text{-----} \quad (3.9)$$

where,  $m$  and  $n$  corresponds to the sides  $L$  and  $W$  respectively.

$\epsilon_r$  can be obtained approximately from [14]

$$W = \frac{c}{2f_0\sqrt{\frac{(\epsilon_r + 1)}{2}}} \quad \text{-----} \quad (3.10)$$

The antenna bandwidth (BW) is generally affected by the width ( $W$ ) which increases or decreases with increase or decrease in  $W$  as does the antenna directivity. The BW and directivity (D) of RMSA is given by the following equations

$$\%BW = \frac{Ah}{\lambda_0\sqrt{\epsilon_r}} \sqrt{\frac{W}{L}} \quad \text{-----} \quad (3.11)$$

$$\text{where } A = 180 \quad \text{for} \quad \frac{h}{\lambda_0\sqrt{\epsilon_r}} \leq 0.045$$

$$A = 200 \quad \text{for} \quad 0.045 \leq \frac{h}{\lambda_0\sqrt{\epsilon_r}} \leq 0.075$$

$$A = 220 \quad \text{for} \quad \frac{h}{\lambda_0\sqrt{\epsilon_r}} \geq 0.075$$

where,  $W$  and  $L$  are the length and width of the RMSA. However, to avoid higher order modes,  $W$  should not exceed  $\lambda$ . The relationship between directivity and width of a RMSA can be approximated by

$$D = 0.2W + 6.6 + 10 \log (1.6\sqrt{\epsilon_r}) \text{ dB} \quad \text{-----} \quad (3.12)$$

The radiation pattern of an RMSA for  $TM_{10}$  mode can be calculated by combining the radiation pattern of two parallel slots of length  $W_e$  and width  $\Delta L$  over an infinite ground

plane separated by a distance of  $L + \Delta L$ . The normalized patterns in the E - plane ( $E_\theta$  in  $\Phi = 0^\circ$  plane (figure 3.1 (c))) and the H -plane is given by the following equations

$$E_\theta = \frac{\sin\left(\frac{k_0 \Delta L \sin \theta}{2}\right)}{k_0 \Delta L \sin \theta} \cos\left(\frac{k_0(L + \Delta L)}{2} \sin \theta\right) \quad \text{-----} \quad (3.13)$$

$$E_\Phi = \frac{\sin\left(\frac{k_0 W_e}{2} \sin \theta\right)}{\frac{k_0 W_e}{2} \sin \theta} \cos \theta \quad \text{-----} \quad (3.14)$$

where  $\theta$  is the angle measured from the broadside direction as shown in figure 3.1 (c) and for very small thickness of the patch antenna ( $k_0 h \ll 1$ ).

In the above expression,  $k_0$  is the wave number given by  $k_0 = 2\pi/\lambda_0$ . The fields are normalized with respect to  $E_\Phi(\theta = 0^\circ)$  and  $V_0$  is given by  $V_0 = h E_0$  is the voltage across the slot.

For thin substrates ( $k_0 h \ll 1$ ),  $E_\theta$  can be reduced to

$$E_\theta = \cos\left(\frac{k_0(L + \Delta L)}{2} \sin \theta\right) \quad \text{-----} \quad (3.15)$$

The radiated power can be obtained by integrating the radiated fields from which the radiation resistance can be obtained. An approximate method for finding radiation resistance is to first calculate the radiation resistance,  $R_r$  of the slot, which is given by

$$R_r = 120 \frac{\lambda_0}{W_e} \quad \text{for } W_e \geq 2 \lambda_0$$

$$R_r = \frac{1}{\left(\frac{W_e}{120 \lambda_0} - \frac{1}{60\pi^2}\right)} \quad \text{for } 0.35\lambda_0 \leq W_e \leq 2 \lambda_0 \quad \text{-----} \quad (3.16)$$

$$R_r = 90 \left(\frac{\lambda_0}{W_e}\right) \quad \text{for } W_e \leq 0.35 \lambda_0$$

Instead of using the above expressions, following single line formula could be used for better accuracy [17]

$$R_r = \frac{w_e^2}{6(60 + w_e^2)} \quad \text{-----} \quad (3.17)$$

where,  $w_e = k_0 W_e$  and  $k_0 =$  free space wave propagation constant  $= \frac{2\pi}{\lambda_0}$

The input impedance of the RMSA varies from zero at its centre to maximum value at the radiating edges. For co-axial feed at a distance  $x$  from the centre, the input impedance ( $R_{in}$ ) of the RMSA at resonant can be calculated using the following formula:

$$R_{in} = R_e \sin^2\left(\frac{\pi x}{L}\right) \text{ for } 0 \leq x \leq L/2 \quad \text{-----} \quad (3.18)$$

where  $R_e = \frac{1}{2(G_r + G_m)}$

where  $G_r = \frac{1}{R_r}$  is the slot conductance and  $G_m$  is the mutual conductance, which

accounts for mutual coupling between the two slots and is given by:

$$G_m = G_r F_g \quad \text{-----} \quad (3.19)$$

$$F_g = J_0(l) + \frac{p^2}{24 - p^2} J_2(l) \quad \text{-----} \quad (3.20)$$

where  $l = k(L + \Delta L)$ ,  $p = k \Delta L$ ,  $J_0(l)$  and  $J_2(l)$  are zero- and second-order Bessel functions respectively.

### 3.3 Simulation for feed point and slit widths

The rectangular patch antenna is designed in the C - band at 4.85 GHz using TLM described in the previous section. The patch antenna specifications are given in table 3.2 and the patch dimensions are marked in figure 3.8 (a). Simulated results show a resonant frequency of 4.2 GHz, which remains unchanged with feed point location as against 4.85 GHz calculated using TLM model while the only return loss changes. Figures 3.3 to 3.5 show the simulated values of return loss ( $RL$ ), VSWR and impedance with feed point location respectively.

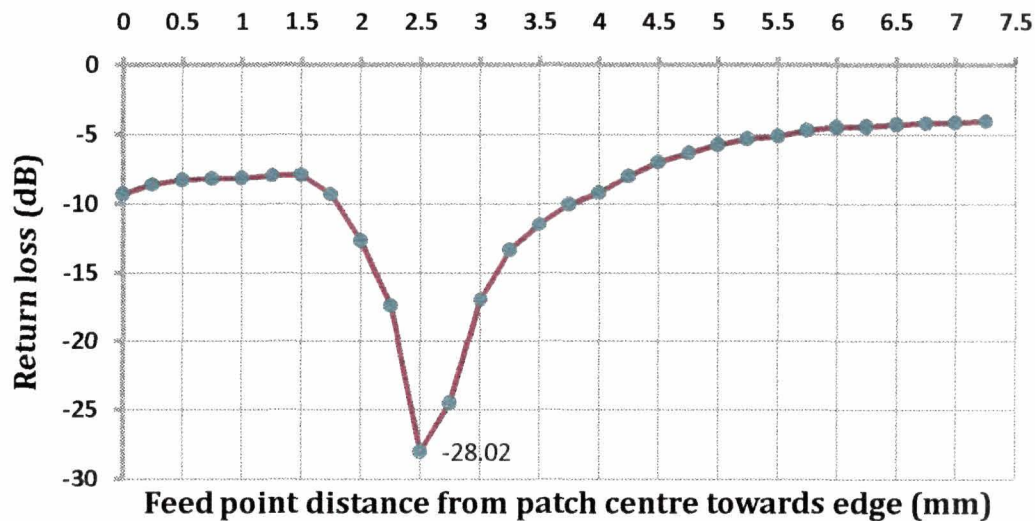
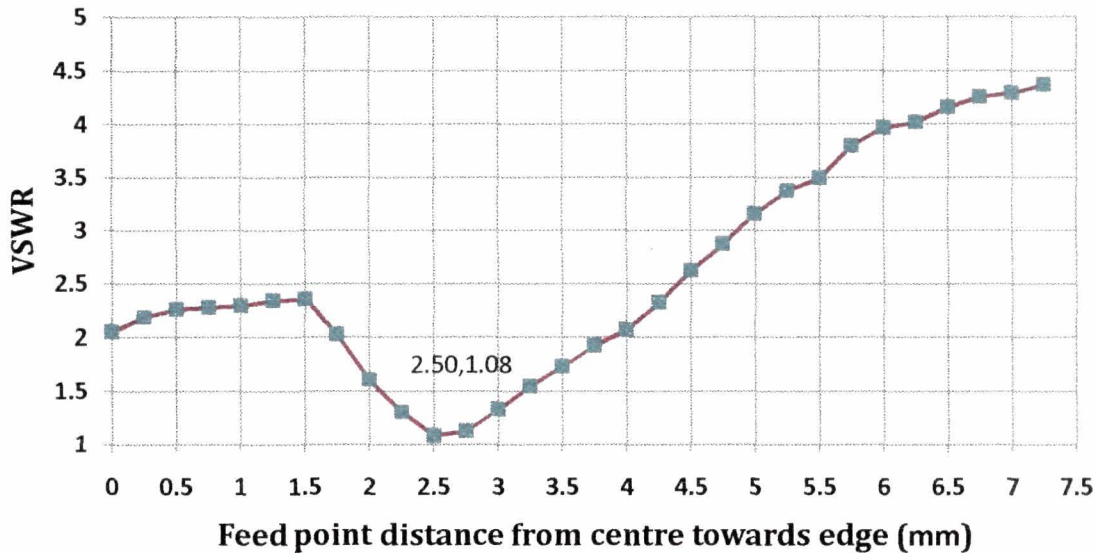


Figure 3.3: Simulated plot of return loss vs. feed point location (at 4.2GHz)

Feed point location for best matching is simulated by moving the feed point location in steps of 0.25 mm starting from the centre along the patch length towards the radiating edge. Simulated return loss ( $RL$ ) value of -28.02 dB is obtained when feed point is moved 2.5 mm from centre towards the radiating edge along the length of the patch as shown in figure 3.3.



**Figure 3.4:** Simulated plot of VSWR vs. feed point location

The corresponding VSWR value at 4.20 GHz is 1.08 for the feed point location at 2.5 mm from the centre towards the radiating edge as shown in figure 3.4. An impedance value of  $46.43 \Omega$  is obtained at this feed point location as shown in figure 3.5. Figure 3.6 shows the simulated smith chart plot.

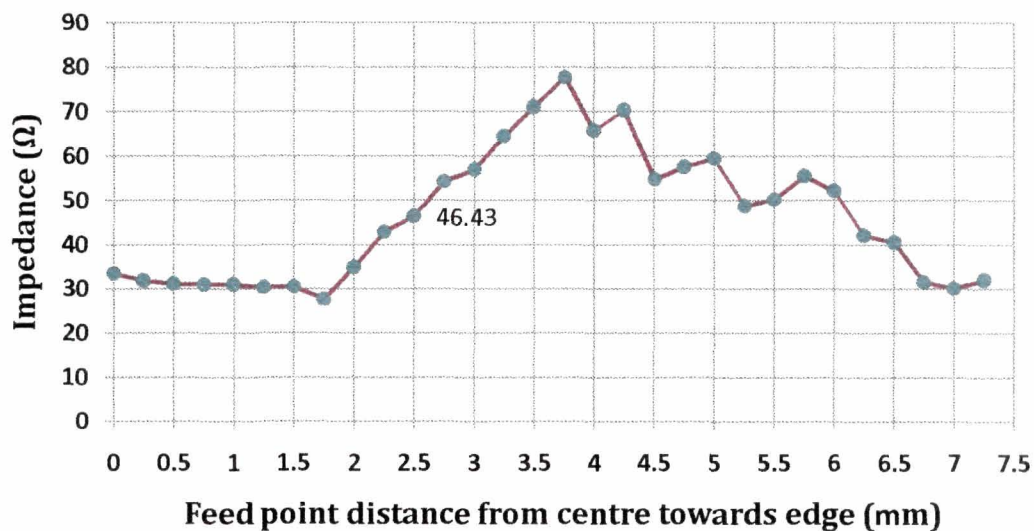


**Figure 3.5:** Simulated plot of impedance (real part) vs. feed point location



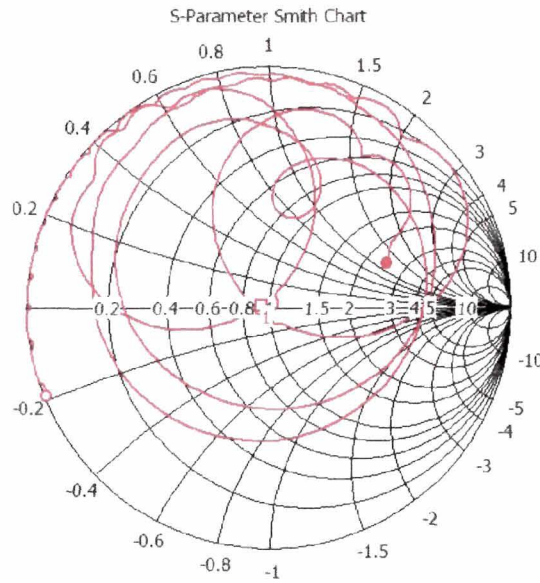
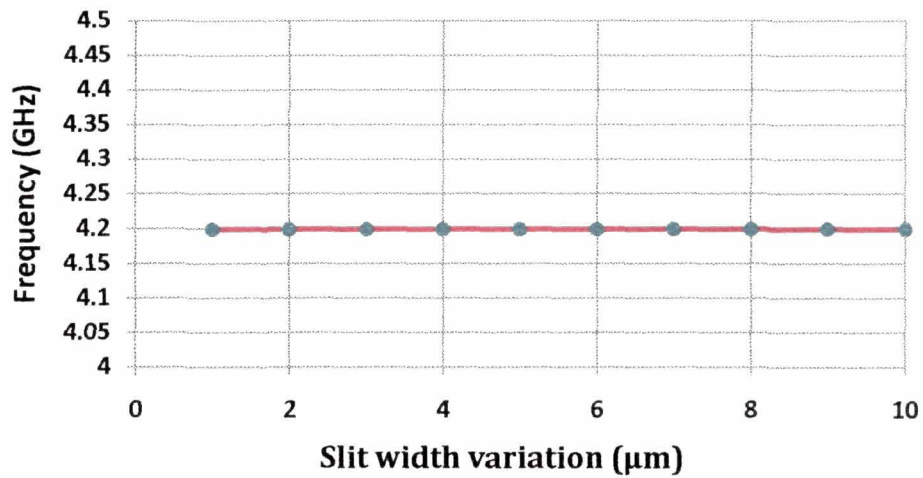


**Figure 3.6:** Simulated plot of smith chart at 4.2 GHz for frequency sweep 2-6 GHz

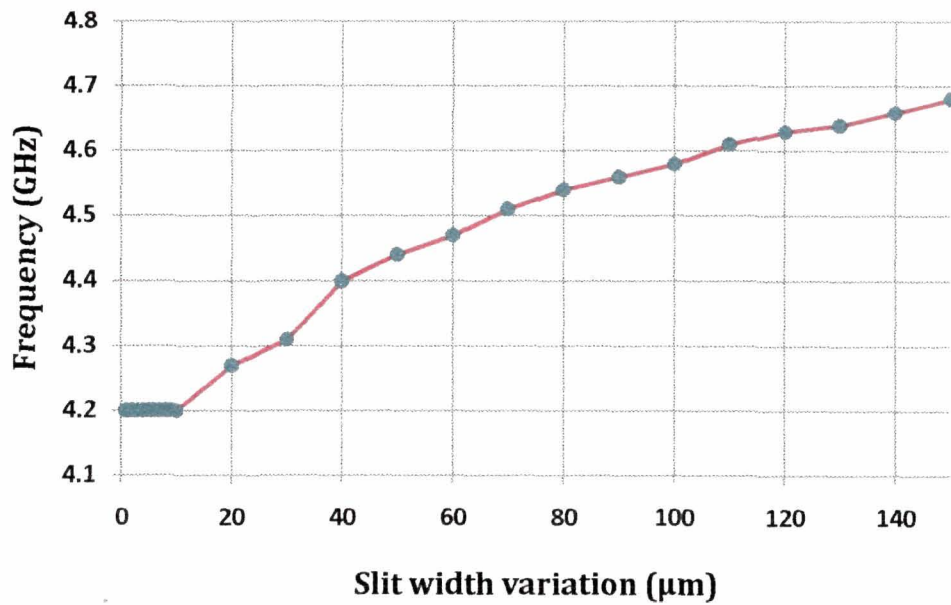
A pair of narrow slits parallel to and near the radiating edges is introduced in the simple patch. The slits introduced are at a distance of 2.5 mm from the radiating edges. Thus, position of the slits on either side of feed point is not equidistant from the feed point. Further, slit widths are varied from  $0\ \mu\text{m}$  to  $10\ \mu\text{m}$  in steps of  $1\ \mu\text{m}$  and  $10$  to  $100\ \mu\text{m}$  in steps of  $10\ \mu\text{m}$  to study the effect of capacitive coupling between the main patch and the isolated patch sections. Effect of slit width variation on resonant frequency and  $RL$  is simulated prior to fabrication of prototypes. The simulated results indicate that when the slit width is varied from  $1\ \mu\text{m}$  to  $10\ \mu\text{m}$ , the resonant frequency remains unaffected at a value of 4.2 GHz (table 3.1 (a)). Subsequently, the slit width is varied from  $10\ \mu\text{m}$  to  $100\ \mu\text{m}$  when the resonant frequency changes from 4.2 GHz to 4.6 GHz. It is observed that the matching degrades as the slit width is increased as is summarized in table 3.1 (a) and (b), probably due to progressive weakening of the capacitive coupling between patch sections. The shift in resonant frequency with slit width variation is shown figure 3.7.

From this table 3.1 (a), it is observed that the best return loss obtained is for a slit width ( $w_s$ ) before  $4\ \mu\text{m}$ , however fabrication facilities for such a narrow slits for which the edges along the conductor thickness also needs to be vertically flat, are not available. Due to this limitations, the smallest slit width that could be fabricated to a reasonably accuracy using the standard etching process is  $100\ \mu\text{m}$ .

As the objective of introducing the slits (and then fabricating them) is to study the its effect on antenna performance, it can be considered as reasonable compromise with the expectation that the general trends of change will be manifested.



(a)



(b)

**Figure 3.7:** Simulated plot of slit width variation vs. shift in resonant frequency(a) 1 -100  $\mu\text{m}$ (b) 10-100  $\mu\text{m}$



**Table 3.1 (a):** Slit width variation (1-10  $\mu\text{m}$ )

<i>Slit width (<math>\mu\text{m}</math>)</i>	<i>Frequency (GHz)</i>	<i>Return loss (dB)</i>
1	4.20	-29.15
2	4.20	-29.15
3	4.20	-29.15
4	4.20	-28.74
5	4.20	-28.74
6	4.20	-28.74
7	4.20	-28.74
8	4.20	-28.74
9	4.20	-28.74
10	4.20	-28.74

**Table 3.1 (b):** Slit width variation (10-100  $\mu\text{m}$ )

<i>Slit width (<math>\mu\text{m}</math>)</i>	<i>Frequency (GHz)</i>	<i>Return loss (dB)</i>
10	4.20	-28.74
20	4.27	-26.47
30	4.31	-25.16
40	4.34	-24.36
50	4.45	-19.30
60	4.48	-17.89
70	4.52	-16.62
80	4.55	-15.99
90	4.57	-15.37
100	4.60	-14.83
110	4.61	-14.30
120	4.63	-13.96
130	4.64	-13.67
140	4.66	-13.39
150	4.68	-13.25

Prototypes of patches are fabricated and tested using the dimensions of simulated values as explained above. The following sections describe the experimental results of designed patch prototypes.

### 3.4 Fabrication of patch with slits

A double-sided copper laminated with glass epoxy substrate of thickness of 1.5 mm has been used for fabrication of antenna, as these are commercially easily available in the market. Although these substrates are relatively lossy as compared to standard microstrip patch antenna substrate materials, prototypes are fabricated using these laminated substrates as the present work essentially focuses on the effects of structural changes on resonant frequency and pattern characteristics.

A coaxially-fed RMSA having patch dimension of  $W = 18$  mm and  $L = 15$  mm (same as simulated patch). The patch is coaxially fed using an SMA probe connector at 2.5 mm from patch centre (table 3.2). Schematic diagrams for the prototypes for simple patch, patch with double slits is shown in figure 3.8 (a) and (b). The patch structure with single slit on one side nearer to the feed point and the side further to the feed point are shown in figure 3.8 (c) and (d) respectively. Table 3.2 gives its dimensions.

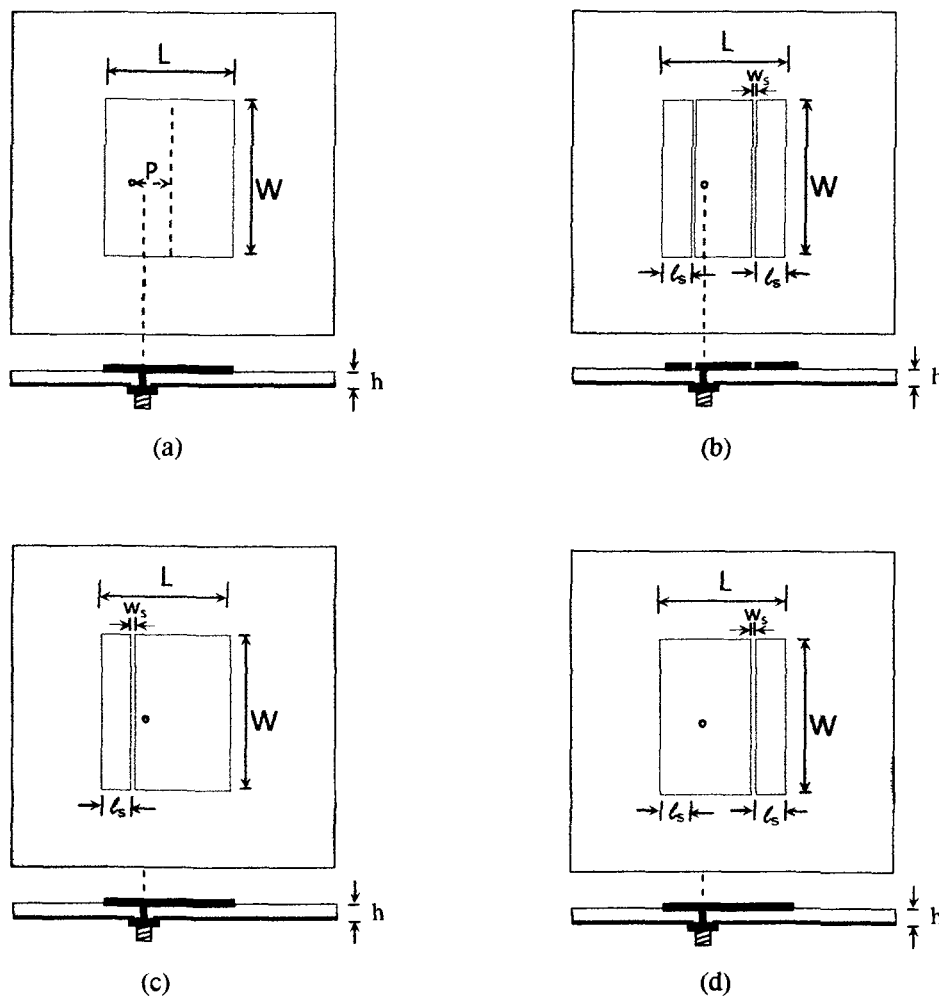


**Figure 3.8:** (a) Planar RMSA  
 (b) Planar RMSA with double slit  
 (c) Planar RMSA with single slit ( $l_s = 2.5$  mm) near to the feed point  
 (d) Planar RMSA with single slit ( $l_s = 2.5$  mm) further from the feed point

**Table 3.2:** Design parameter of RMSA

<i>Parameter</i>	<i>Value</i>
Patch width (W)	18 mm
Patch length (L)	15 mm
Substrate thickness (h)	1.52 mm
Relative dielectric constant ( $\epsilon_r$ ), $\tan\delta$	4.8, 0.001
Feed point distance from centre (p)	2.5 mm
Slit width ( $W_s$ )	100 $\mu\text{m}$
Isolated patch section ( $l_s$ ) dimension along the patch length	2.5 mm

The patches are fabricated using the standard ferric chloride ( $\text{FeCl}_3$ ) etching process. The sample pieces are masked with adhesive tape over the copper surface on both sides. This tape is cut for etching in the requisite dimensions on one of the sides. For connecting the co-axial feed, a hole of diameter equal to the centre probe diameter of the SMA connector is drilled at the feed location on the ground plan side. A small circular section (2.3 mm) centered at this hole is etched on the ground plane for mounting the SMA probe feed. Once measurements on the RMSA is completed, the slits are introduced on the same patch by masking the patch using two parallel masking tape sections leaving a gap of the required width of 100 $\mu\text{m}$ . The specified gap between the tap sections is obtained by multiple cycles of trial and error attempts, each time the gap being measured under a travelling microscope by till eventually arriving at the required gap. A two-stage etching is carried out to obtain sharp and accurate edges of the slit. A relatively concentrated solution for faster etching is used until areas away from the patch are nearly cleared of copper, which is followed by the use of a diluted solution. For both the stages, stirring of the etching solution is done using a small-motorized stirrer. After removing the masking, the patch surface is cleaned using ethanol to remove any residual tape adhesive. A travelling microscope is used for confirming the width of the slit and its uniformity along the slit length. The prototype patch finally selected for measurements has been checked at seven positions along the slit length starting from one end to the other end, showing a maximum error of 5 % (Table 3.3).

**Table 3.3:** Fabricated slit width measurement using travelling microscope

<i>SL. No.</i>	<i>Measurement distance from slit edge (mm)</i>	<i>Slit Width (Micron)</i>
1	1	101
2	3	102
3	6	101
4	9	95
5	12	103
6	15	101
7	18	101

### 3.5 Measured results

Return loss measurements are carried out for the simple patch and patch with slits. Figure 3.9 shows the return loss plot for the simple patch. Return loss plots for the patch with double and single slits on the original patch are shown in figures 3.10. From this figure, the return loss for the patch with single slit is shown separately in figure 3.11.

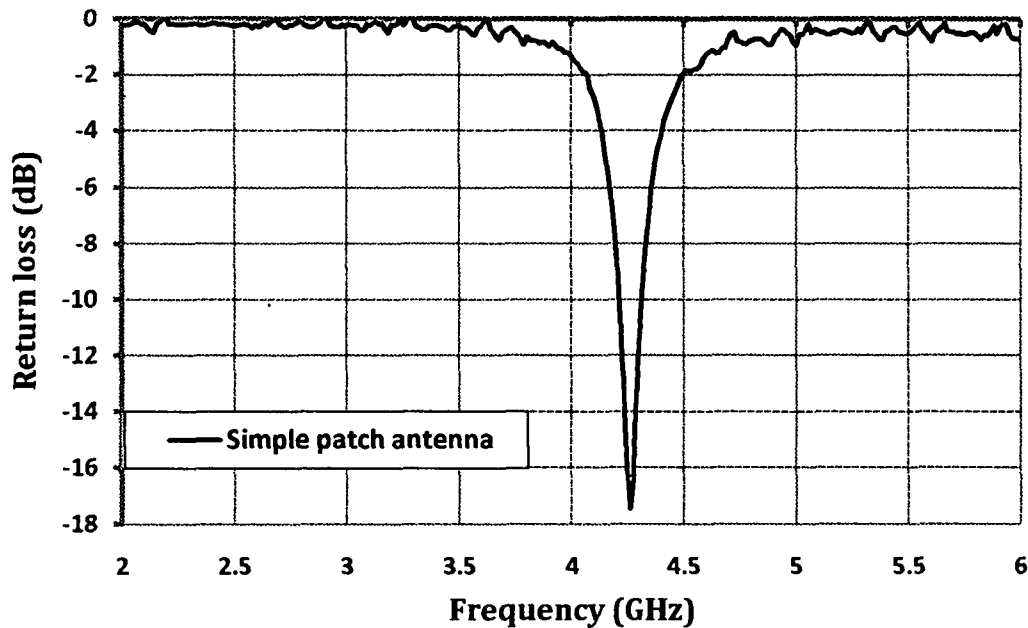


**Figure 3.9:** Return loss vs. resonant frequency for RMSA (feed point at 2.5 mm from patch centre)

The fabricated simple patch resonates at 4.25 GHz with a return loss of -17.46 dB while the simulated results show a resonant frequency of 4.20 GHz with a return loss of -28.74 dB. The shift in measured resonant frequency from simulated value is 1.1% which may be due to fabrication tolerance.

The patch structure is then modified by introducing two slits at equal distances ( $\ell_s = 2.5$  mm) from both the radiating edges (figure 3.8 b).

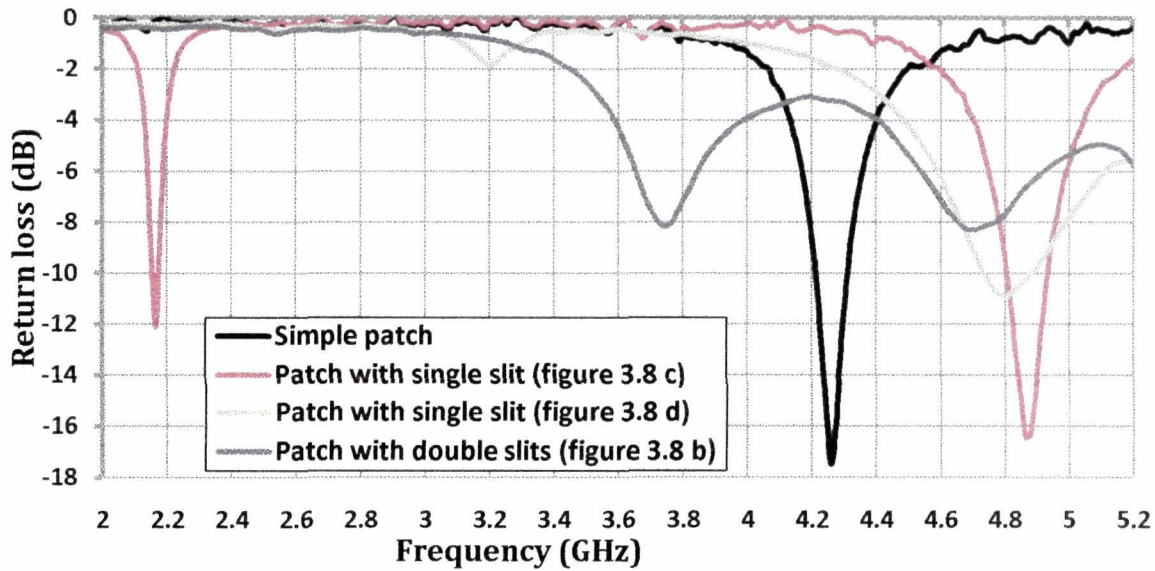


**Figure 3.10:** Return loss vs. frequency for simple patch and patch with slits

Introduction of a pair of slits results in degradation of matching (figure 3.10) although two resonant frequencies one at 3.75 GHz and 4.68 GHz can be seen.

As results with two slits were not very encouraging, instead of changing the position of the slits (which would have required many prototypes, the geometry is modified with one of the two slits removed). The two possible geometries with one slit removed are shown in figures 3.8 (c) and 3.8 (d).

With the single slit at the position shown in figure 3.8 (c), two resonant frequencies are obtained. The higher resonant frequency is above but closer to that for the simple patch (4.25 GHz) at 4.86 GHz. The lower resonant frequency (LRF) on the other hand, is much below at 2.17 GHz in the S- band. Hence, corresponding to the frequency, a significant reduction in antenna size, by as much as 49%, is achieved as is evident from RL plot in figure 3.11.

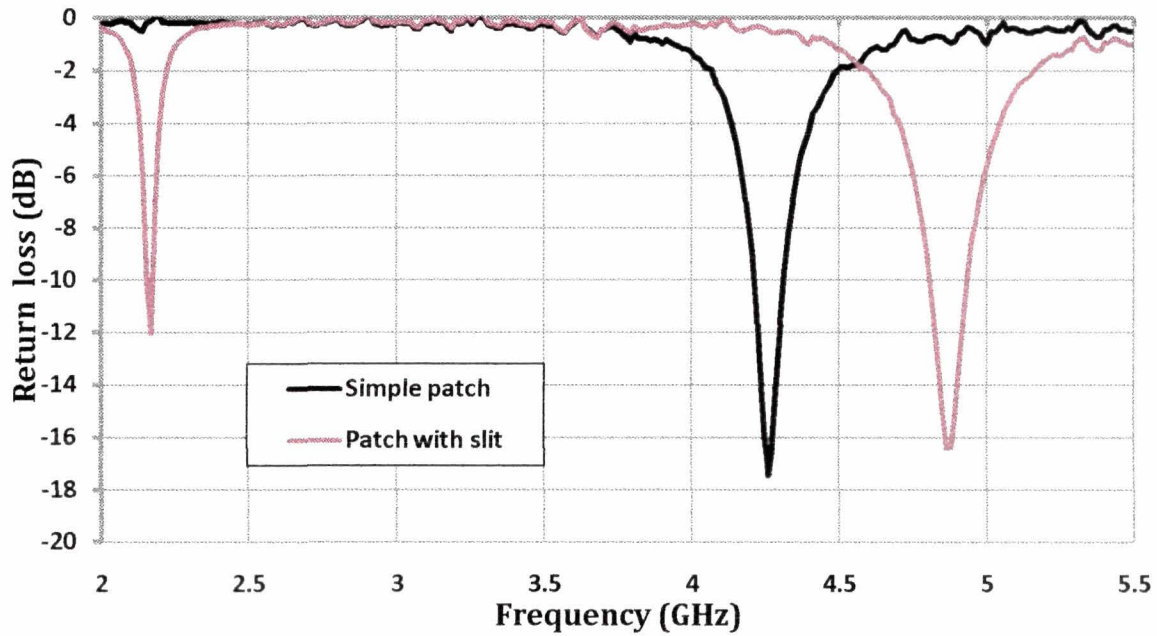


**Figure 3.11:** Measured return loss vs. resonant frequency for simple patch and patch with single slit

In contrast, for the single slit at the relative position as shown in figure 3.8 (d), there is only one resonant frequency which is higher than poorer return loss as compared to the simple patch (figure 3.10). Introduction of this single slit, therefore, results in two desirable effects; significant size reduction and dual frequency operation with the upper frequency moving to the higher side as compared to that of the original patch while a lower resonant frequency showing up in the S- band.

### 3.6 Patch with single partial slit

The slit length, for the geometry shown in (figure 3.8 (c)) which runs through the entire width of the patch as described in the preceding sections is further modified by reducing the slit length leaving a part of the isolated patch section now eclectically connected to the main patch (figure 3.12 (a)). Effect of variation of slit length  $s$  ( $< W$ ) on return loss performance and resonant frequency is discussed in this section.

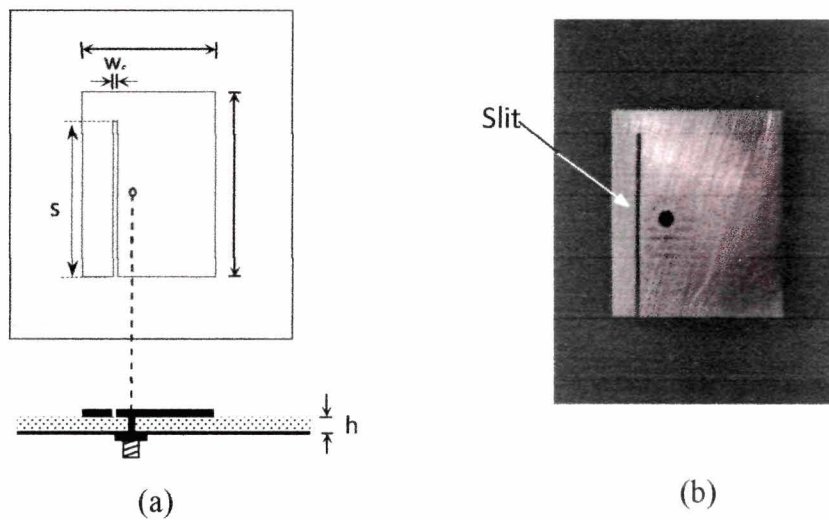


**Figure 3.12:** (a) Patch antenna with partial slit (table 3.4 (a))  
(b) Fabricated patch antenna with partial slit

Patch samples are fabricated with different slit lengths and measurements are carried out for experimentally evaluating the variation in antenna performance characteristics of the fabricated samples.

### 3.6.1 Measured return loss for patch with varying slit length

Measured return loss characteristics for different slit lengths ( $s$ ) are shown in figure 3.13 and plot for change in resonant frequency corresponding to different slit length is shown in figure 3.14.

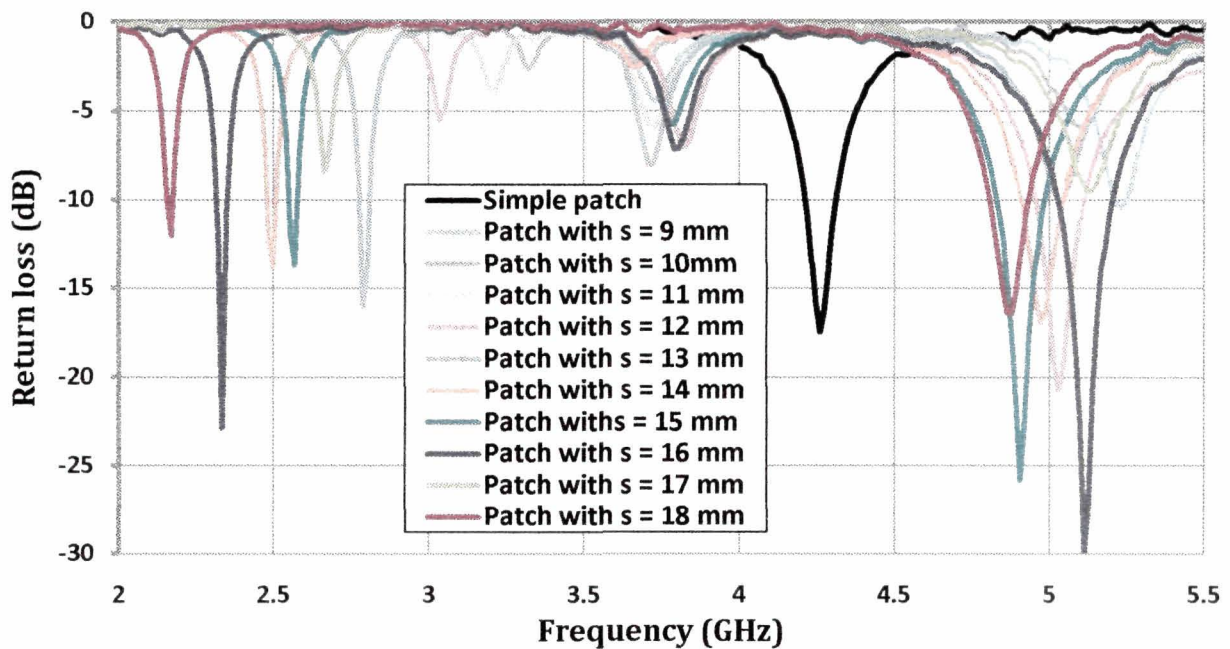


**Figure 3.13:** Measured return loss vs. frequency for different slit length( $s$ )



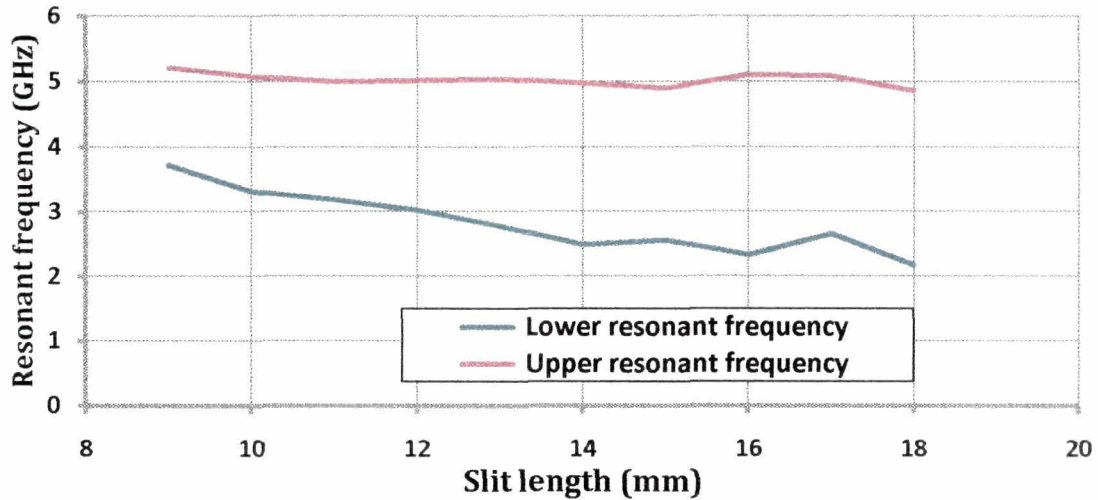


**Figure 3.14:** Slit length vs. resonant frequency (measured)

It can be seen from figure 3.13 that for different slit lengths ( $s < w$ ), the patch resonates at two resonant frequencies. The resonant frequency of the simple patch without slit lies between the two resonant frequencies with partial slits. Moreover, significant improvement in  $RL$  values, both at the lower and upper resonant frequencies are obtained for a slit length of ( $s$ ) 16 mm. The  $RL$  bandwidth ( $BW$ ) of 3.5% at the upper resonant frequency ( $URF$ ) is higher than the  $BW$  of simple patch without slit (2.33%). However, the  $BW$  observed at the lower frequency is only 0.85%. As the slit length is reduced from  $s = w$  to  $s = 9$  mm in steps of 1 mm, both the upper and lower resonant frequencies vary as shown in figure 3.14. As can be seen in the figure, the  $LRF$  has a general reducing trend while the  $URF$  does not vary much with the increase in slit length,  $s$ . Figures 3.15 and 3.16 show the  $RL$  plots for  $LRF$  and  $URF$  respectively for four of the slit lengths ( $s = 13$  mm, 14 mm, 15 mm, 16 mm and 18 mm) for which  $RL$  peaks are at the least -10 dB. The measured values of resonant frequency and return loss for these five slit length are given in table 3.4 (a).



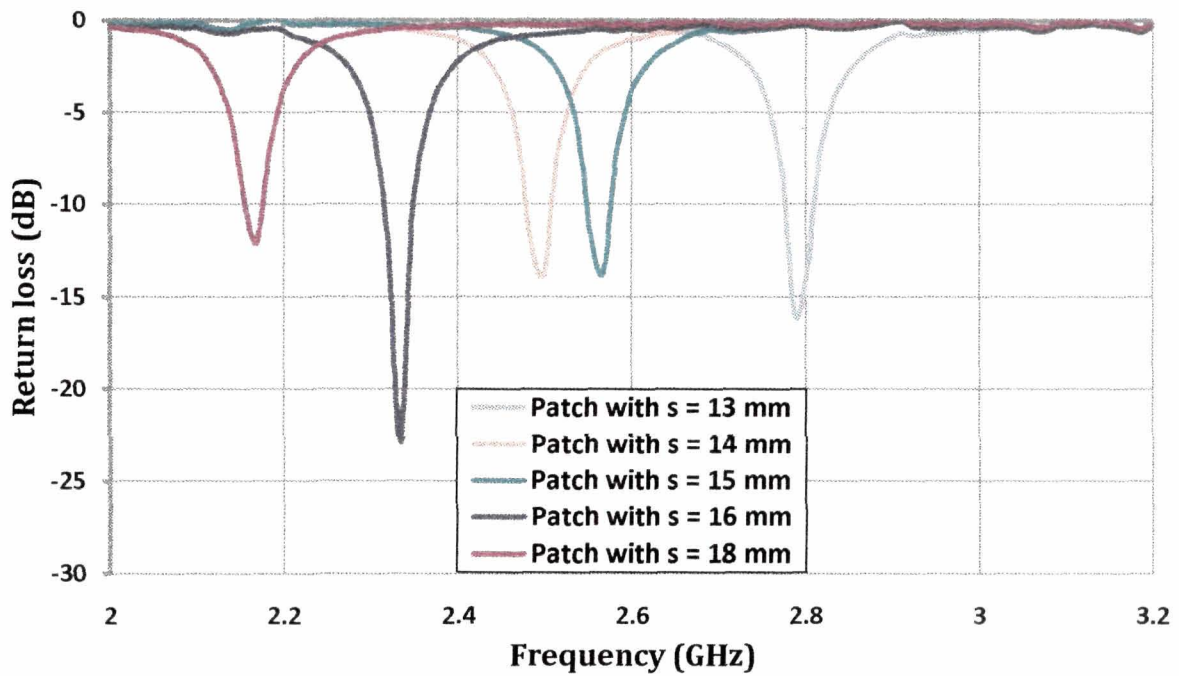


Figure 3.15: Measured return loss plot for different slit length (lower resonant frequencies)

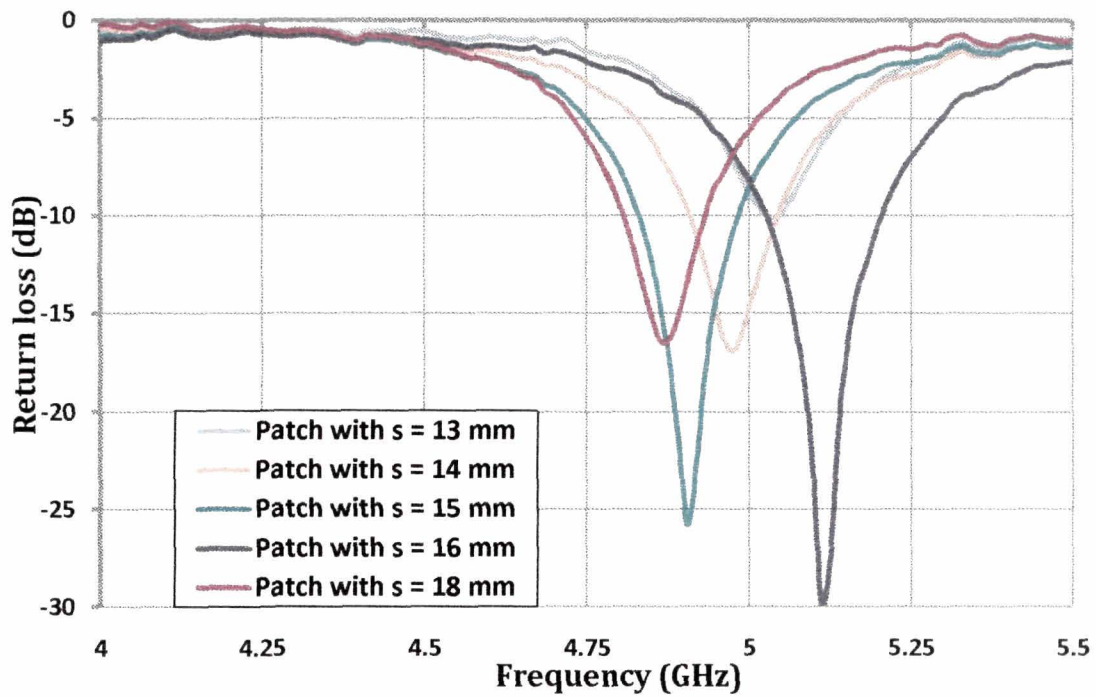


Figure 3.16: Measured return loss plot for different slit length (upper resonant frequencies)

**Table 3.4 (a):** Variation of resonant frequencies and RL with different slit lengths(s)

<i>Antenna type</i>	<i>Lower Frequency (GHz)</i>	<i>Return loss (dB)</i>	<i>Upper Frequency (GHz)</i>	<i>Return loss (dB)</i>
Simple Patch	--	--	4.25	-17.46
s = 18.0 mm = width of patch (w)	2.17	-12.00	4.86	-16.39
s = 16.0 mm	2.33	-22.84	5.11	-29.90
s = 15.0 mm	2.56	-13.71	4.90	-25.81
s = 14.0 mm	2.49	-13.80	4.98	-16.18
s = 13.0 mm	2.78	-15.97	5.04	-10.05

**Table 3.4 (b):** Antenna size reduction corresponding to LRF for different slit lengths(s)

<i>Antenna type</i>	<i>Lower resonant frequency (GHz)</i>	<i>Size reduction (%)</i>
s = 18.0 mm = width of patch (w)	2.17	48.94
s = 16.0 mm	2.33	45.10
s = 15.0 mm	2.56	39.76
s = 14.0 mm	2.49	41.41
s = 13.0 mm	2.78	34.58

The return loss value of -22.84 dB at 2.33 GHz for  $s = 16.0$  mm is a significant improvement in *RL* performance compared to -12 dB at 2.17 GHz with single full ( $s=w$ ) slit. However, the resonant frequency has slightly increased resulting in a marginal sacrifice on size reduction in achieving this improved matching.

Return loss measurements are followed by radiation pattern measurements for all prototypes. The following sub section details the measured results.

### 3.6.2 Radiation pattern measurements for patch with different slit length

Radiation pattern measurements are carried out using an automated pattern measurement system, which includes a signal generator as source, a spectrum analyzer, and a PC controlled turntable as described in chapter 2. E- plane and H- plane radiation patterns for the simple microstrip patch antenna, patch with single slit and patch with varying slit length are carried out at their respective resonant frequencies.

E -plane and H -plane radiation patterns for the simple patch designed at 4.25 GHz are measured. The field patterns are as shown in the figure 3.17 (a) and (b). As can be seen from the figures, the patterns are broad side in nature and are generally obtained for simple

rectangular patch. The corresponding directivities are found to be 4.50 dBi and 3.98 dBi for E - and H – plane patterns.

The field patterns for patch with full slit ( $s = W$ ) at its corresponding  $LRF$  and  $URF$  are shown in figures 3.18 and 3.19 respectively. The dotted lines in the subsequent figures from 3.18 to 3.27 are for the corresponding simple patch at its resonant frequency.

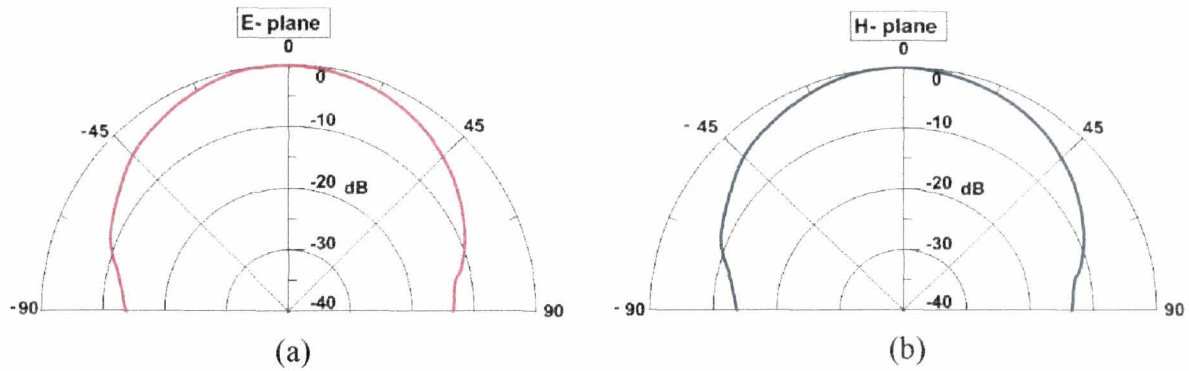


**Figure 3.17:** Measured radiation pattern of simple patch at 4.25 GHz  
(a) E- plane (b) H- plane

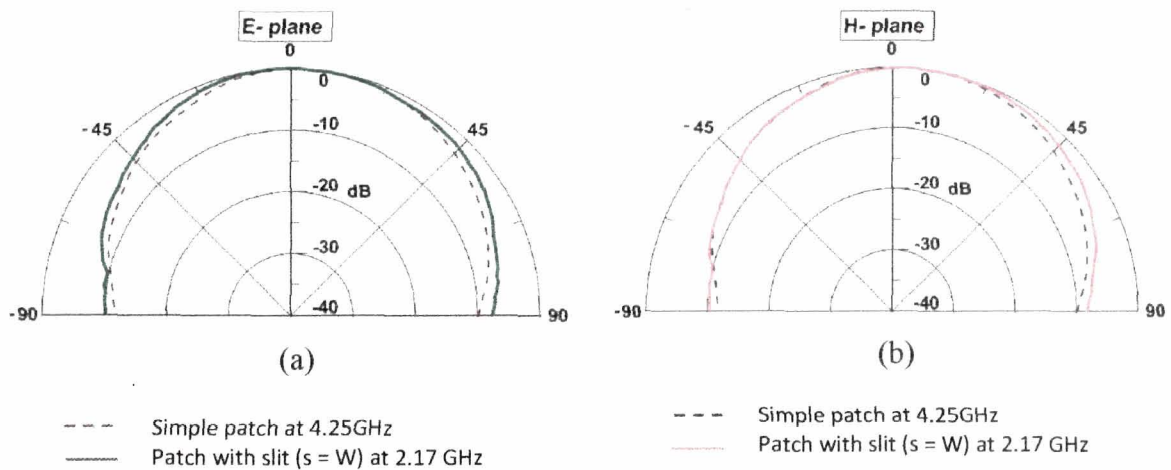


**Figure 3.18:** Measured radiation pattern of patch with slit ( $s = W$ ) at 2.17 GHz  
(a) E- plane (b) H- plane

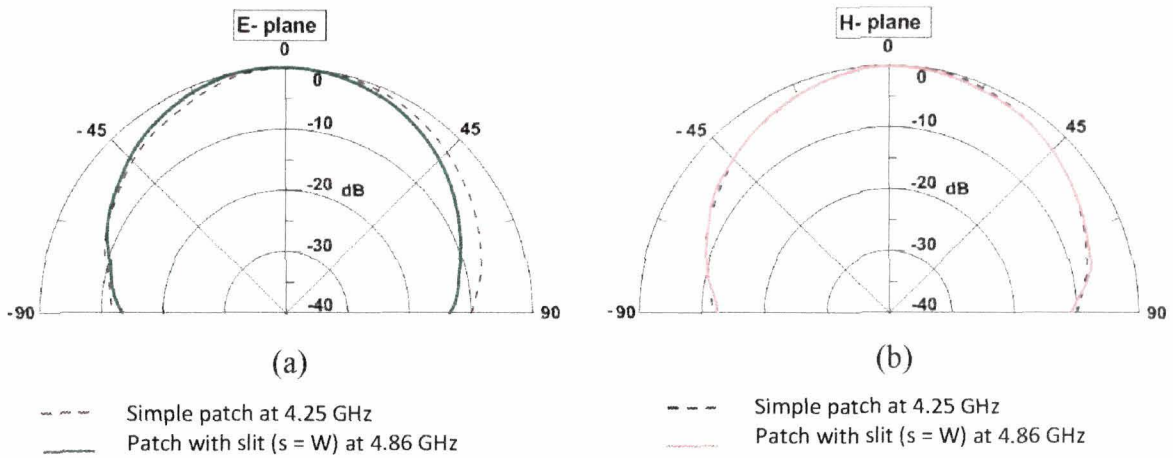


**Figure 3.19:** Measured radiation pattern of patch with slit ( $s = W$ ) at 4.86 GHz

(a) E- plane (b) H- plane

The field pattern characteristics for patch with slit length ( $s =$ ) 16 mm at both the respective frequencies of 2.33 GHz and 5.11 GHz are shown in figures 3.20 and 3.2

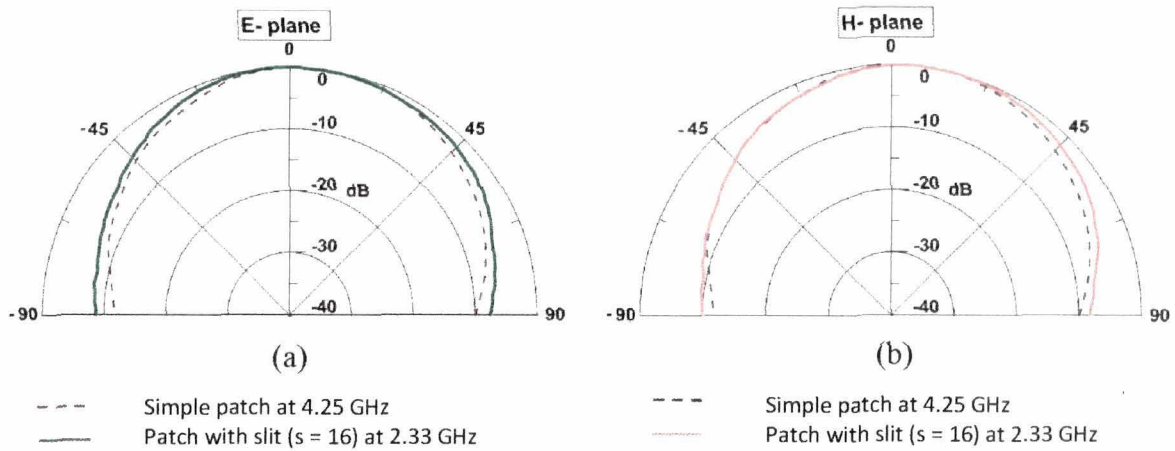


**Figure 3.20:** Measured radiation pattern of patch with slit ( $s = 16$ ) at 2.33GHz

(a) E- plane (b) H- plane

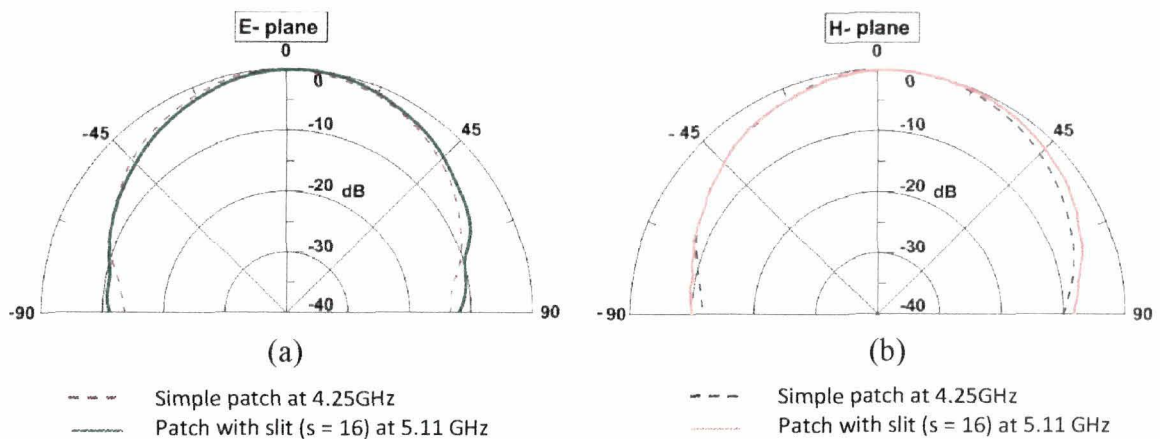


**Figure 3.21:** Measured radiation pattern of patch with slit ( $s = 16$ ) at 5.11GHz

(a) E- plane (b) H- plane

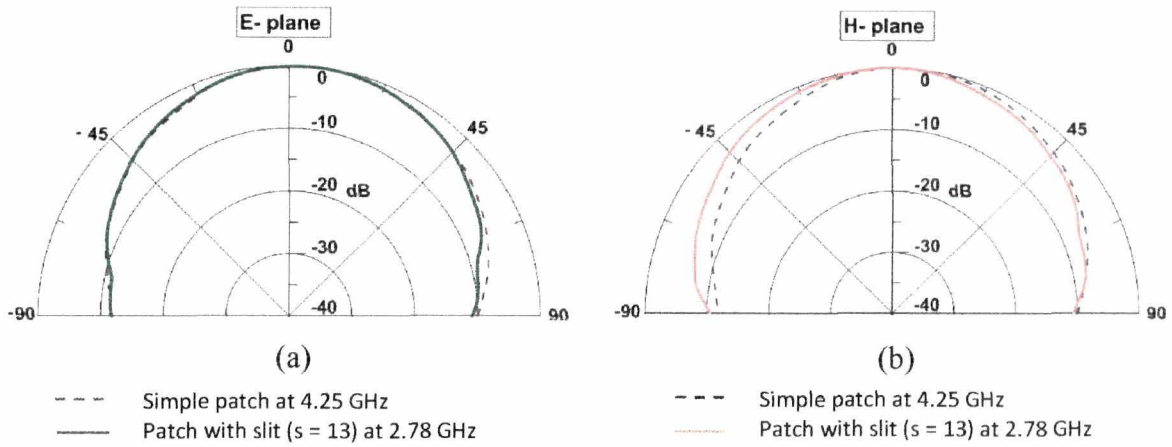


**Figure 3.22:** Measured radiation pattern of patch with slit ( $s = 13$ ) at 2.78 GHz

(a) E- plane      (b) H- plane

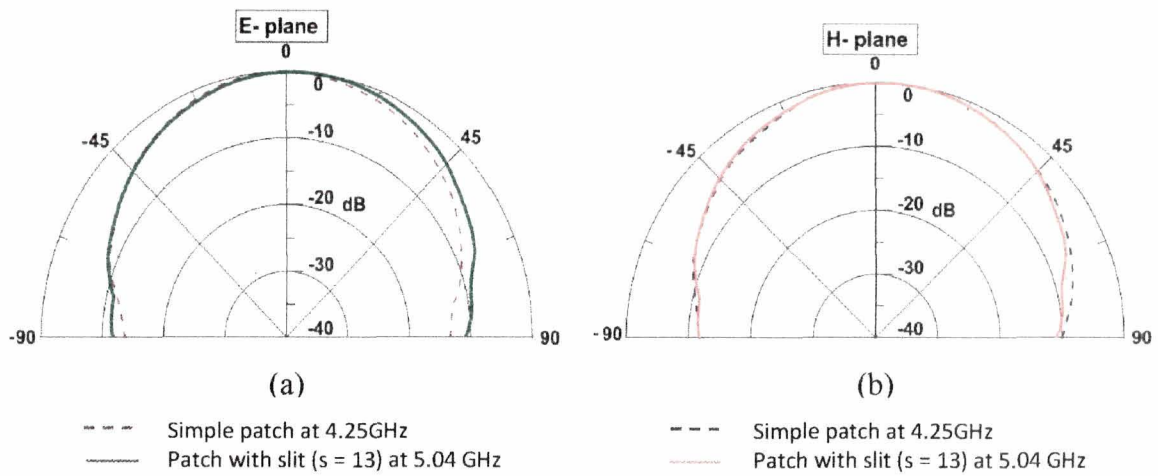


**Figure 3.23:** Measured radiation pattern of patch with slit ( $s = 13$ ) at 5.04 GHz

(a) E- plane      (b) H- plane

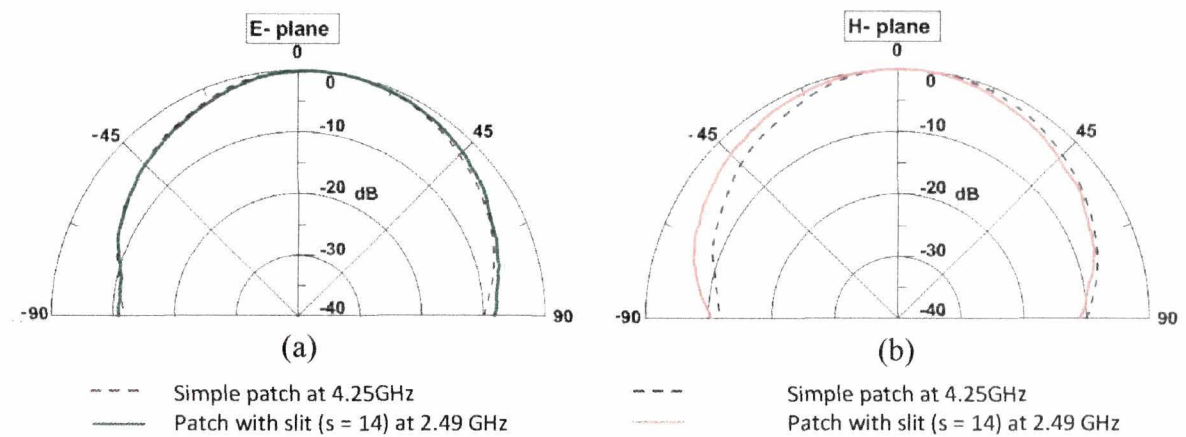
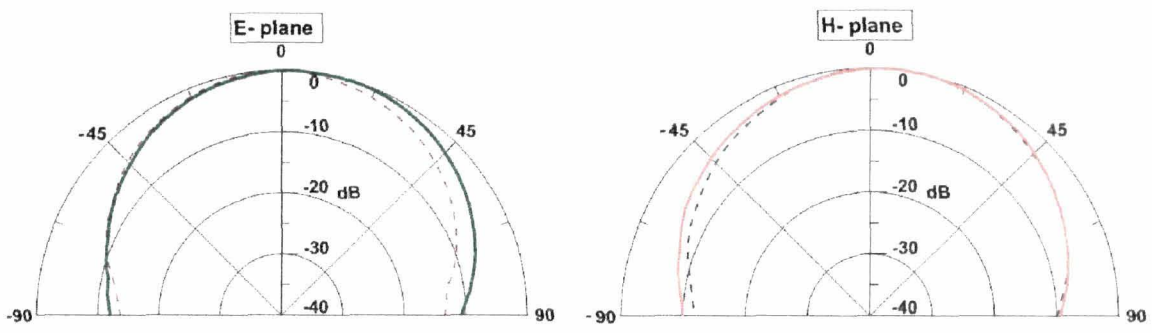


**Figure 3.24:** Measured radiation pattern of patch with slit ( $s = 14$ ) at 2.49 GHz

(a) E- plane      (b) H- plane



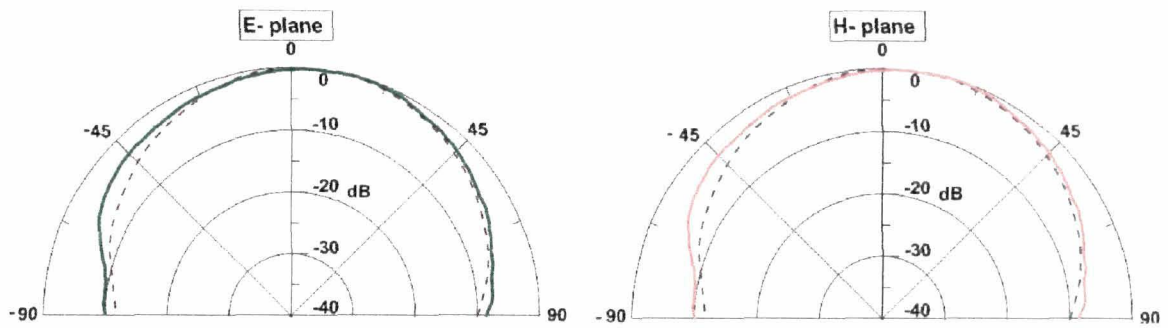


(a) (b)

--- Simple patch at 4.25GHz      --- Simple patch at 4.25GHz  
 — Patch with slit ( $s = 14$ ) at 4.98GHz      — Patch with slit ( $s = 14$ ) at 4.98 GHz

**Figure 3.25:** Measured radiation pattern of patch with slit ( $s = 14$ ) at 4.98 GHz

(a) E- plane      (b) H- plane

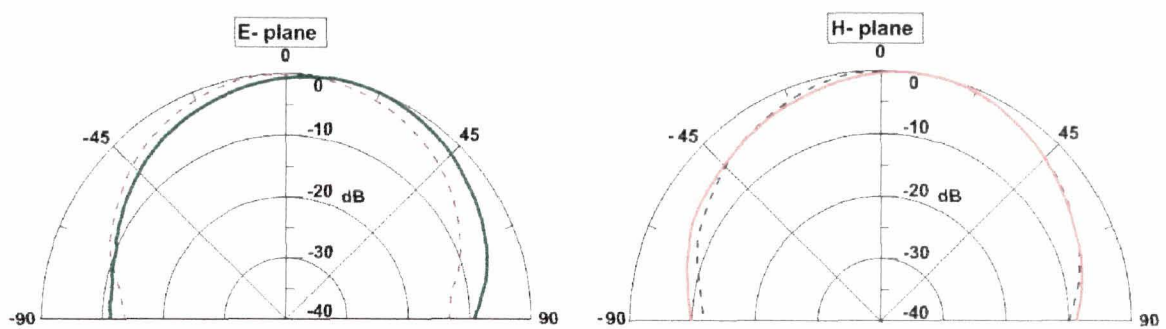


(a) (b)

--- Simple patch at 4.25GHz      --- Simple patch at 4.25GHz  
 — Patch with slit ( $s = W$ ) at 2.56 GHz      — Patch with slit ( $s = W$ ) at 2.56 GHz

**Figure 3.26:** Measured radiation pattern of patch with slit ( $s = 15$ ) at 2.56 GHz

(a) E- plane      (b) H- plane



(a) (b)

--- Simple patch at 4.25GHz      --- Simple patch at 4.25GHz  
 — Patch with slit ( $s = 15$ ) at 4.90 GHz      — Patch with slit ( $s = W$ ) at 4.90 GHz

**Figure 3.27:** Measured radiation pattern of patch with slit ( $s = 15$ ) at 4.90 GHz

(a) E -plane      (b) H -plane

The pattern plots indicate that introduction of the full or partial slits have not significantly altered the radiation patterns of the antennas with slits from that of the simple patch antenna.

Directivities at their respective resonant frequencies calculated from measured radiation pattern plots for simple patch and patch with different slit lengths ( $s$ ) are summarized in the following table (table 3.5). The directivities from table 3.5 are plotted in figures 3.28 and 3.29 for E- and H- plane separately.

**Table 3.5:** Measured directivity with different slit lengths ( $s$ )

<i>Slit length</i>	<i>Lower resonant frequency directivity</i>		<i>Upper resonant frequency directivity</i>	
	<i>E- plane directivity (dBi)</i>	<i>H- plane directivity (dBi)</i>	<i>E- plane directivity (dBi)</i>	<i>H- plane directivity (dBi)</i>
Simple Patch	—————		(4.25 GHz)	
	—————	—————	4.50	3.98
$s = 18.0$ mm = width of patch ( $w_s$ )	(2.17 GHz)		(4.86 GHz)	
	3.73	4.85	4.39	3.91
$s = 16.0$ mm	(2.33 GHz)		(5.11 GHz)	
	3.70	4.85	4.13	3.73
$s = 15.0$ mm	(2.56 GHz)		(4.90 GHz)	
	3.91	3.97	4.27	4.57
$s = 14.0$ mm	(2.49 GHz)		(4.98 GHz)	
	4.37	5.04	4.55	3.96
$s = 13.0$ mm	(2.78 GHz)		(5.04 GHz)	
	4.37	3.31	4.36	4.36

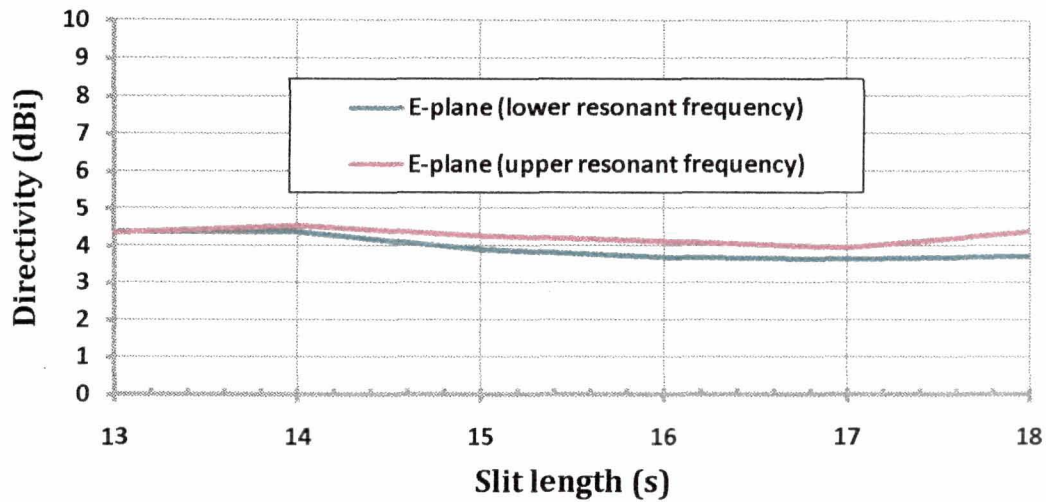


**Figure 3.28:** Measured directivity vs. slit length (s) for E- and H- plane

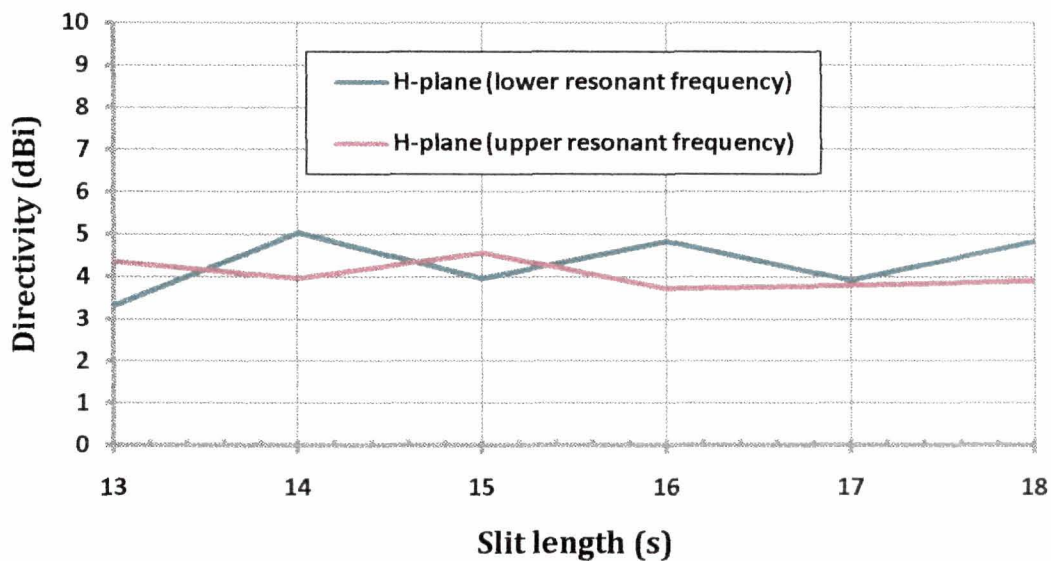


**Figure 3.29:** Measured directivity vs. slit length (s) for E- and H- plane

The E-plane directivities at the lower and upper resonant frequencies are similar to that of simple patch without slit ( $s = 0$ ) whereas directivities in the H- plane for both the resonant frequencies vary to some extent with change in slit length.

### 3.7 Patch with slit isolated elevated sections

Most of the reported efforts in improving bandwidth performance and dual frequency operations are confined to modifications in the planar profile in microstrip antennas, which have their own advantages [17-19]. A coupling mechanism was reported by Choi et al [18] which describes a dual polarized microstrip patch antenna based on both the CPW (Co Planar Wave Guide) fed and the microstrip -T line fed for obtaining dual band performance. There are very few reported works on profiling of the antenna geometry along the direction of its thickness. An out of plane quasi 3-D structure was reported by



Y. Kim et. al. [20] in which enhancement of radiation was obtained. The antenna showed increased radiation power level by 3 dB in both E- and H- plane compared to conventional planar patch antenna. Linear profiling was reported by J.C. Langer et al. [21], on a micro machined out-of plane reconfigurable microstrip antenna using plastic deformation magnetic assembly.

This section presents investigations on a patch which is partially profiled patch conductor with narrow slits at the profile boundary. The profiling is linear where part of the length on both the sides of radiating edges raised (tilted) out of the patch making an angle  $\theta_e$  (elevation angle) with the plane of the patch. The elevation angle ( $\theta_e$ ) is varied to study the effect on antenna performance including bandwidth and resonant frequencies. The following sub sections include the structural design details and performance characterization of the elevated patch with the slits. The objective of the work is to design an antenna to explore the possibilities of bandwidth enhancement by changing only one parameter i.e. the elevation ( $\theta_e$ ) of the patch.

### ***3.7.1 Design and fabrication of elevated patch antenna with slits***

A simple rectangular patch antenna is designed at 4.49 GHz using CST Microwave Studio. Two slits parallel to the radiating edges on both the side of the feed point are introduced as shown in figure 3.30 (a). These isolated patch sections due to slits running through the patch width are profiled by raising the sections at an angle, the end at the slit side being at the substrate plane while the other end elevated above the substrate. The design parameter for the single patch and modification details are summarized in the table 3.6.

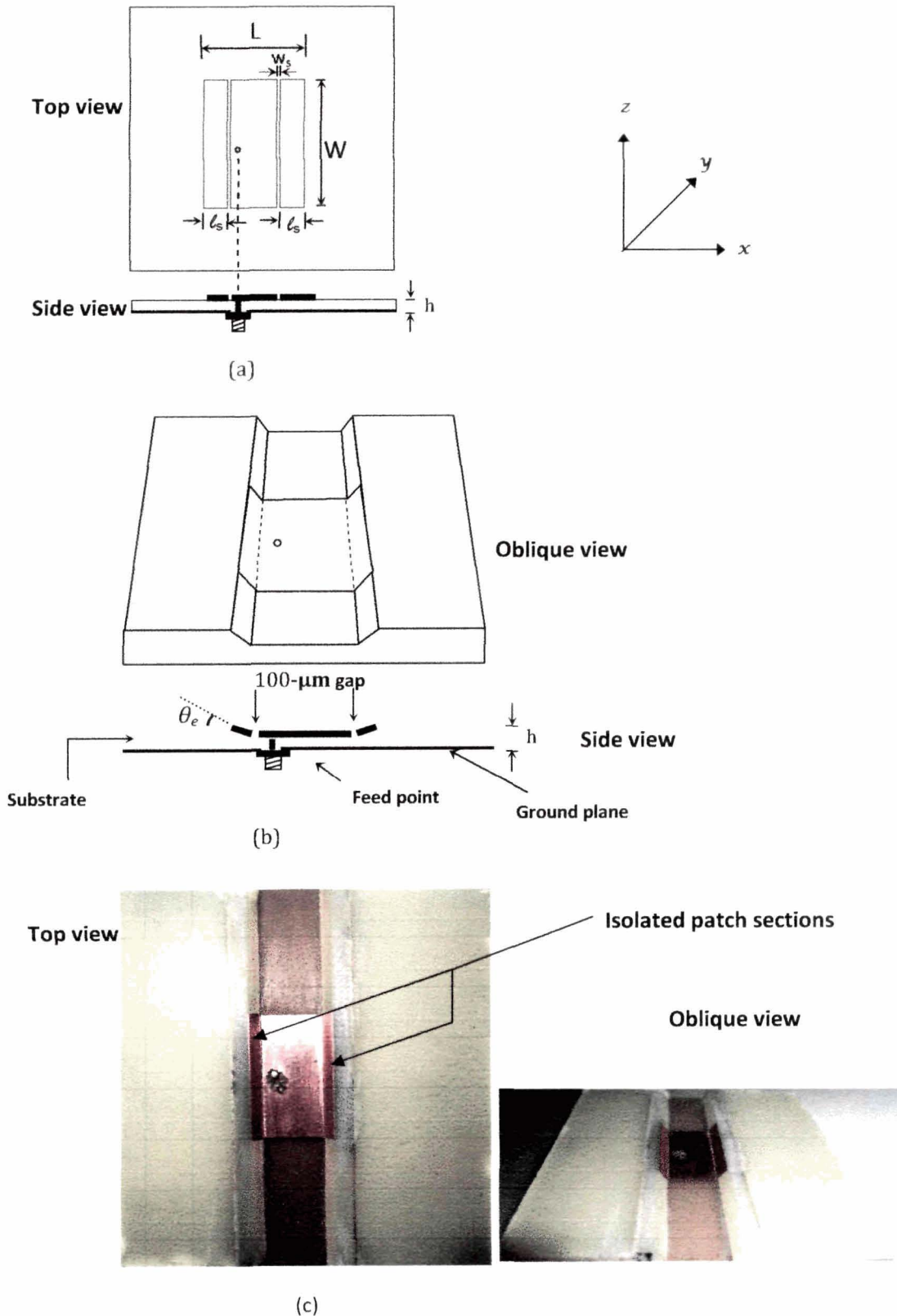


**Figure 3.30:** Microstrip patch antenna with slits

- (a) Planar conventional structure with slits (top and side view)
- (b) Structure with slits and elevated sections (oblique and side view)
- (c) Fabricated profiled antenna with slits (top and oblique view)

**Table 3.6:** Design specification of profiled RMSA

<i>Parameter</i>	<i>Value</i>
Patch width (W)	20.1 mm
Patch length (L)	15 mm
Thickness of the substrate (h)	2.4 mm
Relative dielectric constant ( $\epsilon_r$ ), $\delta$	4.8, 0.001
Feed point location from edge	4.0 mm
Slit width( $w_s$ )	100 $\mu$ m
Isolated conductor dimension along patch length ( $l_s$ )	2.5 mm
Elevation angle ( $\theta_e$ )	45°, 50°, 55°, 65°, 70°, 75°, 85°

The fabrication of the patch with elevated sections is carried out in a number of steps. First, the central planar section of the structure is fabricated using the etching process on a two sided copper laminated substrate (FR<sub>4</sub>) of thickness 1.5mm (figure 3.31). The elevated sections are fabricated by cutting single sided laminated substrate (FR<sub>4</sub>) of thickness 3mm at the required angle ( $\theta_e$ ) using a miter saw (figure 3.32(b)). Two of these sections are fixed on the substrate surface on both side of the main central patch shown in figure 3.30 keeping slanted edge of 100 $\mu$ m away and parallel to the central patch using synthetic adhesive. The gap 100 $\mu$ m is again checked under a travelling microscope. The section is removed and refixed until a gap accuracy of  $\pm 5\%$  along its length is obtained. The dielectric beyond the outer edge of the elevated conductor section is raised to the level of its extending to the main substrate boundary. This is done by cutting a piece of lamination stripped substrate section at the same angle ( $\theta_e$ ) so that it can fit into the wedged gap on the outer side of the elevated sections as shown in figure (figure 3.33 (c)). The extra portion of the raised substrate sections are then cut down the level of the outer edge of the elevated conductor section using a mechanical surface grinder.

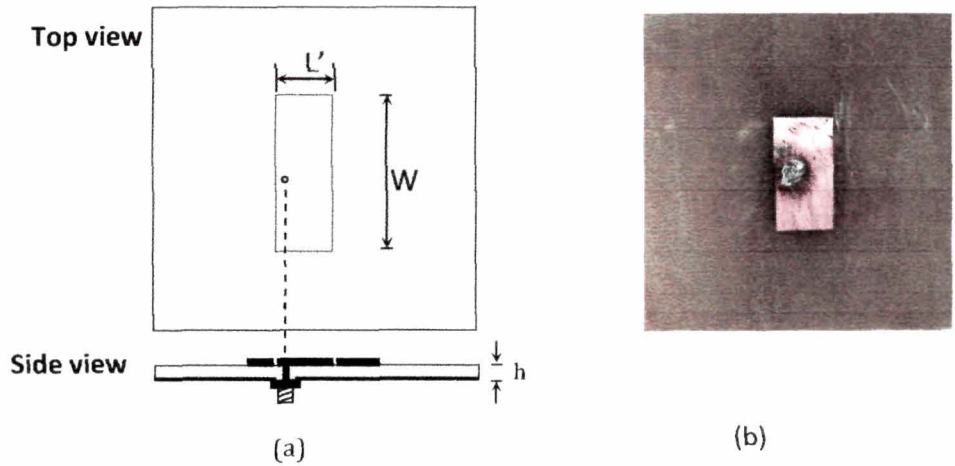


**Figure 3.31:** (a) Planar conventional structure without slits (top and side view)  
 (b) Fabricated central conductor (top view)

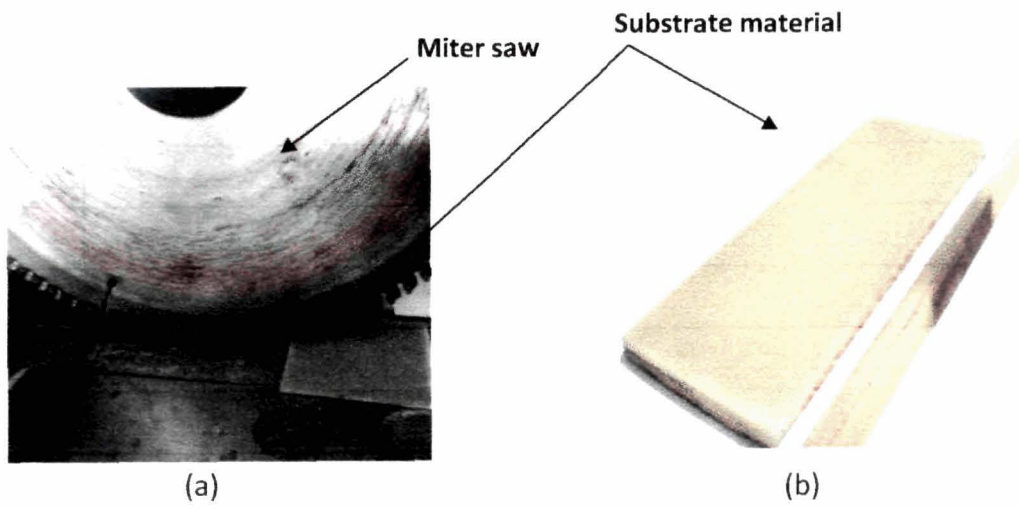


**Figure 3.32:** (a) Miter saw with single sided copper laminated substrate sample  
 (b) Fabricated elevated substrate section ( $\theta_e = 45^\circ$ )

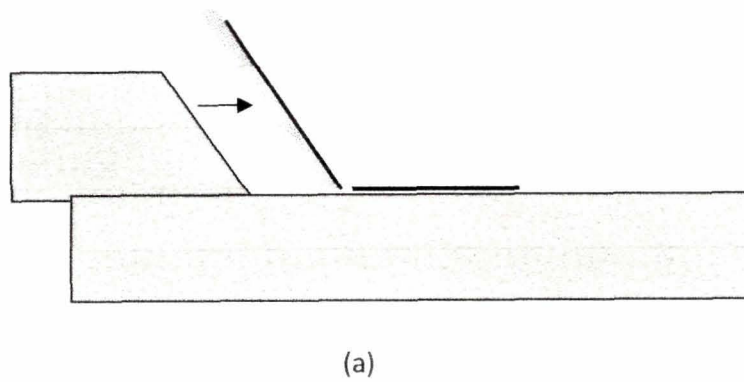




**Figure 3.33:** (a) Isolated substrate section before adding to elevated patch section  
 (b) Fabricated elevated section before addition ( $\theta_e = 45^\circ$ )  
 (c) Isolated substrate section added to elevated patch section

### 3.7.2 Return loss measurement of simple patch antenna

The measured resonant frequency of the simple patch fabricated is 4.42 GHz that is designed at 4.49 GHz using CST Microwave Studio. The measured resonant frequency shifts down by 1.56%.

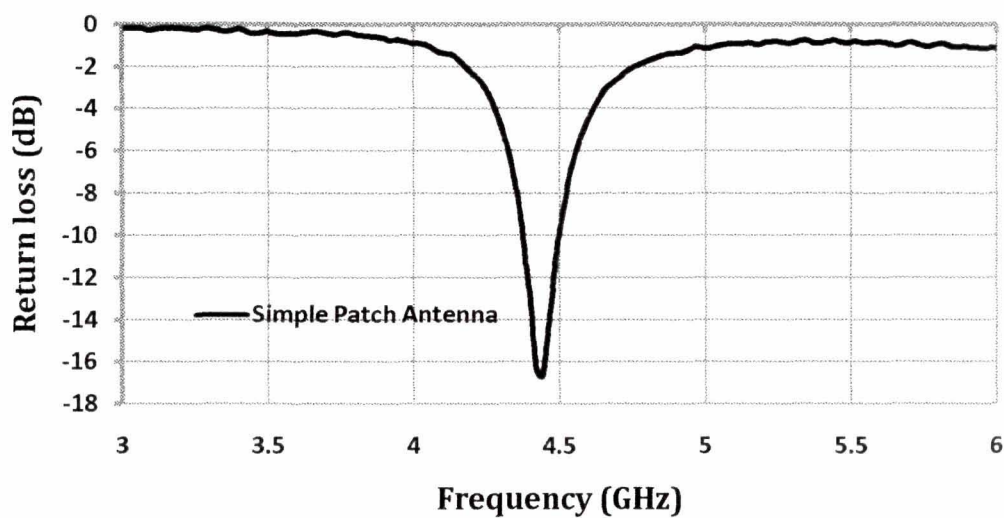
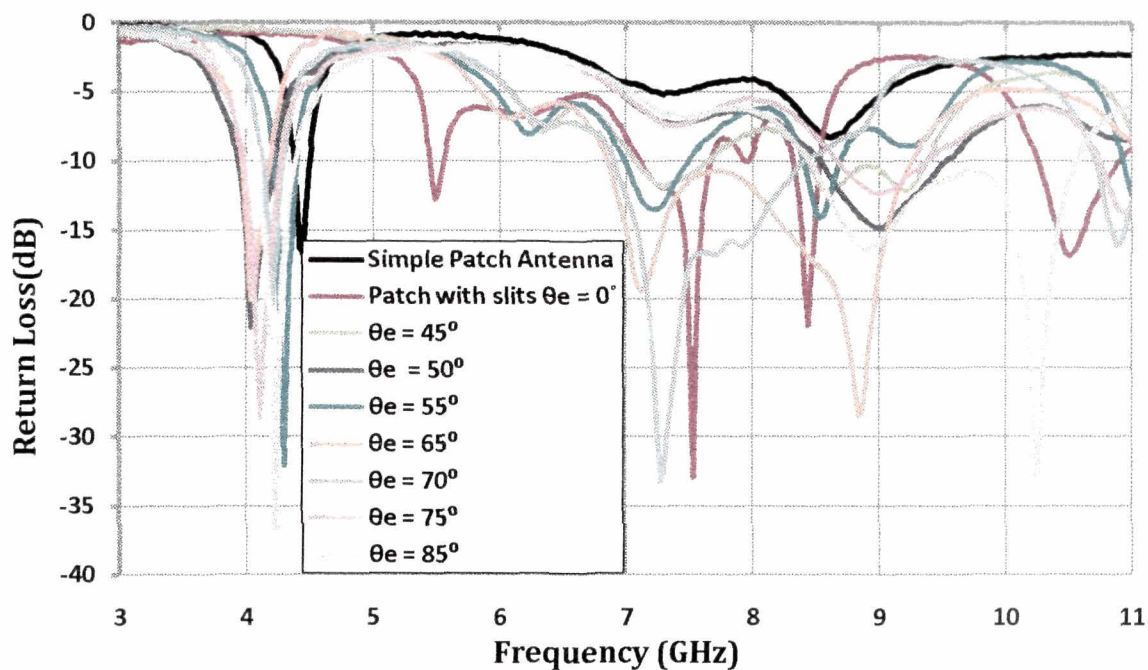


**Figure 3.34:** Return loss vs. frequency of simple patch antenna (resonant frequency = 4.42 GHz)

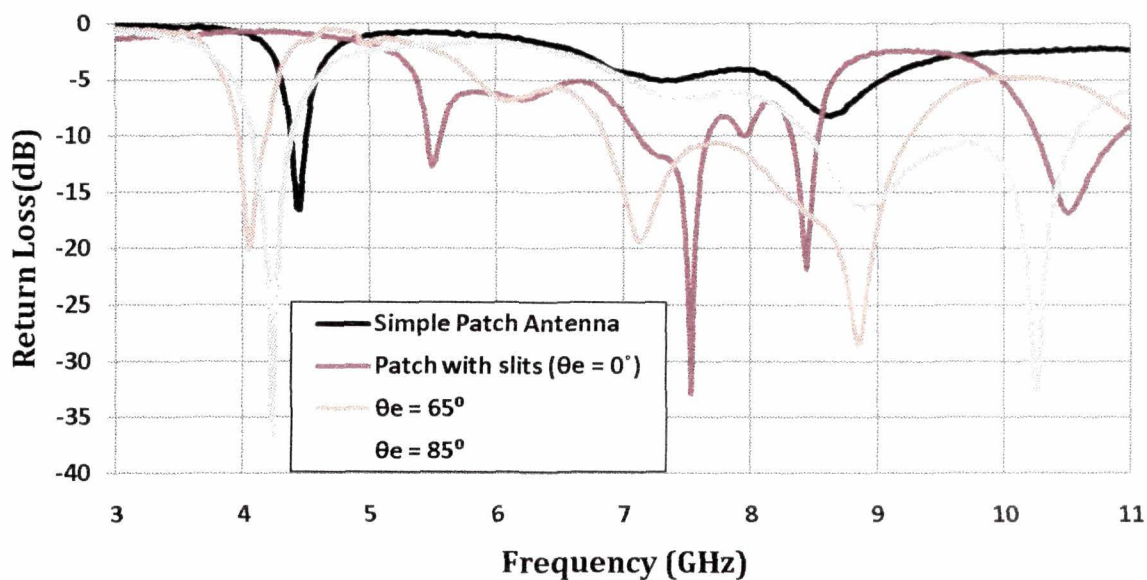
Measured results indicate an  $RL$  value of -16.31 dB at 4.42 GHz for the simple patch as shown in figure 3.34.

### 3.7.3 Return loss measurement of elevated patch antenna

Measurements on antenna performance characteristics is carried out for elevated angles  $\theta_e = 0^\circ$  to  $\theta_e = 85^\circ$  of the isolated radiating edges. The antenna performance characteristics including RL and radiation pattern are carried out for the fabricated patch prototypes.



(a)



(b)

**Figure 3.35:** Measured return loss plot for patch with different  $\theta_e$

(a)  $\theta_e = 0^\circ, 45^\circ, 50^\circ, 55^\circ, 65^\circ, 70^\circ, 75^\circ, 85^\circ$

(b)  $\theta_e = 0^\circ, 65^\circ, 85^\circ$



**Table 3.7:** Resonant frequency and return loss for different elevation angles ( $\theta_e$ )

$\theta_e$	1 <sup>st</sup> RL peak (dB)		2 <sup>nd</sup> RL peak (dB)		3 <sup>rd</sup> RL peak (dB)		4 <sup>th</sup> RL peak (dB)	
	f <sub>L</sub> (GHz)	RL (dB)	f <sub>L</sub> (GHz)	RL (dB)	f <sub>L</sub> (GHz)	RL (dB)	f <sub>L</sub> (GHz)	RL (dB)
0°	5.48	-12.74	7.53	-32.9	8.43	-21.87	10.52	-16.71
45°	7.31	-11.71	8.62	-12.21	9.21	-12.05	---	---
50°	4.04	-22.02	8.89	-14.38	---	---	---	---
55°	4.30	-32.00	7.27	-13.32	8.50	-13.75	---	---
65°	4.04	-20.02	7.08	-18.52	8.83	-28.48	---	---
70°	4.20	-20.43	7.27	-33.17	10.85	-15.65	---	---
75°	4.11	-28.60	8.93	-12.14	10.88	-13.17	---	---
85°	4.23	-36.61	8.98	-15.91	10.26	-32.31	---	---

It can be seen from table 3.7 that for all the  $\theta_e$  values, the antenna resonates at two frequencies with at least 10 dB return loss. The lower resonant frequency is near to the resonant frequency of the simple patch while the upper resonant frequency is almost double of that. When  $\theta_e$  changes from 50° to 45°, the RL peaks barely cross the 10 dB level and hence are not included in the table.

For elevation angle of 85°, there are two prominent return loss peaks in excess of -30 dB, the lower frequency being 4.23 GHz (C-band) and the upper frequency at 8.83 GHz (X - band). Moreover, a wideband behavior is observed with a (-10 dB) frequency range from 8.43 GHz to 10.59 GHz which amounts to a 22.71 % bandwidth as shown in table 3.8.

**Table 3.8:** Best bandwidth enhancement for two specific elevation angles

Elevation angle ( $\theta_e$ )	-10 dB bandwidth at upper operating frequency band		
	$f_L$ (GHz)	$f_U$ (GHz)	Bandwidth (%)
65°	6.84	9.24	29.82
85°	8.43	10.59	22.71

$f_L$ —10dB lower cut off frequency in the band

$f_U$ —10dB upper cut off frequency in the band

From the measure results, it is observed that wide band characteristics as well as improved matching is observed for elevations beyond the elevation angle  $\theta_e = 45^\circ$  (table 3.6). Figure 3.36 shows measured values of return loss with different elevation angles.

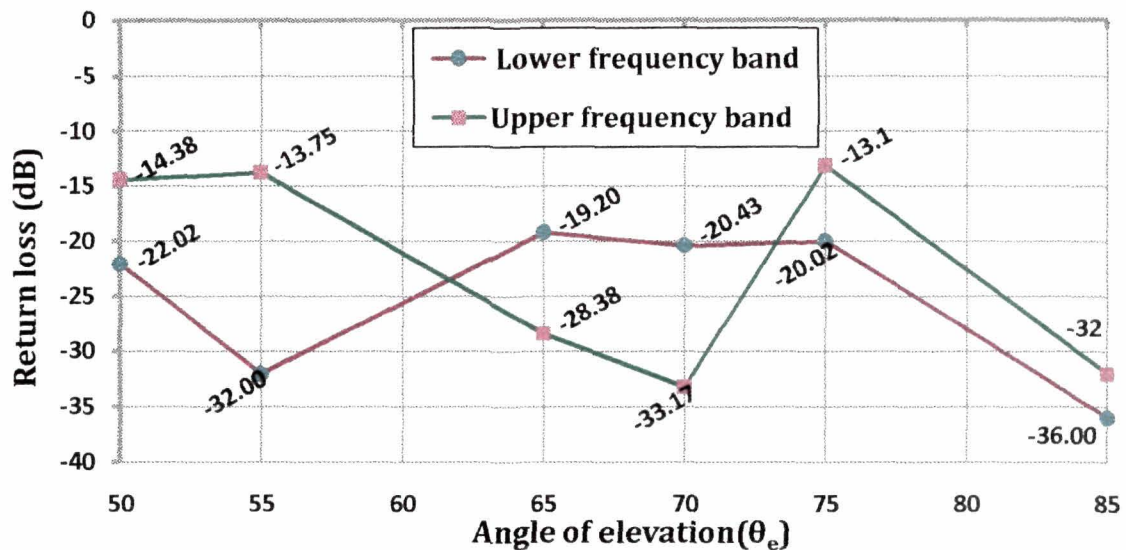


**Figure 3.36:** Measured plot for two best return loss values (at  $f_L$  and  $f_U$ ) vs. angle of elevation ( $\theta_e$ )

The measured results indicate that dual frequency operation can be obtained without any major size increase of the simple patch by simply introducing slits although both the frequencies are on the higher side. The small shift in the lower resonant frequency due to elevation angle change can be compensated by minor adjustments in the patch dimensions, as the shift in frequency of the upper band is more sensitive to elevation angle change whereas the accompanying shift in the lower frequency is much smaller.

Radiation pattern measurements are carried out for simple patch and patches with two of the elevation angles ( $\theta_e = 65^\circ$  and  $85^\circ$ ).

#### 3.7.4 Radiation pattern measurements of profiled patch antenna

E - plane and H - plane radiation patterns for the simple microstrip patch antenna resonating at 4.42 GHz are measured. The patterns are shown in figure 3.37 (a and b) respectively. The corresponding directivities are found to be 4.64 dBi and 3.95 dBi for E- and H- plane patterns. Both the patterns are broadside in nature like the conventional patch antennas.

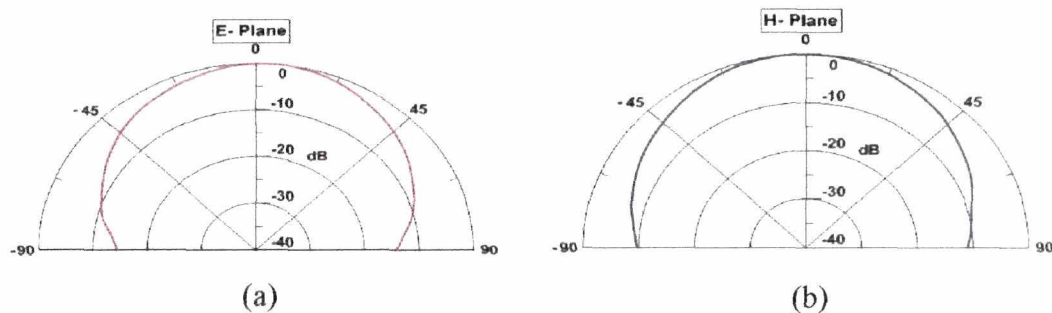


**Figure 3.37:** Measured radiation pattern for simple patch at 4.42 GHz  
(a) E - plane (b) H - plane



Patterns for the planar patch with slits ( $\theta_e = 0^\circ$ ) at the two resonate frequencies are shown in figures 3.38 and 3.39.

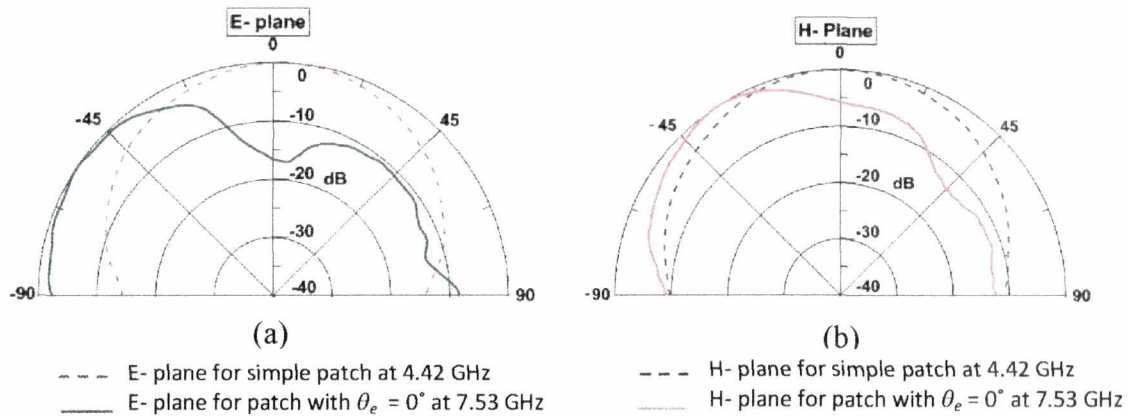


**Figure 3.38** Measured radiation pattern for patch with slits ( $\theta_e = 0^\circ$ ) at 7.53 GHz

(a) E - plane (b) H - plane

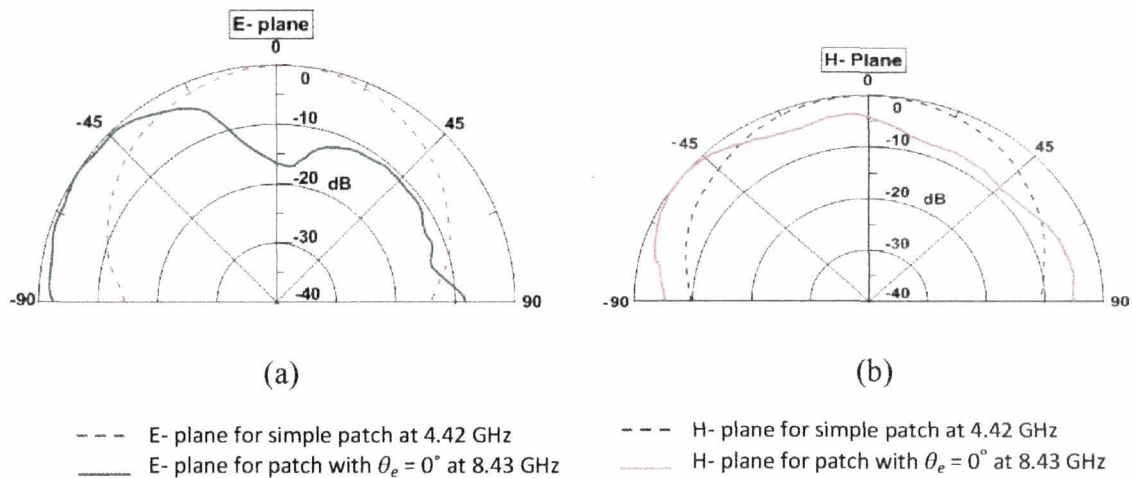


**Figure 3.39:** Measured radiation pattern for patch with slits ( $\theta_e = 0^\circ$ ) at 8.4 GHz

(a) E - plane (b) H - plane

As can be seen from the figures with the introduction of the slits, both the E- and H- plane patterns are deviated from the broad side direction at 7.53 GHz as compared to the simple patch. Patterns at the other resonant frequency (8.43 GHz) for the same structure ( $\theta_e = 0^\circ$ ) are also deviated from broadside direction as shown in figure 3.39.

Measured E- and H- plane patterns for  $\theta_e = 65^\circ$  and  $85^\circ$  at frequencies of peak return losses are measured shown in the following figures (3.40 to 4.43).

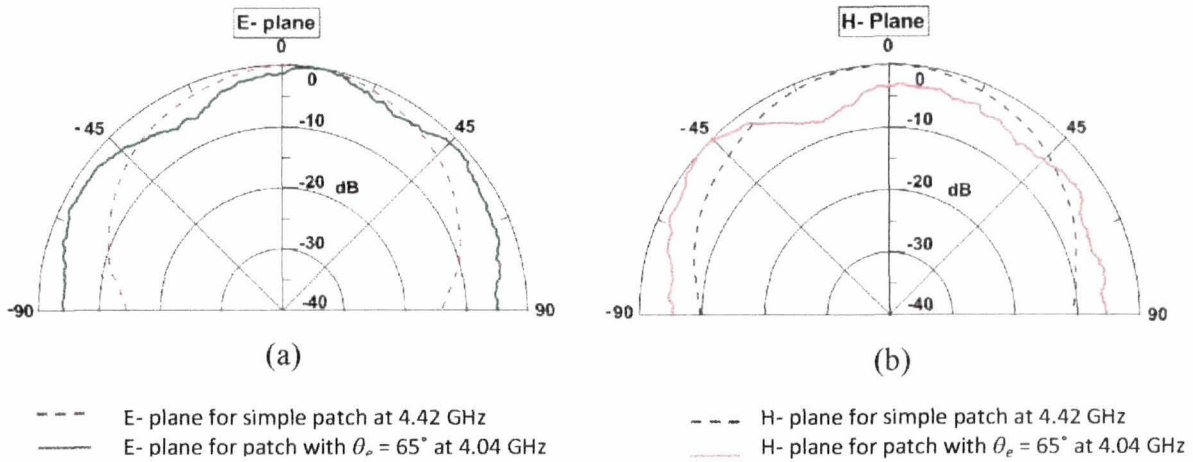


**Figure 3.40:** Measured radiation pattern of patch with slits ( $\theta_e = 65^\circ$ ) at 4.04 GHz  
 (a) E - plane      (b) H - plane

For  $\theta_e = 65^\circ$ , the principal plane pattern at 8.83 GHz is given in figure 3.38 while figure 3.39 and 3.40 show the field patterns at 4.23 GHz and 10.26 GHz respectively for  $\theta_e = 85^\circ$ .

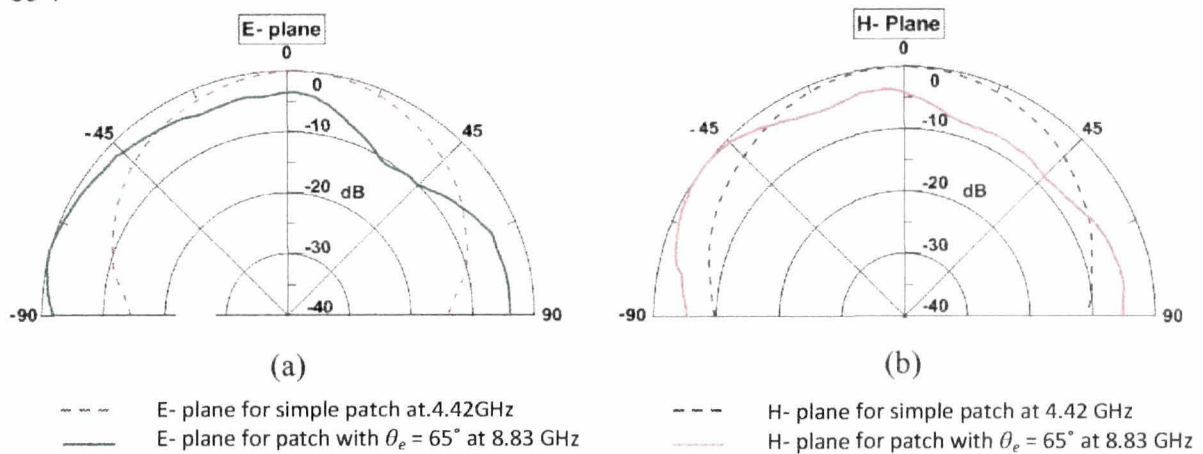


**Figure 3.41:** Measured radiation pattern of patch with slits ( $\theta_e = 65^\circ$ ) at 8.83 GHz  
 (a) E - plane      (b) H - plane

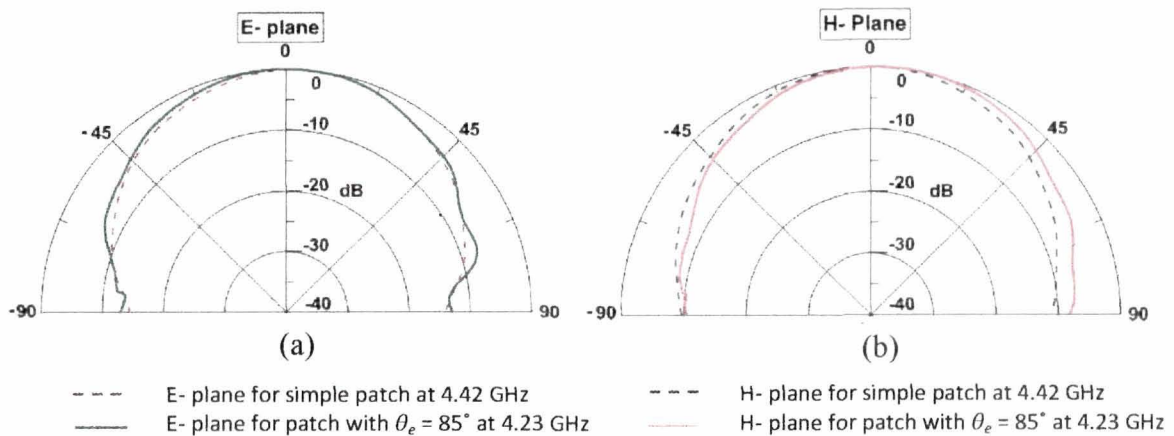


**Figure 3.42:** Measured radiation pattern of patch with slits ( $\theta_e = 85^\circ$ ) at 4.23 GHz  
 (a) E - plane      (b) H - plane

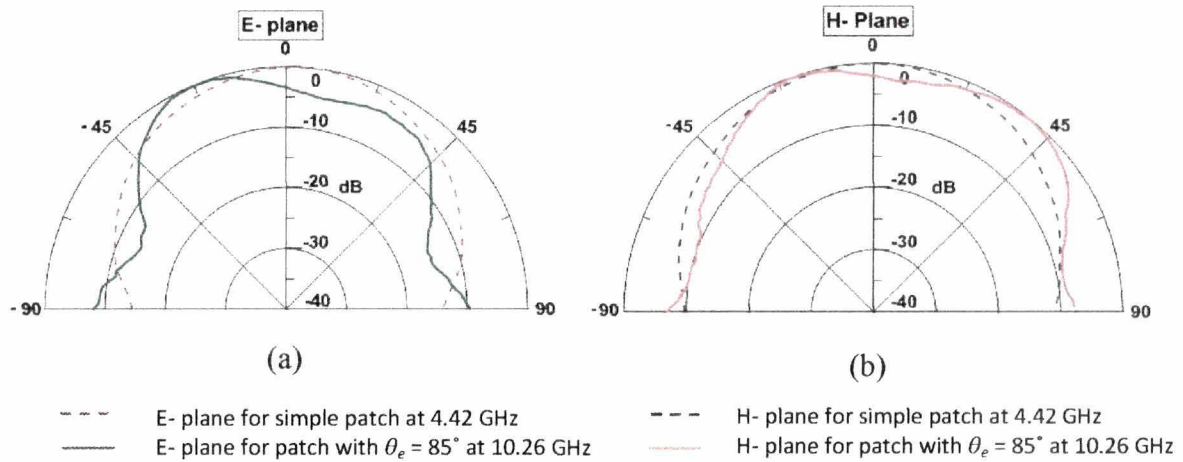


**Figure 3.43:** Measured radiation pattern of patch with slits ( $\theta_e = 85^\circ$ ) at 10.26 GHz

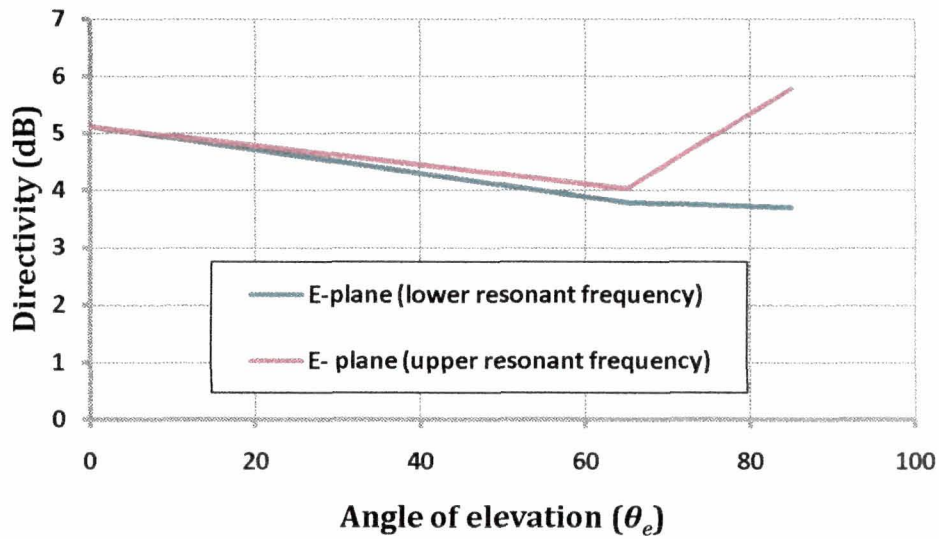
(a) E - plane      (b) H - plane

Radiation patterns for the lowest resonating operating frequencies of the patches are similar to the conventional rectangular patch. At higher frequencies, the beam maxima of the E - plane shifts away from the broadside possibly due to the two slits together with the outer sections seeing a phase difference because of the asymmetric positioning of the feed point along the direction of the patch length. With the increasing elevation angles, some realignment towards the broadside direction is observed. As expected, the H - plane pattern at the first resonating frequency is symmetrical (figure 3.39 (b)) because of the symmetry of the structure.

Table 3.9 gives the directions calculated from the radiation patterns in the two principal planes. Figures 3.44 and 3.45 show the variation of directivities at both the lower and frequencies with the two best RL values with change in angle of elevation ( $\theta_e$ ).

**Table 3.9:** Measured directivity for two frequencies ( $f_L$  and  $f_U$ ) with best return loss values

	Lower resonant frequency $f_L$ (GHz)		Upper resonant frequency $f_U$ (GHz)	
	E- plane directivity(dBi)	H- plane directivity (dBi)	E- plane directivity (dBi)	H- plane directivity (dBi)
Simple Patch	4.25 GHz		-----	
	4.64	3.96		
$\theta_e = 0^\circ$	7.5 GHz		8.43 GHz	
	5.12	5.07	5.12	4.84
$\theta_e = 65^\circ$	4.04 GHz		8.83 GHz	
	3.79	4.41	4.04	4.84
$\theta_e = 85^\circ$	4.23 GHz		10.26 GHz	
	3.70	3.75	5.78	5.27

**Figure 3.44:** Measured directivity vs. angle of elevation ( $\theta_e$ ) for E- plane



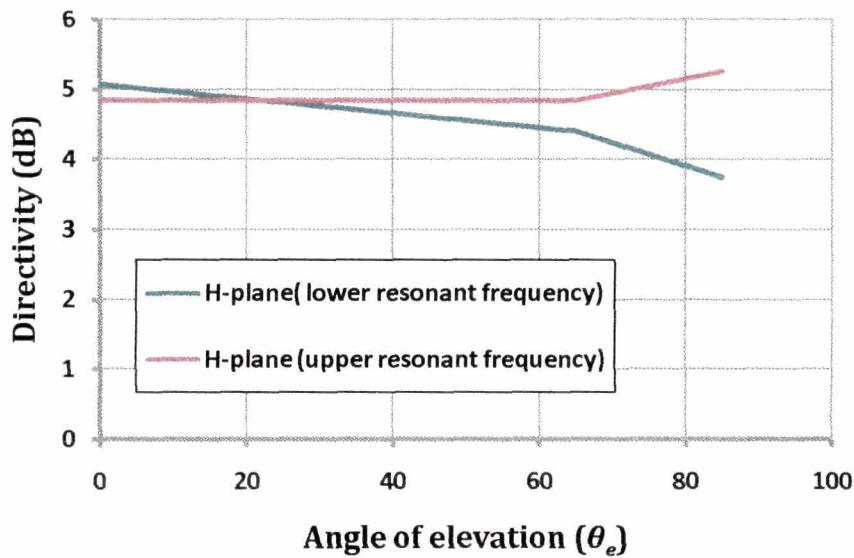


Figure 3.45: Measured directivity vs. angle of elevation ( $\theta_e$ ) for H- plane

As can be seen from the figures, directivities in the E- plane for the two resonant frequencies ( $f_L$  and  $f_U$ ) are almost identical except for the elevation angle of  $\theta_e = 85^\circ$ . However, directivity in the H-plane for  $f_U$  is increased for the elevation angle value of  $\theta_e = 85^\circ$ .

### 3.8 Chapter Summary

Two structures of microstrip patch antenna has been designed, fabricated and tested in this chapter. The first structure is a planar patch antenna with a  $100 \mu\text{m}$  slit near the radiating edge closer to the feed point location. The design is modified by varying the slit lengths to less than the width of the patch. The second structure is a profiled patch antenna with two slits. The patch sections isolated due the slits are linearly profiled with slit side end being at the substrate plane while the other end elevated above the substrate plane. Both the structures yield dual and multi band characteristics with tunability of lower and higher frequencies. Measured results of first structure have demonstrated that introduction of the slit results in both size reduction and dual band operation. In addition, variation of slit length results in tuning of both the lower and upper resonant frequencies. Slit length of 16 mm results in improved matching at both the frequencies with return loss values  $-22.84 \text{ dB}$  and  $-29.90 \text{ dB}$  corresponding to the dual operating frequencies of 2.33 GHz and 5.11 GHz respectively. The size reduction achieved is as high as 49 %. Hence, the antenna design can be used as a reconfigurable structure with tuning of both upper and lower frequencies though both the frequencies cannot be tuned independently. Although, in this work, separate patches are made for different slit lengths to study the effect of slit length

variation on two resonant frequencies, the design can be used for reconfigurable antennas using switching technologies including MEMS to vary the slit length electronically. Understandably, the use of active switching technologies to alter the effective slit length for tuning will lead quantitative change in the results obtained here. Inevitably, this will require further investigation but nonetheless the essential feature of tunability is clearly established in the present investigation.

Measured results for the second structure have demonstrated that dual frequency operation can be obtained without any major size changes of the simple patch by simply introducing slits although both the frequencies are on the higher side. Moreover, for specific ( $\theta_e = 65^\circ, 85^\circ$ ) the lowest resonant frequency is restored nearer to that of the simple patch while at the same time a broadband upper frequency operation is achieved. For these elevation angles, the structure can operate simultaneously at both C - and X - band with a -10 dB bandwidth of  $> 2.0$  GHz at the upper operating frequency band which is a considerably large bandwidth, which is not seen for its conventional counterpart. The large upper frequency operating band can be adjusted according to specific application requirements by changing the elevation angles, even while the lower resonant frequency is kept the same. The small shift in the lower resonant frequency due to elevation angle change can be compensated by minor adjustments in the patch dimensions, as the shift in frequency of the upper band is more sensitive to elevation angle change whereas the accompanying shift in the lower frequency is much smaller.

## References

- [1] J.T. Aberle, S.H. Ohn, D.T. Auckland and S.D. Rogers, "Reconfigurable antennas for portable wireless devices", *IEEE Antennas Propag. Mag.*, Vol. 45, pp.148-152.
- [2] P. Bhartia, and I.J.Bahl, "A frequency agile microstrip antennas" *IEEE Antennas Propagation Symp. Digest*, Vol. 20, pp.304–307, May 1982.
- [3] P.M. Haskins, and J.S. Dahele, "Varactor-diode loaded passive polarisation agile patch antenna", *Electron. Lett.*, Vol.30, pp.1074-1075, 1994.
- [4] J.T. Song, I.H. Jo, and Y.H. Kim, "Frequency agile microstrip antenna using piezoelectric substrate", *Jpn, J. Appl. Phys*, Vol. 40, pp.515-517, 2003.
- [5] R. Jr., Jackson, and R. Ramadoss, "A MEMS-based electronically tunable circular microstrip patch antenna", *J. Micromech. Microeng.*, Vol. 17, pp. 1-8, 2007.
- [6] N.X Sun, J. W. Wang, A. Diagle, C. Pettiford, H. Mosallaei, and Vittoria, C., "Electronically tunable magnetic patch antenna with meta magnetic films", *Electron. Lett.*, Vol 43, pp.434-436, April2007.
- [7] A.K. Bordoloi, P. Borah, S. Bhattacharyya and N.S. Bhattacharyya "A novel approach for post fabrication fine tuning and matching of microstrip patch antenna using adjustable air pocket in substrate layer," *Loughborough Antennas and Propagation Conference (LAPC2011)*, Loughborough University, Loughborough, U.K., 14-15 Nov. 2011.
- [8] S.-Hyuk Wi, Y.-Shil Lee and J Gwan Yook, "Wideband Microstrip patch antenna with U shaped parasitic elements", *IEEE Trans. Antennas Propag.*, Vol 55, pp. 1196-1199, 2007.
- [9] P. Borah, A. K. Bordoloi, N. S. Bhattacharyya, and S. Bhattacharyya, "Bridged "V" shaped patch antenna for dual band communication", *Electronics Lett.*, Vol 48, pp. 419- 420, 2012.
- [10] D.H. Choi, Y.J. Cho and S.O. Park, "Dual-band and dual-polarised microstrip antenna", *Electron. Lett.*, Vol.42, pp.1034-1036, 2006.
- [11] M. Du. Plessis, and J. H. Cloete, "Tuning Stub for Microstrip Patch antenna," *IEEE AP-S Int. Symp. Digest*, pp. 964–967, June 1993.
- [12] K. P. Ray, and G. Kumar , "Tunable and Dual-Band Circular microstrip Antenna with Stubs," *IEEE Trans. Antennas Propag.*, Vol. 48, pp. 1036–1039, July 2000.
- [13] X. Xia Zhang and F. Yang, "Study of a Slit cut on a Microstrip Antenna and its application, *Microwave Opt. Technolo. Lett.*, Vol.18,pp. 297-300, 1998.
- [14] I. J. Bahl, and P. Bhartia, *Microstrip Antennas*, Dedham, MA: Artech House, 1980.
- [15] G. Kumar, and K. P Ray, "Broad band microstrip patch antennas" MA: *Artech House*, 2003.
- [16] C.A. Balanis, "Antenna theories- analysis and design", *John Willey and Sons*, 2005.
- [17] W. He, R. Jin, and J. Geng, E- shaped patch with and circular polarization for millimetre - wave communication, *IEEE Trans. Antennas Propag.*, Vol. 56 pp. 893-895, 2008.
- [18] C.-Wei Su, J.-Sheen Row, and J.-Feng Wu, "Design of a single-feed dual-frequency microstrip antenna", *Microwave Opt Technol Lett.*, Vol.47, pp. 114-116, 2005.
- [19] D.H Choi, Y.J. Cho and S.O. Park, "Dual-band and dual-polarised microstrip antenna", *Electron. Lett.*, 2006, Vol. 42, pp. 1034-1036, 2005.
- [20] Yonghoon Kim, Gi Young Lee, and Sangwook Nam, "Efficiency enhancement of microstrip antenna by elevating radiating edges of patch", *Electronics Lett.*, Vol. 39, pp.1363-1364, 2003.
- [21] J.C. Langer, J. Zou, C. Liu and J.T. Bernhard, "Micro machined reconfigurable out of plane microstrip patch antenna using plastic deformation magnetic actuation", *IEEE Microwave and Wireless Components Letters*, Vol. 13, pp.120-122, 2003.

---

## CHAPTER IV

# MICROSTRIP PATCH ANTENNA WITH NOTIONALLY SUPERPOSED MICROSTRIP LINE

---

### 4.1 Introduction

### 4.2 Design of patch with asymmetrically superposed strip line section

#### *4.2.1 Feed point location*

### 4.3 Antenna performance studies with varying strip line width and tilt angle

#### *4.3.1 Variation of strip line width and its effect on RL performance*

#### *4.3.2 Variation of tilting angle and its effect on RL performance*

#### *4.3.3 Variation of tilt angle and its effect on antenna size*

### 4.4 Measured results

#### *4.4.1 Return loss measurements of simple and modified patch with the strip line*

### 4.5 Comparison of measured and simulated results

#### *4.5.1 Return loss performance*

#### *4.5.2 Antenna size reduction: Results from measurements and simulation*

### 4.6 Radiation pattern measurements of modified patch with tilted superposed strip line section

### 4.7 Chapter summary

### References



## 4.1 Introduction

A single tunable antenna eliminates the need for multiple antennas for operation in multiple frequency bands. Various techniques have been used to tune the resonant frequency, which include adjusting the effective length of the patch using varactor diodes [1–4]. Patch antennas can also be optically tuned over a narrow frequency range of about 100 MHz using an optically controlled pin diode as reported in [3]. A microstrip patch in L-band was reported where tuning was achieved with multiple varactors mounted at both the radiating edges [4]. In the early 1980, a manually tunable circular microstrip patch antenna was reported by Lee et al. [5, 6]. The tuning was achieved by manually adjusting the air gap between the substrate and the ground plane using a spacer. Recently, MEMS-based electro statically tunable microstrip antennas had been reported in [7, 8] where a MEMS-based tunable square patch antenna was fabricated on a flexible Kaptonplymide film using printed circuit processing technique.

Size reduction has been of considerable interest in the development of compact broadband microstrip antenna for present day wireless hand held devices. Several techniques have been proposed to effectively reduce the size of the patch antenna. These include use of high dielectric constant materials [9], using shorting post / wall [10] and cutting slots on the patch [11].

In this chapter, a simple patch antenna is initially designed in the C-band. The patch is modified leading to a geometry obtained by asymmetrically superposing a finite strip line section near one of the radiating edges as shown in figure 4.1 (b). As shown in the figure, the line section is tilted at an angle  $\theta_t$  with respect to one of the radiating edges. Throughout this chapter, the notionally superposed strip line section will be referred to as strip line.

The effect on resonant frequency with change of tilt angle  $\theta_t$  is studied to explore the possibility of tuning the patch antenna by simply rotating (changing  $\theta_t$ ) the strip line. In addition, possible shift of resonant frequency (due to the tuning achieved) to the lower side can effectively result in size reduction of the antenna.

## 4.2 Design of patch with asymmetrically superposed strip line section

### 4.2.1 Feed point location

The rectangular microstrip patch antenna (RMSA) in the C- band is designed using CST Microwave Studio to resonate at 4.55 GHz. Dimension of the patch antenna are shown in figure 4.1(a). As an initial design aid, simulated results using CST MicrowaveStudio for different feed point location are obtained for maximizing the value

the simple patch. Simulation is carried out for evaluating antenna performance characteristics before fabricating the sample prototypes. Before deciding on the specifications of the modified patch, the strip line centre position is varied for both  $m$  and  $n$  (figure 4.1 (b)) to ascertain the position which yields the best  $RL$  performances. The patch specifications are given in table 4.2. Simulated values of return loss ( $RL$ ), impedance (real) and VSWR corresponding to different feed point location are obtained as in figures 4.2 to 4.4 respectively.

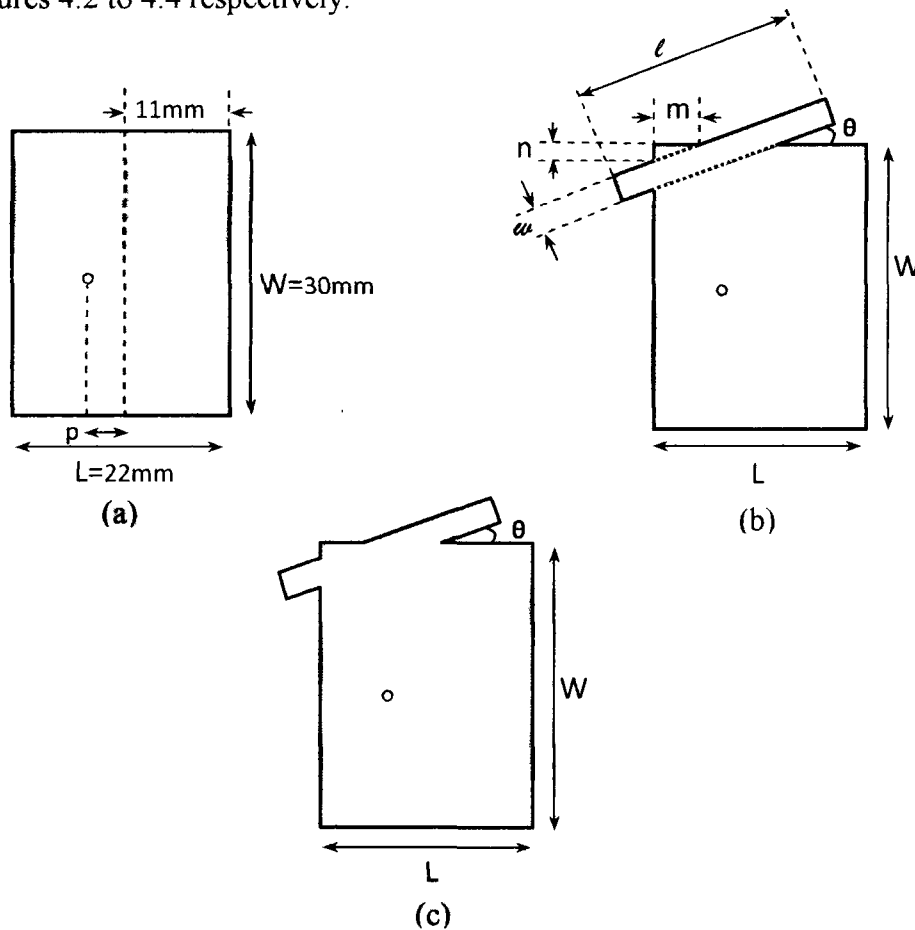


**Figure 4.1:** (a) Dimension for simple patch resonating at 4.55 GHz (CST Microwave Studio)  
 (b) Simple patch shown with notionally superposed strip line section  
 (Dimensions are given in table 4.2)  
 (c) Actual modified patch geometry

Results are obtained by moving the feed point in increments of  $0.25\text{ mm}$  along the length from the patch centre (figure 4.2)

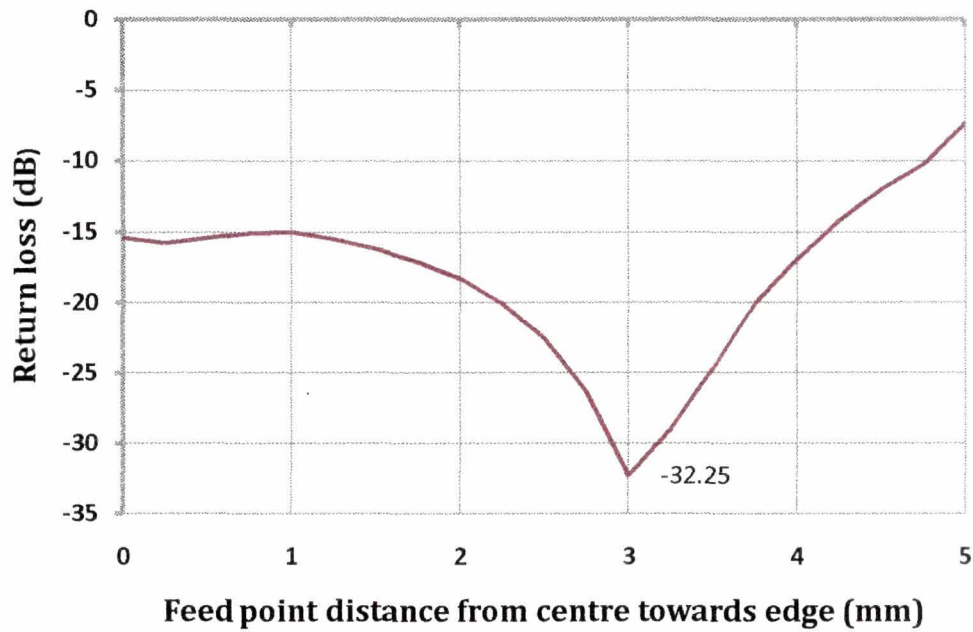


**Figure 4.2:** Simulated return loss vs. feed point location (from patch centre)

Simulated results indicate that a maximum return loss ( $RL$ ) value of  $-33.25$  dB is obtained when feed point is located at 3 mm from the centre towards one of the radiating edges.

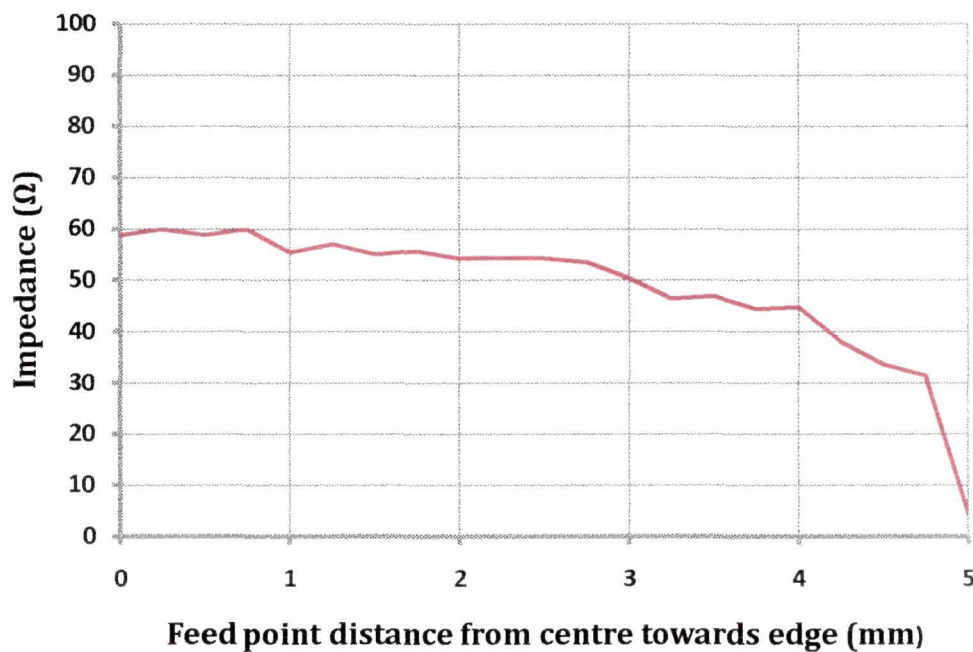


**Figure 4.3:** Simulated plot of impedance ( $\Omega$ ) vs. feed point location

Impedance (real part) value at this feed point location is  $50.36 \Omega$  (figure 4.3). The corresponding value of VSWR is found to be 1.035 as shown in figure 4.4.

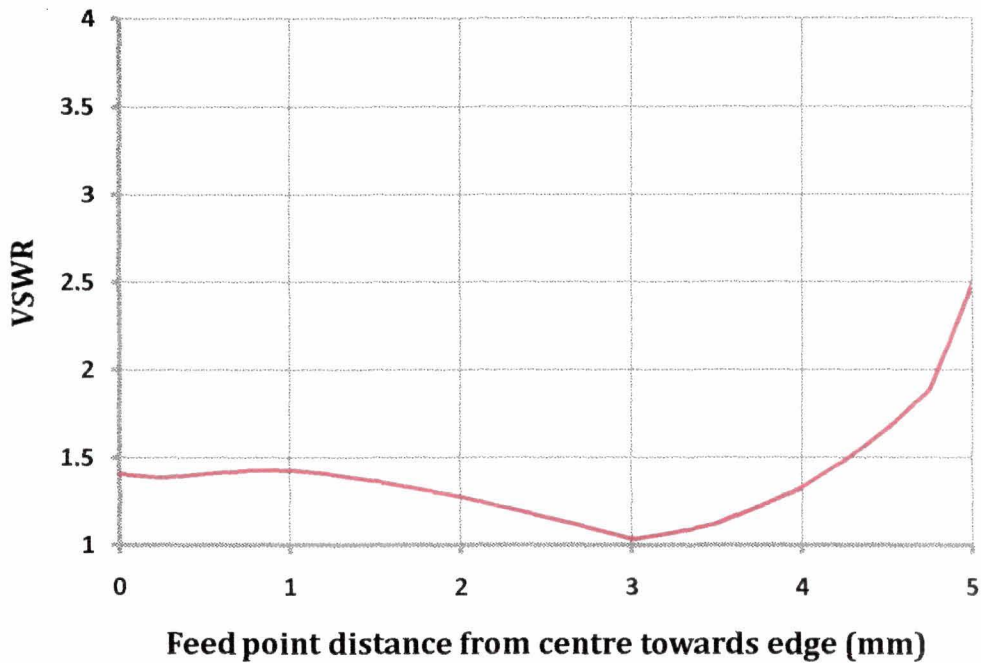


**Figure 4.4:** Simulated plot of VSWR vs. feed point location

With this feed point, a simple strip line section near one of the radiating edges is superposed (figure 4.1 b).

### 4.3 Antenna performance studies with varying strip line width and tilt angle

Simulation studies using CST Microwave Studio has been carried out on the effect of strip line width ( $w$ ) and tilt angle ( $\theta_t$ ) on the return loss performance and resonant frequency. The same set of data from simulated results are presented in two separate subsections, 4.3.1 and 4.3.2 to highlight the effect of  $\theta_t$  and  $w$  on return loss performance

#### 4.3.1 Variation of strip line width and its effect on RL performance

The width of the strip line is varied with four values of  $w$  (=1mm, 2mm, 3mm, 4mm) with different tilt angle  $\theta_t$  (= 10°, 20°, 30°, 40°, 45°). The effect of width variation of the strip line on antenna performances including resonant frequency and  $RL$  are shown in figures 4.5 to 4.9 for different tilt angle ( $\theta_t$ ). It is observed from figure 4.5 that with varying strip line width ( $w$ ), return loss value corresponding to the lower resonant frequency ( $LRF$ ) is almost same for tilt angle  $\theta_t = 10^\circ$  with very little change (0.05 GHz) in the resonant frequency. However the return loss for the upper resonant frequency ( $URF$ ) marginally degrades from -26.13 dB to -24.72 dB when the strip line width changed from 1 mm to 2 mm. Subsequent increase in width to 3 mm and then onto 4 mm results in an almost linear improvement in the return loss values from -24.72 dB to -31.92 dB. Increasing  $w$  to 5 mm results in a degradation of the  $RL$  values for both the

resonant frequencies. Hence, the best trade off for both the resonant frequencies from the return loss performance aspect is for a strip line width of 4 mm.

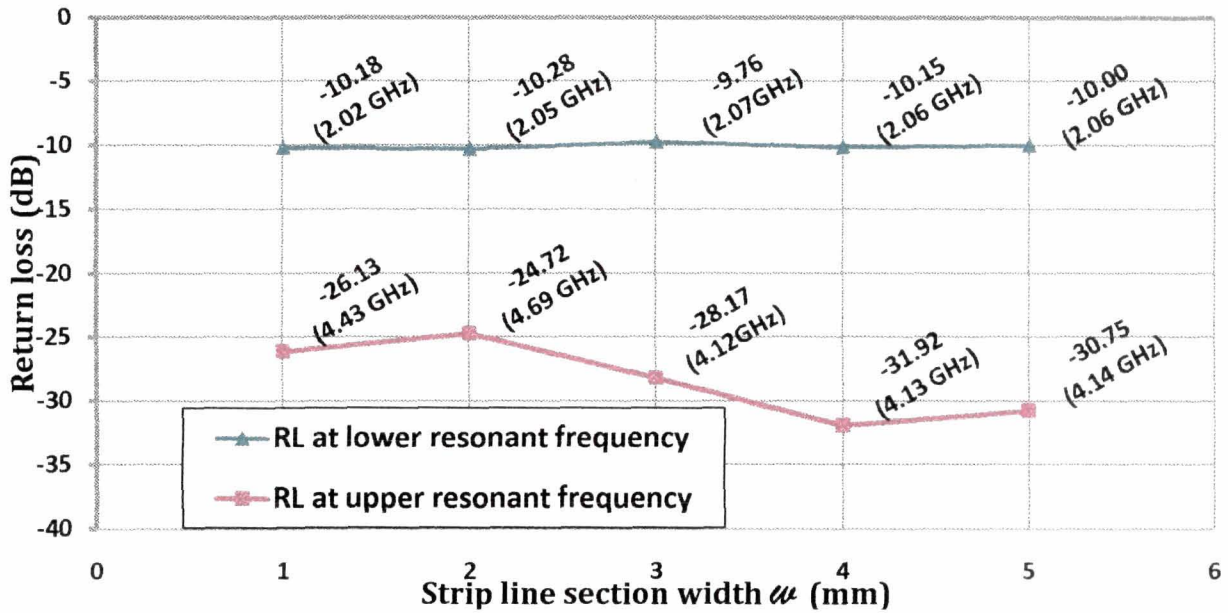


Figure 4.5: Variation of RL value with strip line for  $\theta_t = 10^\circ$  (resonant frequency shown in brackets)

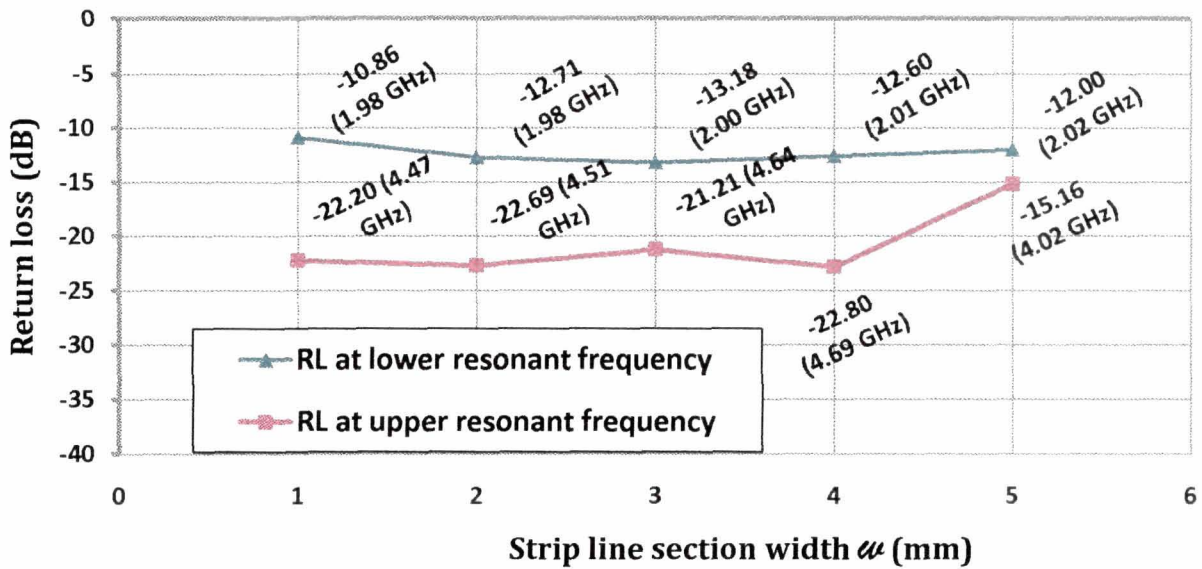


Figure 4.6: Variation of RL value with strip line for  $\theta_t = 20^\circ$  (resonant frequency shown in brackets)

**For tilt angle  $\theta_t = 20^\circ$**

Figure 4.6 shows the variation of RL values with  $\omega$  for  $\theta_t = 20^\circ$ . While the return loss for the LRF initially increases reaching a maximum value of -13.18 dB for  $\omega = 3$  mm, the return loss value for URF is much less affected with change in  $\omega$  as compared to  $\theta_t = 10^\circ$ . The best trade off for both the resonant frequencies from the return performance aspect is a strip line width of 3 mm. Although for  $\omega = 3$  mm, the best RL value obtained



is -13.18 dB for the *LRF*. The *RL* for the *URF* is -21.2 dB which improves to -22.80 dB for  $w = 4$  mm with only a slight degradation (a difference of 0.58 dB) of *RL* value for the *LRF* from -13.18 dB to -12.60 dB. Further increase in  $w$  leads to poorer *RL* performance for both the resonant frequencies.

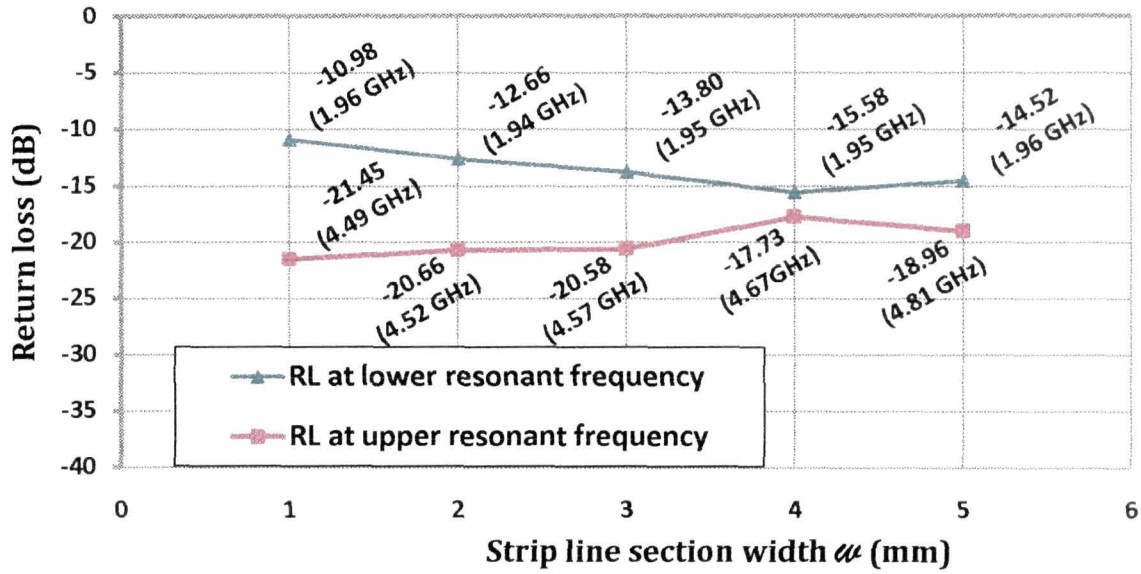
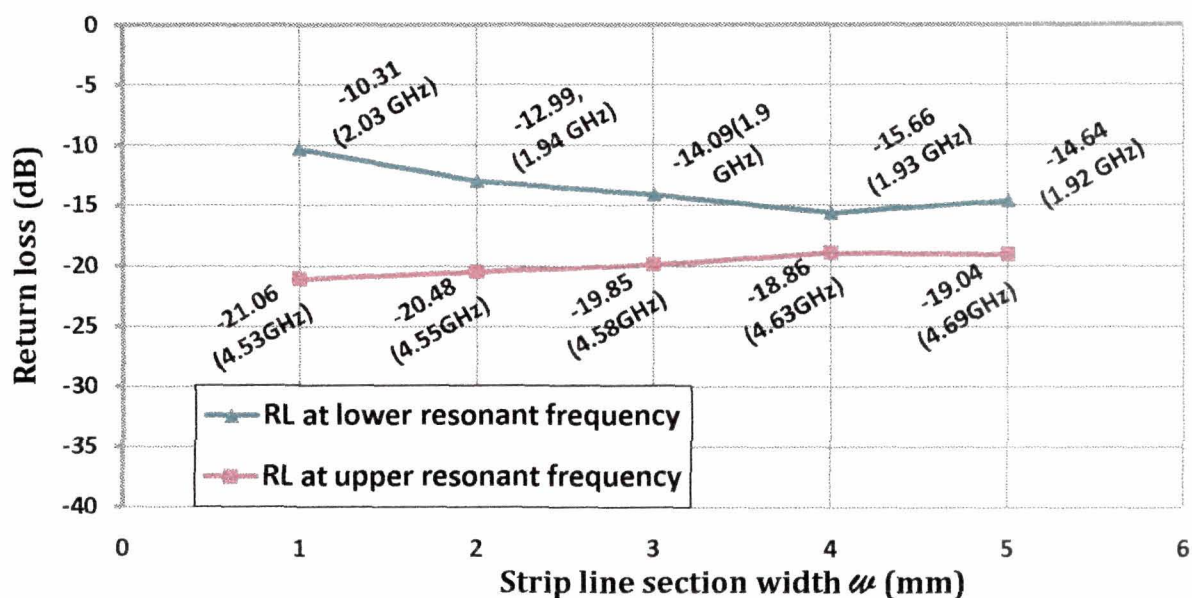


Figure 4.7: Variation of RL value with strip line for  $\theta_t = 30^\circ$  (resonant frequency shown in brackets)

**For tilt angle  $\theta_t = 30^\circ$**

The simulated results indicate that when the strip line width ( $w$ ) is changed from 1 mm to 4 mm with tilt angle  $\theta_t = 30^\circ$ , *RL* values corresponding to the *LRF* gradually improves from -10.98 dB at 1.96 GHz for  $w = 1$  mm to -15.58 dB at 1.95 GHz for  $w = 4$  mm. For the *URF* a slight degradation of return loss value is observed when the strip line width is changed from 1 mm to 2 mm with return loss value changing from -21.45 dB to -20.66 dB while the value is almost same when the strip line width is further changed to 3 mm. For  $w = 4$  mm, the return loss improves to -15.58 dB for the *LRF* while for the *URF*, the return loss degrades to -17.73 dB. When  $w$  is increased to 5 mm, *RL* performance for the *LRF*, which in any case is poorer than that for the *URF*, deteriorates even further although the *RL* for the *URF* improves. For a dual frequency antenna, therefore, a strip line width of 4 mm will be the desired width from amongst the five different width studied.



**Figure 4.8:** Variation of RL value with strip line for  $\theta_t = 40^\circ$  (resonant frequency shown in brackets)

**For tilt angle  $\theta_t = 40^\circ$**

As can be seen from the figure 4.8, for tilted angle  $\theta_t = 40^\circ$ , return loss value for the *LRF* improves from -10.31 dB at 2.03 GHz. to -15.66 dB at 1.93 GHz when  $w$  changes from 1 mm to 4 mm as against the degrade in the return loss value for the *URF* from -21.06 dB at 4.53 GHz to -18.86 dB at 4.63 GHz. As is the case with  $\theta_t = 30^\circ$ , the *RL* in this case degrades for the *LRF* with an accompanying improvement in *RL* for the *URF*. Hence, for  $\theta_t = 40^\circ$ , the best trade off for both the resonant frequencies from the return loss performance aspect is a strip line width of  $w = 4$  mm.

**For tilt angle  $\theta_t = 45^\circ$**

For  $\theta_t = 45^\circ$ , change in return loss value for both the upper and *LRF* with change in  $w$  is similar to that for  $\theta_t = 40^\circ$  with minor difference in resonant frequency and return loss values as can be seen by comparing figures 4.9 with 4.8. It is therefore apparent that for  $\theta_t = 45^\circ$ , a strip line width ( $w$ ) of 4 mm is desirable for best *RL* performance in both the resonant frequencies.

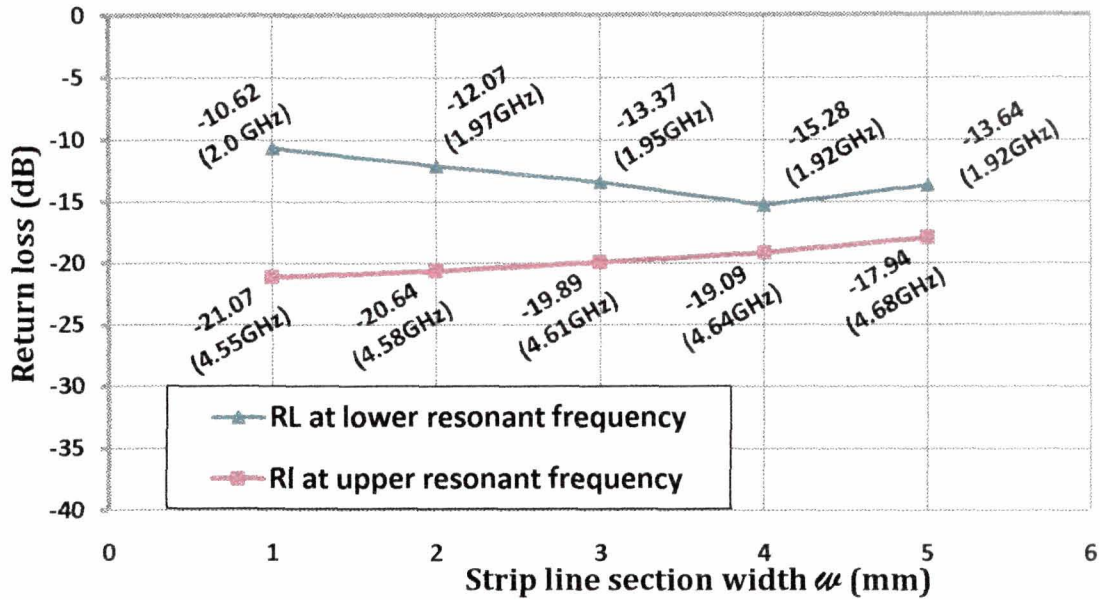


Figure 4.9: Variation of RL value with strip line for  $\theta_t = 45^\circ$  (resonant frequency shown in brackets)

### 4.3.2 Variation of tilting angle and its effect on RL performance

As the RL performance is dependent for this modified patch structure on both the strip line width  $w$  and the tilt angle  $\theta_t$ , the same set of data used in subsection 4.3.1 are again used here to show the effect of tilt angle on the RL of antenna which are shown in figures 4.10 to 4.13.

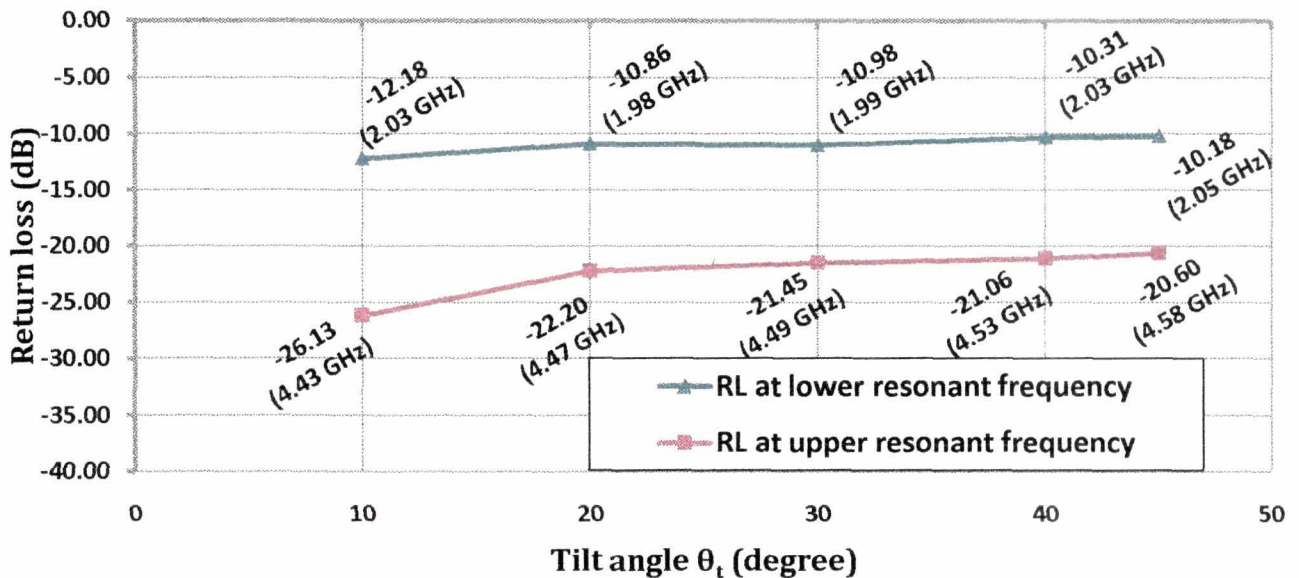


Figure 4.10: Variation of RL value with tilt angle ( $\theta_t$ ) for strip line  $w = 1$  mm

#### Strip width 1 mm and 2 mm

The return loss value for both the upper and lower resonant frequencies degrade with increase in  $\theta_t$  from  $10^\circ$  to  $45^\circ$  (figure 4.10). For  $w = 2$  mm, there is some



improvement in the return loss value for the *LRF* at the cost of the return loss value of the *URF* from  $\theta_t = 10^\circ$  to  $20^\circ$  (figure 4.11). There is no significant change in the *RL* value for both the resonant frequency when  $\theta_t$  increases from  $20^\circ$  to  $30^\circ$  and to  $40^\circ$ , which eventually shows deteriorating trend when  $\theta_t$  increases to  $45^\circ$ .

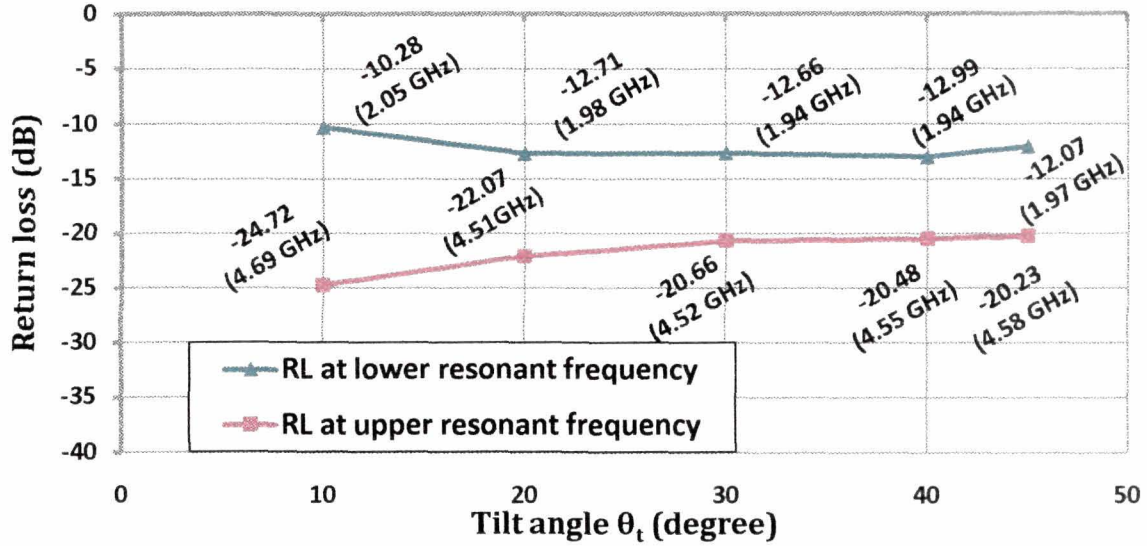


Figure 4.11: Variation of RL value with tilt angle ( $\theta_t$ ) for strip line  $w = 2$  mm

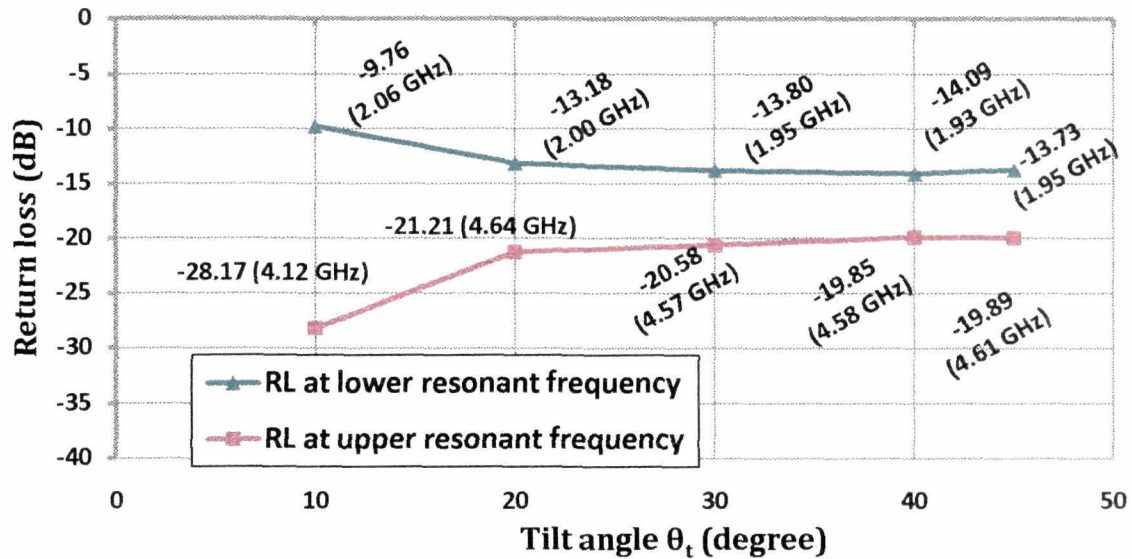


Figure 4.12: Variation of RL value with tilt angle ( $\theta_t$ ) for strip line  $w = 3$  mm

**Strip width 3 mm**

Simulated results indicate that for  $w$  of 3 mm (figure 4.12), the return loss value for the *LRF* improves with change in  $\theta_t$  from  $10^\circ$  to  $20^\circ$ , but to a lesser extent as compared to the degradation of return loss value for the *URF*. For  $\theta_t = 20^\circ, 30^\circ, 40^\circ$  and  $45^\circ$  the return

loss values for both the resonant frequencies do not differ by much but nonetheless, the best compromise again can be seen for  $\theta_t = 40^\circ$ .

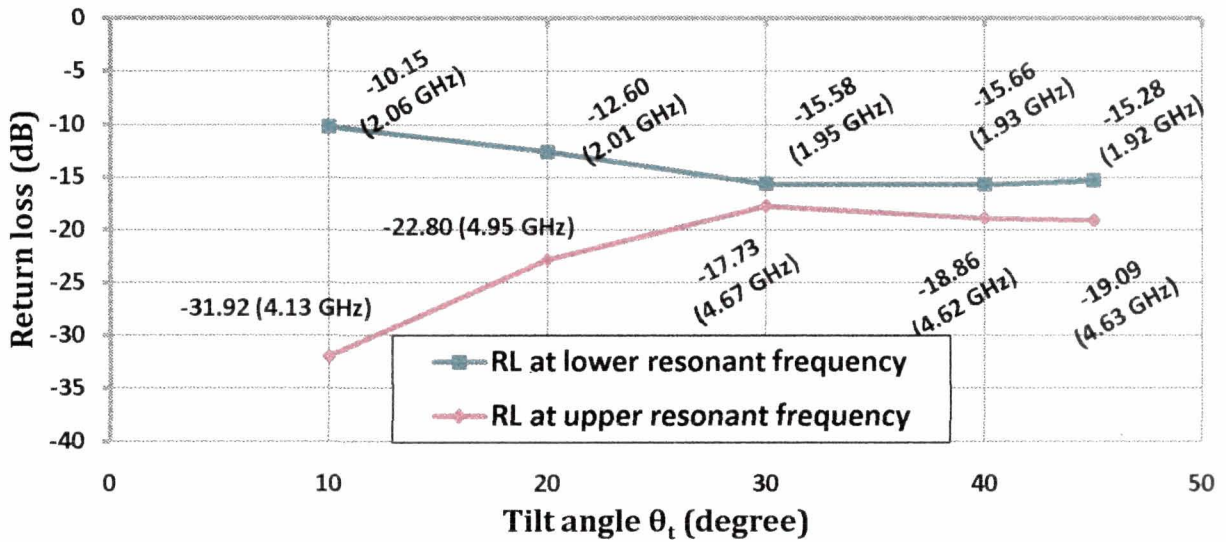


Figure 4.13: Variation of RL value with tilt angle ( $\theta_t$ ) for strip line  $w=4$  mm

**Strip width 4 mm**

Figure 4.13 shows the variation of return loss with tilt angle ( $\theta_t$ ) for a line width of 4 mm from amongst all the tilt angles and strip line widths studied, the best return loss value of -31.92 dB is observed for the *URF* whereas the return loss for the *LRF* is just near the acceptable level of -10.00 dB. From  $10^\circ$  through  $20^\circ$  onto  $30^\circ$  the return loss value for the *URF* degrades rapidly with a much lesser improvement in the return loss for the *LRF*.

From  $\theta_t = 30^\circ$  to  $40^\circ$  and then to  $45^\circ$ , although the change in return loss value is not significant, the best *RL* for the *LRF* again is found to be for  $\theta_t = 40^\circ$ .

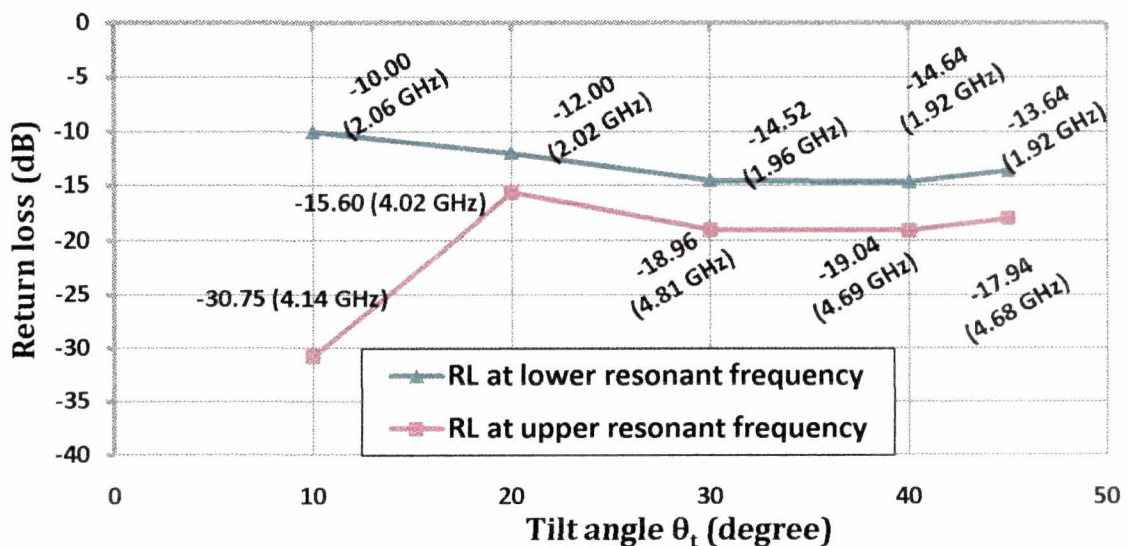


Figure 4.14: Variation of RL value with tilt angle ( $\theta_t$ ) for strip line  $w=5$  mm

### ***Strip width 5 mm***

With the increase of  $\theta_t$ , improvement of  $RL$  of the  $LRF$  is observed from  $\theta_t = 10^\circ$  to  $20^\circ$  and then on to  $30^\circ$  to  $40^\circ$  as shown figure 4.14. However, for the  $URF$ , a steep degradation of the  $RL$  value is observed when  $\theta_t$  changes from  $10^\circ$  to  $20^\circ$ . Thereafter, with increase in  $\theta_t$ , the pattern of variation of  $RL$  follows almost that for the  $LRF$ .

As can be seen from figures 4.5 to 4.14, when the simple patch is modified by superposing the strip line, the patch resonates at two different frequencies instead of one in the unmodified simple patch. While both the frequencies are lower than the resonant frequency of the simple unmodified patch (4.55 GHz), one of the resonant frequencies (the lower one) is less than half the  $URF$  for all combinations of  $\theta_t$  and  $w$  studied.

From the simulated plots, the best  $RL$  performance trade off for both the resonant frequencies is found for strip line width of  $w = 4$  mm, for  $\theta_t = 30^\circ$ ,  $40^\circ$  and  $45^\circ$  and the antenna behaves as dual band patch with acceptable range of return loss values for both the frequencies. Moreover tuning of both the resonant frequencies is observed for different strip width ( $w$ ) with maximum tuning observed for patch with strip line width  $w = 4$  mm.  $URF$  tuning is found to be 0.82 GHz and corresponding tuning in  $LRF$  is 0.140 GHz for varying value of tilt angle with the strip width of 4 mm. The shift in upper and lower resonant frequencies is simultaneously accompanied by improvement and degradation of  $RL$  values at both the resonant frequencies. The variation of return loss values for both the resonant frequencies with different strip line width for varying values of tilt angle is shown in figures 4.15 (a & b) which visualizes the variations more distinctly.

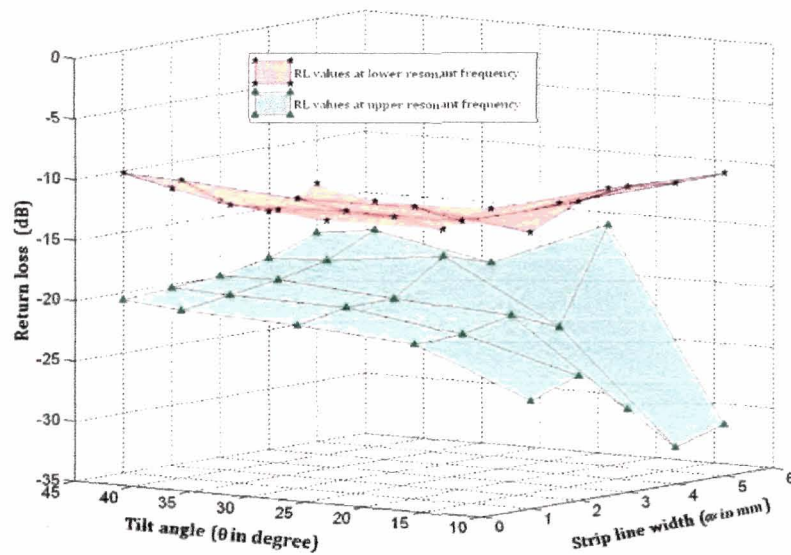


**Figure 4.15(a):** 3-D plot of return loss as a function of  $\theta_t$  and  $\omega$  (simulated) for lower and upper resonant frequency

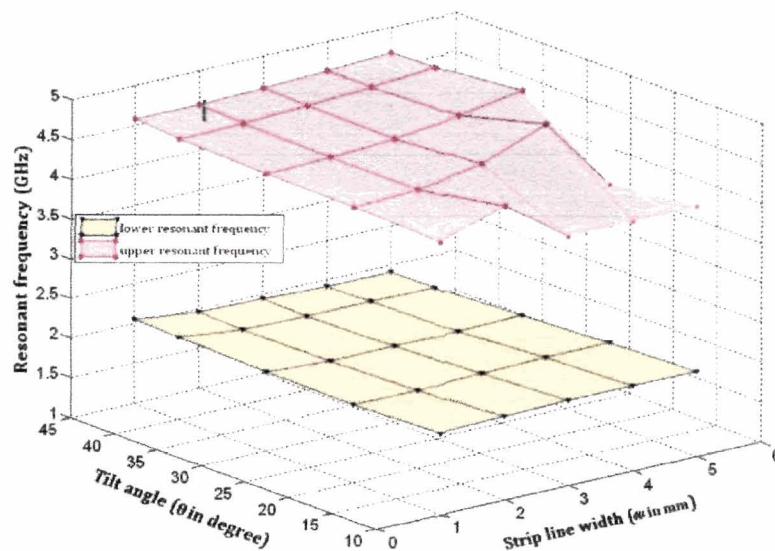


**Figure 4.15(b):** 3-D plot of resonant frequency as a function of  $\theta_t$  and  $\omega$  (simulated) for lower and upper resonant frequency

### 4.3.3 Variation of tilt angle and its effect on antenna size

Simulated results indicate that the antenna with different values of strip width( $\omega$ ) with varying tilt angle $\theta_t$ , the modified patch antenna resonates in two distinct frequencies, as can be seen from figures 4.5 to 4.14. Since the  $LRF$  is less than half of the resonant frequency for the simple patch for all the values of  $\theta_t$  and  $w$  studied, the modified patch can reduce the size in excess of 54%. Following figure 4.16 shows the size reduction (%)



for the modified patch with different strip line with tilt angle ( $\theta_t$ ) for different strip line width ( $w$ ).

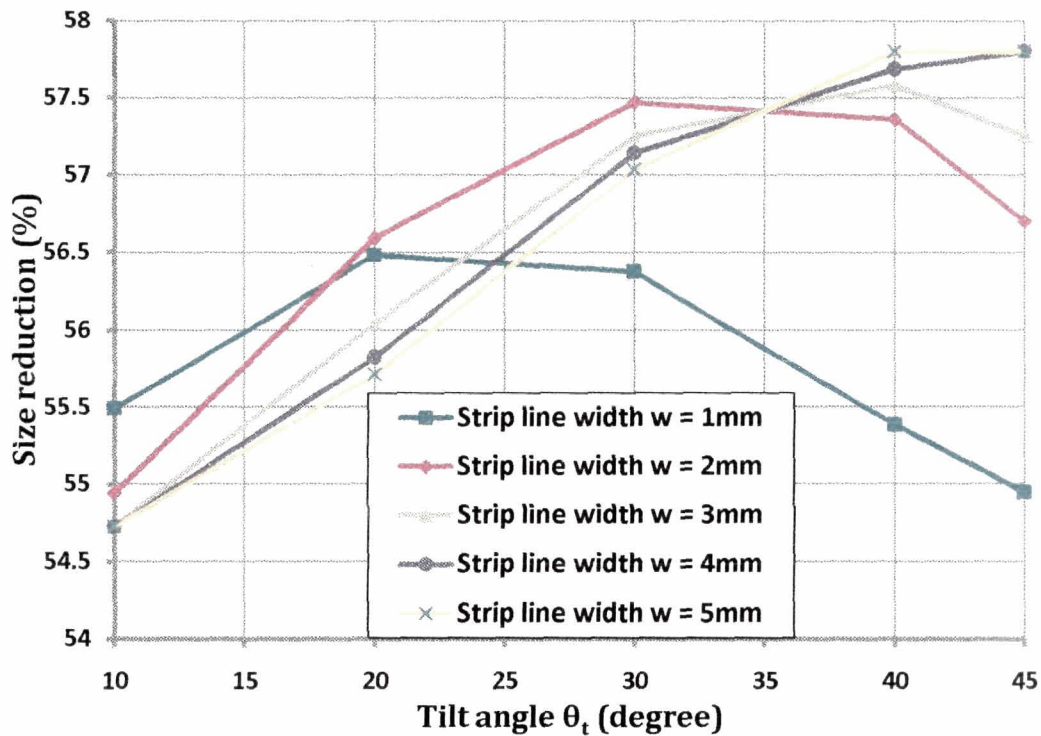


**Figure 4.16:** Size reduction (%) for with different strip line width ( $w$ ) for varied tilt angle ( $\theta_t$ )

As can be seen from the figure, a size reduction of 57.80% is achieved for a strip line width ( $w$ ) of 4 mm and 5 mm with  $\theta_t = 45^\circ$ . With equivalent size reduction for the two strip line widths,  $w = 4$  mm is preferable because of its better *RL* performance. Table 4.1 gives the *LRF* values and the corresponding size reduction for different  $\theta_t$  with  $w = 4$  mm.

**Table 4.1:** Size reduction for strip line width  $w$  of 4 mm

Antenna type	Lower resonant frequency (GHz)	Size reduction (%)
Simple Patch		4.55
$\theta = 10^\circ$	2.06	54.73
$\theta = 20^\circ$	2.01	55.82
$\theta = 30^\circ$	1.95	57.14
$\theta = 40^\circ$	1.93	57.69
$\theta = 45^\circ$	1.92	57.80
Resonant frequency of corresponding simple patch	4.55 GHz	

#### 4.4 Measured results

The fabricated simple and modified patches are shown in figure 4.17 (a) and 4.17 (b) respectively. A standard SMA connector is used to feed the antenna.

Measurements carried out on the modified path structure shown in figure 4.1 (c) mainly focuses on studying the following aspects:

1. Size reduction
2. Multiple/ dual resonant frequency
3. Tuning of the resonant frequencies.

The simple and modified patch geometries shown in figures 4.1(a) to 4.1(c) are fabricated on glass epoxy copper laminated substrates with specifications given in table 4.2.

**Table 4.2:** Specifications of RMSA and strip line (in reference to figure 4.1 (b))

<i>Parameter</i>	<i>Value</i>
Patch width (W)	22 mm
Patch length (L)	30 mm
Height of the substrate (h)	1.52 mm
Dielectric constant ( $\epsilon_r$ )	4.8
Feed point distance from centre (p)	3 mm
Strip line width ( $w$ )	4 mm
Strip line width ( $l = W$ )	30 mm
m	2.25 mm
n	1.0 mm
$\theta_t$	10°, 20°, 30°, 40°, 45°



**Figure 4.17:** (a) Fabricated simple patch designed at 4.75 GHz

(b) One of the fabricated patch antenna with superposed strip line ( $\theta_t = 40^\circ$ )

#### 4.4.1 Return loss measurements of simple and modified patch with the strip line

Measurements are carried out for all the fabricated patch antenna structures including the *RL* plot for the simple patch is shown in figure 4.18 along with the simulated plot.

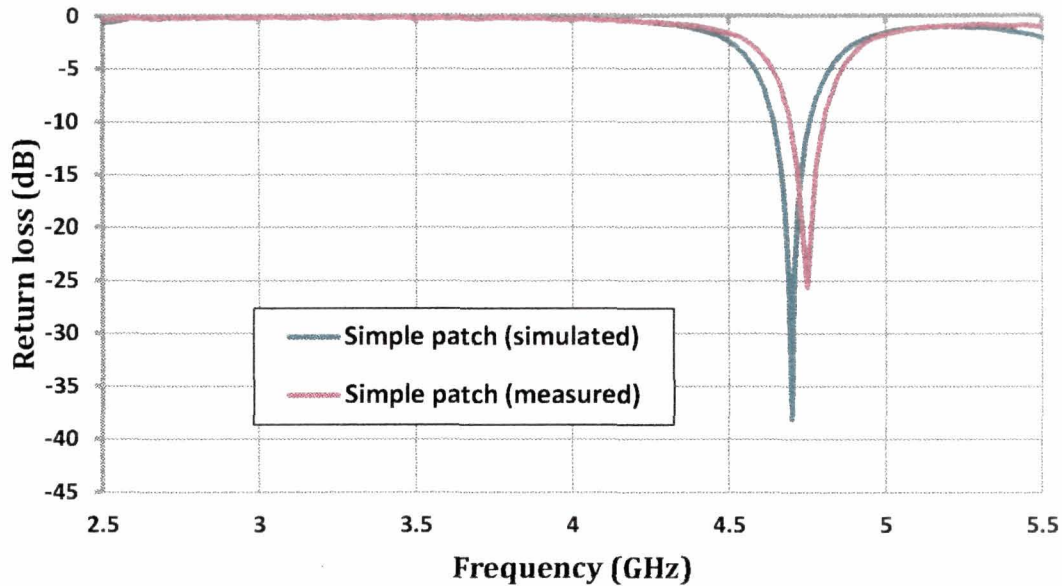


**Figure 4.18:** Measured and simulated return loss plot for the simple patch

Measured results indicate that the simple patch antenna resonates at 4.75 GHz with a *RL* value of -25.57 dB whereas the simulated value with the same dimension of the patch resonates at 4.7 GHz with *RL* of -32.25 dB. The measured resonant frequency is deviated from the simulated value by about 1%. This frequency difference may be due to fabrication tolerances.

Measured *RL* plots of the modified patch structures with varying tilt angle ( $\theta_t = 10^\circ$ ,  $20^\circ$ ,  $30^\circ$ ,  $40^\circ$ ,  $45^\circ$ ) are shown in figure 4.19. *RL* plots for both the upper and lower frequencies are shown separately in figures 4.20 and 4.21. The relevant values from these plots are given in table 4.3.

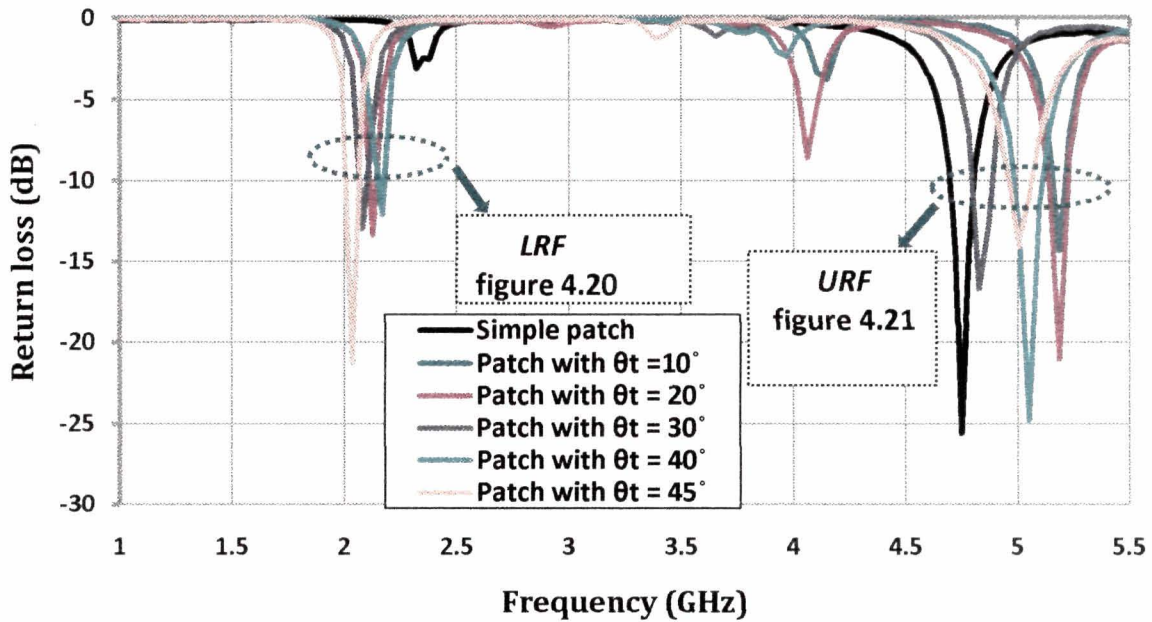


**Figure 4.19:** Measured return loss plots for different values of tilt angle,  $\theta_t$  (both *LRF* and *URF*)

It is observed from the measured results that the patch with tilt angles ( $\theta_t$ ) resonate at two frequencies, which are widely separated. The results indicate change in both the upper and lower resonant frequencies with varying tilt angle ( $\theta_t$ ). The *LRF* which is 2.17 GHz for  $\theta_t = 10^\circ$  and  $40^\circ$  with *RL* values of -11.32 dB and 12.08 dB respectively goes down to 2.04 GHz with a significantly improved *RL* value of -21.22 dB.

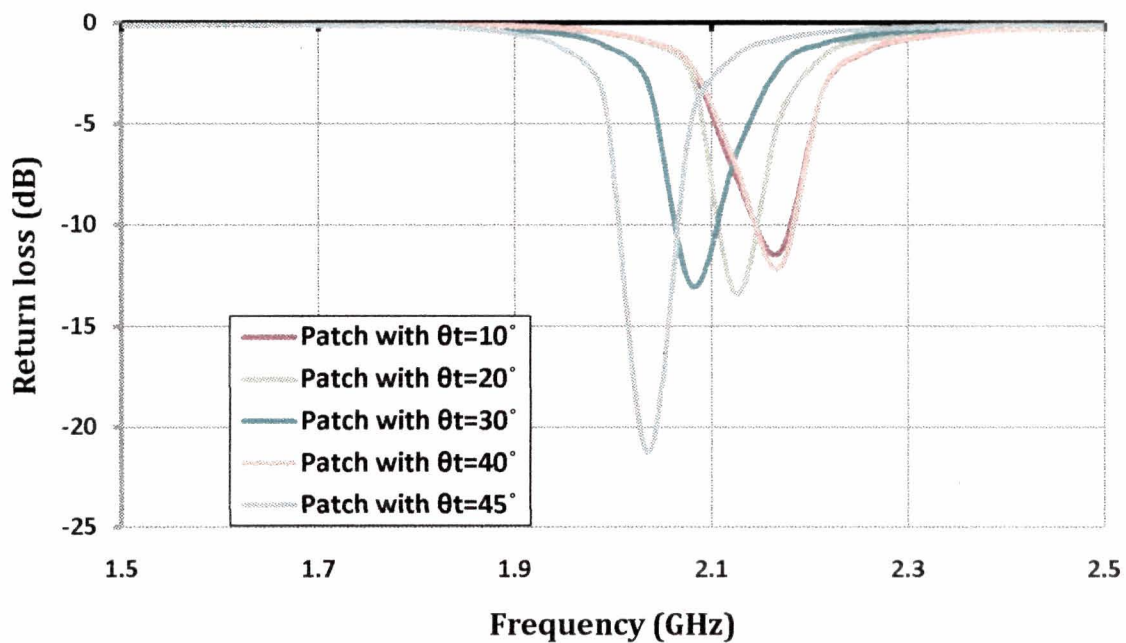


**Figure 4.20:** Measured return loss plot for different values of tilt angle,  $\theta_t$  for lower resonant frequency



From the measured result (figure 4.20), it is observed that the patch with tilt angle  $\theta_t = 10^\circ$  resonates at a lower frequency of 2.17 GHz with a  $RL$  value of -11.32 dB. When the tilt angle is increased to  $20^\circ$ , resonant frequency comes down to 2.13 GHz with an improved  $RL$  value of -13.37 dB. As the  $\theta_t$  is increased to  $30^\circ$ , resonant frequency further comes down to 2.08 GHz with slight degradation of  $RL$  value (-12.99 dB) in comparison to the patch with tilt angle  $\theta_t = 20^\circ$ . For tilt angle  $\theta_t = 40^\circ$ , the patch resonates at 2.17 GHz, the same frequency at which resonates for tilt angle,  $\theta_t = 10^\circ$  accompanied by a slightly better  $RL$  value of -12.08 dB. The measured results show that for the patch with tilt angle,  $\theta_t = 45^\circ$ , the resonant frequency shifts to the lowest value of 2.04 GHz accompanied by the best  $RL$  of -21.22 dB amongst all the tilt angles studied ( $\theta_t = 10^\circ, 20^\circ, 30^\circ, 40^\circ$  and  $45^\circ$ ). The tuning range for the  $LRF$  is 0.13 GHz.

The  $URF$  (figure 4.21) also goes down from 5.19 GHz for,  $\theta_t = 10^\circ$  and 5.05 GHz for  $\theta_t = 40^\circ$  to 5.01 GHz for  $\theta_t = 45^\circ$ . However, as can be seen from table 4.3 the  $RL$  for the  $LRF$  with  $\theta_t = 40^\circ$  is 12.08 dB while for the  $URF$  it is much better with a  $RL$  of -24.74 dB. The condition reverses when  $\theta_t$  is increased to  $45^\circ$  for which the  $RL$  of the  $LRF$  is -21.22 dB while for the  $URF$  it is reduced to -14.04 dB.

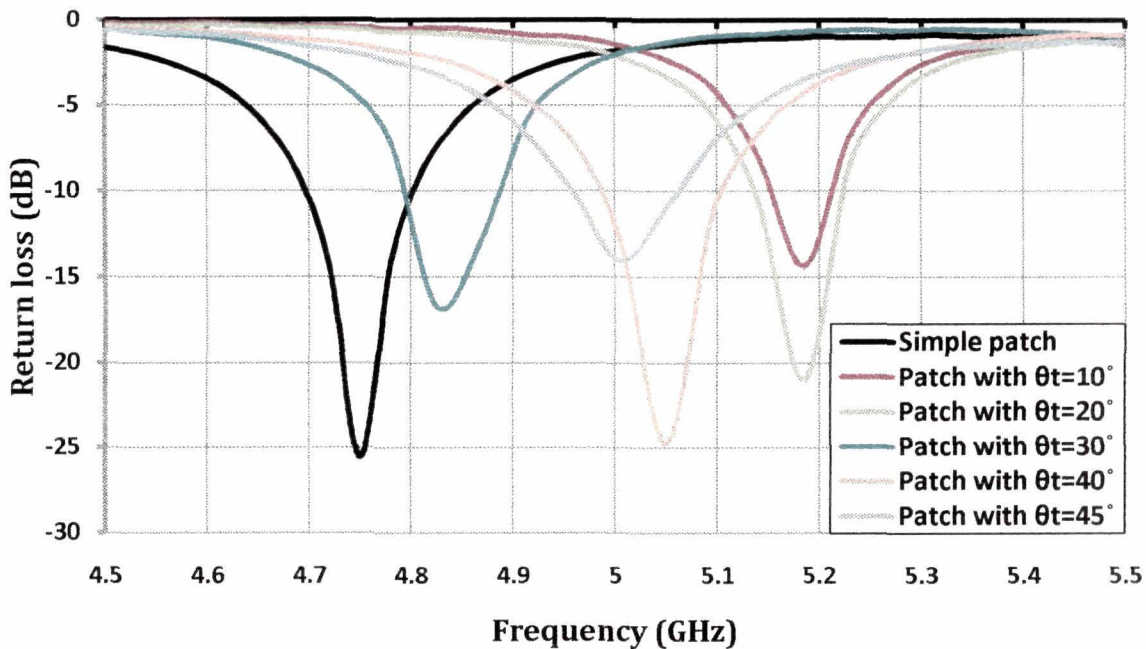


**Figure 4.21:** Measured return loss plot for different values of tilt angle,  $\theta_t$  for upper resonant frequency

**Table 4.3:** Variation of resonant frequencies and return loss with different tilt angle ( $\theta_t$ )

<i>Antenna type</i>	<i>Lower resonant frequency<sub>1</sub> (GHz)</i>	<i>Return loss (dB)</i>	<i>Upper resonant Frequency (GHz)</i>	<i>Return loss (dB)</i>
Simple Patch	--	--	4.75	-25.57
$\theta_t = 10^\circ$	2.17	-11.32	5.19	-14.33
$\theta_t = 20^\circ$	2.13	-13.37	5.12	-20.98
$\theta_t = 30^\circ$	2.08	-12.99	4.83	-16.66
$\theta_t = 40^\circ$	2.17	-12.08	5.05	-24.74
$\theta_t = 45^\circ$	2.04	-21.22	5.01	-14.04

As is evident from the measured data (table 4.3), tuning ratio upto 2.46 between *LRF* and *URF* is achieved. Moreover, size reduction up to 57% is obtained for varying tilt angle of  $\theta_t$  summarized in table 4.4. It may be mentioned that while calculating the size reduction, contribution of the strip line to the area is ignored, which if taken into account will result in a slightly lower size reduction but will still remain significant being as much as 55.4%. In addition, if the overall rectangular area (marked by the dotted line in figure 4.1(c)) occupied by the modified patch is considered, the size reduction works out to be 44.3%.

**Table 4.4:** Size reduction with different angle of rotation ( $\theta_t$ )

<i>Antenna type</i>	<i>Lower resonant frequency (GHz)</i>	<i>Upper resonant frequency (GHz)</i>	<i>Size reduction (%)</i>
Simple Patch	4.75		
$\theta_t = 10^\circ$	2.17	5.19	54
$\theta_t = 20^\circ$	2.13	5.12	55
$\theta_t = 30^\circ$	2.08	4.83	56
$\theta_t = 40^\circ$	2.17	5.05	54
$\theta_t = 45^\circ$	2.04	5.01	57

Variation of resonant frequency corresponding to different tilt angles ( $\theta_t$ ) is shown figure 4.22.

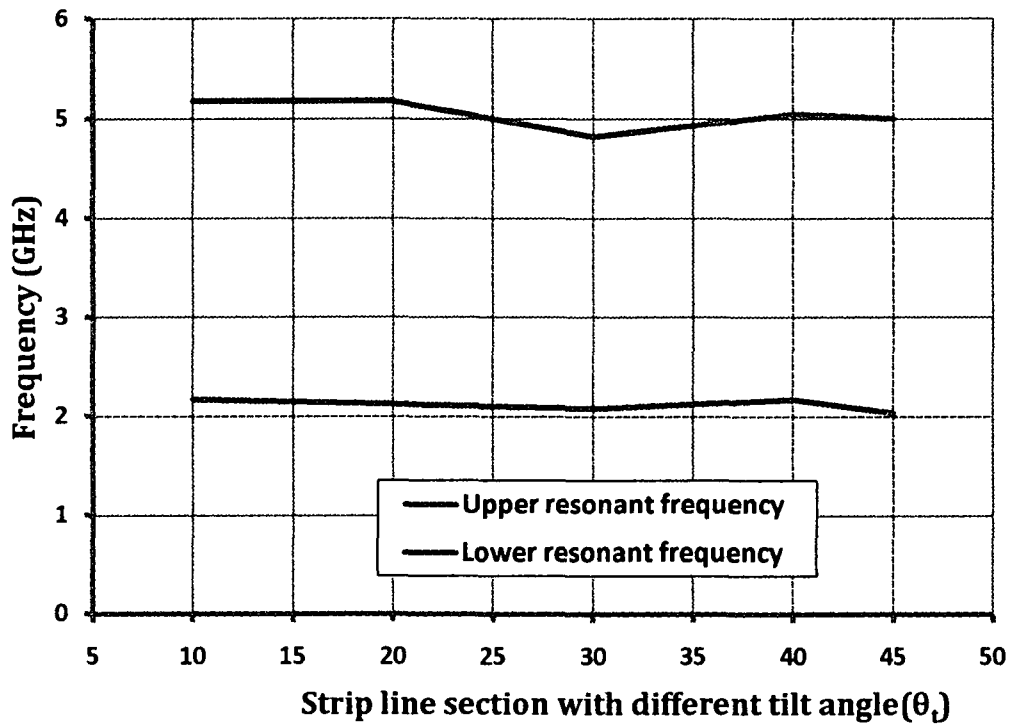


Figure 4.22: Variation of resonant frequency with different tilt angle ( $\theta_i$ )

#### 4.5 Comparison of measured and simulated results

The measured results obtained for the patch with strip line width  $w$  of 4 mm are compared with simulation results obtained for the patch with the same dimensions (table 4.3).

##### 4.5.1 Return loss performance

The simulated and measured  $RL$  plots for both the resonant frequencies of the patch antennas with different tilt angles ( $\theta_i$ ) are shown in figures 4.23 to 4.32. (Variations of the lower and upper resonant frequencies are shown in separate figures).

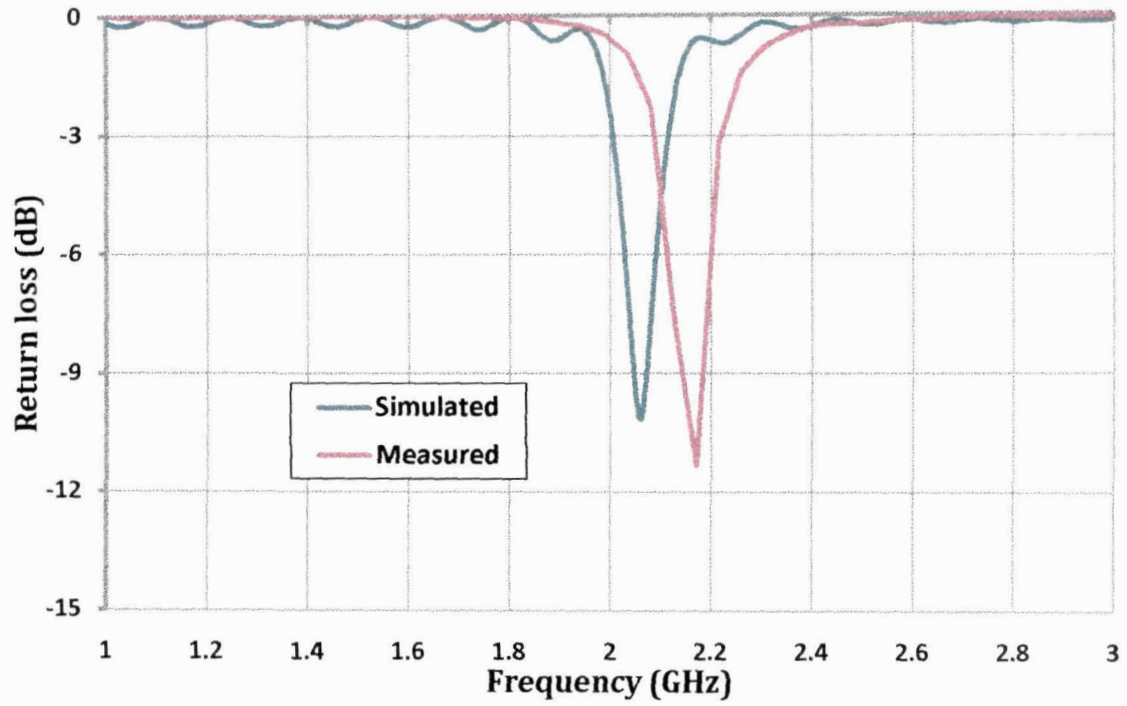


Figure 4.23: Return loss vs. frequency for  $\theta_t = 10^\circ$  (lower resonant frequency)

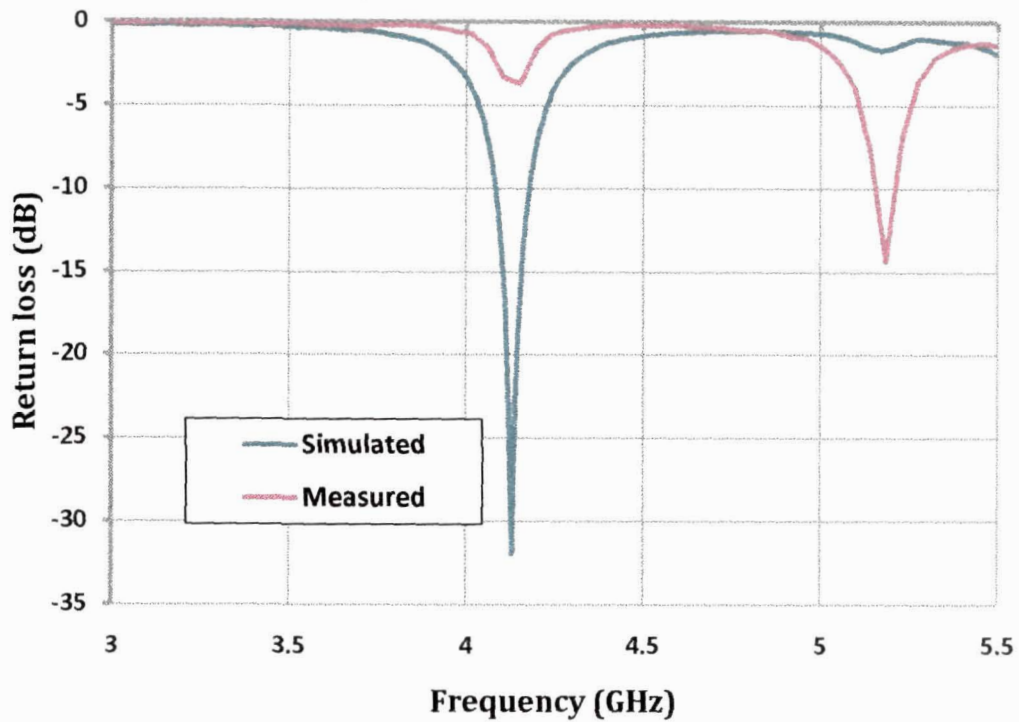


Figure 4.24: Return loss vs. frequency for  $\theta_t = 10^\circ$  (upper resonant frequency)

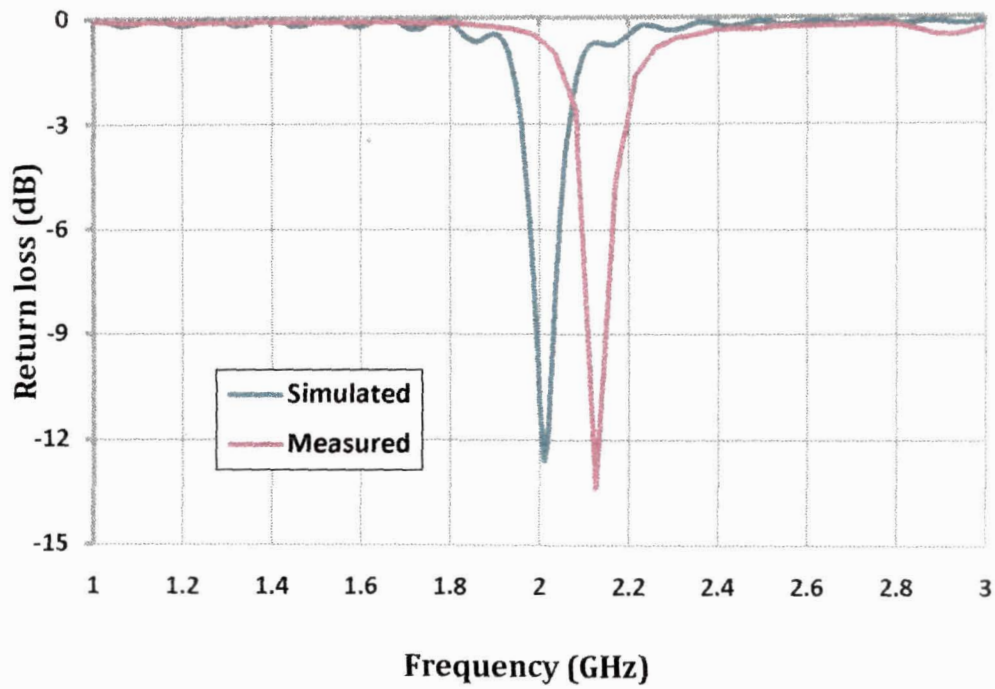


Figure 4.25: Return loss vs. frequency for  $\theta_t = 20^\circ$  (lower resonant frequency)

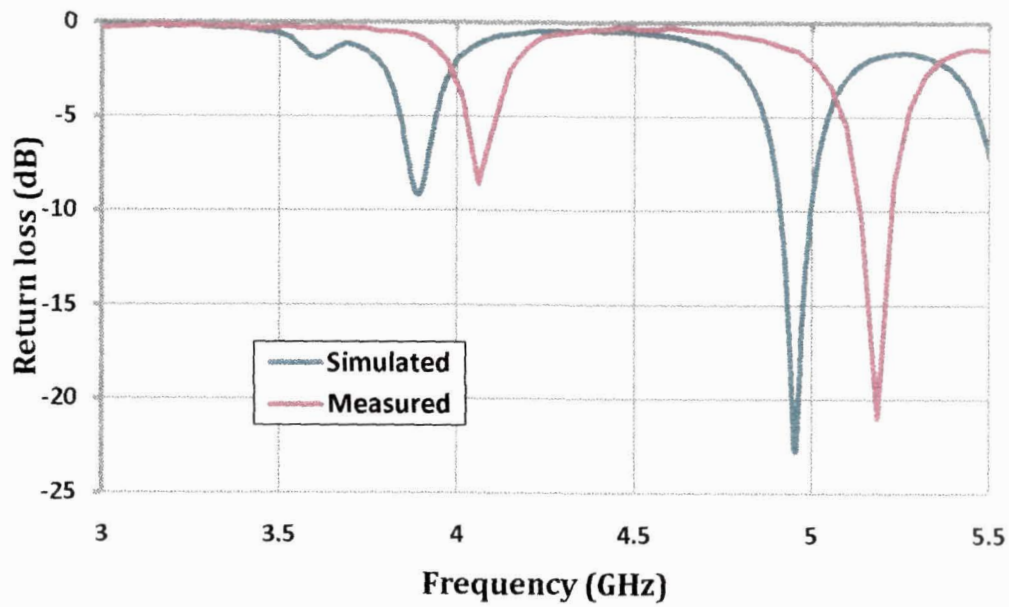


Figure 4.26: Return loss vs. frequency for  $\theta_t = 20^\circ$  (upper resonant frequency)

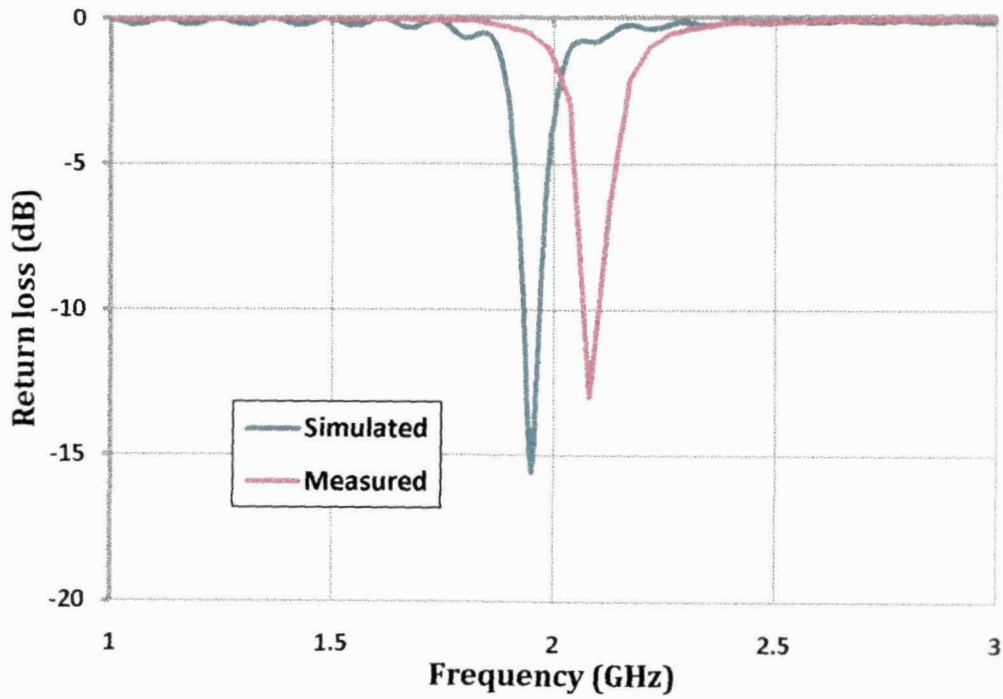


Figure 4.27: Return loss vs. frequency for  $\theta_t = 30^\circ$  (lower resonant frequency)

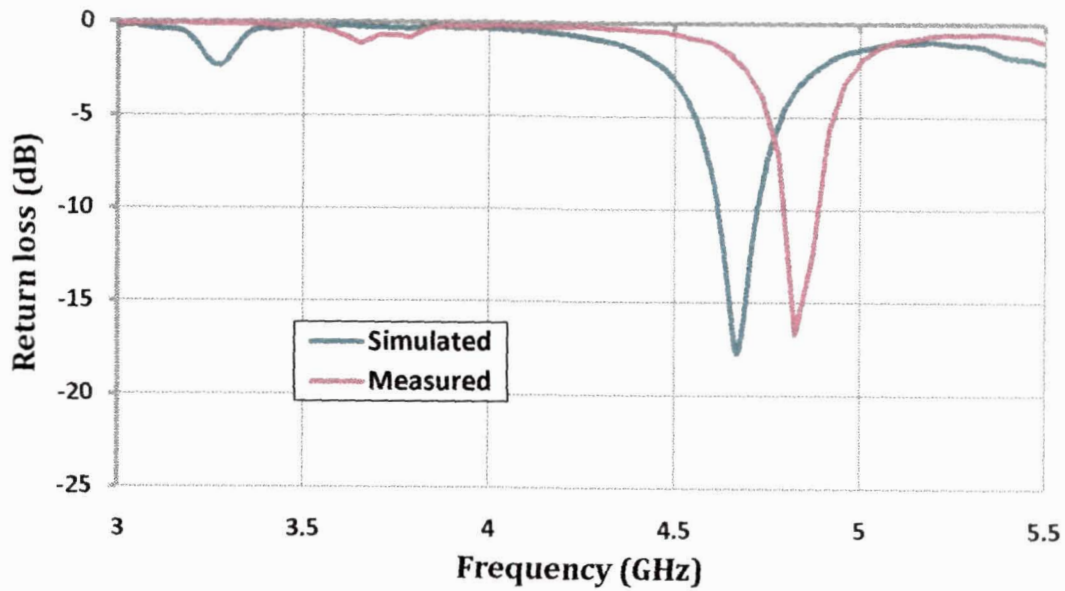


Figure 4.28: Return loss vs. frequency for  $\theta_t = 30^\circ$  (upper resonant frequency)

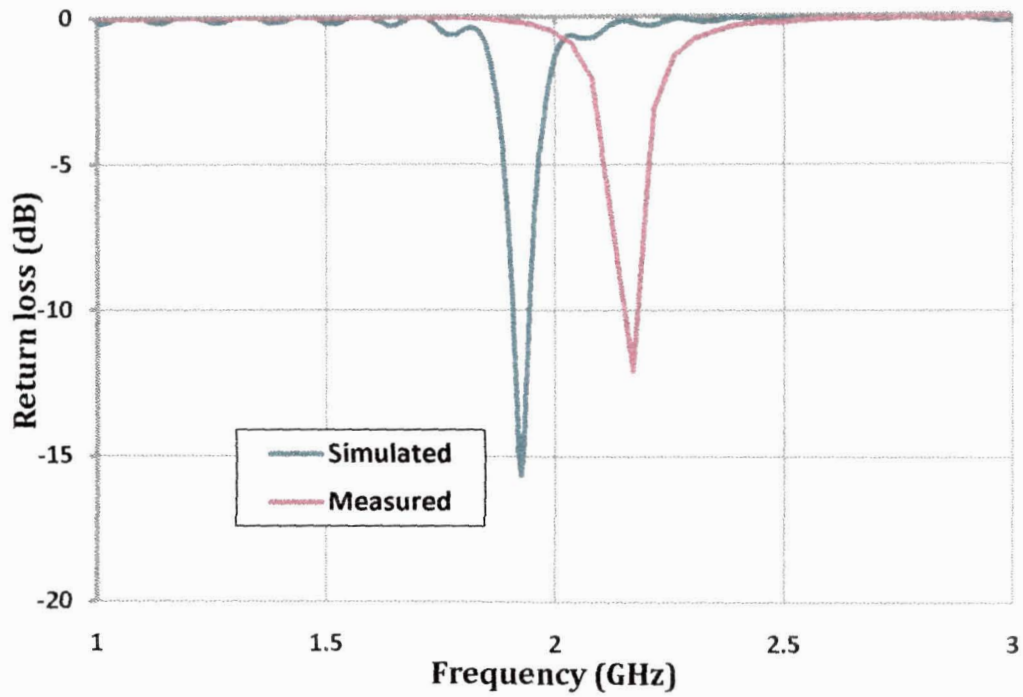


Figure 4.29: Return loss vs. frequency  $\theta_t = 40^\circ$  (lower resonant frequency)

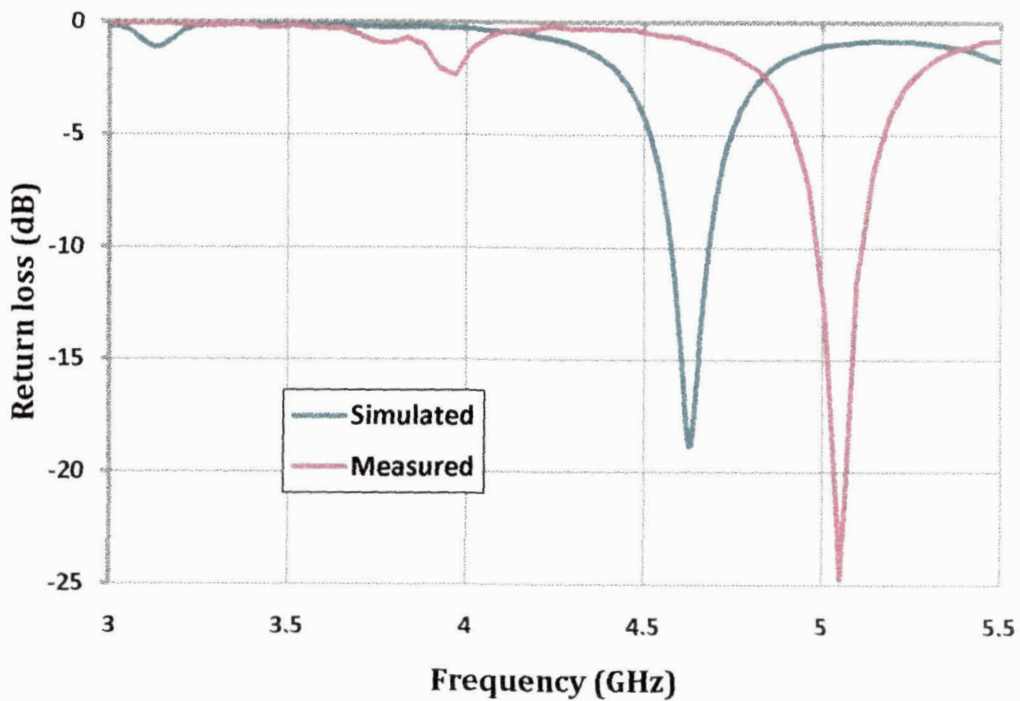
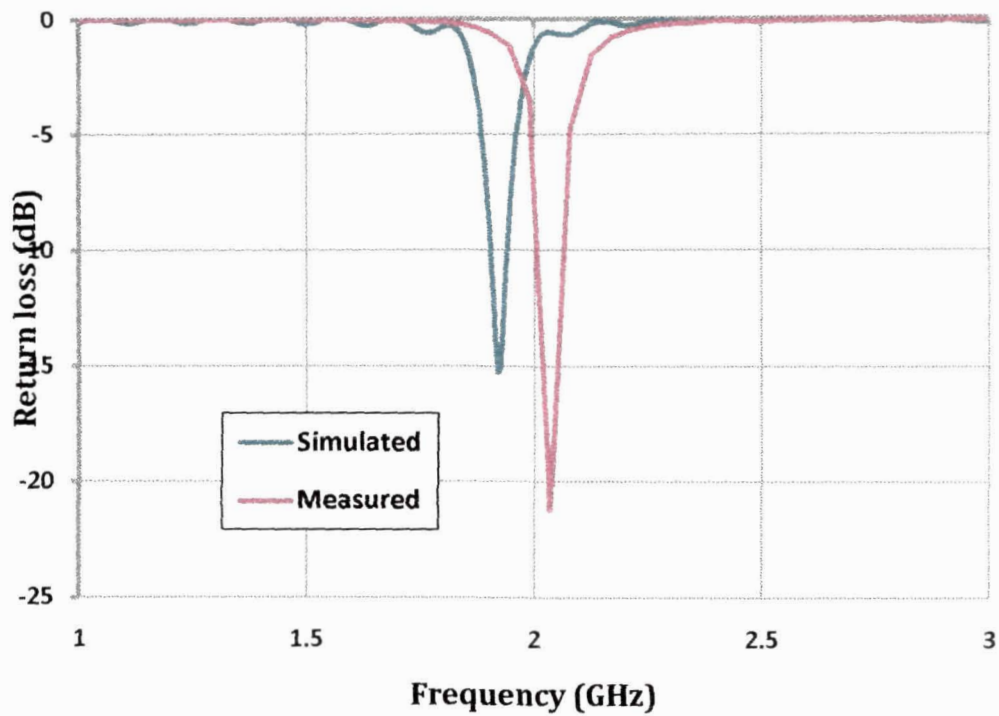
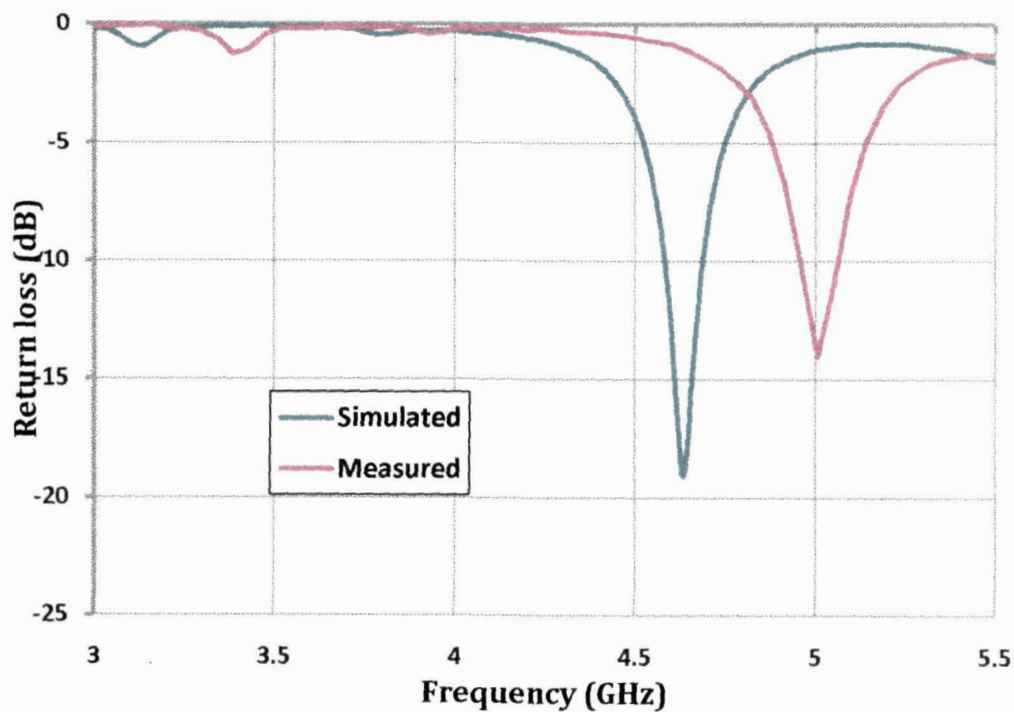


Figure 4.30: Return loss vs. frequency for  $\theta_t = 40^\circ$  (upper resonant frequency)





**Figure 4.31:** Return loss vs. frequency for  $\theta_t = 45^\circ$  (lower resonant frequency)



**Figure 4.32:** Return loss vs. frequency for  $\theta_t = 45^\circ$  (upper resonant frequency)

It is seen from figures 4.17 to 4.26 that the measured operating frequencies (both upper and lower) are higher than the simulated ones. Nonetheless, the performance trends indicated by simulation have been, to a large extent, qualitatively in agreement with measured results for the fabricated prototype. The difference between measured and



simulated values of resonant frequencies range from 0.1-0.2 GHz for the *URF* for  $\theta_t = 40^\circ$  and  $45^\circ$  (table 4.6 and figures 4.35 and 4.36). For  $\theta_t = 10^\circ$  the difference is large between measured and simulated values. In the case of return loss values at the lower resonant frequencies, there is reasonably good agreement for  $\theta_t = 10^\circ$  and  $20^\circ$  while for  $\theta_t = 30^\circ$ ,  $40^\circ$  and  $45^\circ$ , the difference ranges from 2.59 dB to 5.5 dB (figure 4.33). As is the case of *LRF* agreement between measured and simulated *RL* values is poor for  $\theta_t = 10^\circ$ . For  $\theta_t = 20^\circ$  and  $30^\circ$ , the agreement is reasonably good while for  $\theta_t = 40^\circ$  and  $45^\circ$  the difference between measured and simulated *RL* values is greater, the difference being of the order of 5 to 6 dB (figure 4.34).

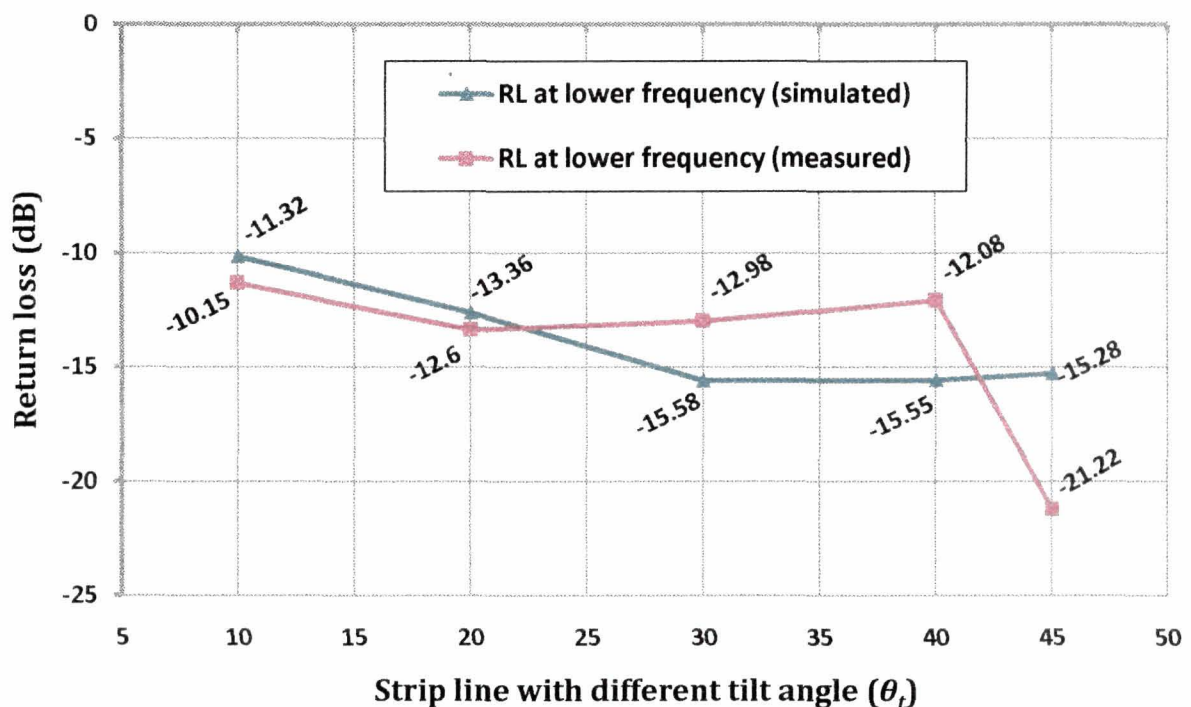


**Figure 4.33:** Comparison plot of return loss values with tilt angle  $\theta_t$  for lower resonant frequency

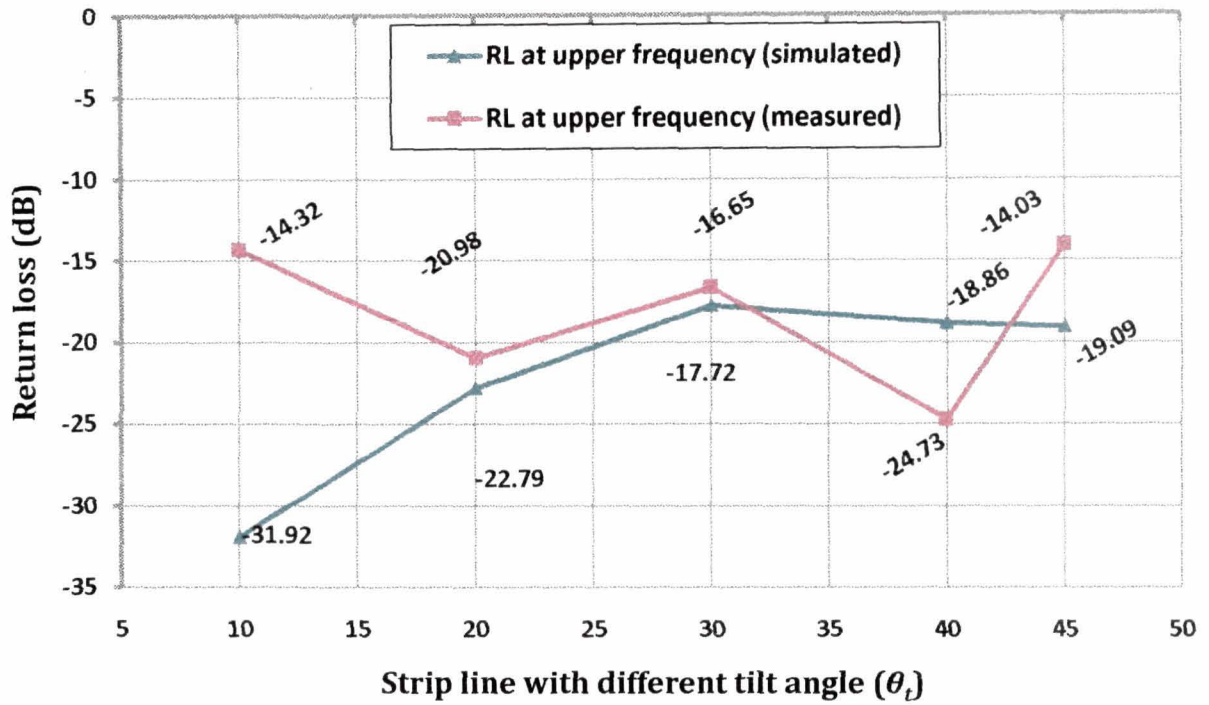


**Figure 4.34:** Comparison plot of return loss values with tilt angle  $\theta_t$  for upper resonant frequency

The measured and simulated values for the *LRF* and *URF* for different tilt angles ( $\theta_t$ ) are summarized in the table 4.5.

**Table 4.5:** Resonant frequencies for different tilt angles ( $\theta_t$ )

Antenna type	Lower resonant frequency (GHz)		Upper resonant frequency (GHz)	
	Measured	Simulated	Measured	Simulated
$\theta_t = 10^\circ$	2.17	2.06	5.19	4.13
$\theta_t = 20^\circ$	2.13	2.01	5.02	4.96
$\theta_t = 30^\circ$	2.08	1.95	4.83	4.67
$\theta_t = 40^\circ$	2.17	1.93	5.05	4.63
$\theta_t = 45^\circ$	2.04	1.92	5.01	4.64
Simple patch	Resonant frequency (GHz)			
	Measured		Simulated	
	4.75		4.55	

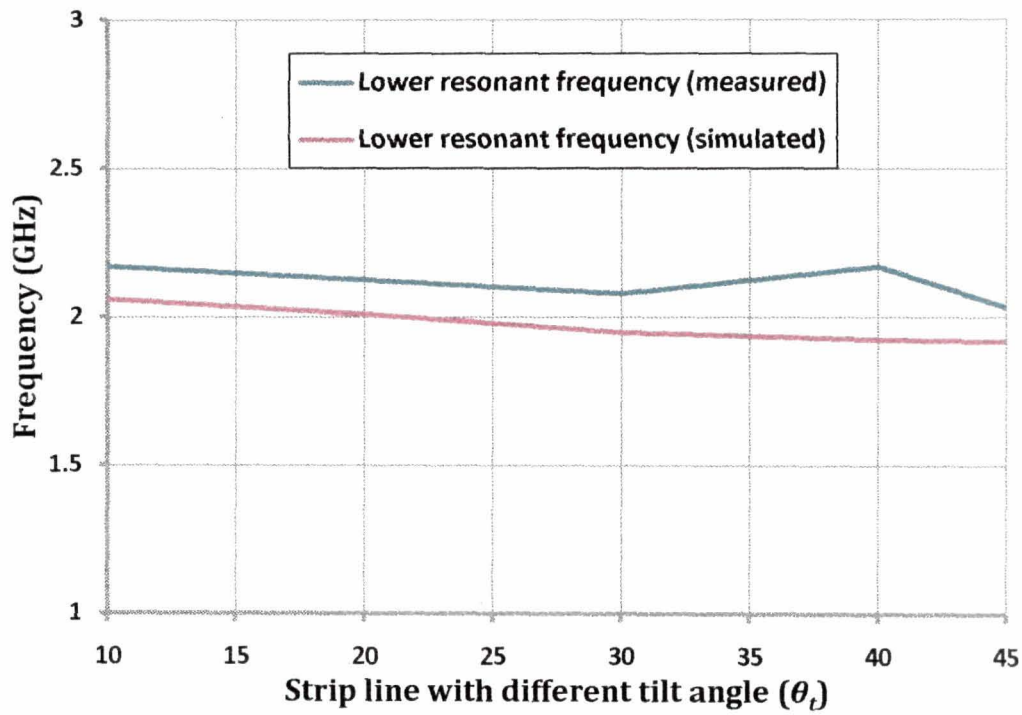


**Figure 4.35:** Measured and simulated values of the lower resonant frequency as a function of tilt angle ( $\theta_t$ )

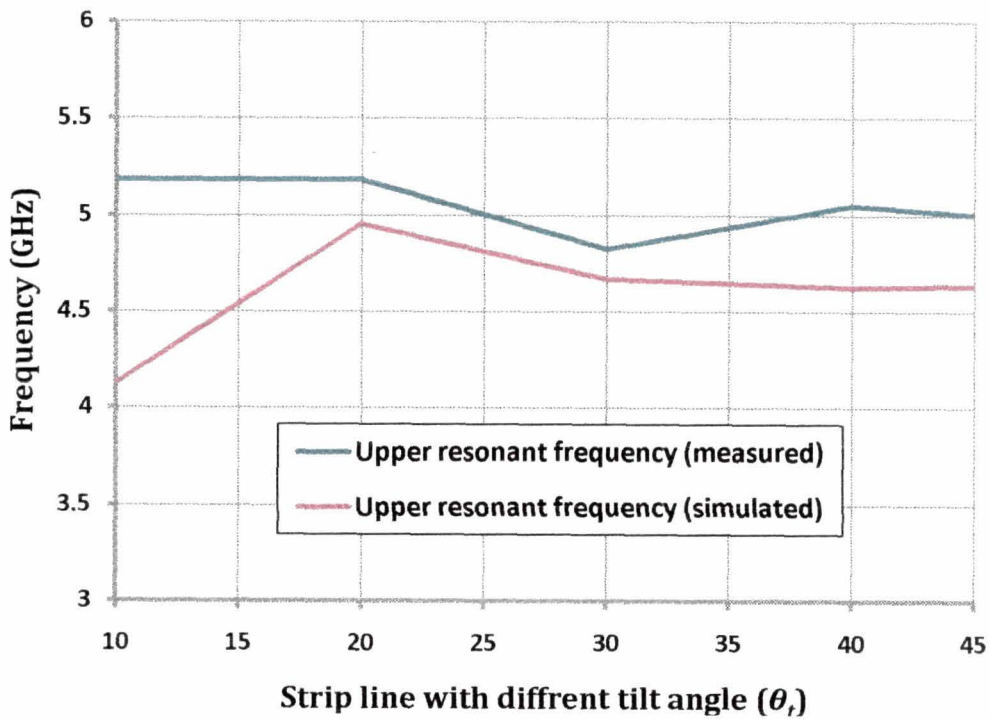


**Figure 4.36:** Measured and simulated values of the upper resonant frequency as a function of tilt angle ( $\theta_t$ )

**Table 4.6:** Resonant frequency difference between measured and simulated values

	Lower resonant frequency (GHz)		Difference of lower resonant frequencies (GHz)	Upper resonant frequency (GHz)		Difference of lower resonant frequencies (GHz)
	Measured	Simulated		Measured	Simulated	
Simple Patch	4.75	4.55	0.2	4.75	4.55	0.2
$\theta_t = 10^\circ$	2.17	2.06	0.11	5.19	4.13	1.06
$\theta_t = 20^\circ$	2.13	2.01	0.12	5.02	4.96	0.06
$\theta_t = 30^\circ$	2.08	1.95	0.13	4.83	4.67	0.16
$\theta_t = 40^\circ$	2.17	1.93	0.24	5.05	4.63	0.42
$\theta_t = 45^\circ$	2.04	1.92	0.12	5.01	4.64	0.37

**4.5.2 Antenna size reduction**

The modified patch structure with all varying parameters of strip line widths ( $w$ ) and tilt angles ( $\theta_t$ ) results in size reduction. Figure 4.37 shows the percentage of size reduction with strip line width of 4 mm for varying tilt angle ( $\theta_t$ ).

As already discussed the modified patch structure shown in figure 4.1(c) resonates at two distinct frequencies, one of which is less than half of that for the corresponding simple patch. The uniqueness of the modified patch with superposed strip line lies in the fact that, this significant lowering of one of the resonant frequency has been observed for all the combination of  $\theta_t$  and  $w$  that are studied in simulation and the ones for which measurements are carried out.

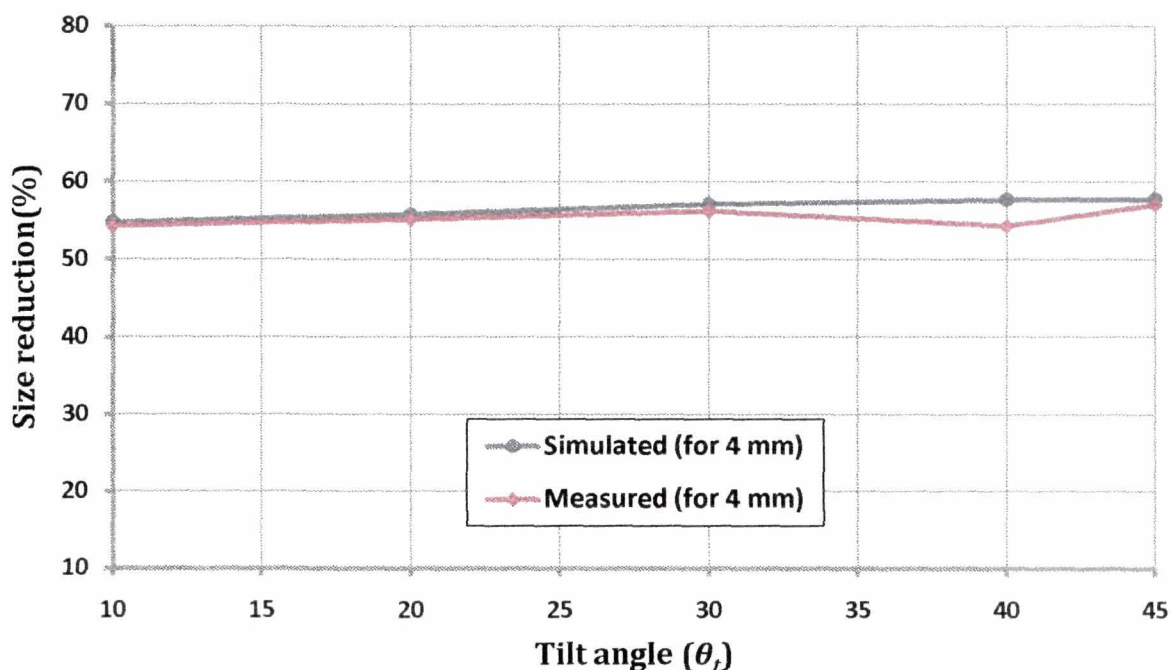


**Figure 4.37:** Comparison plot showing the reduction in size with different tilt angle ( $\theta_t$ )



As can be seen from the figure 4.35, antenna size reduces with increase in tilt angle ( $\theta_t$ ) from  $10^\circ$  to  $30^\circ$  in both measurement and simulation. In fact, for simulated results, the trend of increase in size reduction with increase in  $\theta_t$  from  $10^\circ$  to  $45^\circ$  is closely followed by the measured results but with a lower size reduction. The only point where some visible anomaly in this correlating trend between measured and simulated results is seen is for a tilt of  $40^\circ$ . Here, the measured size reduction goes down close to 54% as against a regular increasing behavior for the simulated results. Incidentally, when the tilt angle ( $\theta_t$ ) further increases to  $45^\circ$ , the measured result reverts back to follow the original increasing trend.

Radiation pattern measurements for all the fabricated patch structures are carried out to obtain a comparative understanding of the effect of the patch modification on the spatial radiation characteristics of the antenna.

#### 4.6 Radiation pattern measurements of modified patch with tilted superposed strip line section

E - plane and H - plane radiation patterns for the simple microstrip patch resonating at 4.75 GHz are measured. The field patterns are shown in figures 4.38 (a & b). The corresponding directivities are found to be 4.61 dBi and 5.55 dBi for the E- and H- plane patterns respectively. Both the patterns are broadside in nature and are similar to the conventional patch antenna.

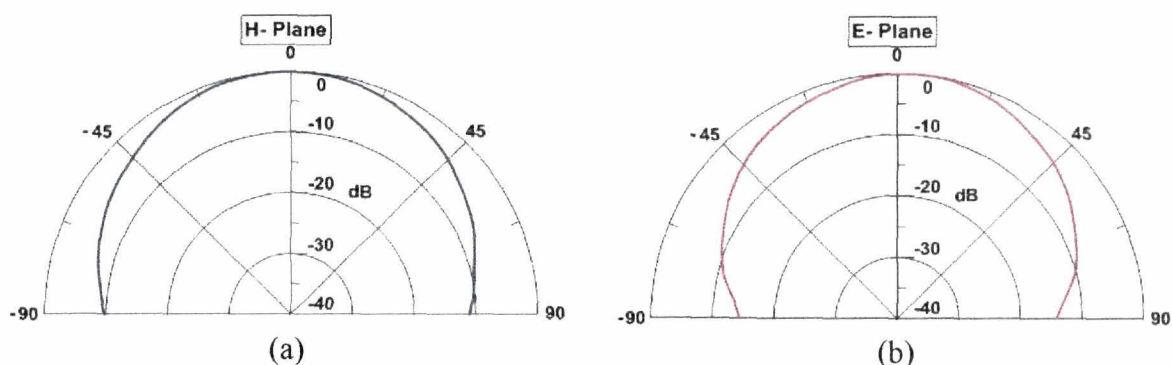


**Figure 4.38:** Measured radiation patterns of simple rectangular patch at 4.75 GHz

(a) E- plane (b) H- plane

The E- plane and H- plane radiation patterns for  $\theta_t = 10^\circ, 20^\circ, 30^\circ, 40^\circ$  and  $45^\circ$  in both *LRF* and *URF* respectively are shown in figures 4.39 to 4.48.

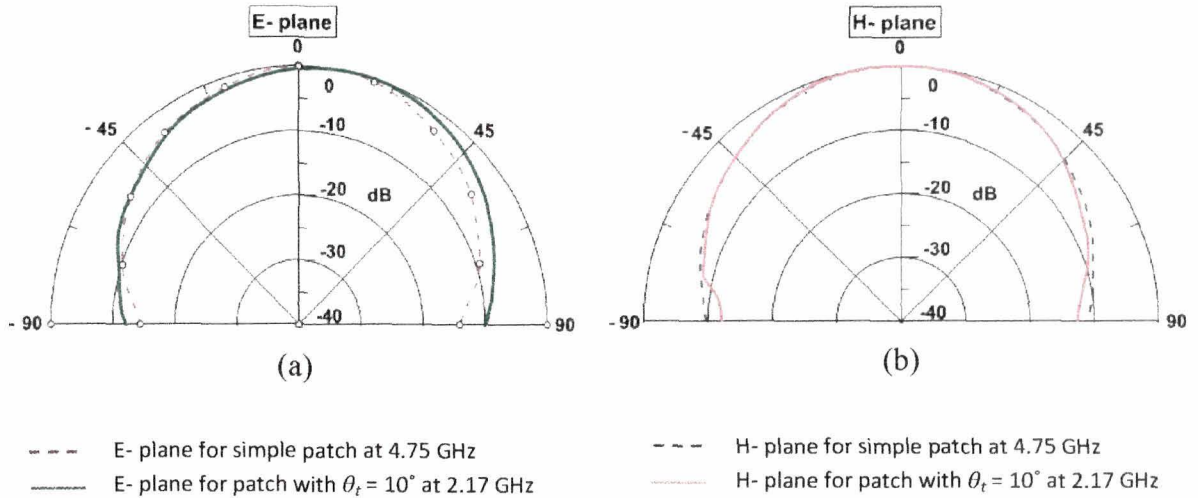


**Figure 4.39:** Measured radiation patterns of patch with  $\theta_t = 10^\circ$  at 2.17 GHz

(a) E- plane      (b) H- plane

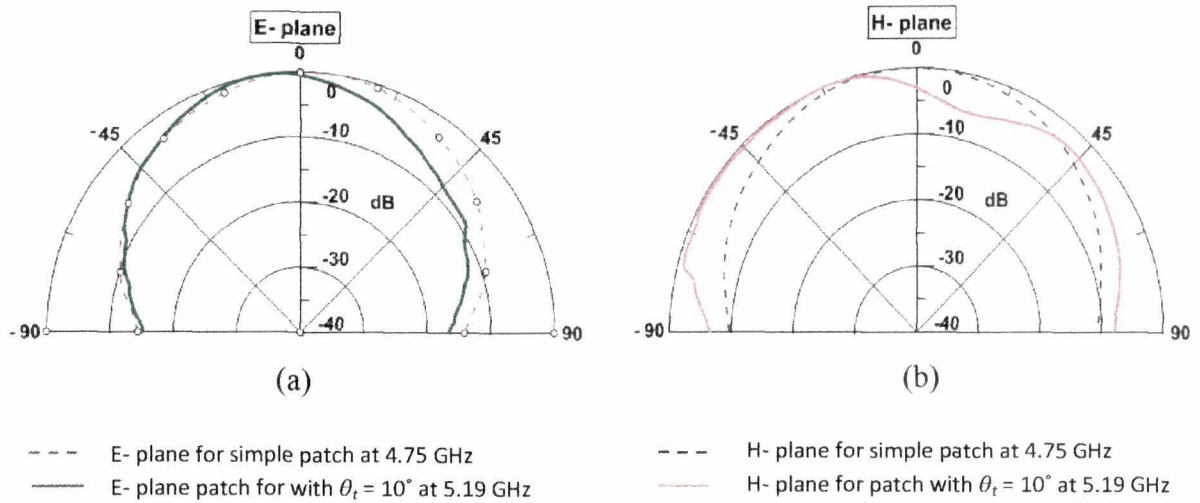


**Figure 4.40:** Measured radiation patterns of patch with  $\theta_t = 10^\circ$  at 5.19 GHz

(a) E- plane      (b) H- plane

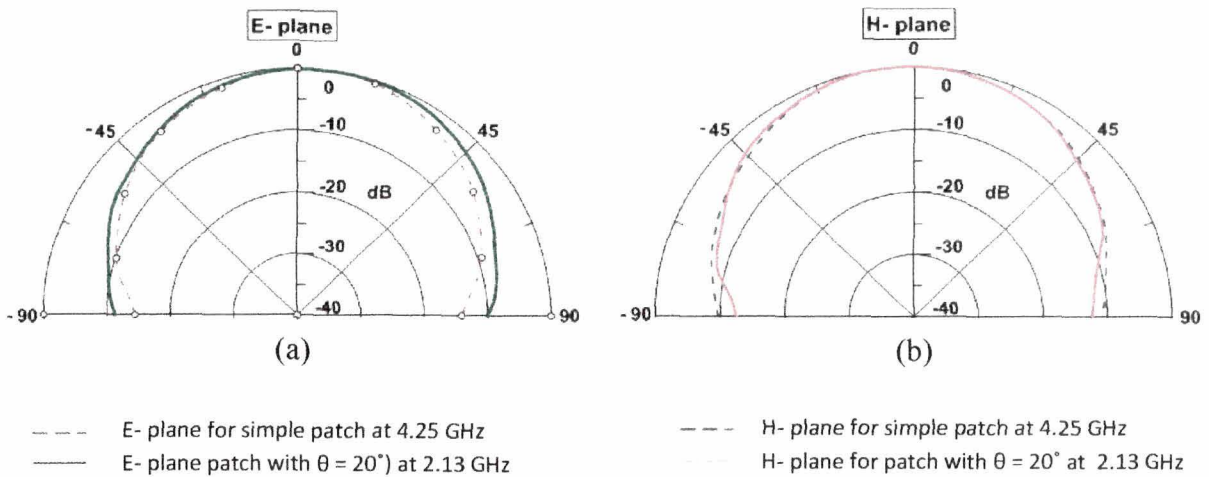


**Figure 4.41:** Measured radiation pattern of patch with slit ( $\theta = 20^\circ$ ) at 2.13 GHz

(a) E- plane      (b) H- plane

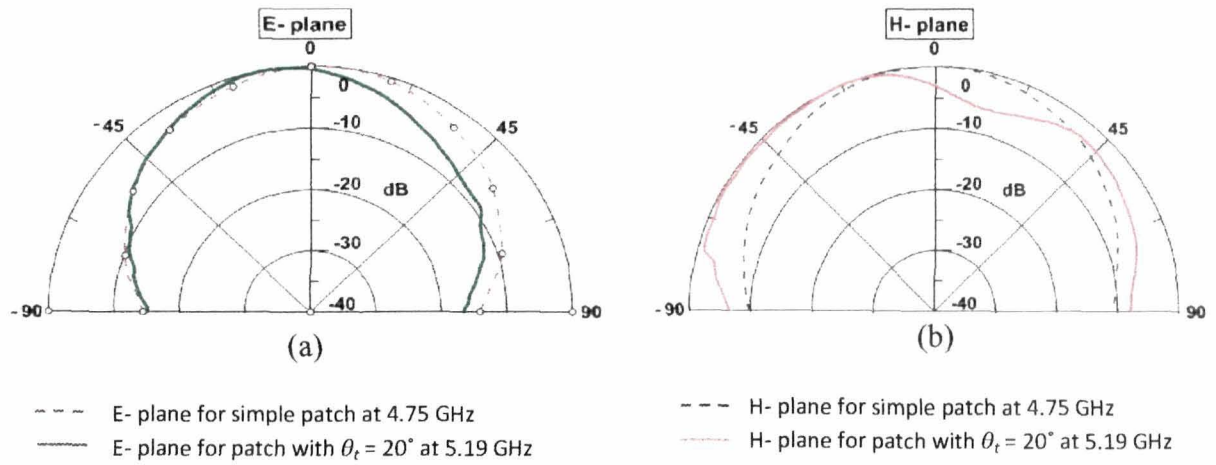


**Figure 4.42:** Measured radiation patterns of patch with  $\theta_t = 20^\circ$  at 5.09 GHz

(a) E- plane      (b) H- plane

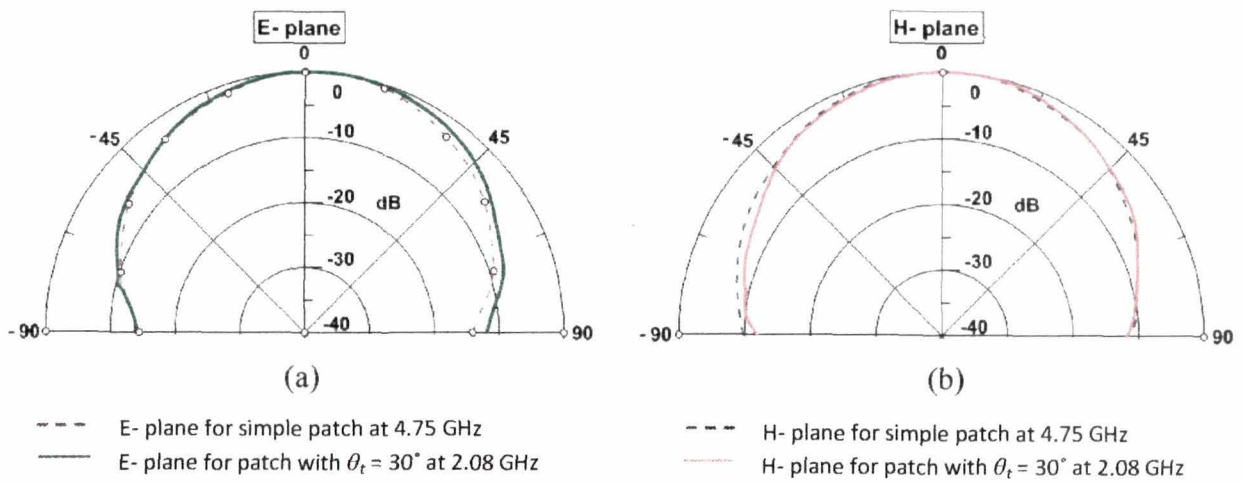


**Figure 4.43:** Measured radiation pattern of patch with  $\theta_t = 30^\circ$  at 2.08 GHz

(a) E- plane      (b) H- plane

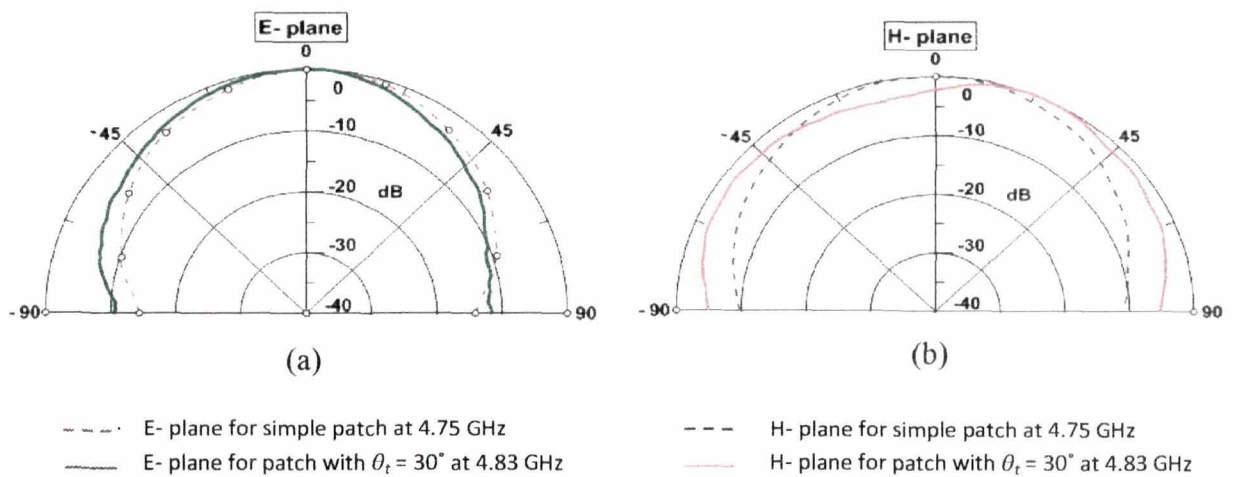


**Figure 4.44:** Measured radiation patterns of patch  $\theta_t = 30^\circ$  at 4.83 GHz

(a) E- plane      (b) H- plane

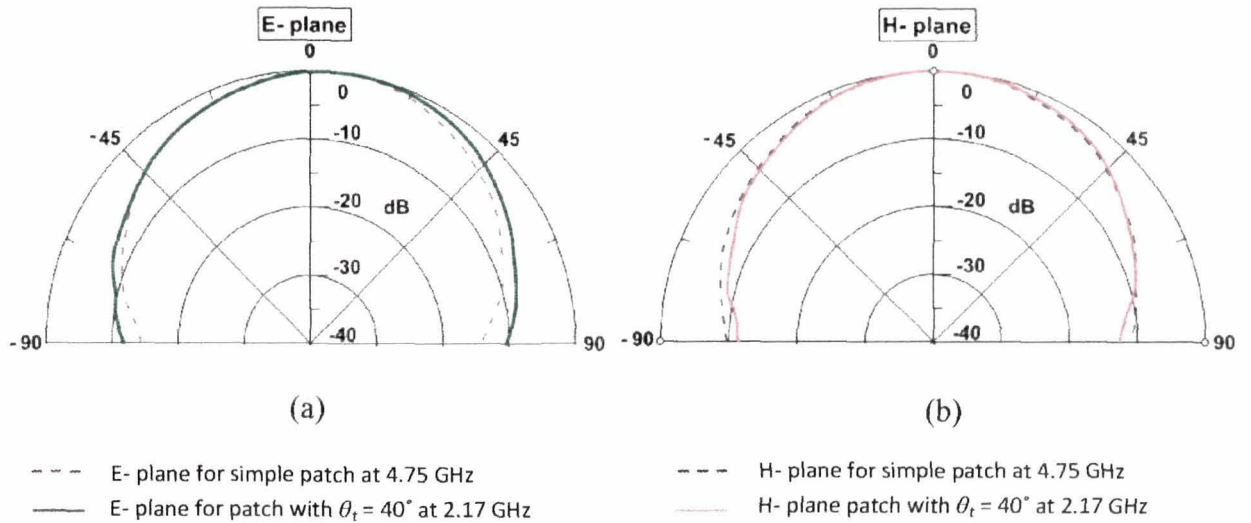


**Figure 4.45:** Measured radiation patterns of patch  $\theta_t = 40^\circ$  at 2.17 GHz

(a) E- plane                      (b) H- plane

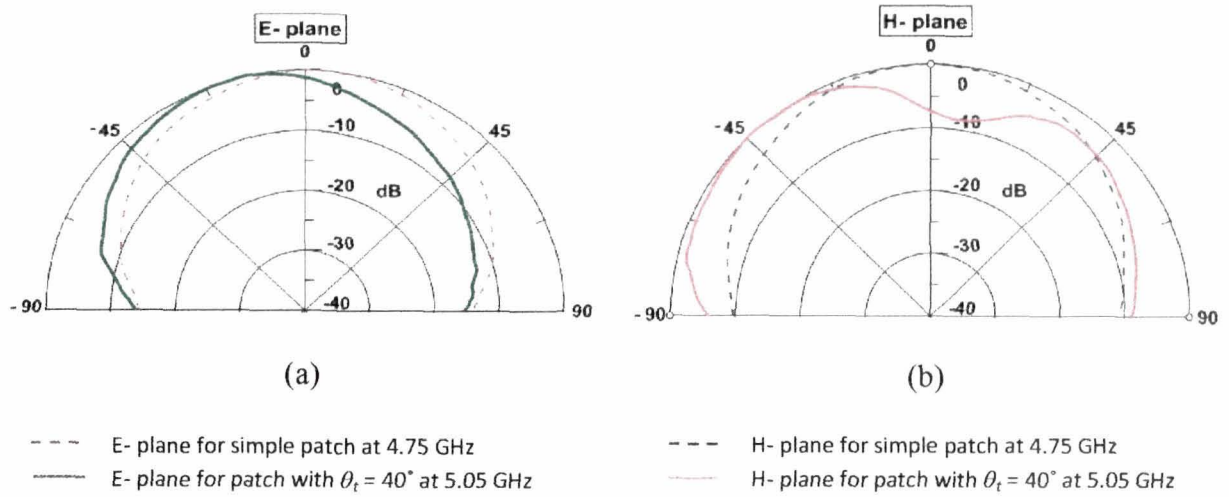


**Figure 4.46:** Measured radiation patterns of patch with  $\theta_t = 40^\circ$  at 5.05 GHz

(a) E- plane                      (b) H- plane



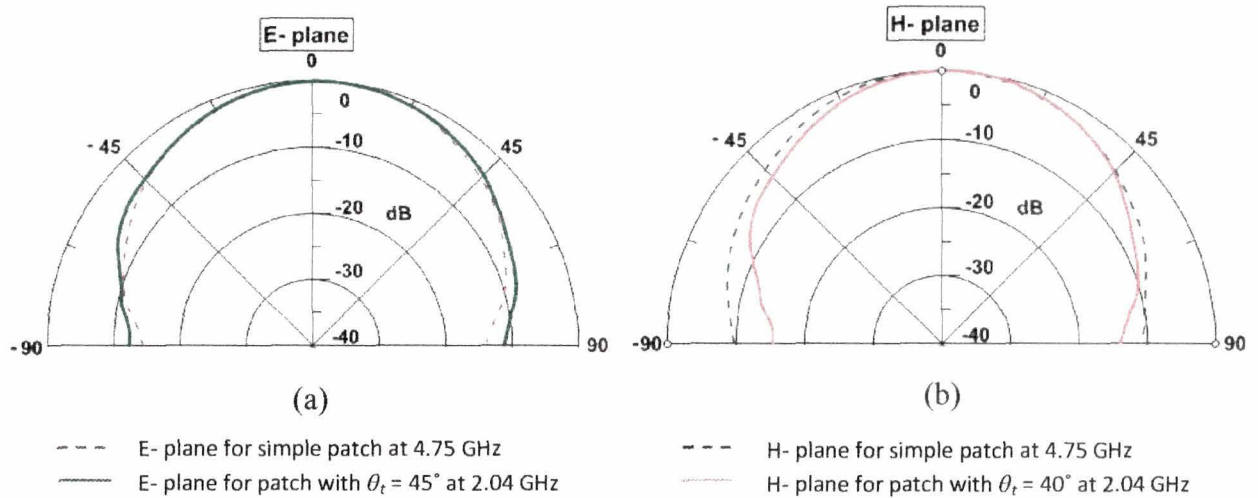


Figure 4.47: Measured radiation patterns of patch with  $\theta_t = 45^\circ$  at 2.04 GHz

(a) E- plane (b) H- plane

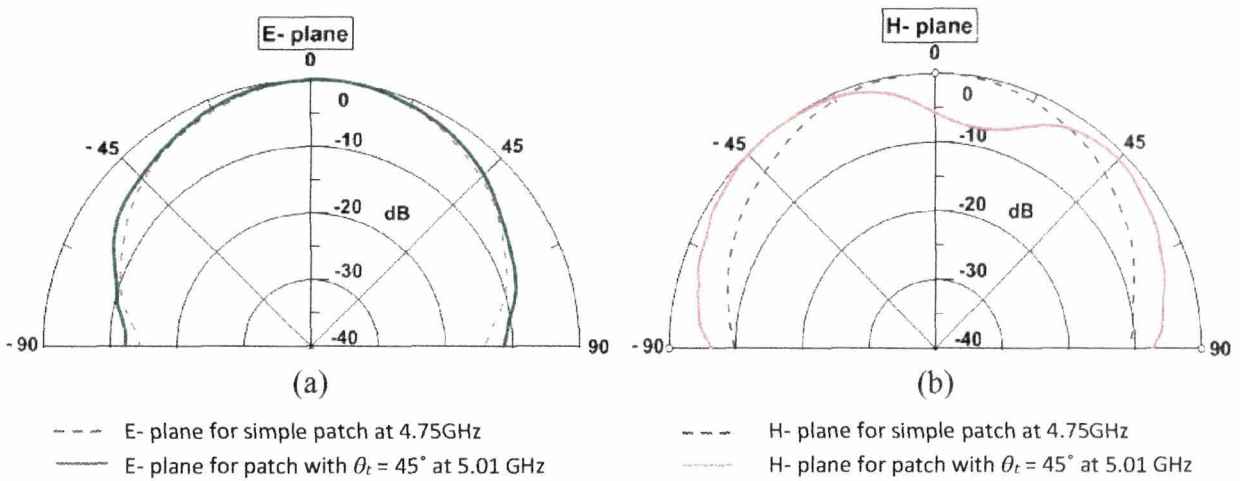


Figure 4.48: Measured radiation patterns of patch with  $\theta_t = 45^\circ$  at 5.01 GHz

(a) E- plane (b) H- plane

**Table 4.7:** Measured directivity for different tilt angles ( $\theta_t$ ) of the strip line section

Patch with tilt angle ( $\theta_t$ )	Directivity (dBi)			
	LRF (GHz)		URF (GHz)	
	E- plane	H- plane	E- plane	H- plane
$\theta_t = 10^\circ$	at 2.17 GHz		at 5.19 GHz	
	3.77	3.88	5.99	3.56
$\theta_t = 20^\circ$	at 2.13 GHz		at 5.09 GHz	
	3.68	4.03	5.90	3.26
$\theta_t = 30^\circ$	at 2.08 GHz		at 4.83 GHz	
	4.17	4.00	4.25	3.30
$\theta_t = 40^\circ$	at 2.17 GHz		at 5.05 GHz	
	3.76	3.89	5.42	3.85
$\theta_t = 45^\circ$	at 2.04 GHz		at 5.01 GHz	
	4.36	4.37	4.36	3.31
Simple patch	Directivity (dBi)			
	E- plane		H- plane	
	at 4.55 GHz			
	4.61		4.35	

Table 4.7 summarizes the measured directivities obtained from radiation patterns in figures 4.38 to 4.48 for the modified patch with  $\theta_t = 10^\circ, 20^\circ, 30^\circ, 40^\circ$  and  $45^\circ$  for the E- plane and H- plane in both the LRF and URF. The same values are plotted in figures 4.49 and 4.50 for the E- plane and H- plane respectively

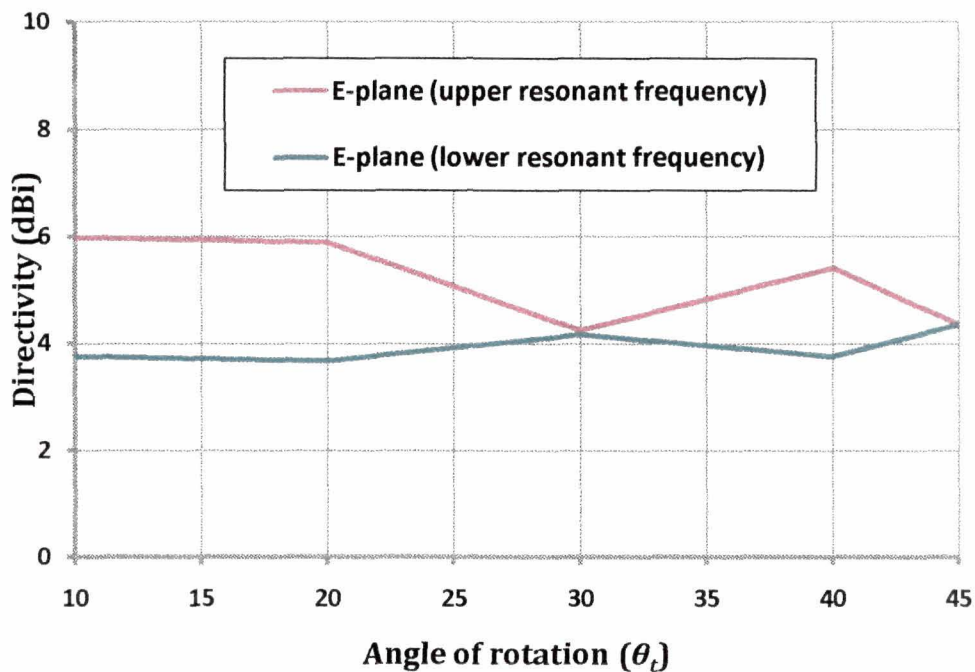


**Figure 4.49:** Measured directivity vs. tilt angle ( $\theta_t$ ) for E- plane

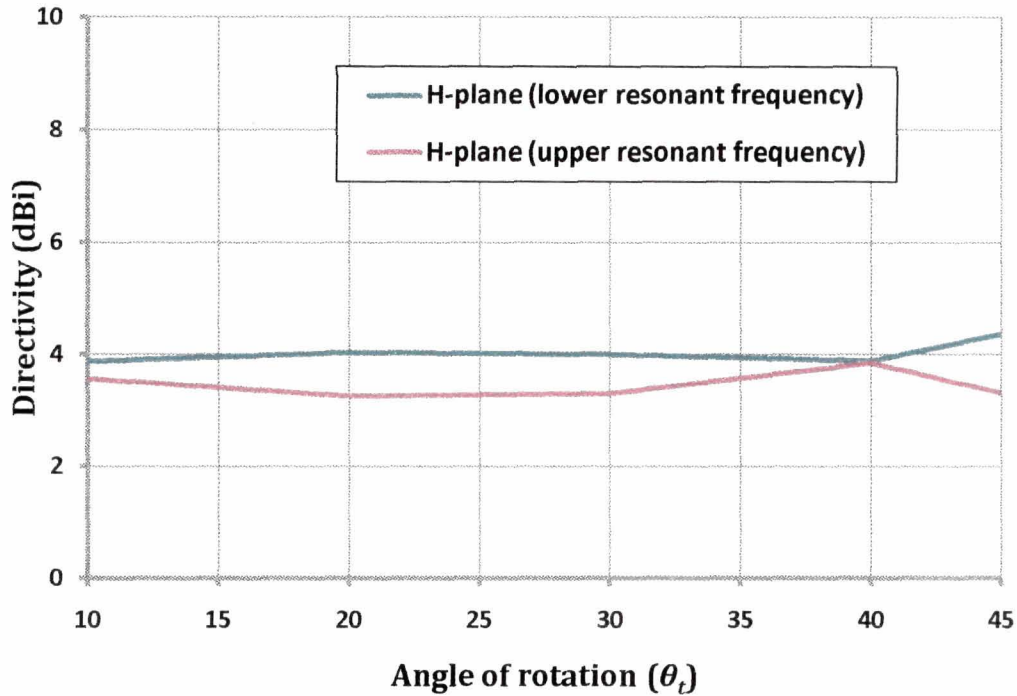


**Figure 4.50:** Measured directivity vs. tilt angle ( $\theta_t$ ) for H- plane

From figures 4.39 to 4.48, it is seen that E- plane radiation patterns for both *LRF* and *URF* are reasonably similar for all the fine  $\theta_t$  values to that for the simple patch at its resonating frequency. In case of H-plane patterns, again similarity with the H-plane pattern for the simple patch can be seen with no significant difference. However, for the H-plane patterns at higher resonating frequency for the modified patch, an asymmetrical dip slightly away from the broadside direction is seen. It may be mentioned that comparisons are made with patterns for the simple rectangular patch which resonates at 4.75 GHz which is near the *URF* for the modified patch.

The directivity measured from pattern plot is summarized in the table 4.7 and shown in figures 4.49 and 4.50.

#### 4.7 Chapter summary

A patch geometry obtained when a finite strip line section is notionally superposed on the rectangular patch near one of its radiating edges has been studied for its frequency/ frequencies of resonance and return loss performance. The modified structure is simulated for different relative orientations of the strip line section before fabricating the prototypes. The fabricated modified patch resonates at two different frequencies, one in the S- band and another in the C- band for all the  $\theta_t$  values studied. Both the resonant frequencies can be found over a small range by changing  $\theta_t$ . The *LRF* is tuned from 2.04 GHz to 2.17 GHz by varying  $\theta_t$  from  $10^\circ$  to  $45^\circ$  while the *URF* is tuned from

4.83 GHz to 5.19 GHz. However, since both the resonant frequencies shift simultaneously, only one of them can be independently tuned by adjusting  $\theta_t$ . Importantly, a significant reduction in size which is about 54% for all  $\theta_t$  values studied is obtained, with a maximum reduction of 57% for  $\theta_t = 45^\circ$ . For all  $\theta_t$  values, an  $RL$  of at least -10 dB is obtained. The best  $RL$  for the  $LRF$  is obtained at  $\theta_t = 45^\circ$  while for the  $URF$ , it is for  $\theta_t = 40^\circ$ . Hence, according to application requirements, the  $RL$  can be maximized for either the  $URF$  or the  $LRF$  simply by changing the tilt angle. There is no major deviation of the directivity from that of the simple patch. The E- plane and H- plane radiation patterns excepting the H- plane patterns for the higher resonant frequencies where a dip in the pattern slightly away from the broadside direction is seen.

The designs studied in this chapter is essentially to study the performance of a modified patch where, possibly, an equivalent structure can be fabricated using an actual strip line pivoted through its centre at the appropriate location of the patch and rotated to tune the frequency or adjusting the  $RL$  while at the same time obtaining dual- frequency operation. There is likely to be some shift in the results obtained here with such a reconfigurable structure. In addition, precise mechanical fabrication and ensuring of reliable electrical contact over the overlapping region of the rectangular patch and the strip line will be a challenge for the designer.

**References**

- [1] R. R., Garg P., Bhartia, I., Bahl and A., Ittipiboon, "Microstrip Antenna Design Handbook" (Boston, MA: Artech House), 2000.
- [2] P. Bhartia, and I.J.Bahl, "A frequency agile microstrip antennas" *IEEE Antennas Propagation Symp. Digest*, Vol. 20, pp.304–307, May 1982.
- [3] A. S., Daryoush, K., Bontzos and P., R., Hercsfeld, "Optically tuned patch antenna for phased array applications", *IEEE Int. Antennas Propag., Symp. Dig.*24361–4, 1986.
- [4] Z. Jin and A., Mortazawi, "An L-band tunable microstrip antenna using multiple varactors" *IEEE Int. Antennas Propag. Symp. Dig.* Vol.4, pp. 524–527, 2003.
- [5] K. F., Lee, K., Y., Ho, and J., S., Dahele, "Circular-disk microstrip antenna with an air gap" *IEEE Trans. Antennas Propag.* Vol.32, pp. 32 880–4, 1984.
- [6] J. S., Dahele and K.F., Lee, "Theory and experiment on microstrip antennas with air gaps", *IEEE Proc. (Part H)*, Vol. 132, pp. 455–60, 1985.
- [7] J., P., Gianvittorio and Y.,Rahmat-Samii "Reconfigurable patch antennas for steerable reflect array applications", *IEEE Trans. Antennas Propag.*, Vol. 54,1388–92, 2006.
- [8] R. V., Goteti, R., Jackson and R., Ramadoss, "MEMS based electrostatically tunable microstrip patch antenna fabricated using printed circuit processing techniques", *IEEE Antennas Wireless Propag. Lett.*, Vol. 52, pp. 28–30, 2006.
- [9] C. Y., Huang, and J.Y. W, "Compact microstrip antenna loaded with very high permittivity superstrate", *Antennas and Propagation Society International Symposium, IEEE*, Vol. 2, pp.21-26, 1998.
- [10] R. Waterhouse, "Small microstrip patch antenna, *Electronics Letters*, Vol.31, No. 8, 604–605, 1995.
- [11] Haneishi, and Y. Suzuki, "Circular polarization and bandwidth", *Handbook of Microstrip Antennas*, J. R. James, P. S. Hall, Peter Peregrinus, London, 1989.

## CHAPTER V

# SPIKE EDGED RECTANGULAR PATCH ANTENNA

---

### 5.1 Introduction

### 5.2 Design of patch with number spike section on radiating edges

#### *5.2.1 Feed point location*

### 5.3 Simulated antenna performance studies with spikes at radiating edges

#### *5.3.1 Return loss performance of patch with six spikes on each edge*

### 5.4 Measured results

#### *5.4.1 Return loss measurements of simple patch*

#### *5.4.2 Comparison of measured and simulated results*

### 5.5 Radiation pattern measurement of SEMPA and SEMPA with strip line

### 5.6 Chapter summary

### References

## 5.1 Introduction

The advantage of microstrip antenna for modern day communication is well known and has already been highlighted in preceding chapters including chapter I [1-8]. Many designs of single and dual band microstrip patch antennas using E slots and U slots have been reported for triangular, square and circular [7-8] MPA shapes. The inherently bandwidth of conventional microstrip patch antenna poses a challenge for microstrip antenna designers to meet broadband requirements [2-3]. Various broadband techniques had been reported in the literature to address this limitation, which in general include increasing patch height over ground plane [4], using a lower substrate permittivity [5], and multilayer structures consisting of several parasitic radiating elements with different sizes above the driven element [6].

In this chapter a spike edge rectangular patch antenna (SEMPA), where spike shaped triangular conductor sections are added to the rectangular patch at the radiating edges has been investigated. The effect on resonant frequency on addition of a number of spikes in the shape of equilateral triangle is studied. The antenna is fabricated and measured results are presented in this chapter. In addition, two adjacent spikes have been bridged using a strip line section for studying its possible effect on resonant frequencies and matching. In addition, the position of the strip line is moved from the spike tips to below the tips. The approach is adopted with an objective of achieving tuning by variation of only one parameter which may reduce design complexity.

## 5.2 Design of patch with number of spike sections on radiating edges

### 5.2.1 Feed point location

The basic square patch antenna is designed in the C- band using CST Microwave Studio at 4.40 GHz. Dimension of the patch are indicated in the figure 5.1. Simulated results for different feed point locations are obtained for maximizing the value of RL of the simple patch. The values of return loss ( $RL$ ), impedance (real) and  $VSWR$  corresponding to different feed point locations are shown in figures 5.2 to 5.4 respectively.



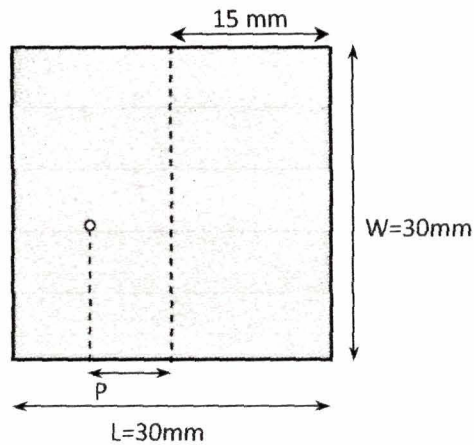


**Figure 5.1:** Simple square patch resonating at 4.40 GHz (CST Microwave Studio)

Results are obtained by moving the feed point in increments of 0.5 mm along the length of the patch from the patch centre (figure 5.2)

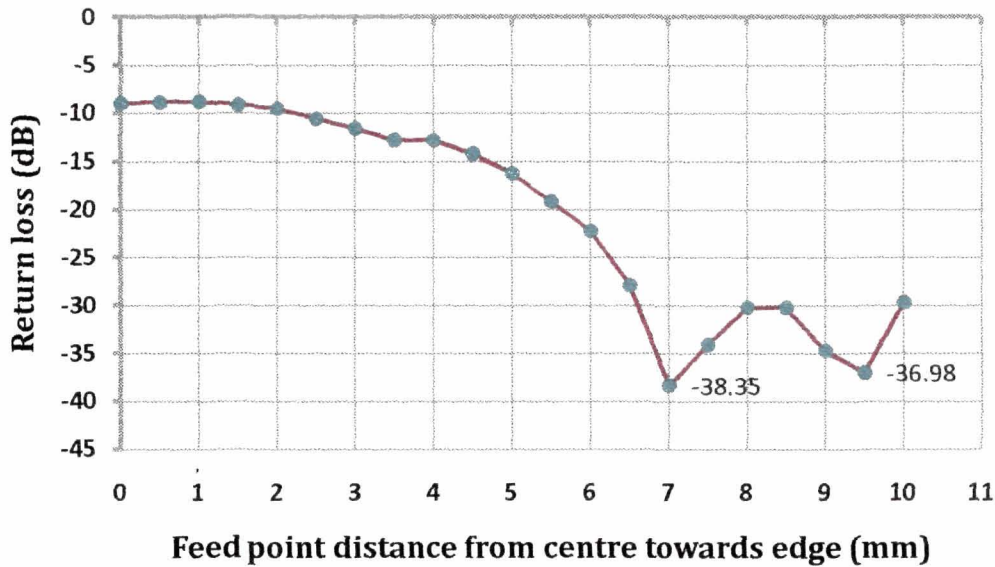


**Figure 5.2:** Simulated return loss vs. feed point distance from patch centre

Simulated results indicate two feed point location for which more than -35 dB  $RL$  is obtained. The  $RL$  values observed at the locations of 7 mm and 9.5 mm are -38.35 dB and -36.98 dB for the resonant frequency of 4.4 GHz in the C- band.

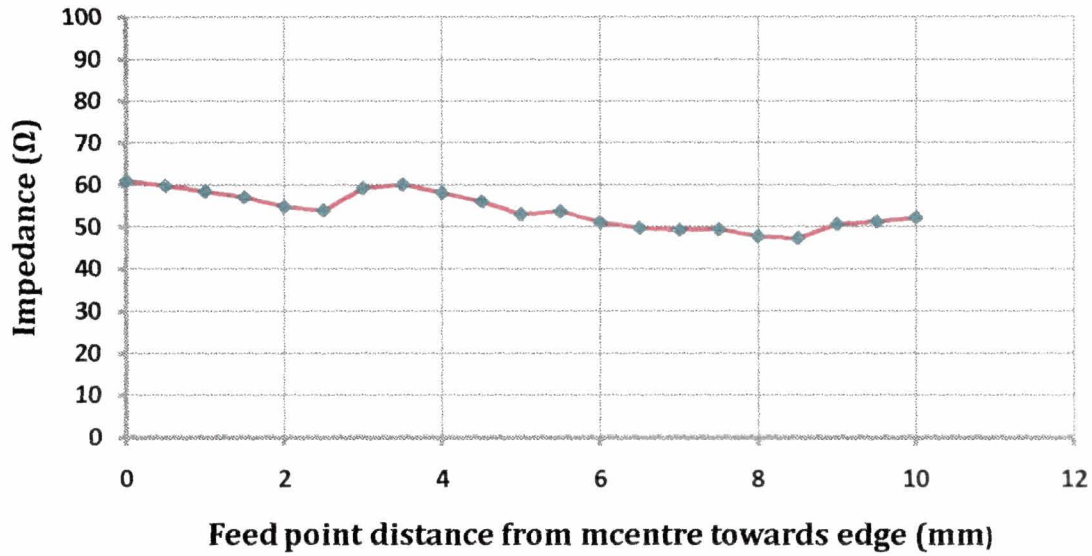


**Figure 5.3:** Simulated plot of impedance ( $\Omega$ ) vs. feed point location

Impedance (real part) values at these two feed point locations are  $49.54 \Omega$  for 7 mm and  $51.41 \Omega$  for 9.5 mm. The corresponding values of *VSWR* are 1.024 and 1.029 respectively as shown in figure 5.4.

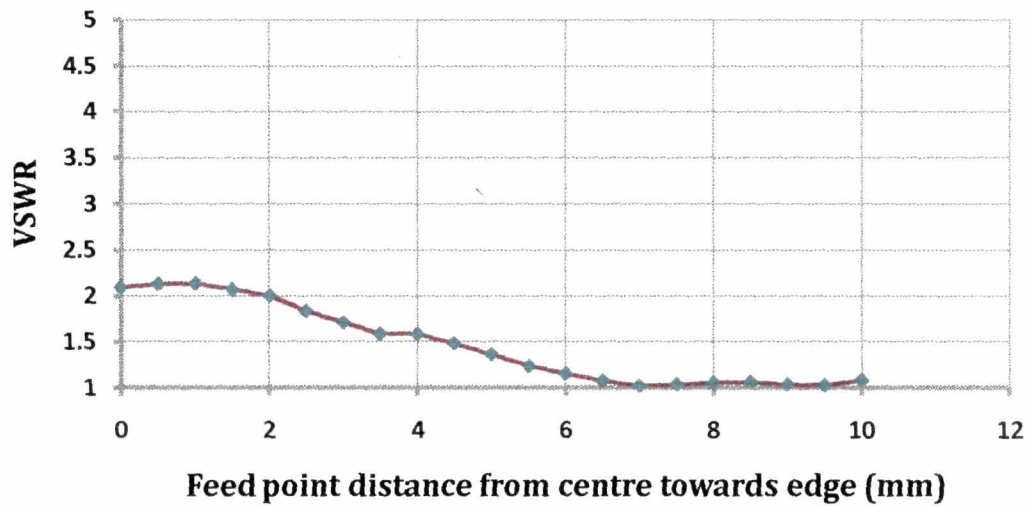


**Figure 5.4:** Simulated plot of VSWR vs. feed point location

The patch is modified by adding six numbers of equilateral triangles on each radiating edge, each with sides 5 mm measuring, as shown in figure 5.5. The design parameters of the patch with spike edge are given in table 5.1.

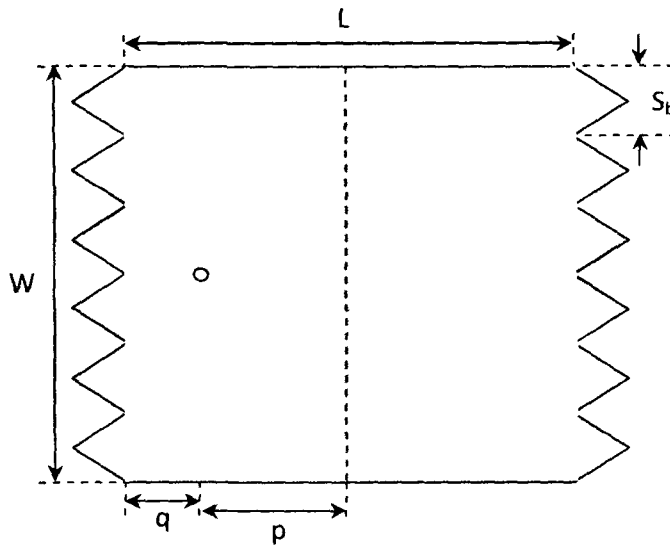


**Figure 5.5:** Patch structure with spikes at radiating edges

**Table 5.1:** Design parameters of the spike edged patch

Parameters	Values (mm)
L	30
W	30
p	7 / 9.5
q	8 / 5.5
$S_b$	5

As the simple patch with two feed point locations gives return loss values below -35 dB (figure 5.2), the best feed point location out of these is studied with the modified patch structure shown in figure 5.5.

### 5.3 Simulated antenna performance studies with spikes at radiating edges

Simulations are carried out for  $RL$  performance on the spike edged patch (figure 5.5). Thereafter, alternate spikes are removed from both the edges leaving three spikes on each edge. One design is obtained by removing these spikes from the same end (figure 5.7) and another in which spikes are removed from opposite ends of the two edges (figure 5.9).

Although, modification of the geometry in general might alter the feed point location for best match, in this study, the feed points considered are limited to the two locations for which good match is obtained for the simple patch. The modified spike edged rectangular microstrip patch antenna (SEMPA) antenna with six spikes at both the radiating edges is initially studied (figure 5.5).

### 5.3.1 Return loss performance of patch with six spikes on each edge

The return loss performance of the patch shown in figure 5.5 is evaluated for the two feed point locations obtained (figure 5.2) at 7 mm and 9.5 mm from centre toward the edge along the patch length.

The simulated RL plot for the two feed point locations are shown in figure 5.6.

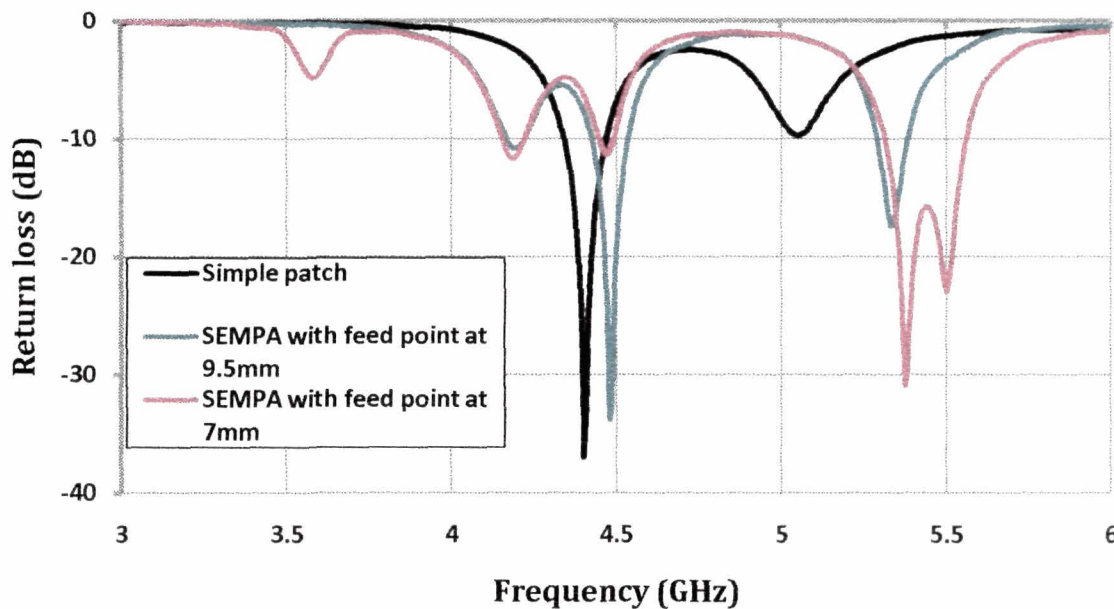


**Figure 5.6:** Simulated return loss plots for feed points at 7 mm and 9.5 mm from patch centre

As can be seen from the RL plots in figure 5.6, the resonant frequency of 4.4 GHz for the simple patch slightly shifts to the higher side at 4.48 GHz for feed point,  $p = 9.5$  mm. without any appreciable loss in RL performance. Noticeably a second RL peak at 5.33 GHz with a value of -17.4 dB is observed. From the figure, it is seen that for  $p = 7$  mm, the structure shows two feeble resonances, one at 4.17 GHz with an RL value of -11.54 dB and other at 4.46 GHz with an RL value of -10.91 dB. However, a prominent twin peaked RL is seen. These peaks are -30.91 dB at 5.37 GHz and -22.97 dB at 5.5 GHz. As a good RL is obtained at lower frequency the feed point at  $p = 9.5$  mm is use in the subsequent studies.

As already mentioned, the spike edged geometry shown in figure 5.5 is further modified by removing alternating spikes symmetrically from both the edges. The resulting structure is shown in figure 5.7. The RL performance of this structure is compared with that for the structure shown in figure 5.5 as is shown in figure 5.8(a). It can be seen that

the RL performance degrades when the alternate spikes are symmetrically removed from the structure in figure 5.5.

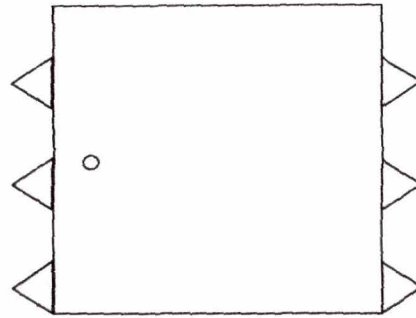


Figure 5.7: Patch structure with alternate spikes at symmetric positions

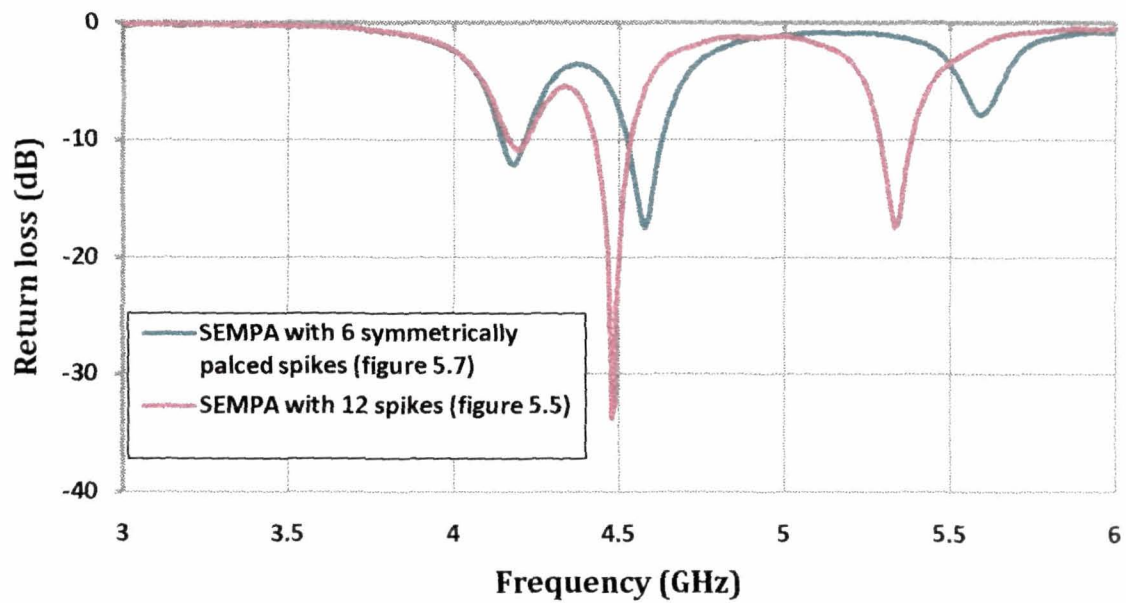
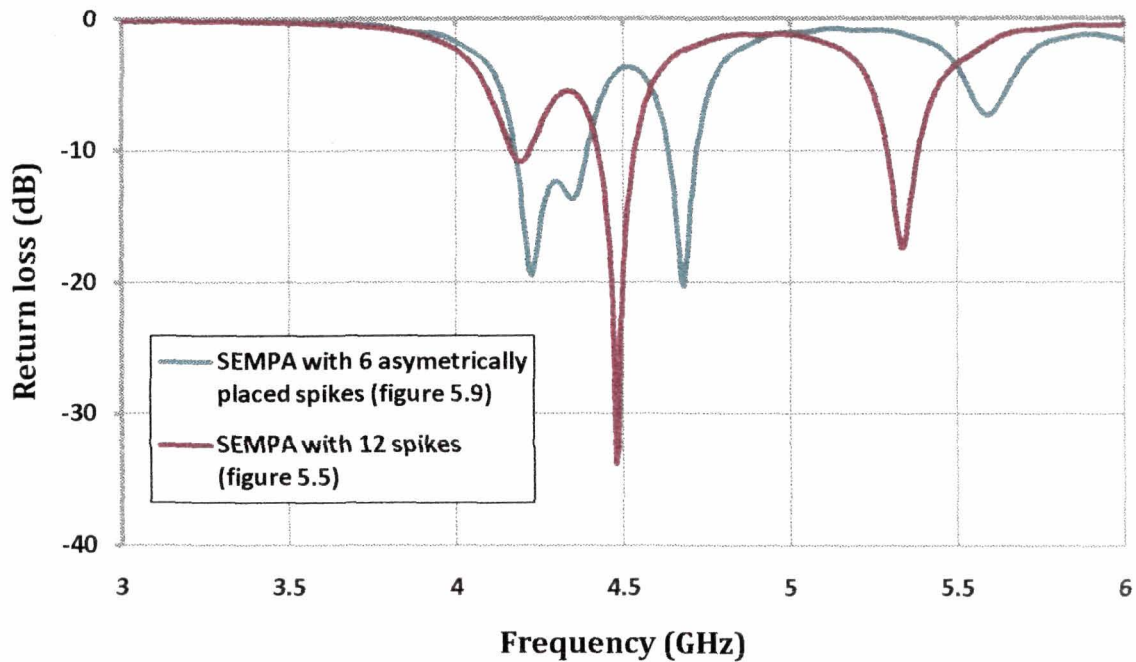


Figure 5.8(a): Simulated return loss plots for patch with 12 and 6 symmetrically placed spikes ( $p=9.5$  mm)





**Figure 5.8(b):** Simulated return loss plots for patch with 12 and 6 asymmetrically placed spikes ( $p=9.5$  mm)

Another geometry is obtained by removing alternate spikes from opposite ends of the two edges from one structure shown in figure 5.5. The resulting geometry is shown in figure 5.9. The simulated return loss plot for this geometry along with the plot for the patch with 12 spikes is shown in figure 5.8(b).

There are two prominent and almost equal return loss peaks at 4.22 GHz (-19.5 dB) and 4.68 GHz (-20.27 dB). It is evident, therefore, that for the asymmetrically positioned 6 spike geometry, the return loss performance as a dual band antenna is better than that for the symmetrically positioned 6 spike geometry. In addition, the lower resonant frequency is lower than that for the simple patch, although at the cost of return loss performance. Figure 5.10 shows the same plots together with the plots shown in figure 5.8(a).

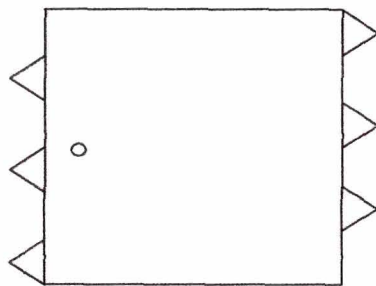


**Figure 5.9:** Patch structure with alternate spikes at asymmetric positions

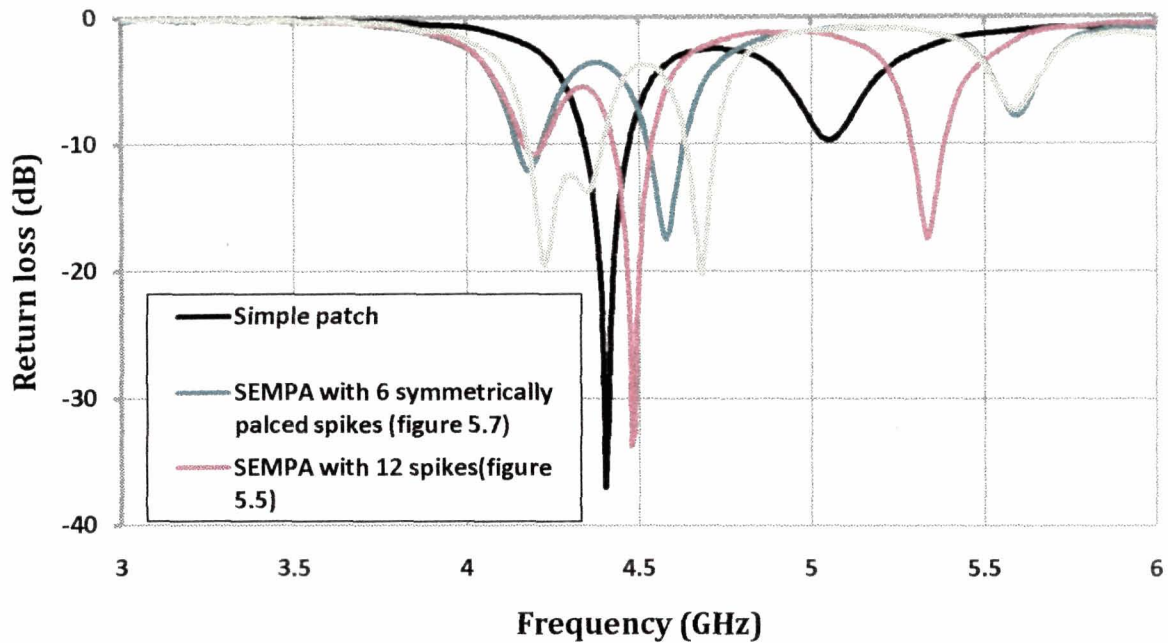


**Figure 5.10:** Simulated return loss for simple patch and modified geometries

To sum up, the patch with asymmetrically placed spikes on both the radiating edges exhibits the best dual band characteristics.

#### 5.4 Measured results

The simple and modified patch geometries as shown in figures 5.1 and 5.9 are fabricated on glass epoxy copper laminated substrate with specifications given in table 5.2. The fabricated simple and the modified patch structures are shown in figure 5.11(a) and 5.11(b). Measurements are carried out on the fabricated patches.

**Table 5.2:** Design parameter of MPA with spikes

<i>Parameter</i>	<i>Value</i>
Patch width ( $W$ )	30 mm
Patch length ( $L$ )	30 mm
Height of the substrate ( $h$ )	1.52 mm
Dielectric constant ( $\epsilon_r$ )	4.8
Feed point distance from centre ( $p$ )	9.5 mm
Spike dimension (each side)	5 mm



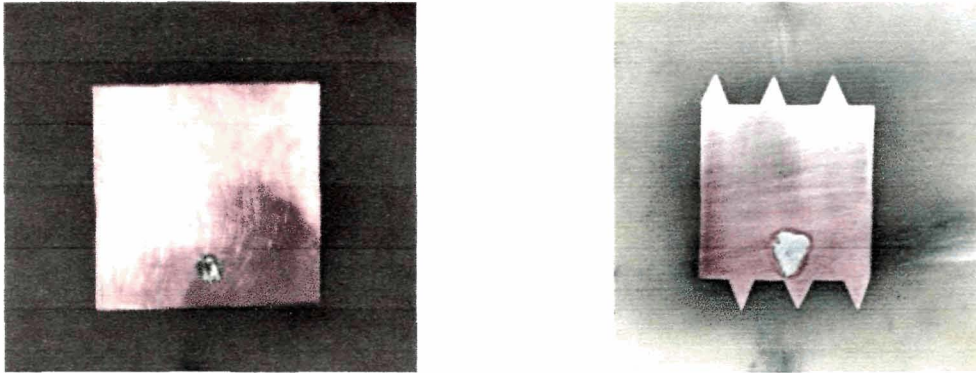


**Figure 5.11:** (a) Fabricated simple patch.

(b) Fabricated patch antenna with spikes

#### 5.4.1 Return loss measurement of simple patch

Measurements are carried out for the fabricated simple patch antenna. RL plot for the simple patch is shown in figure 5.12 along with the simulated plot.

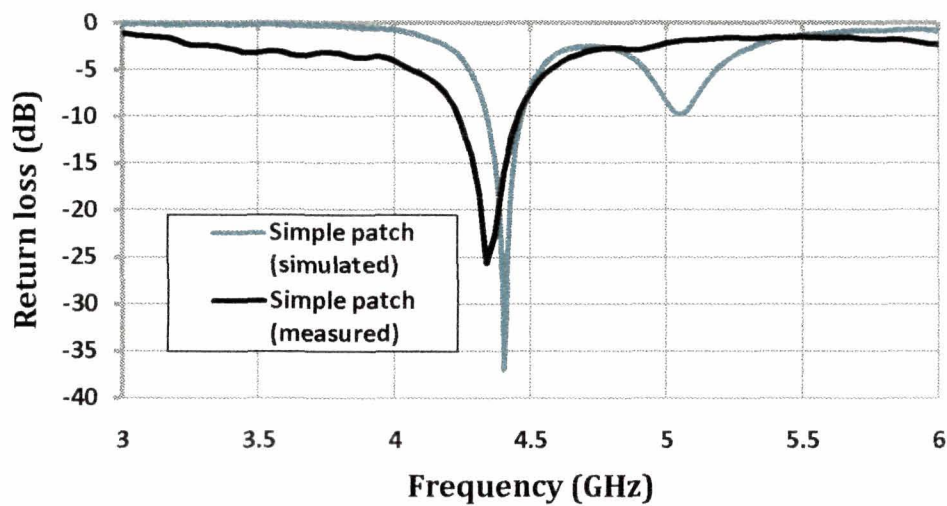


**Figure 5.12:** Simulated RL plot (p=9.5 mm)

Measured results indicate that the patch resonates at 4.34 GHz (with a return loss value of -25.72) which indicates a slight shift of 1.36% from the simulated frequency of 4.4 GHz (-36.97 dB), possibly due to fabrication tolerances.

The antenna is thereafter fabricated with spikes added as shown in figure 5.11 (b).

#### 5.4.2 Return loss measurements of modified patch with spikes

Measurement is carried out for the spike edged antennas which are positioned at the

radiating edges asymmetrically Figure 5.13 shows the measured return loss plot of the spike edged square patch (SEMPA) antenna along with the plot for the simple patch

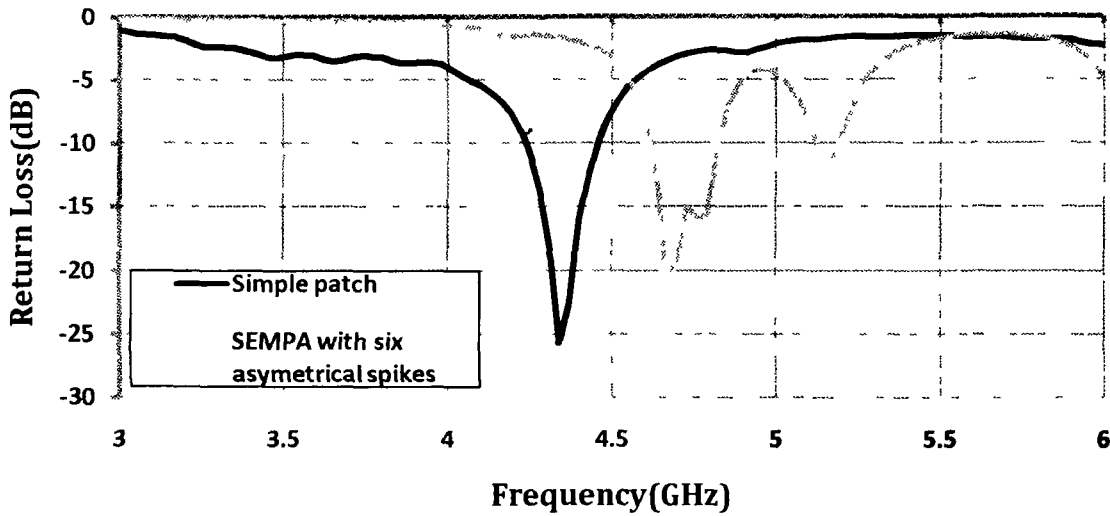


**Figure 5.13:** Return loss plot for simple patch and SEMPA

It can be seen from the plots that when spikes are added to the simple square patch, the resonant frequency shifts to a higher value at 4.67 GHz with a return loss value of -21.27 dB in comparison to the resonant frequency of 4.34 GHz for the unmodified patch. The shift in resonant frequency is accompanied by slight degradation of return loss value by about 4 dB. Moreover, the patch resonates at another frequency at 5.09 GHz with a return loss value of -11.92 dB. It can be seen that both the measured resonant frequencies are higher than the corresponding simulated values shown in figure 5.10. Moreover, the measured return loss at the higher resonant frequency is poorer than the simulated value at its higher resonating frequency.

The patch structure is further modified by connecting two adjacent spike vertices on the far side of the feed point by a strip line of width 2 mm (characteristic impedance of strip line =  $50.53\Omega$ ) as shown in figure 5.14(a). This strip line is then extended to connect the remaining vertex by the third spike figure 5.14(b). Return loss characteristics for these two geometries (figure 5.14(a) and (b)) are shown in 5.15(a) and 5.15(b) respectively. As is seen from figure 5.15 (a), the patch geometry in figure 5.14(a) resonates in only one frequency at 4.79 GHz with return loss of -24.20 dB. This is almost similar to the return loss characteristic of the basic simple square patch, with only an increase in the resonant frequency and a marginally inferior return loss value.

On extending the strip line to connect all three vertices on one side of the SEMPA

(figure 5.14(b)), the structure resonates at 3 different frequencies, two of them close together (twin peaks) forming a common -10 dB bandwidth of 4.42 %. Figure 5.15(b) shows these three resonant frequencies; the twin frequencies are 4.89 GHz (-17.78 dB) and 5.04 GHz (-19.93 dB) while the third resonant frequency is at 5.40 GHz with a return loss of -20.24 dB.

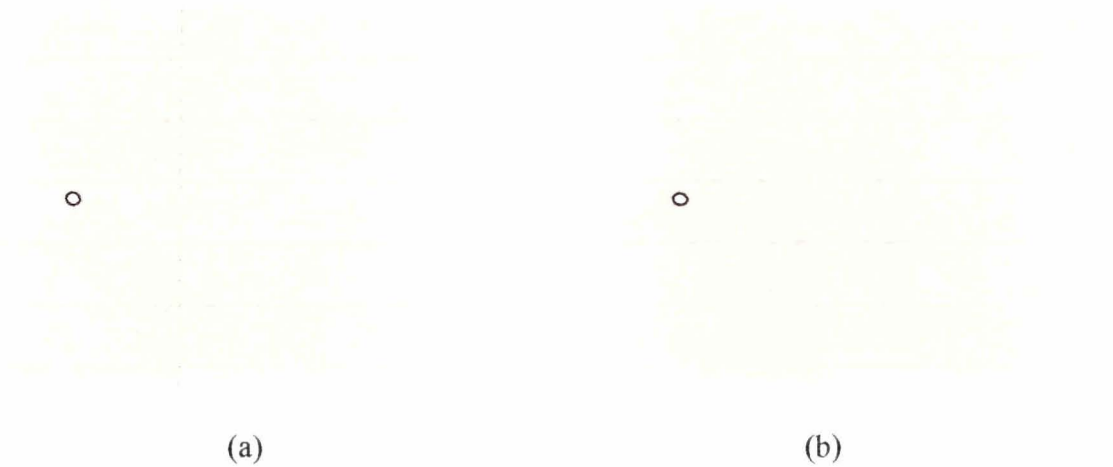


**Figure 5.14:** (a) SEMPA with strip line connecting 2 spike vertices

(b) SEMPA with strip line connecting 3 spike vertices

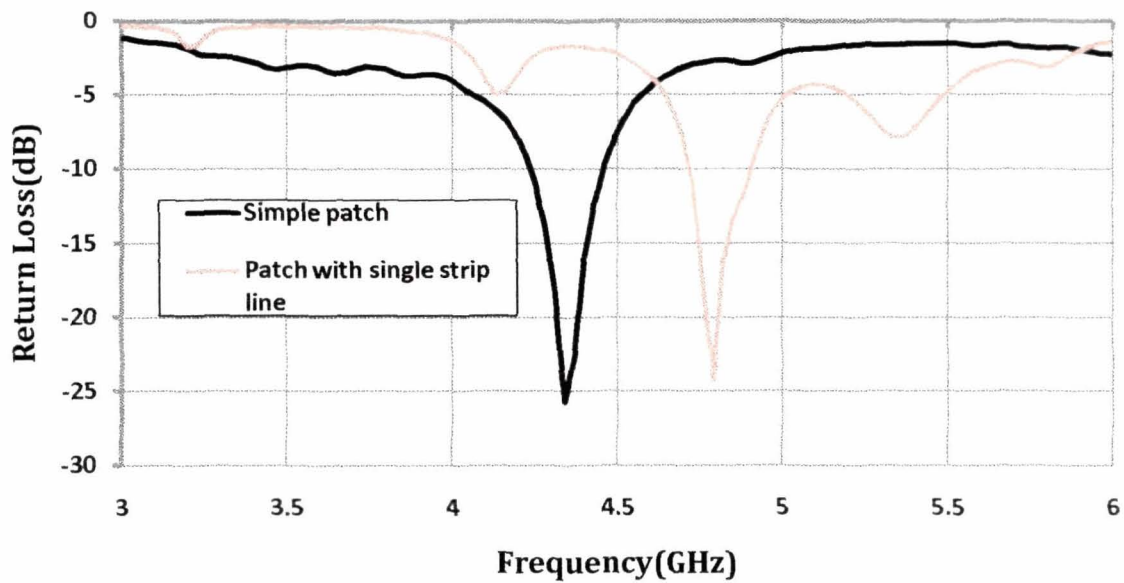


**Figure 5.15 (a):** Return loss plots for SEMPA with strip line connecting two outer spike vertices (figure 5.14 (a))

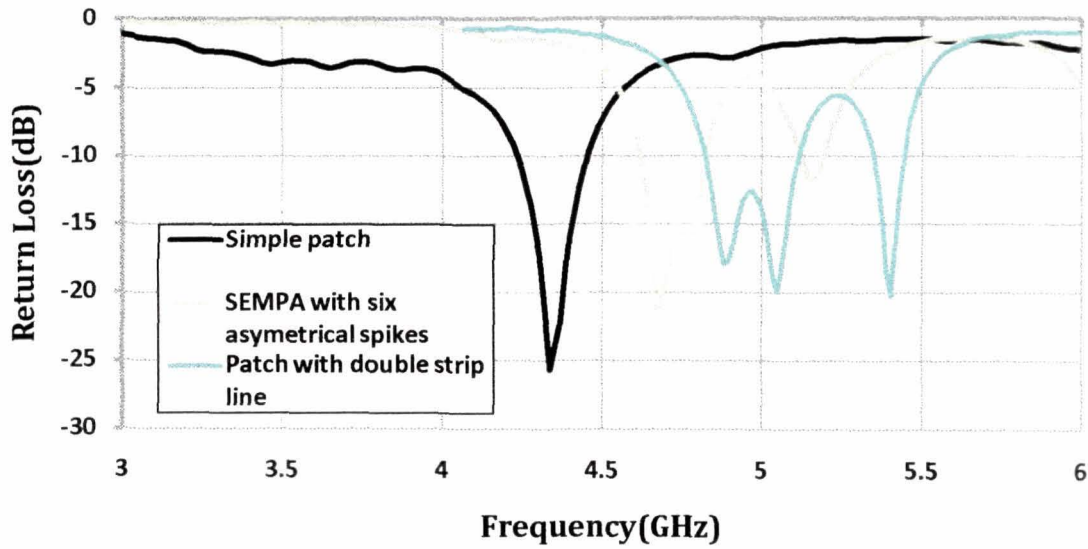


**Figure 5.15 (b):** Return loss plots for SEMPA with strip line connecting three outer spike vertices (figure 5.14 (b))

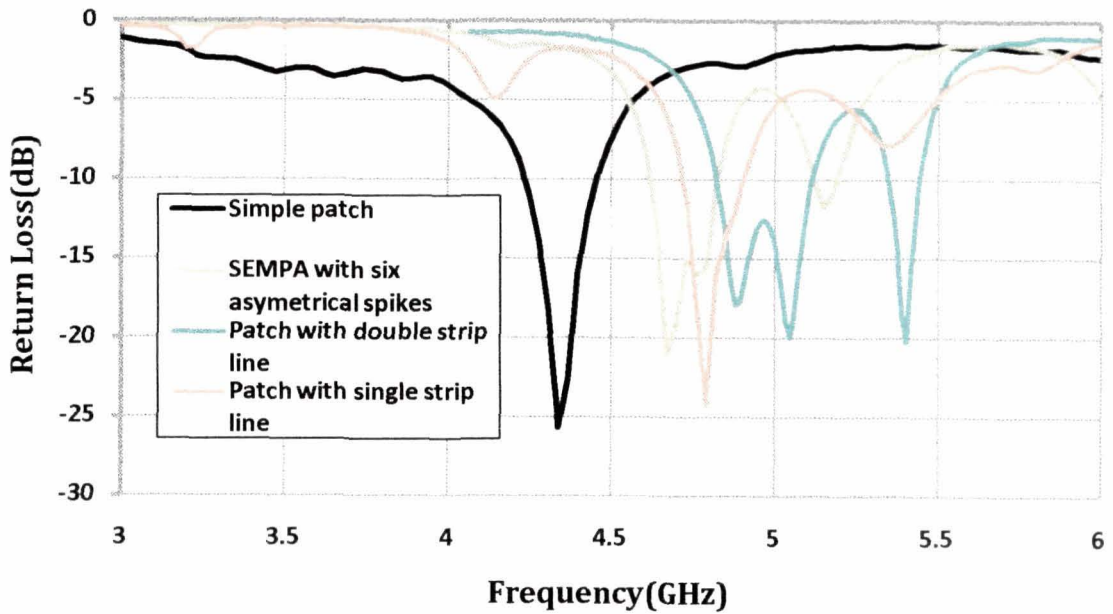


**Figure 5.15 (c):** Return loss plots for in figure 5.14 (a) and 5.14 (b)

The resonant frequencies with the corresponding return loss values for the SEMPA and modified SEMPA are summarized in table 5.3.



**Table 5.3:** Variation of resonant frequency and return loss of the modified SEMPA

Patch configuration	Lower resonant frequency (GHz)	Return loss at lower resonant frequency (dB)	Upper resonant frequency (GHz)	Return loss at upper resonant frequency (dB)
SEMPA	4.67	-21.27	5.09	-11.92
SEMPA with single strip line	4.79	-24.20	----	----
SEMPA with double strip line	4.89	-17.78	5.40	-19.93
	5.04	-19.93(twin peaks)		

As the SEMPA of figure, 5.14(a) with the strip line connecting a pair of vertices is found to resonate at only one frequency, the strip line is moved down along the height of the spike (figure 5.16(a)) to study its effect on resonant frequency. One of the fabricated patches with  $d=1$  mm is shown in figure 5.16 (b). The return loss plots for three different positions of the strip line ( $d = 0$  mm, 1 mm, 2 mm) are shown in figure 5.17. It is seen that for  $d = 1$  mm and 2mm, the antenna resonates again at two different frequencies exhibiting dual band performance. Both the upper and lower resonant frequencies for these two 'd' values are slightly higher than those for the SEMPA geometry without the strip line.

The best combination of return loss values for both the resonant frequencies is seen for  $d=2$  mm. Its performance is comparable to the other geometry (figure 5.14(b)) demonstrating the best return loss performance as is observed from tables 5.3 and 5.4.

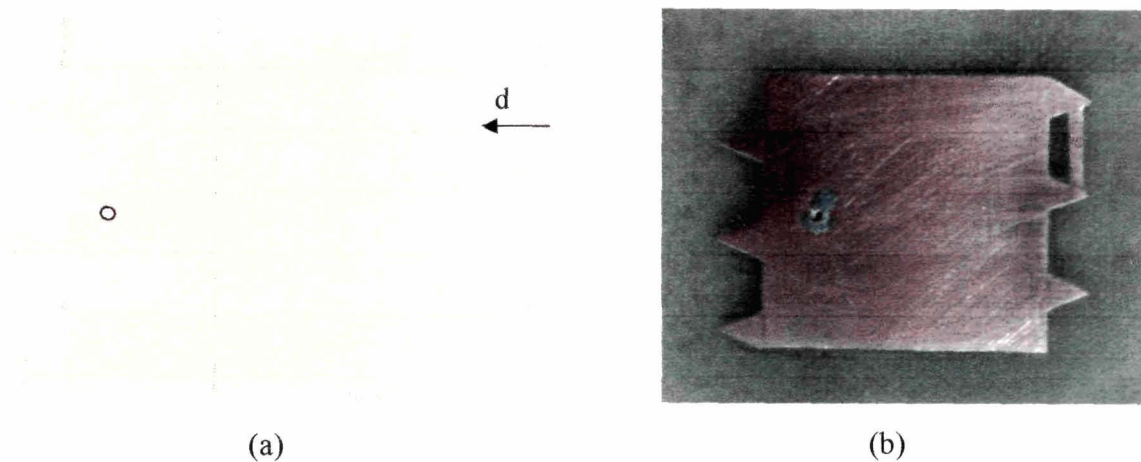


**Figure 5.16:** (a) SEMPA geometry with strip line showing shifting of the strip line  
(b) Fabricated SEMPA with single strip ( $d=1$ mm)

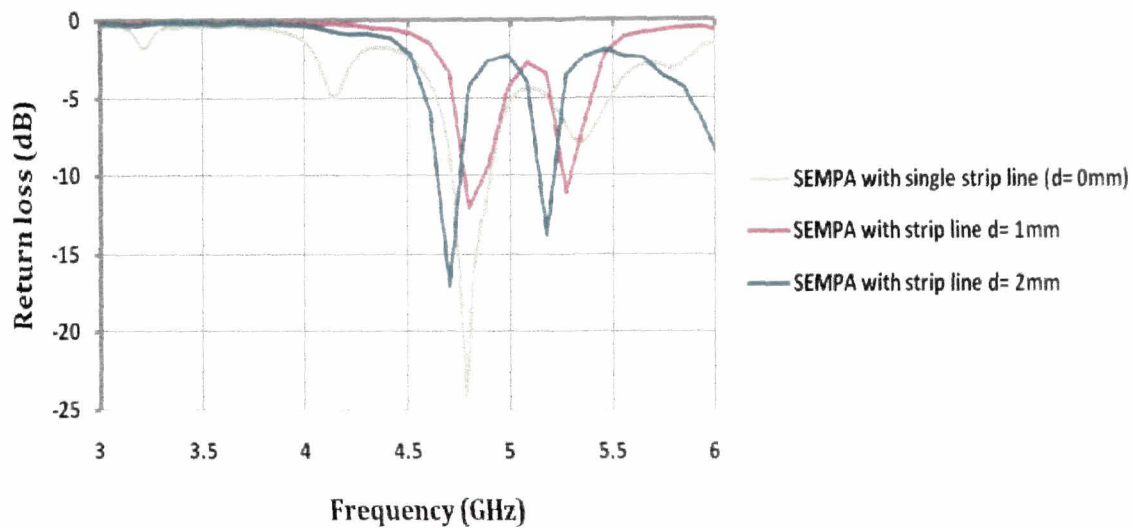


**Figure 5.17:** Return loss plots for SEMPA with strip line at 3 different positions

**Table 5.4:** Resonant frequencies and RL values of SEMPA with strip line positions

Strip line position (Fig 5.16(a))	Lower resonant frequency (GHz)	Return loss at lower resonant frequency (dB)	Upper resonant frequency (GHz)	Return loss at upper resonant frequency (dB)
SEMPA with single strip line at $d = 0$ mm	4.79	-24.20	---	---
SEMPA with strip line at $d = 1$ mm	4.80	-11.97	5.28	-11.06
SEMPA with strip line at $d = 2$ mm	4.71	-17.04	5.18	-13.72

### 5.5 Radiation pattern measurement of SEMPA and SEMPA with strip line

The radiation pattern for SEMPA and SEMPA with single and double strip line sections are shown in figures 5.18 to 5.23

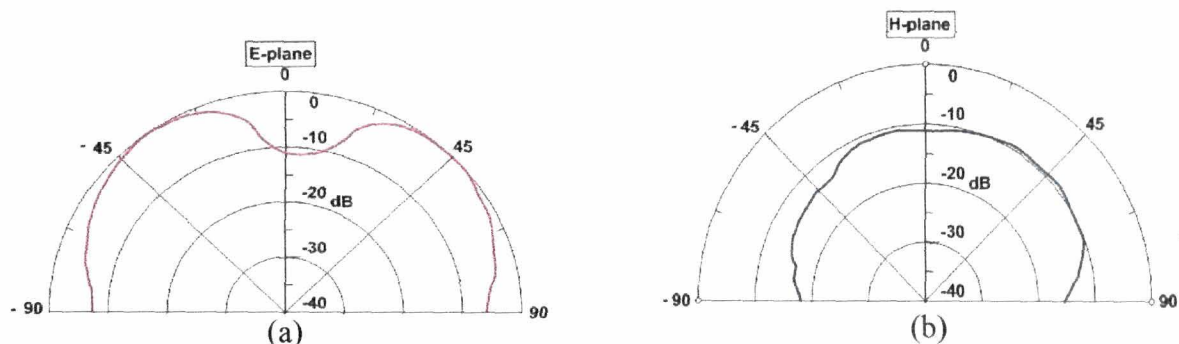


**Figure 5.18:** Measured radiation pattern of SEMPA at 4.67 GHz

(a) E - plane      (b) H- plane

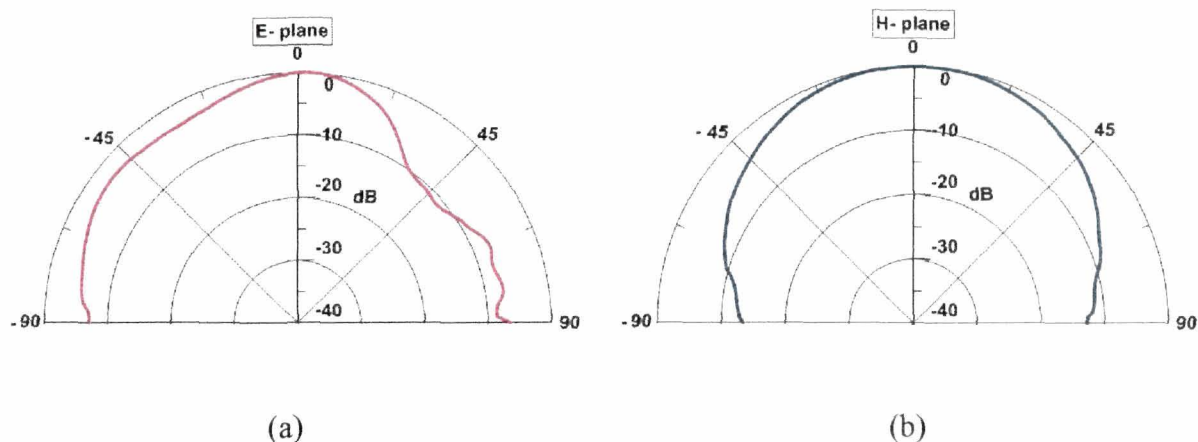


**Figure 5.19:** Measured radiation pattern of SEMPA at 5.09 GHz

(a) E – plane    (b) H – plane

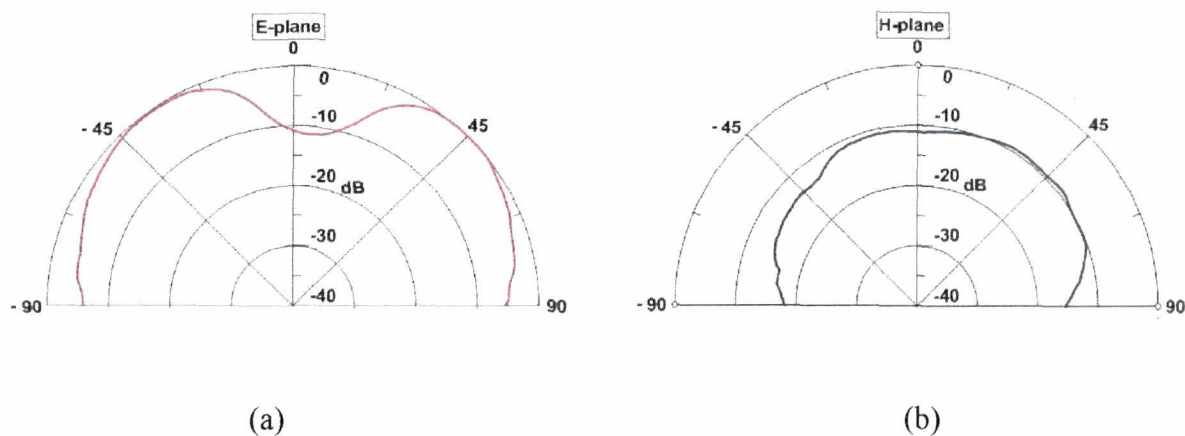


**Figure 5.20:** Measured radiation pattern at 4.79 GHz of SEMPA with strip line connecting

2 vertices  
(a) E – plane    (b) H – plane

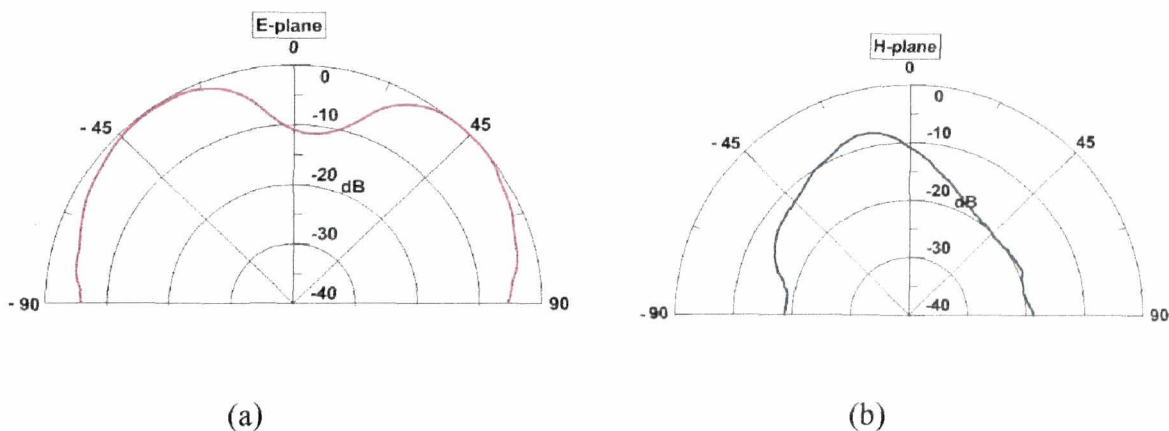


**Figure 5.21:** Measured radiation pattern at 4.89 GHz of SEMPA with strip line connecting

3 spike vertices  
(a) E – plane    (b) H – plane



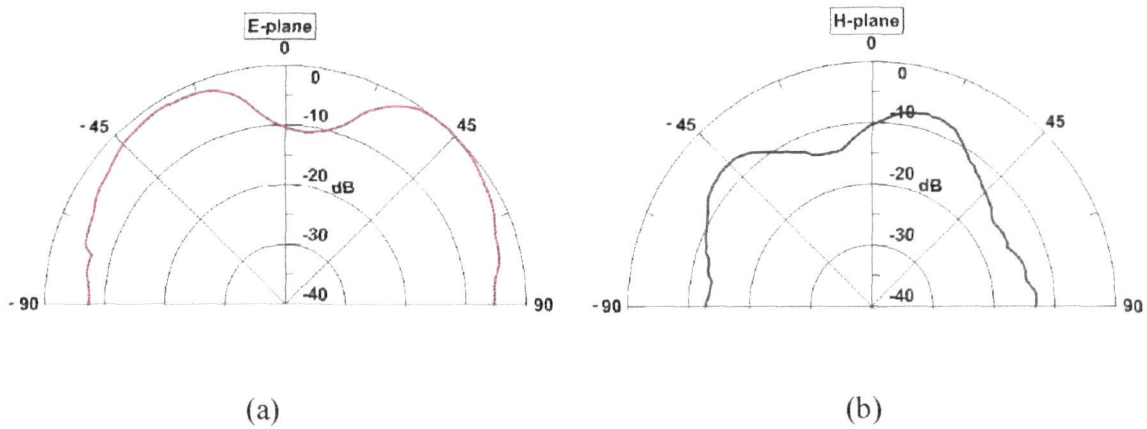


**Figure 5.22:** Measured radiation pattern at 5.40 GHz of SEMPA with strip line connecting 3 spike vertices.

(a) E – plane (b) H – plane

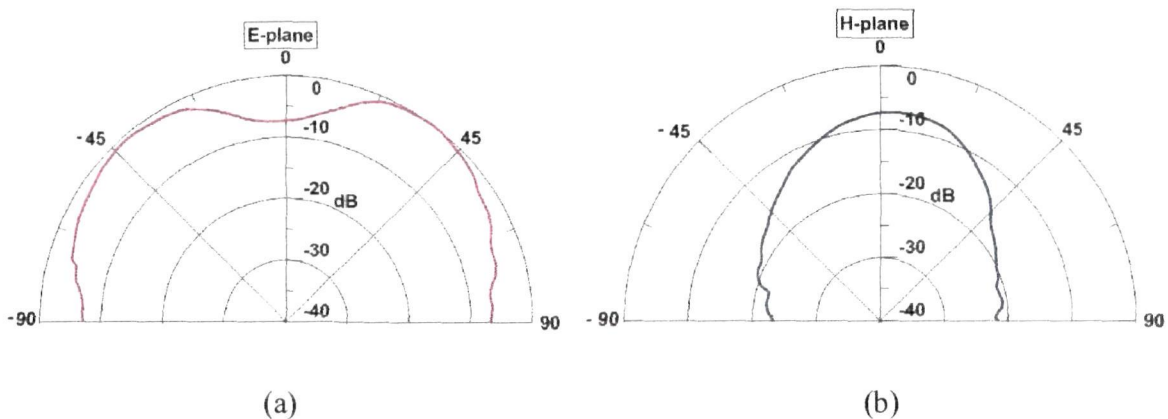


**Figure 5.23:** Measured radiation pattern at 5.40 GHz of SEMPA with strip line connecting 3 spike vertices.

(a) E – plane (b) H – plane

At the lower resonant frequency of 4.67 GHz for the SEMPA, a dip in the broadside direction going down to between -10 dB can be seen for the E-plane pattern (fig 5.18(a)). Excluding the E-plane pattern at the higher resonant frequency of the same structure, all the other E-plane patterns at all resonating frequencies exhibit this dip in the broadside direction. As this dip is observed also for the geometries with strip line bridging of the spike vertices, this pattern alteration can be inherently attributable to the SEMPA structure itself.

For the H-plane patterns again expecting the pattern for SEMPA at 5.09, all the other H-plane patterns shows a peak relative power which is around -10 dB. These patterns also

show some variation including asymmetric with respect to the broadside direction. For the pattern at 5.09 GHz (SEMPA), interestingly, the pattern closely conforms to that of a simple rectangular/square patch.

**Table 5.5:** Measured directivity with SEMPA and SEMPA with strip line

	<i>Lower resonant frequency (GHz)</i>		<i>Upper resonant frequency (GHz)</i>			
	<i>E- plane directivity (dBi)</i>	<i>H- plane directivity (dBi)</i>	<i>E- plane directivity (dBi)</i>	<i>H- plane directivity (dBi)</i>	-----	-----
SEMPA	(4.67 GHz)		(5.09 GHz)		-----	
	3.59	4.35	4.41	4.12		
SEMPA with single strip line			(4.79 GHz)			
	-----	-----	4.41	4.12		
	3.36	7.60	3.59	4.35		
SEMPA with double strip line	4.89 GHz		5.04 GHz		5.40 GHz	
	3.36	7.6	3.81	5.08	3.83	5.90

Table 5.4 summarises the measured directivities obtained from radiation patterns in figures 5.18 to 5.23 for with SEMPA and SEMPA with strip line bridging of vertices for both the E- and H- planes.

## 5.6 Chapter summary

A square patch antenna is modified by adding equilateral triangular spikes at both the radiating edges. The numbers of spikes are changed and strip lines in different configuration connect spike vertices. It is seen that the patch exhibits dual frequency behaviour when three numbers of spikes are asymmetrically added to the two radiating edges, the spikes being spaced apart from each other by 5 mm, a distance equal to the length of a side of the equilateral triangular spike. On bridging to adjacent and extreme spike tips on the far side of the feed point using a strip line of width 2 mm, the dual band behaviour disappears. However, when the strip line is moved down the height of the spikes, dual band is again obtained. For a particular moving distance (2 mm), the return losses at the two resonant frequencies are comparable to the best obtained amongst the geometries studied in this chapter. The best dual band return loss performance is obtained. The value being -19.93 dB at 5.04 GHz and -20.24 dB at 5.40 GHz. The E- plane patterns

in general show a dip in the broadside direction for the SEMPA which also seen for the SEMPA structures with strip lines. The H- plane pattern maxima coincides with the dip of the E- plane pattern (in most cases) indicating higher radiation in the E- plane. Such pattern behaviour may find applications where radiation in one plane is desired in preference to its transverse plane.

---

**References**

- [1] W. He. R., Jin and J., Geng, "E-shaped patch with wideband and circular polarization for millimetre wave communication," *IEEE Trans. Antennas Propag.*, Vol. 56, No.3, pp.893-895, 2008.
- [2] Y. P., Zhang and J., J., Wang, ' Theory and analysis of differentially driven microstrip antennas", *IEEE Trans. Antennas Propag.*, Vol.54, No.4, pp. 1092-1099, 2006.
- [3] A. A., Desmukh, and G., Kumar, "Compact broadband E-shaped microstrip antennas," *Electronic Letters*, Vol. 41, No 18, pp. 989-990, 2005.
- [4] Sanad, "Double C-Patch antennas having different aperture shapes," *IEEE Trans. Antennas Propag. Dig.*, pp. 2116-2119, 1995.
- [5] N. A., Murald, "Microstrip U-shaped dual band antennas," *Applied Electromagnetics*, APACE 2005, Asia –Pacific Conference, 2005.
- [6] B. L., Ooi, "A novel stacked E-shaped patch antenna," *Antennas and Propagation Society International Symposium*, 2001 IEEE, Vol.4, pp. 478-481, 2001.
- [7] Wi. Sang-Hyuk, "Wideband microstrip patch antenna with U-shaped parasitic elements," *IEEE Trans. Antennas Propag.*, 2007, Vol.55, No.4., pp.1196-1199.
- [8] D. Singh, "Small H-shaped antennas for MMIC applications," *IEEE Trans. Antennas Propag.*, Vol. 2, pp. 708–711, 2003.

## **CHAPTER VI**

# **MICROSTRIP PATCH ANTENNA WITH SUBSTRATE POCKET**

---

### **6.1 Introduction**

### **6.2 Design and fabrication of patch with air pocket underneath the patch (Prototype 1)**

#### ***6.2.1 Return loss measurements of patch with substrate pocket and plunger (Prototype 1)***

### **6.3 Design and fabrication of patch with air pocket underneath the patch (Prototype 2)**

#### ***6.3.1 Return loss measurement of patch with substrate pocket and plunger (Prototype 2)***

### **6.4 Chapter summary**

### **References**

## 6.1 Introduction

Tuning in microwave antennas can be achieved using various techniques, such as, by using pin diodes, varactor diodes and MEMs switches [4, 5] as well as by varying substrate properties with ferrites [6] and ferroelectrics. There has been considerable interest in the development of tunable antennas because of increasing number of global wireless standards [1-3]. Multiband antennas are required in order to achieve miniaturisation in mobile and wireless systems such as PCs, bluetooth and wireless local area network.

A tunable antenna provides an alternative to a broadband antenna in which an antenna with a small band width is tuned over a frequency range. Tunable multi-frequency antennas, rather than broadband antennas, can be a preferred alternative when the system needs to operate only at one frequency at any given time. Various tunable configurations have been reported in the literature. One method to realise post-fabrication tunability is by changing the length of a small stub attached to the regularly shaped microstrip antenna [6, 8].

In this chapter, a technique for tuning a microstrip antenna by moving a dielectric plunger in and out of a cut out pocket in the patch substrate is presented. The pocket is created underneath the patch with a thickness equal to or less than the thickness of the substrate with the same cross section as that for the plunger.

Two patch prototypes are fabricated using a vertical milling machine using two different approaches to introduce the pocket in the substrate layer.

## 6.2 Design and fabrication of patch with air pocket underneath the patch (Prototype 1)

A single side copper laminated FR4 substrate board is used as the base layer for assembling the antenna structure. Two dielectric slabs, DS1 and DS2 (figure 6.1) are machined to the requisite dimensions (table 6.1) from the same type of laminated board. Another dielectric section, DS3, is cut out on a milling machine. All these three sections are secured at appropriate locations on the base layer substrate using cyanoacrylate based adhesive. The patch and the feed line is cut out together from a copper foil of thickness 0.025mm. This is secured at the position shown in figure 6.1 (b) using the same adhesive. To prevent sagging of the copper foil section, a brass slab accurately fitting into the recess beneath the patch area is placed before applying the adhesive and pressing the patch-feed line sheet with a weight of 5 kg. The dielectric

plunger section is also cut out to accurately fit the substrate pocket with the length extended out of the patch ground plane when the plunger is completely inserted into the pocket (figure 6 1(c)) Figure 6 2(a) and (b) shows the fabricated structure without and with the plunger section respectively

**Table 6.1:** Specifications for the patch and assembled segments

<i>Parameters (figure 6.1)</i>	<i>Value</i>
Substrate slab thickness ( $T_{DS}$ )	1.5 mm
Width of dielectric slabs, DS1 and DS2 ( $W_{DS}$ )	23.5 mm
Air pocket thickness ( $T_{ap}$ )	1.5 mm
Length of dielectric slab, DS1 and DS2 ( $L_{DS}$ )	40.5 mm
Air pocket width ( $W_{ap}$ )	18.0 mm
Patch dimensions ( $L \times W$ )	23 mm $\times$ 26 mm
Ground plane substrate layer thickness ( $T_{GS}$ )	1.5 mm
Feed strip line width ( $W_f$ ) edge fed	2 mm
Feed strip line length ( $l_f$ )	18.5 mm
Dimension of dielectric slab along patch length, DS3 (= $l_s$ )	19.5 mm
Ground plane dimension ( $G_L \times G_W$ )	60 mm $\times$ 65 mm
Plunger dimensions ( $W_p \times L_p$ )	25 mm $\times$ 18 mm
Plunger thickness	1.5 mm
Resonant frequency of patch with pocket and without plunger	3.25 GHz
Relative permittivity of substrate, $\epsilon_r$	4.8



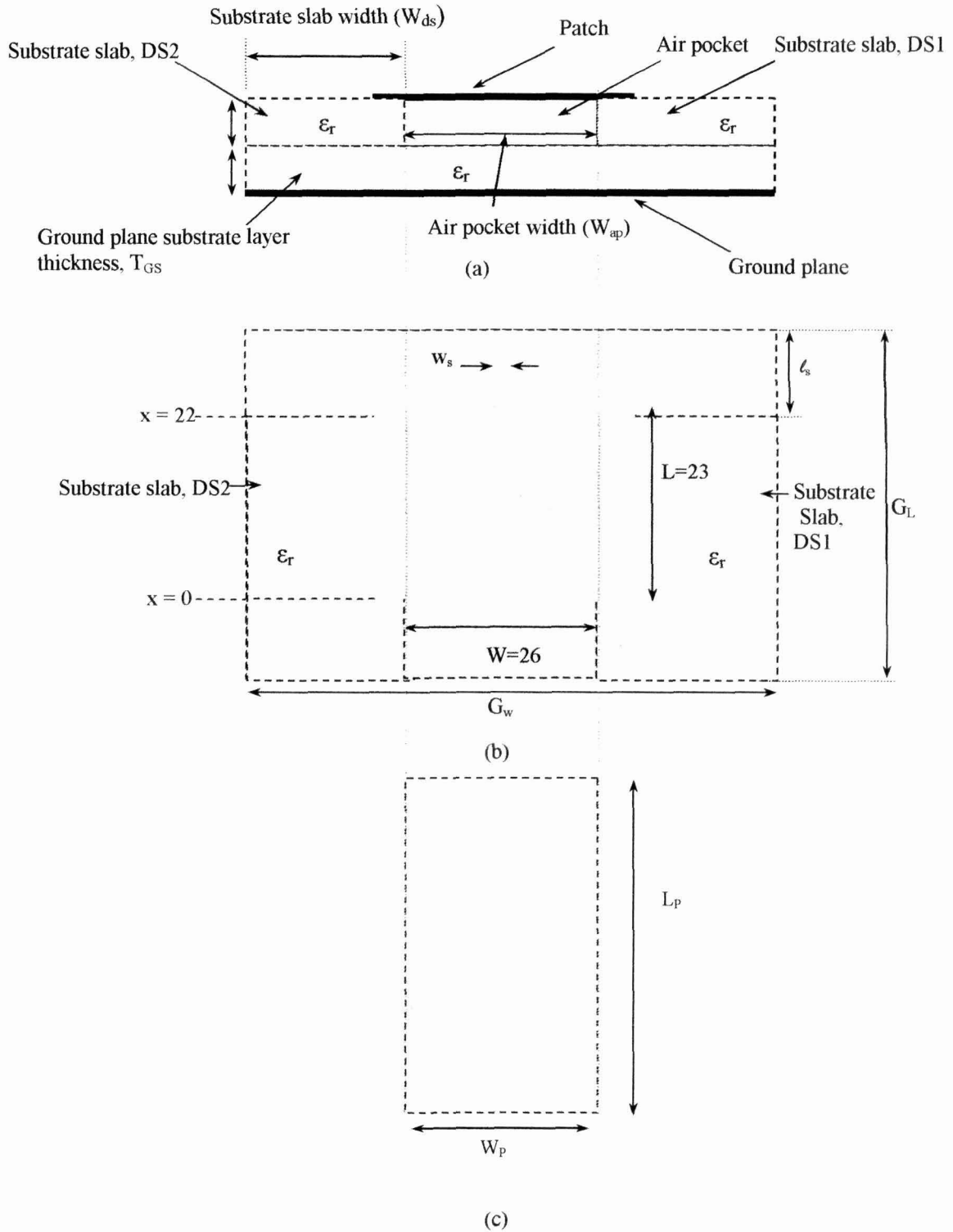


**Figure 6.1:** Antenna geometry demarcating assembled segments  
 (a) End view looking into air pocket  
 (b) Top view  
 (c) Plunger dimension

Measurements are carried out for return loss performance of the fabricated patch prototype (figure 6.1 (a)).

### 6.2.1 Return loss measurements of patch with substrate pocket and plunger (Prototype 1)

Return loss measurements are carried out for the patch structure with the dielectric plunger section inserted into the air pocket as shown in figure 6.2 (b). Figure 6.3 shows the measured return loss plots for the patch antenna for plunger positions resulting in different percentages (87.5%, 75%, 62.5%, 50%, 25% and 0%) of the air pocket filled by the plunger beneath the patch conductor.

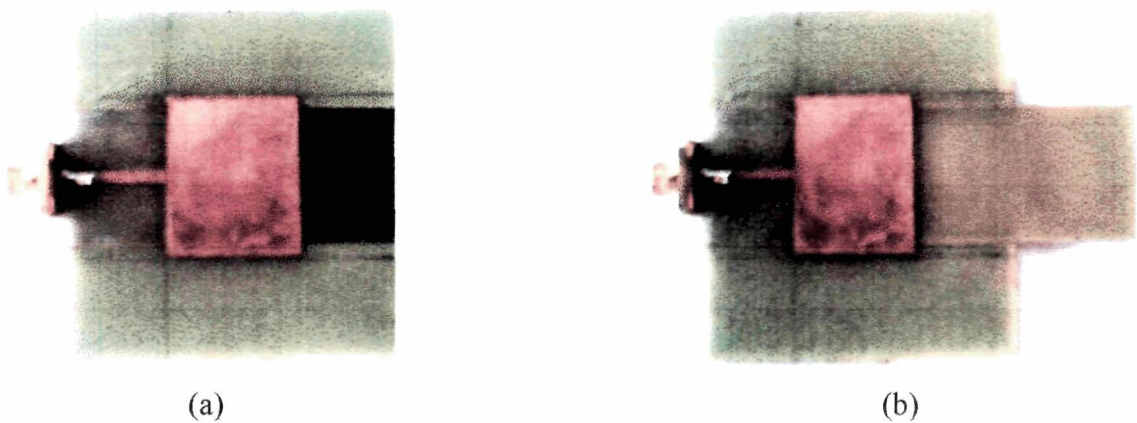


**Figure 6.2:** (a) Fabricated patch with air pocket beneath the patch  
(b) Fabricated patch with plunger section inserted into the air pocket

**Table 6.2:** Resonant frequency with position of plunger

<i>Air pocket thickness (<math>T_{ap}</math>)=1.5mm</i>							
<i>Air pocket width (<math>W_{ap}</math>)=18mm</i>							
Position of plunger tip (x) (figure 6.1(b)) (mm)	0	5.5	10.5	13.4	16.4	19.2	22
Percentage of air pocket filled by plunger dielectric	0%	25%	47.7%	60.9%	74.5%	87.2%	100%
Resonant frequency (GHz)	3.4	3.25	3.2	3.3	3.25	3.25	3.25

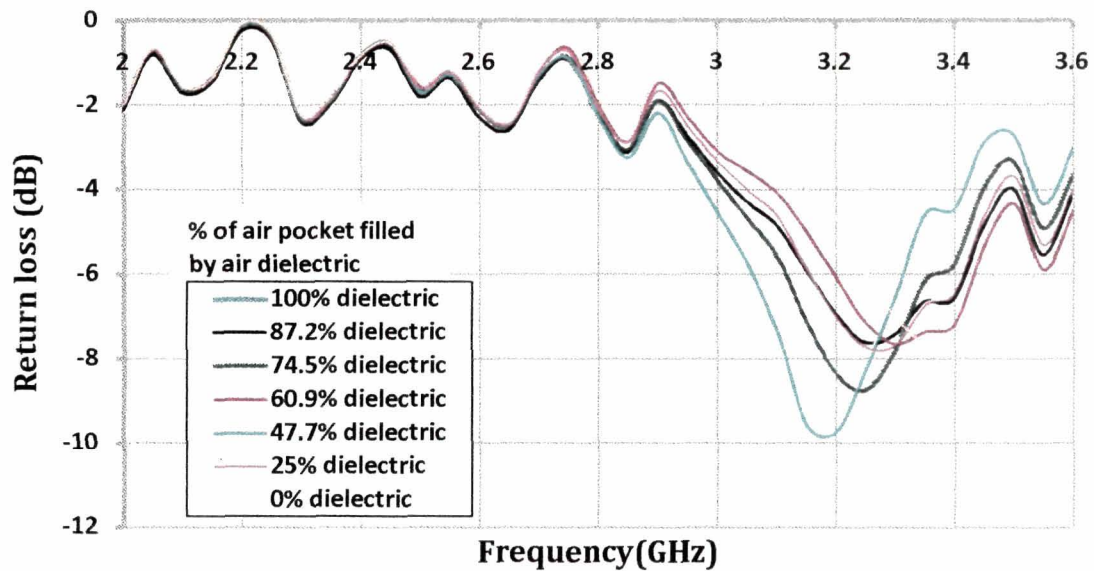


**Figure 6.3:** Measured return loss plot for patch with different dielectric section (%) below the patch

Measurements show that the resonant frequency of the structure can be fine tuned over a small range by moving the plunger within the air pocket (figure 6.3 and table 6.2). However, the resonant frequency values given in table 6.2 show an erratic trend of change in resonant frequency with effective volume of the air pocket. It is observed that with increase in the effective air pocket volume, the return loss degrades but partially recovers when the plunger is fully out of the air pocket. The resonant frequency with plunger end position ( $x$ ) (indicated in figure 6.1(b)) is shown in figure 6.4. It is evident from the results presented in figure 6.3 and table 6.2 that the return loss in general is very poor, not even reaching the -10dB level which is generally considered as a standard minimum performance criteria. One reason may be that the patch, even without the air pocket, shows a poor matching as it is edge fed using a strip line, to start with. Notwithstanding this shortcoming, measurements on this prototype 1 have exhibited the viability of tuning the antenna using this technique. The resonant frequency with different air pocket in the dielectric is shown in figure 6.4.

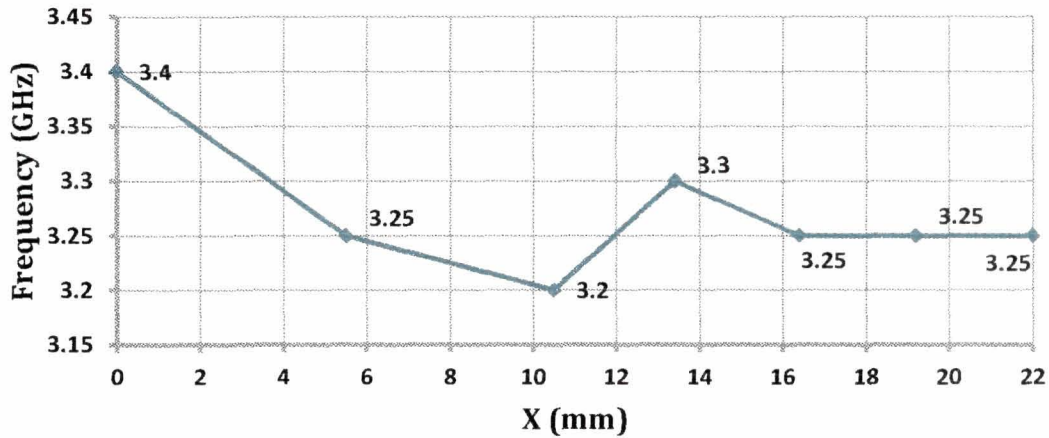


**Figure 6.4:** Shift in resonant frequency with different air pocket beneath the patch

### 6.3 Design and fabrication of patch with air pocket underneath the patch (Prototype 2)

A single sided copper clad substrate board is cut to the required ground plane dimensions given in table 6.3. The substrate side is then machined in a vertical milling machine through its length,  $G_L$  at the centre of the substrate width  $G_w$  to a depth of 1.5mm with a width of 20mm (figure 6.5(a) and (b)). The cutting has to be carried out all through the length of the ground plane since the cutting tool is round and would have left rounded corners if cut only upto the required distance. As the substrate has to be removed down to the copper cladding, the copper side is stuck using adhesive on a smooth metal plate to avoid deformation and resultant damage to the copper cladding before machining. Thereafter, the board is carefully removed from the metal plate using a combination of heating and cleaving.

**Table 6.3:** Specifications for the patch with air pocket

<i>Parameters</i>	<i>Value</i>
Air pocket width ( $W_{ap}$ )	20.0 mm
Patch dimensions (L X W)	22 mm X 29 mm
Feed strip line width - edge fed ( $W_f$ )	2 mm
Feed strip line length ( $l_s$ )	18.5 mm
Plunger dimensions ( $W_p \times L_p$ )	20 mm X 40 mm
Plunger thickness, Air pocket thickness ( $T_{ap}$ ), Substrate thickness ( $h$ )	1.5 mm
Ground plane dimension ( $G_L \times G_w$ )	60mm x 65mm
Resonant frequency of patch with air pocket and without plunger	4.25 GHz
Dimension of filler slab under feed strip line, ( $T_{ap} \times W_p \times l_s$ )	1.5mm x 20mm x 18.5 mm

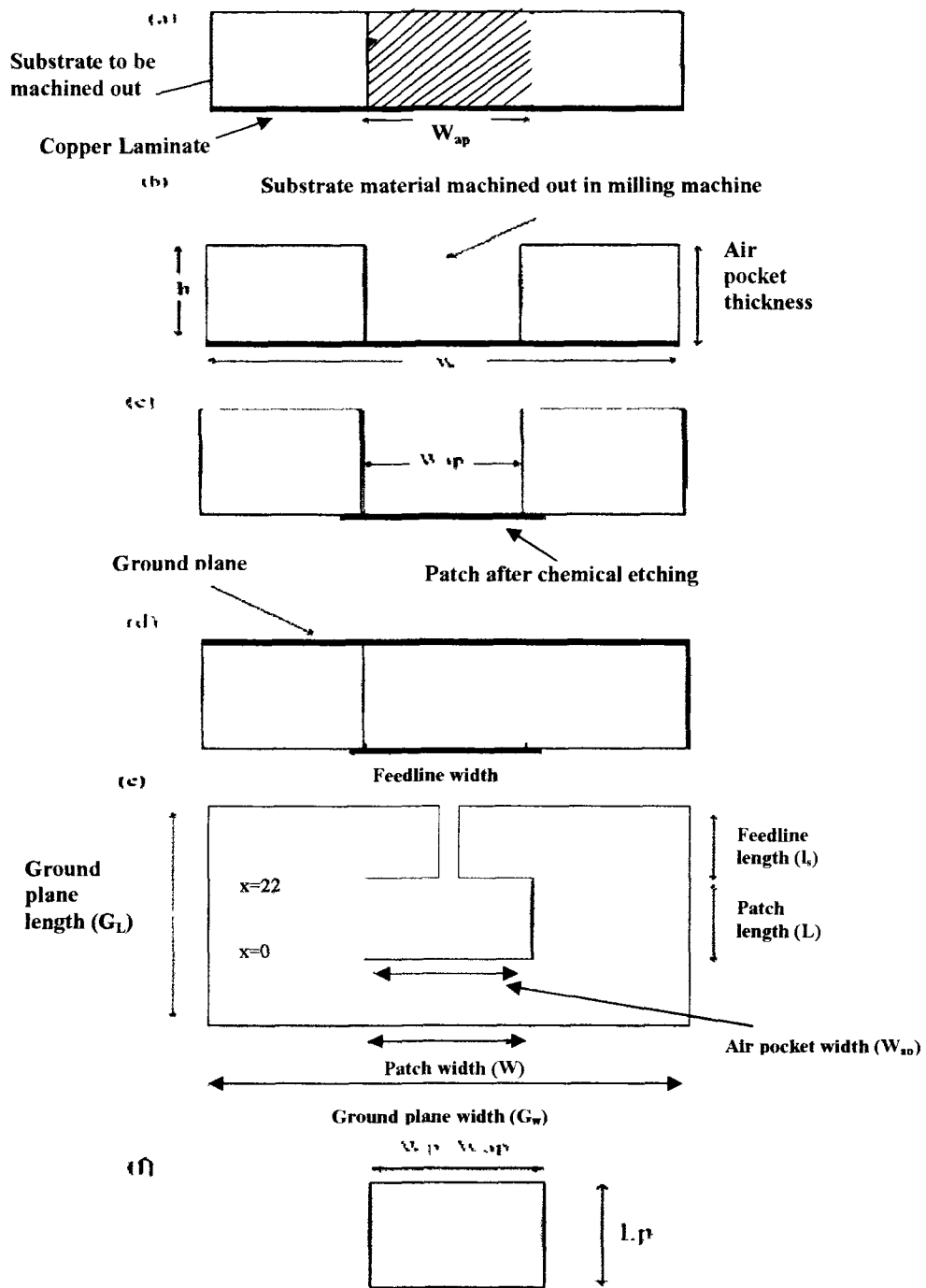


**Figure 6.5:** (a) Single side copper clad substrate showing region to be machined out (end view)  
 (b) Copper clad substrate after machining of region R (end view)  
 (c) Patch on substrate after etching (end view)  
 (d) Patch on substrate with ground plane introduced (end view)  
 (e) Top view of the antenna structure  
 (f) Plunger dimensions



The patch and the feed line is etched out chemically to the required dimensions (figure 6.5 (c)). A filler dielectric slab with dimensions given in table 6.3 is pasted underneath the feed strip line to fill the cut out region under the line. A copper foil of thickness 0.025 mm is pasted onto the substrate on the side opposite to the patch to form the ground plane (figure 6.5 (d)). Again, sufficient pressure is applied to squeeze out the extra adhesive and secure a good bonding (figure 6.5(d)). Figure 6.5(e) and (f) shows the top view of the patch structure and the plunger dimensions respectively. Figure 6.6 shows the substrate being cut on the vertical milling machine to create the air pocket.

The substrate material is thus aligned and milled away with 20 mm cutter leaving two substrate section attached above the copper layer (on other side of the substrate material) as shown in figure 6.6.

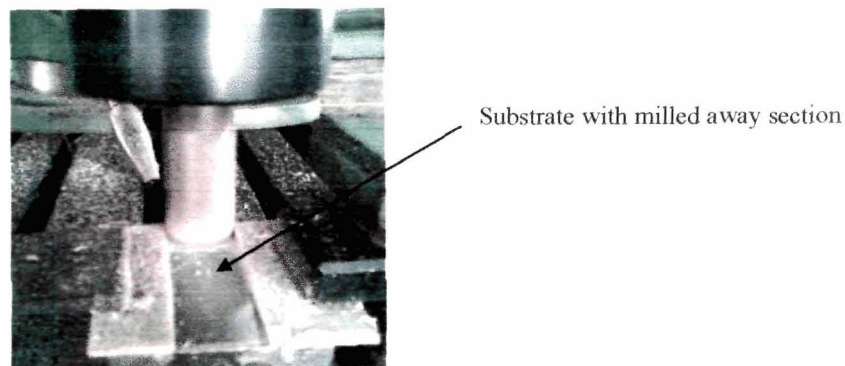


**Figure 6.6:** Picture showing the process of preparing patch with milled away section.

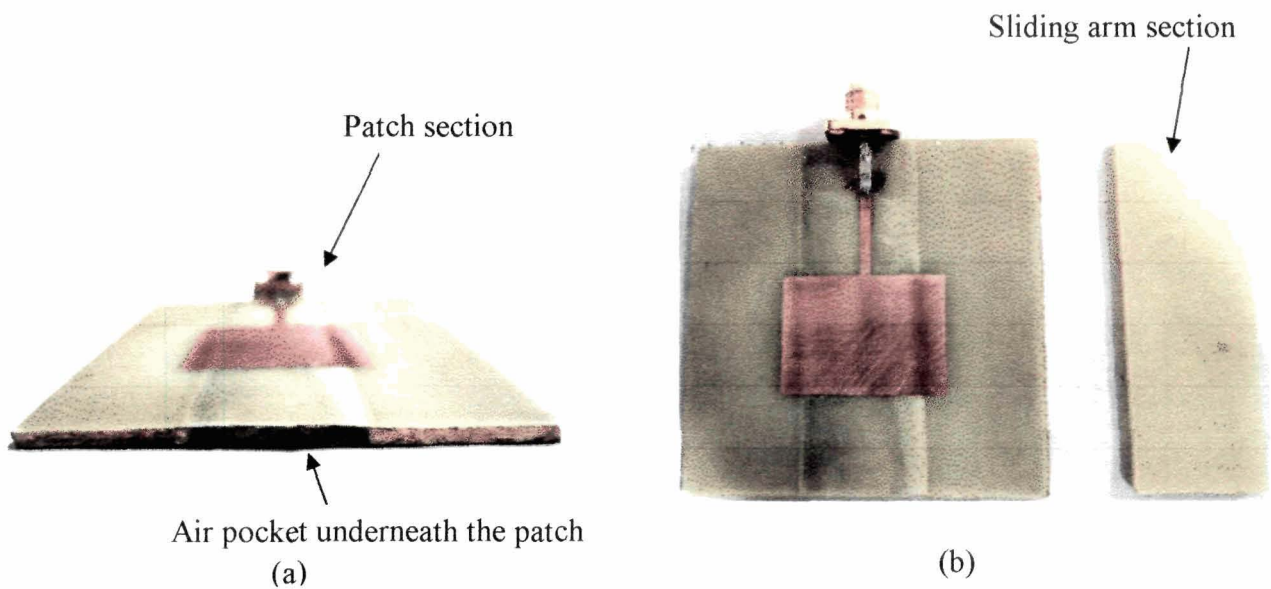


**Figure 6.7:** (a) Fabricated patch structure with air pocket (oblique end view)  
 (b) Fabricated patch and plunger section.

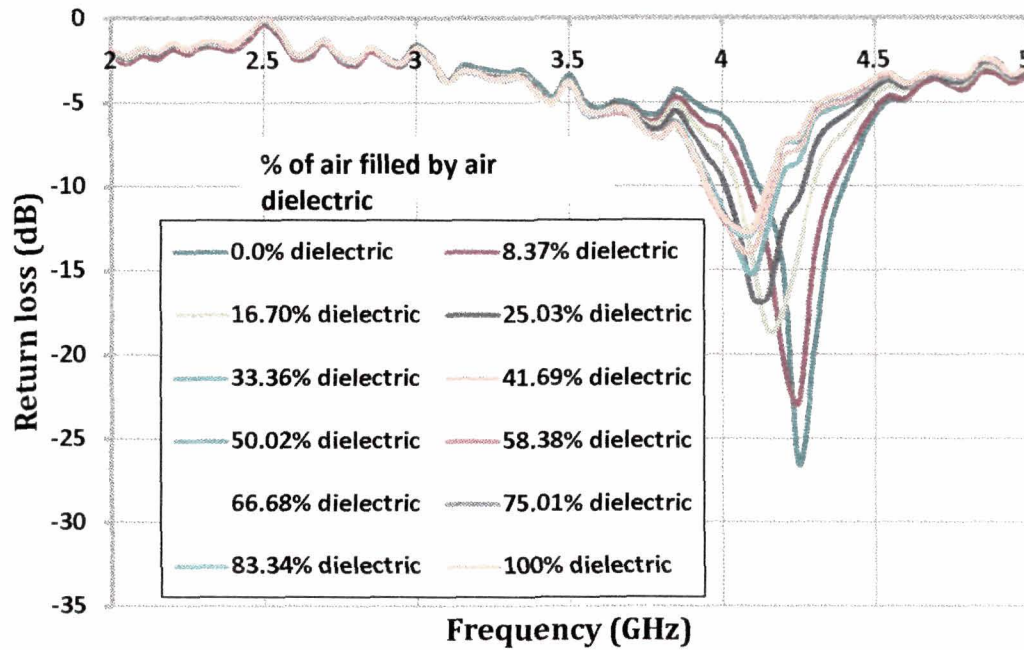
**6.3.1 Return loss measurement of patch with substrate pocket and plunger (Prototype 2)**

Figure 6.7 (a) and (b) shows the fabricated patch structure and plunger. The measured return loss performance with the variation of dielectric (%) below the patch using the second technique (subsection 6.2.2) is shown in figure 6.8. Percentage of air pocket in dielectric substrate with the sliding is given in table 6.3. Return loss measurements are carried out for the patch structure with plunger section inserted into the air pocket.

**Table 6.4:** Resonant frequency with plunger end position

<i>Air pocket thickness (<math>T_{ap}</math>)= 1.5 mm</i>												
<i>Air pocket width (<math>W_{ap}</math>)= 20 mm</i>												
Position of plunger tip (x)	0	1.83	3.6	7.3	9.1	10.98	12.8	14.4	16.4	18.3	20.1	22
Percentage of air pocket filled by plunger dielectric (figure 6.6)	0	8.37	16.7	25.0	33.3	41.6	50.0	58.3	66.6	75.0	83.3	100
Resonant frequency (GHz)	4.25	4.25	4.15	4.10	4.10	4.05	4.05	4.05	4.05	4.05	4.05	4.05





**Figure 6.8:** Measured return loss plot for patch with different dielectric section (%) below the patch

The measured results indicate that as the air pocket beneath the patch is reduced by moving the plunger inwards, the resonant frequency is lowered (figures 6.8 and 6.10). The measured return loss, however, varies erratically with plunger position. Variation in return loss ranges from -12.57dB to -26.59dB, all being better than -10 dB (figure 6.8 and 6.9). The maximum value of return loss is found to be -26.59 dB at 4.25 GHz. Minimum value of return loss as observed from figure 6.9 is -12.52 dB at 4.05 GHz for a plunger position of  $x=18.7$ mm.

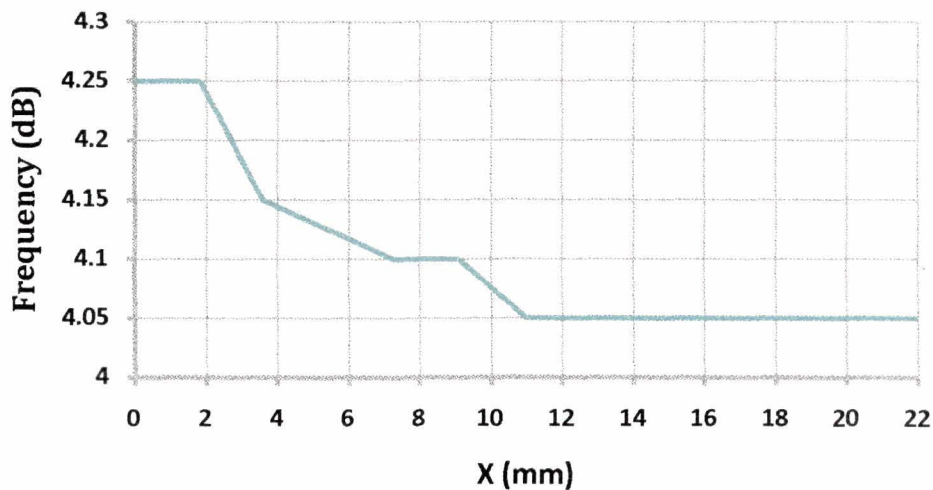


**Figure 6.9:** Measured return loss for patch with different air pocket dimension at the respective resonant frequencies

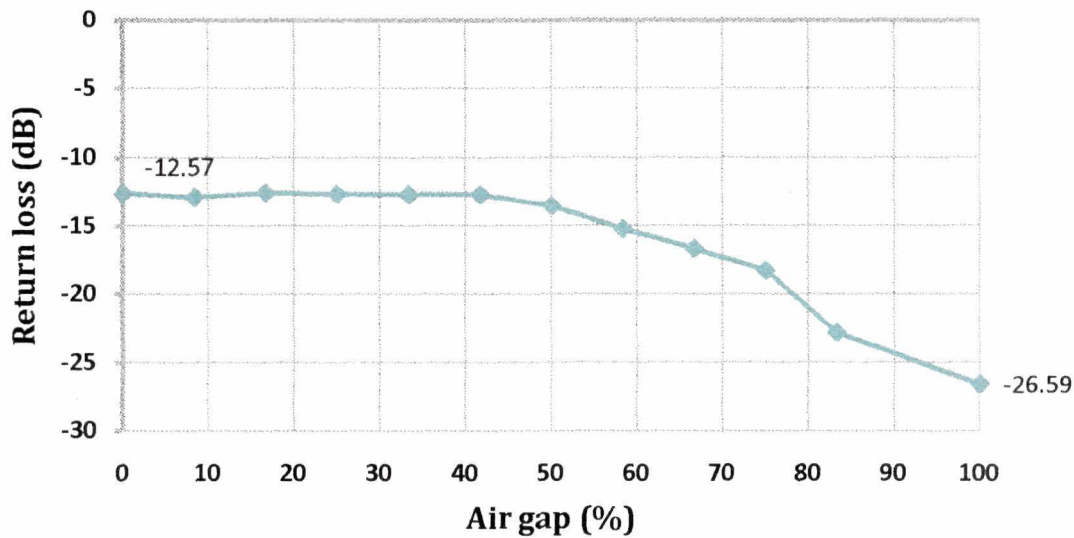


**Figure 6.10:** Measured resonant frequency vs. different air pocket dimension

#### 6.4 Chapter summary

Two patch structures are fabricated with an air pocket in the substrate. A plunger with the same width and thickness as the air pocket is inserted into the air pocket to different depth. In one prototype, the structure is assembled using dielectric slabs of appropriate dimensions on a copper clad substrate. The patch is a copper foil pasted at the appropriate location. Tuning over a small range is achieved by moving the dielectric plunger in the air pocket. The return loss obtained was poor. This is possibly due to poor matching of the strip line edge feed, as the same structure without the air pocket also showed poor return loss performance. Moreover, the resonant frequency shift is also erratic with a unidirectional movement of the plunger in the air pocket. A possible reason for this may be the fabrication method where the copper foil patch pasted gets little support on the dielectric sides. This causes deformity of the patch surface contour (convexing). Movement of the plunger randomly distributes this convexed profile creating variable air gap between the patch conductor and the plunger dielectric.

A second prototype is made using a different fabrication approach. The air pocket is created from the dielectric side by milling out the dielectric material down to the copper cladding. Hence, in this approach, the ground plane is pasted, which gets better supporting dielectric surface area, instead of the patch conductor as has been done in the first prototype. The resonant frequency, in this prototype, decreases in general with

---

the plunger moving in to the air pocket. It is, therefore, possible using the air pocket and plunger approach to design a reconfigurable antenna which can be tuned over a small frequency range. Possible applications of the technique may be in retuning the resonant frequency of a patch which may have drifted due to factors such as ageing/ degradation of substrate material. Other possible uses may be in precisely tuning the resonant frequency after fabrication where manufacturing tolerances do not allow requisite precision of the resonant frequency of the antenna manufactured.

---

**References**

- [1] J.T., Aberle, S.H., Ohn, D.T., Auckland, and S.D., Rogers, "Reconfigurable antennas for portable wireless devices", *IEEE Antennas Propag. Mag.*, Vol. 45, No 6, pp. 148, 2003.
- [2] P., Bhartia, and I. J. Bahl, "A frequency agile microstrip antennas", *IEEE Antennas Propagation Symp. Dig.*, Vol. 20, pp. 304–307, 1982.
- [3] P.M., Haskins, and J.S., Dahele, "Varactor-diode loaded passive polarisation agile patch antenna", *Electron. Lett.*, Vol. 30, No 13, pp. 1074, 1994.
- [4] J.T., Song, I.H., Jo, and Y.H., Kim, "Frequency agile microstrip antenna using piezoelectric substrate", *Jpn. J. Appl. Phys*, Vol. 40, p.L515, 2003.
- [5] R Jr., Jackson, and R. Ramadoss, "A MEMS-based electronically tunable circular microstrip patch antenna", *J. Micromechec. Microeng*, Vol. 17, pp. 1-8, 2007.
- [6] N.X., Sun, J. W Wang, A., Diagle, C., Pettiford, H., Mosallaeiand, and C., Vittoria, "Electronically tunable magnetic patch antenna with meta magnetic films", *Electronics Letters*, Vol.43 No 8, 2007.
- [7] M. Du Plessis, and J. H. Cloete, "Tuning Stub for Microstrip Patch antenna," *IEEE AP-S Int. Symp. Digest*, pp. 964–967, 1993.
- [8] K. P., Ray, and G. Kumar, "Tunable and Dual-Band Circular microstrip Antenna with Stubs," *IEEE Trans. Antennas Propagation*, Vol. 48, pp. 1036-1039, 2000.

## **CHAPTER VII**

### **CONCLUSIONS AND FUTURE WORK**

---

#### **7.1 Conclusion**

#### **7.2 Future work**

## 7.1 Conclusion

The work carried out is essentially motivated by the need to address the well known and inherent limitations of the most popular antenna type in the current era—the microstrip patch antenna. Its low bandwidth limitation has led to numerous innovative designs to enhance the bandwidth, with accompanying trade off, to cater to specific needs. In this same context of bandwidth limitations, a tunable or a multi-frequency antenna may be a more convenient approach in circumventing these limitations, at least in many of the applications.

Intuition plays a major role in antenna technology and hence ideas and approaches of earlier workers form the basis for newer design concepts. The designs presented in this work, draw clues from earlier designs in tackling the limitations mentioned.

In one of the designs studied, a pair of very narrow parallel slits (compared to patch length) is introduced on the patch conductor. The modification results in two resonant frequencies, both on the higher side of the resonant frequency of the original patch, but with lower return loss values. Two resonant frequencies are observed again when one of the slits is removed, retaining only the slit nearer to the feed point. The return loss values are less than that for the simple patch at its resonant frequency (4.86 GHz, -17.46 dB). The lower resonant frequency of 2.17 GHz has a return loss of -12 dB while for the higher resonant frequency at 4.86 GHz, it is -16.4 dB. A size reduction of 76% corresponding to the lower resonant frequency is achieved, which is comparable to the best reported in the literature, using a very simple design. On varying the length of this slit, both the resonant frequencies change and the return losses also vary. This length variation can, therefore, be used to tune the resonant frequencies and adjust the matching. The best return loss performance for both the resonant frequencies can be seen for a slit length of 16 mm (patch width = 18 mm). For this slit length, the lower resonant frequency is 2.33 GHz with a return loss of -22.84 dB while for the upper resonant frequency, these values are 5.11 GHz and -29.9 dB respectively. Both the E- and H-plane patterns at the two resonant frequencies are consistent with the patterns for the conventional simple patch. When the isolated patch sections due to the two parallel slits mentioned earlier are elevated symmetrically at an angle above the substrate, multiple resonant frequencies are observed at different elevation angles which were not seen for the original simple patch. The best results are obtained for elevation angles of 65° and 85°. For an elevation

angle of  $65^\circ$ , the two best resonant frequencies are at 4.04 GHz and 8.83 GHz with return losses of -20.02 dB and -28.48 dB respectively. For an elevation angle of  $85^\circ$ , the two resonant frequencies are 4.23 GHz and 10.26 GHz with return loss values of -36.61 dB and -32.31 dB. All these four return loss values are better than -16.31 dB for the original simple patch at 4.42 GHz. Significant bandwidth enhancements are also obtained at these two elevation angles. A large -10 dB return loss bandwidth is obtained covering the frequency range from 6.84GHz to 9.24 GHz for the  $65^\circ$  elevation angle which amounts to a percentage bandwidth of 29.9%. For elevation angle  $85^\circ$ , the frequency range is from 8.43GHz to 10.59 GHz with a bandwidth of 22.71%.

Size reduction is obtained for another patch geometry formed by notionally superposing a stripline on a rectangular patch making an angle (tilt angle) with the radiating edge. In addition to one resonant frequency near that for the simple patch, another resonant frequency, which is less than half of that for the simple patch, is observed. Hence the design can be used as a dual frequency antenna with one frequency in S- band and the other in the C- band. Both the resonant frequencies change to some extent with change in tilt angle; again providing a method for tuning. For a specific tilt angle, a size reduction of 57% is achieved. All the radiation patterns are similar to the patterns for the conventional patch. This is an advantage as transmitted/ received power level concerns are eliminated for communication link in a particular direction when frequencies are tuned or bands are changed. Moreover, the notionally superposed stripline can be converted to an actual stripline which can be rotated, converting the structure into a reconfigurable antenna. The limitation is that only one resonant frequency can be independently tuned.

Dual band operation is obtained when triangular conductor sections (spikes) are added to the two radiating edges of a rectangular patch. The two operating frequencies are closer (less than 1 GHz apart) in comparison to the previous patch structures studied, where the band separation was higher. The structure turns into a tri-band antenna when all the three vertices of the three spikes on one particular edge of the patch are connected by a strip line. Also, when a strip line section connecting two of the vertices is moved down the height of the spikes, dual band performance is achieved at specific heights. The resonant frequencies can be slightly tuned by changing the stripline position along the spike height.



A dielectric plunger moving within an air pocket in the substrate layer of a rectangular patch is found to tune the operating frequency. However matching is poor. A second fabrication approach is adopted allowing extension of the air pocket throughout the substrate height which was not possible with the first approach used for fabricating the antenna. The structure fabricated using this approach yields better results with the return loss being at least -10 dB for all plunger positions. The feeding method, which in this study is microstrip line edge feeding, can also, be modified through further study to improve the matching.

The investigations on the different patch structures designed indicate that performance improvement; specifically broadband characteristics, dual or multi-frequency operation, pre- or post fabrication tuning as well as size reduction can be achieved to a reasonable extent without seriously compromising on the basic advantages of the microstrip patch antenna. Many of the designs are simple as compared to other techniques reported in the literature with equivalent performance enhancements.

## **7.2 Future work**

The work presented in the dissertation is, in some sense, time limited for a degree. It is therefore inevitable that a more detailed study of parameter variation is left to be done. In addition, the work was carried out within the limitations of available resources.

The slitted patch structures, presented in the third chapter, can be fabricated using accurate CNC prototyping techniques to obtain more accurate results. Further studies with slits of different configurations, such as meandered slits etc. can reveal interesting results. The notionally superposed strip line design can be made mechanically reconfigurable by incorporating a rotating strip line section.

A more detailed study with different spike dimensions, number of spikes, non linear spike profile and spike loading can be areas for further study.

## List of publications

### International Journal paper:

- [1] "Bridged 'V'-shaped patch antenna for dual-band communication," *Electronics Letters*, Vol.48, no.8, pp.419-420, April. 2012.
- [2] "Broadband Microstrip antenna with 100  $\mu\text{m}$  slits on elevated edges for C- and X-band communication" *Microwave And Optical Technology Letters*, Vol. 55, No. 6, pp.1285-1287, 2013.

### International Conference:

- [3] "A novel approach for post fabrication fine tuning and matching of microstrip patch antenna using adjustable air pocket in substrate layer," *Loughborough Antennas and Propagation Conference (LAPC2011)*, doi:10.1109/LAPC.2011.6114026, Loughborough University, Loughborough, U.K., 2011.
- [4] "Design of a novel "V" shaped microstrip antenna with a back reflector," *Loughborough Antennas and Propagation Conference (LAPC2011)*, doi: 10.1109/LAPC.2011.611397, Loughborough University, Loughborough, U.K., 2011.
- [5] "A Novel Spike Edged Rectangular Patch Antenna in C-band for Wireless Application," *The 2011 IEEE Applied Electromagnetic Conference (AEMC 2011)*, doi:10.1109/AEMC.2011.6256831, India, 2011.

### National Conference:

- [6] Computational performance evaluation of a probe coupled U-type waveguide rotary joint designed in X-band for military applications
- [7] Design of a star shaped patch for potential use as antenna for wearable communication systems

# Appendix

# A

---

## LPT port testing test programme:

```
include<math.h>
#include <stdio.h>
#include<conio.h>
#include <dos.h>
Void main ()
{
char r []={2,4,6,8};
FILE *f1;
int a[18000];
int b[18000];
clrscr ();
Int k=1, x=0;
float s= 0.01;
float d;
f1= fopen ("deg.txt","w");
for (int i=0;i<=18000;i++)
{
outportb (0x378,r[i%4]);
d=(s*k);
printf ("% .4f deg:\n",d);
fprintf (f1, "% .4f\n ",d);
a[x]=d;
X++;
delay (1);
K++;
}
for (int m=0;m<=18000 && d<=360 ;m++)
{outportb(0x378,r[m%4]);
d=(s*k);
```

```

printf("%.4f deg:\n",d);
fprintf(f1,"%0.4f\n ",d);
b[x]=d;
x++;
delay (1);
k++;
}
outportb (0x378,15);
}

```

---

**Measurement of power Vs frequency:**

```

#include"StdAfx.h"
#include<visa.h>
#include<iostream>
#include<windows.h>
#include<stdlib.h>
#include<dos.h>
#include<conio.h>
#include<stdio.h>
short_stdcall Inp32(short PortAddress);
void_stdcall Out32(short PortAddress, short data);

void main ()
{

char a[] = {2,4,8,16}; //motor 4 bit sequence(anti-clockwise)
int y, stepsperreadingi,g,freq;
float readingangle,stepsperreading,angularposition;
FILE *fp;
ViSessiondefaultRM,vi,defaultRMsp,visp;//Declares variables of
type ViSession
// for instrument communication

```

```

        ViStatus viStatus = 0,viStatussp = 0; //
Declares a variable of type ViStatus
        char rdBuffer [2000],rdBuffersp [2000]; //
Declare variable to hold string data
        viStatus=viOpenDefaultRM(&defaultRM);//Initialize VISA system
        viStatussp=viOpenDefaultRM(&defaultRMsp);
        viStatus=viOpen(defaultRM,
"USB0::0x0957::0x1F01::MY49060341::0::INSTR",VI_NULL,VI_NULL, &vi);
        if(viStatus) // If problems then prompt user
        {
                printf("Could not open USB signal Gen!\n");
                printf("Check instruments and connections\n");
                printf("\n");
                exit(0);}

        viStatussp=viOpen(defaultRMsp, "TCPIP0::192.168.100.4::inst0::INSTR",
VI_NULL, VI_NULL, &visp);
        if(viStatussp)
        { // If problems then prompt user
                printf("Could not open Spectrum Analyser!\n");
                printf("Check instruments and connections\n");
                printf("\n");
                exit(0);
        }

        if (g>0 )
        {
                printf("Source RF state is : on\n");
        }
        else
        {
                printf("Source RF state is : off\n");
        }
}

```